UNCLASSIFIED

AD 444114

DEFENSE DOCUMENTATION CENTER

FOR

SCIENTIFIC AND TECHNICAL INFORMATION

CAMERON STATION, ALEXANDRIA, VIRGINIA

UNCLASSIFIED

4441114

TRANSACTIONS OF THE NINTH CONFERENCE
OF
ARMY MATHEMATICIANS

D D C

AUG 17 1964

DDC-IRA D

Sponsored by

The Army Mathematics Steering Committee

on Behalf of

THE OFFICE OF THE CHIEF OF RESEARCH AND DEVELOPMENT

NO OTS

U. S. Army Research Office-Durham

Report No. 64-1
June 1964

TRANSACTIONS OF THE NINTH CONFERENCE

OF ARMY MATHEMATICIANS

Conducted at

Watervliet Arsenal
Watervliet, New York

5-6 June 1963

FOREWORD

Watervliet Arsenal served as the host for the Ninth Conference of Army Mathematicians. As the preceding two meetings were conducted in the midwest, the sponsor of this series of conferences - the Army Mathematics Steering Committee - deemed it desirable to have the next conference in the east. So when Dr. Robert E. Weigle asked this group to hold their ninth meeting at Watervliet, New York, the AMS was pleased to accept his invitation. Clinical type sessions were introduced into the Army Mathematicians Conferences at this 5-6 June 1963 meeting.

Colonel Keith T. O'Keefe, Commanding Officer of Watervliet Arsenal, called the conference to order and welcomed the group to his installation. In the light of his remarks it seems desirable to quote the following comments from the phamplet entitled "Watervliet Arsenal".

"In the same building where weapons experts of a century ago sought ways to improve maskets and percussion caps, Watervliet Arsenal scientists now use radio isotopes to probe the basic atomic structure and behavior of materials.

This typical example of Watervliet's quest for new knowledge in an old environment aptly symbolizes a continuity of purpose which began 150 years ago on a tract of Hudson River farmland just north of Albany. The traditions of research, knowledge, and craftsmanship implanted then, now motivate the scientists, designers and technicians creating armament for the arenas of space in the Age of the Atom.

Watervliet entered the first of its three major historical eras - a 30 year 'Age of Adolescence' in 1813. A young nation - facing a new threat from an old enemy - established the Arsenal as a supply bastion for troops guarding the invasion routes of Lake Champlain and the Mohawk Valley. This first brief mission was followed by years of struggle as

the small-arms and ammunition depot, beset by the 'growing pains' of economic difficulties, gradually evolved into a manufacturing arsenal. And, despite limitations of space and facilities, Watervliet's manufacturing capacity by the end of the first era encompassed a surprising variety of materiel: gun carriages, fuzes, rockets, percussion caps, sponges and leather accounterments.

Furious activity followed by grinding slowdowns characterized Watervliet's second era when overnight expansions of staff and facilities demanded by two major wars were succeeded by corresponding reductions during post-war 'lean years'.

The Mexican War not only instantly multiplied production demands but also, and more significantly, spurred and tested the Arsenal's ingenuity. Traditions of 'know how' and 'can do' were born as wartime improvisation and invention conceived better and quicked manufacturing methods. Research began in earnest as experiments with rubber harversacks and mineralized wood for gun carriages were carried out with the same dedication that characterizes Arsenal scientists today.

The considerable demands imposed on the Arsenal by the Mexican conflict were dwarfed in 1861 as Watervliet faced - and surmounted - the tremendous challenge of the Civil War. For four years 2000 men and women worked day and night producing prodigious quantities of gun carriages, rifle cartridges, cannon shot, shell casings, scabbards, harness, and scores of other items. But, after Appomatox, all-out production stopped short. Reductions in force - and funds - soon slowed the pace of progress almost to a standstill as the middle era came to a close.

Almost two decades passed before Arsenal fortunes took an upswing. Then, in 1883, the third era dawned brightly as, by Act of Congress, Watervliet was selected to be the 'Army Gun Factory'. Thus began

the proud mission the Arsenal continues to fulfill today - to perform research, design, production - control and procurement assignments for all US Army cannon. Since then Watervliet's design achievements - the first 16-inch gun, the 'Long Tom' of World War II, the gigantic 280mm atomic cannon, and many more - cannon, howitzers, recoilless rifles and mortars - have spoken with steel-throated eloquence in defense of the nation and the free world.

Now on the threshold of the future, as tested talents are turned to work on space- borne components, plus a continuing emphasis on atomic-armed conventional weapons, the Arsenal is proving anew that it is ready today to meet the challenges of tomorrow. "

The Ninth Conference of Army Mathematicians was attended by forty-seven (47) scientists from twenty-one (21) Army installations, two (2) commercial concerns, and eight (8) universities. In addition, the host had nine (9) of its own staff present; thus the total attendance ran to sixty-five (65) persons. Those in attendance had the pleasure of listening to twenty (20) contributed technical papers, to four (4) clinical papers, and one invited address given by Professor Richard C. DiPrima from Rensselaer Polytechnic Institute. The Army Mathematics Steering Committee asked that most of these papers be made available in printed form. In addition to the papers appearing in this book, a paper presented at the conference carrying a security classification of SECRET will appear in a classified appendix.

Dr. Robert Weigle served as the Chairman on Local Arrangements. Those in attendance were indebted to him for an excellent banquet and for handling the large number of organizational problems associated with a meeting of this size. The Committee on Arrangements would like to thank the speakers, the chairmen, the panelists, and the many individuals of the host installation who contributed so much of their time and effort in order to make this conference an interesting and successful scientific event.

TABLE OF CONTENTS

---

* This paper was presented at the Conference. It does not appear in these Transactions.

** This paper carries a security classification of SECRET. It will appear in an appendix to this report.

---

* This paper was presented to the Conference. It is not reproduced here.

* This paper was presented to the Conference. It is not reproduced here.

PROGRAM

Wednesday, 5 June 1963

0815-0845   REGISTRATION: Benet Laboratory

0845-0855   CALLING OF CONFERENCE TO ORDER:
             Robert E. Weigle, Local Chairman
             WELCOMING:
             Colonel Keith T. O'Keefe, Commanding Officer
             of Watervliet Arsenal

0855-1005   TECHNICAL SESSION I
             Chairman: F. W. Schmiedeshoff, Watervliet Arsenal

0855-0930   Some Experiences with Several Procedures for Obtaining
             Non-linear Least Squares' Fits
             Wallace Chandler and Herbert Maisel, U. S. Army
             Strategy and Tactics Analysis Group

0930-1005   On the Numerical Solution of Linear Difference Equations
             with Auxiliary Conditions at Both Ends
             T. N. E. Greville, Mathematics Research Center,
             United States Army, University of Wisconsin

0855-1005   TECHNICAL SESSION II
             Chairman: Julian L. Davis, Explosive and Propellants
             Laboratory, Picatinny Arsenal

0855-0930   Steady-State Temperatures in a Slab Containing a Plane
             Insulating Filament, Part I: Formulation and Solution by
             Conformal Mapping
             J. E. Zweig, M. J. Pascual, S. D. Beck,
             Watervliet Arsenal

0930-1005   Steady-State Temperatures in a Slab Containing a Plane
             Insulating Filament, Part II: Solution to the Infinite System
             by Numerical Induction
             M. J. Pascual and J. E. Zweig, Watervliet Arsenal

1005-1035   BREAK

TECHNICAL SESSION V (CONT.)

TECHNICAL SESSION VII (CONT.)

1600-1640   Classification of Microfibers and Couple Stresses
             M. Sadowsky, Watervliet Arsenal

1520-1640   TECHNICAL SESSION VIII
             Chairman: Badrig Kurkjian, Harry Diamond Laboratories

1520-1600   Thin Cylindrical Shells Subject to Localized Axial (Shear)
             Loading
                 John F. Mescall, U. S. Army Materials Research Agency,
                 Watertown Arsenal

1600-1640   Rectangular Tensile Sheet with Edge Cracks
                 Oscar L. Bowie, U. S. Army Materials Research Agency,
                 Watertown Arsenal

1800   SOCIAL HOUR and DINNER

                        Thursday, 6 June 1963

0815-0950   CLINICAL SESSION A
             Chairman: Fred Frishman, Mathematics Branch, Physical
                       Sciences Division, U. S. Army Research Office,
                       Washington, D. C.
             Panelists: R. J. Duffin, Carnegie Institute of Technology
                        T. N. E. Greville, Mathematics Research
                            Center, U. S. Army, University of
                            Wisconsin
                        F. J. Murray, Duke University
                        T. W. Schmidt, U. S. Army Research Office -
                            Durham
                        J. J. Stoker, Courant Institute of Mathematical
                            Sciences
                        Arthur Wouk, Mathematics Research Center, U. S.
                            Army, University of Wisconsin

0815-0900   A Sturm-Liouville Problem Associated with the Perturbation
             Velocity Field in a Rotating Cylindrical Mass of Fluid, the
             Angular Velocity of which is a Function of the Radius R
                 W. E. Scott, Exterior Ballistics Laboratory, Ballistic
                 Research Laboratories, Aberdeen Proving Ground, Md.

CLINICAL SESSION A (CONT.)

0900-0950   Dynamic Formulation of the Coefficient of Restitution
                    E. H. Jakubowski, Research and Engineering Division,
                    Springfield Armory

0950-1020   BREAK

1020-1145   CLINICAL SESSION B
                   Chairman: Joseph Weinstein, U. S. Army Electronics
                                    Research and Development Laboratory
                   Panelists: R. J. Duffin, Carnegie Institute of Technology
                                    T. N. E. Greville, Mathematics Research Center,
                                        U. S. Army, University of Wisconsin
                                    F. J. Murray, Duke University
                                    T. W. Schmidt, U. S. Army Research Office -
                                        Durham
                                    J. J. Stoker, Courant Institute of Mathematical
                                        Sciences
                                    Arthur Wouk, Mathematics Research Center, U. S.
                                        Army, University of Wisconsin

1020-1105   The Propagation of Shock Waves through Soil-Analytical Methods
                 and Problems
                    Detrich E. Gudzent, Structures and Mechanics Laboratory,
                    Directorate of Research and Development, U. S. Army
                    Missile Command, Redstone Arsenal

1105-1145   Short Range Electronics Position Determination
                    Duncan Harkin, U. S. Army Engineer Geodesy, Intelligence
                    and Mapping Research and Development Agency

1145-1310   LUNCH

1310-1350   TECHNICAL SESSION IX
                   Chairman: G. B. Parrish, U. S. Army Research Office -
                                    Durham

                 Membrane Natural Frequencies for Axi-Symmetric Vibration
                 of Deep Spherical Caps
                    Edward W. Ross, Jr., U. S. Army Materials Research
                    Agency, Watertown Arsenal

1310-1350   TECHNICAL SESSION X
             Chairman: R. L. Helmbold, Combat Operations Research
                        Group, Fort Belvoir

1310-1350   Coordinate Systems and Error Analysis
                Hodge W. Doss, Jr., Operations Research Department
                Institute of Science and Technology, The University of
                Michigan. Representing the U. S. Army Signal Air
                Defense Engineering Agency.

1350-1430   BREAK

1430-1530   GENERAL SESSION
             Chairman: Ralph Brown, U. S. Army Munitions Command,
                        Frankford Arsenal

             Stability of Flow between Rotating Cylinders and Related Topics
                Professor Richard C. DiPrima, Rensselaer Polytechnic
                Institute

ON THE NUMERICAL SOLUTION OF LINEAR

DIFFERENCE EQUATIONS WITH AUXILIARY CONDITIONS AT BOTH ENDS*

T. N. E. Greville**

Mathematics Research Center, United States Army,
University of Wisconsin

1. **INTRODUCTION.** This report concerns the numerical solution of the difference equation.

$$(1) \qquad u_x = \sum_{i=1}^{n} a_{ix} u_{x-i} + g_x \qquad\qquad (x = n+1, n+2, \ldots, p)$$

for $u_1, u_2, \ldots, u_p$, subject to the auxiliary conditions (which we shall call "end conditions")

$$(2) \qquad \sum_{j=1}^{n} b_{ij} u_j = h_i \qquad\qquad (i = 1, 2, \ldots, m)$$

$$(3) \qquad \sum_{j=1}^{n} b_{ij} u_{p-n+j} = h_i \qquad\qquad (i = m+1, m+2, \ldots, n),$$

where $0 < m < n$. While (1), (2) and (3) may be regarded as a system of p simultaneous linear equations in p unknowns, solution of this system by standard methods would fail to take advantage of the special form of the matrix of coefficients.

The method to be suggested here involves choosing n appropriate
starting values and constructing, by successive applications of (1), a
sequence of numerical values satisfying the difference equation (1) (but
not the end conditions (2) and (3)). In a similar manner n further,
linearly independent sequences are constructed satisfying the correspond-
ing homogeneous equation

(4)
$$u_x = \sum_{i=1}^{n} a_{ix} u_{x-i} \, .$$

These n sequences constitute a fundamental set : that is, a basis for the
general solution of (4) , and the general solution of (1) is obtained by
adding the general solution of (4) to any particular solution of (1). The
solution of (1) satisfying the end conditions is therefore obtained as
a suitable linear combination of the n + 1 sequences.

The special case of linear difference equations with constant
coefficients (in which the coefficients a_{ix} are replaced by coefficients
a_i independent of x) is discussed separately, as it permits of consider-
able simplification in the numerical procedures. The simplification
arises from the fact that, once a particular solution of (4) is available,
further linearly independent solutions are obtained in this case merely
by replacing x by x + 1, x + 2, etc. Finally numerical examples are
given, both for the general case and the special case of constant
coefficients.

The methods described are believed to be especially suited for
use with a desk calculator, but could easily be programmed for a
computer. However, the proposed methods are impractical in some
cases, because the elements of the sequences used increase or decrease
too rapidly.

2. THE CASE OF CONSTANT COEFFICIENTS. For this case standard
methods of a totally different character are available [1, 2] . Thus if
$r_i (i = 1, 2, \ldots , n)$ denote the roots of the auxiliary equation

$$(5) \qquad t^n - \sum_{i=1}^{n} a_i t^{n-i} = 0 ,$$

and if v_x $(x = 1, 2, \ldots, p)$ is a particular solution of (1), the general solution, in the case of simple roots, is

$$(6) \qquad u_x = v_x + \sum_{j=1}^{n} c_j r_j^x ,$$

where the c_j are arbitrary constants. In the case of a conjugate pair of complex roots, $r_j = \rho e^{i\theta}$ and $r_{j+1} = \rho e^{-i\theta}$, the terms $c_j r_j^x + c_{j+1} r_{j+1}^x$

can be replaced, if desired, by

$$\rho^x (c_j' \cos x\theta + c_{j+1}' \sin x\theta) .$$

If r_j is a multiple root of multiplicity k, then c_j (or c_j') is replaced by an arbitrary polynomial in x of degree $k - 1$.

Substitution of (6) in (2) and (3) and solution of the resulting system of equations for the undetermined coefficients c_j gives the desired result. However, if the auxiliary equation (5) is of high degree, and especially if it has many complex roots, the procedures just mentioned, as well as the computation of the roots themselves, may be complicated and time consuming.

For a solution not involving the roots of the auxiliary equation we first choose arbitrary starting values y_i ($i = 1, 2, \ldots, n$) and proceed to develop the rest of the y-sequence, up to and including y_p by successive applications of the equation

$$(7) \qquad y_x = \sum_{i=1}^{n} a_i y_{x-i} + g_x \qquad\qquad (x = n + 1, n + 2, \ldots, p).$$

As linear independence is not involved in this instance, it is permissible to take

$$y_1 = y_2 = \ldots = y_n = 0,$$

and this choice has computational advantages. When this is done, we have

$$y_{n+1} = g_{n+1}, \qquad y_{n+2} = a_1 g_{n+1} + g_{n+2}, \ldots .$$

In a similar manner, we take n starting values w_i ($i = 1, 2, 3, \ldots, n$) and develop a sequence satisfying the homogeneous equation

$$(8) \qquad w_x = \sum_{i=1}^{n} a_i w_{x-i} \qquad (x = n+1, n+2, \ldots, p+n-1).$$

In this case it is required that at least one of the starting values be different from zero, and the process is extended over a longer range, up to and including w_{p+n-1}. It can be assumed without loss of generality that $a_n \neq 0$. Care must be taken that the starting values do not satisfy a homogeneous linear difference equation with constant coefficients of order less than n whose auxiliary polynomial is an exact divisor of the left member of (5). This requirement is met if all the starting values but w_1 (or all but w_n) are taken as zero.

We now note that the n sequences

$$w_1, \qquad w_2, \qquad \ldots, \qquad w_p$$

$$w_2, \qquad w_3, \qquad \ldots, \qquad w_{p+1}$$

$$\ldots \ldots \ldots \ldots \ldots \ldots \ldots \ldots \ldots \ldots \ldots \ldots \ldots$$

$$\ldots \ldots \ldots \ldots \ldots \ldots \ldots \ldots \ldots \ldots \ldots \ldots \ldots$$

$$w_n, \qquad w_{n+1}, \qquad \ldots, \qquad w_{p+n-1}$$

are linearly independent, for any linear dependence among them would imply that w-sequence satisfies a difference equation of order less than n, and its auxiliary polynomial would necessarily be an exact divisor of the left member of (5). This condition was specifically avoided in the choice of starting values. As each sequence is a solution of (8), it follows that they constitute a fundamental set of solutions.

In consequence, the general solution of (7) can be written in the form

$$(9) \qquad u_x = y_x + \sum_{i=1}^{n} K_i w_{x+i-1} \qquad (x = 1, 2, \dots, p),$$

where the K_i are arbitrary constants. Substitution of (9) in (2) and (3) gives n simultaneous equations for obtaining the particular values of these constants that yield the desired solution. In fact we have

$$\sum_{j=1}^{n} d_{ij} K_j = f_i \qquad (i = 1, 2, \dots, n)$$

where

$$d_{ij} = \begin{cases} \sum_{k=1}^{n} b_{ik} w_{j+k-1} & (i = 1, 2, \dots, m) \\[2mm] & (j = 1, 2, \dots, n) \\[2mm] \sum_{k=1}^{n} b_{ik} w_{p-n+j+k-1} & (i = m+1, m+2, \dots, n) \end{cases}$$

$$f_i = \begin{cases} h_i - \sum_{k=1}^{n} b_{ik} y_k & (i = 1, 2, \ldots, m) \\[2em] h_i - \sum_{k=1}^{n} b_{ik} y_{p-n+k} & (i = m+1, m+2, \ldots, n). \end{cases}$$

These relations may be clearer when expressed in terms of matrices. Let D denote the matrix of coefficients d_{ij}, K the column-vector of coefficients K_i, and f the column-vector of quantities f_i; let B denote the matrix of coefficients b_{ij}, partitioned into the first m rows B_1 and the last $n - m$ rows B_2. Let $W^{(n)}$ and $W^{(p)}$ denote the persymmetric, alternant matrices $[3, pp.112, 122]$

$$W^{(n)} = \begin{bmatrix} w_1 & w_2 & \cdots & w_n \\ w_2 & w_3 & \cdots & w_{n+1} \\ \hdotsfor{4} \\ w_n & w_{n+1} & \cdots & w_{2n} \end{bmatrix}$$

and

$$W^{(p)} = \begin{bmatrix} w_{p-n+1} & w_{p-n+2} & \cdots & w_p \\ w_{p-n+2} & w_{p-n+3} & \cdots & w_{p+1} \\ \hdotsfor{4} \\ w_p & w_{p+1} & \cdots & w_{p+n-1} \end{bmatrix};$$

let h denote the column-vector of quantities h_i, and finally let $y^{(x)}$ denote the column-vector formed of n consecutive elements of the y-sequence, ending with y_x. Then

$$Dк = f,$$

where

$$D = \begin{bmatrix} B_1 W^{(n)} \\ \\ B_2 W^{(p)} \end{bmatrix}, \qquad f = h - \begin{bmatrix} B_1 y^{(n)} \\ \\ B_2 y^{(p)} \end{bmatrix}.$$

The process of successive application of (7) and (8) by which the y- and w-sequences were developed can also be expressed in terms of matrices. Let

$$Q = \begin{bmatrix} 0 & 1 & 0 & \cdots & 0 \\ 0 & 0 & 1 & \cdots & 0 \\ \cdots\cdots\cdots\cdots\cdots\cdots\cdots\cdots\cdots \\ \cdots\cdots\cdots\cdots\cdots\cdots\cdots\cdots\cdots \\ 0 & 0 & 0 & \cdots & 1 \\ a_n & a_{n-1} & a_{n-2} & \cdots & a_1 \end{bmatrix}$$

let $w^{(x)}$ denote the analogue of $y^{(x)}$ for the w-sequence, and finally let $g^{(x)}$ denote a column-vector of n elements having g_x as its final element preceded by $n-1$ zeros. Then*

---

*A similar discussion appears in $\begin{bmatrix}4\end{bmatrix}$, which generalizes methods described in $\begin{bmatrix}5\end{bmatrix}$ and $\begin{bmatrix}1\end{bmatrix}$.

$$w^{(x+1)} = Qw^{(x)} \qquad\qquad y^{(x+1)} = Qy^{(x)} + g^{(x+1)} \,,$$

or, more generally,

$$(10) \qquad w^{(x+\nu)} = Q^\nu w^{(x)} \qquad\qquad y^{(x+\nu)} = Q^\nu y^{(x)} + \sum_{i=1}^{\nu} Q^{\nu-i} g^{(x+i)}.$$

It will be noted that the characteristic equation of Q is identical with the auxiliary equation (5) ; in fact, Q is the transpose of the "companion matrix" [6, 7] of the auxiliary polynomial.

A word of caution is in order concerning this method. It will sometimes fail, for reasons most readily explained in terms of equation (6). When x becomes large, this expression is dominated by the term involving the root* of maximum absolute value. If the particular solution being sought should happen to have a zero coefficient associated with this root, the coefficients K_i in (9) would have to be obtained very accurately in order to give reasonably accurate values of u_x near the upper end of the sequence. Unless p is small, it may not be possible to carry enough significant figures in the calculations to determine these coefficients with the accuracy required.

3. <u>THE GENERAL CASE</u>. In the general case one cannot obtain additional solutions of the homogeneous difference equation by the expedient of replacing x by $x+1$, $x+2$, etc., and it is necessary to employ additional sets of starting values. One may, of course, use n such sets, which can then be regarded as a "starting matrix". The n sets of starting values must be linearly independent, or, in other words, the starting matrix must be nonsingular. If it is taken as the unit matrix, this is tantamount to expressing all subsequent terms of the sequence as linear functions of the first n terms by successive substitution in the difference equation, and finally substituting these functions in the end conditions in order to evaluate the first n terms.

---

*In the case of two or more roots of maximum absolute value this discussion can be suitably modified.

However, it is computationally more efficient to use the m equations (2) to eliminate m of the first n values. This has the desirable effect of reducing the number of sets of starting values required, and also the number of simultaneous equations to be solved in the final step, from n to $n - m$. We shall use the matrix notation of the preceding section, further partitioning the submatrix B_1 into the first $n - m$ columns, B_{11}, and the last m columns, B_{12}, and shall define the vector $u^{(x)}$ in analogy with $y^{(x)}$ and $w^{(x)}$. The vector $u^{(n)}$ will also be partitioned into the first $n - m$ elements $u_*^{(n)}$ and the last m elements $u_{**}^{(n)}$, and the vector h similarly partitioned into h_1 and h_2. Then

$$(11) \qquad B_{11} u_*^{(n)} + B_{12} u_{**}^{(n)} = h_1 .$$

As it can be assumed that the m equations (2) are independent, B is of rank m, and (11) can be solved for $u_{**}^{(n)}$ to give

$$(12) \qquad u_{**}^{(n)} = B_{12}^{-1} h_1 - B_{12}^{-1} B_{11} u_*^{(n)} .$$

The two terms of the right member of (12) will be utilized to construct, respectively, the starting vector $y^{(n)}$ for the y-sequence and the starting matrix $W^{(n)}$ for the w-sequence. In fact, we have

$$(13) \qquad u^{(n)} = y^{(n)} + W^{(n)} u_*^{(n)} ,$$

where

$$y^{(n)} = \begin{bmatrix} O \\ \\ B_{12}^{-1} h_1 \end{bmatrix}, \qquad\qquad W^{(n)} = \begin{bmatrix} I_{n-m} \\ \\ -B_{12}^{-1} B_{11} \end{bmatrix} .$$

It will be noted that $W^{(n)}$ is now an $n \times (n - m)$ rectangular matrix, rather than an $n \times n$ square matrix as in the preceding section.

Using the elements of $y^{(n)}$ and those of the individual columns of $W^{(n)}$ as separate sets of starting values, and successively applying to each the difference equation (1) in the former case and (4) in the latter, we shall ultimately arrive at the ending vector $y^{(p)}$ and the ending matrix $W^{(p)}$. At each step along the way, the relation

$$(14) \qquad u^{(x)} = y^{(x)} + W^{(x)} u_*^{(n)} \qquad (x = n, \, n + 1, \, \ldots, \, p)$$

must be satisfied. The end conditions (3) therefore take the form

$$(15) \qquad B_2 u^{(p)} \equiv B_2 y^{(p)} + B_2 W^{(p)} u_*^{(y)} = h_2 \quad .$$

If there is a unique solution (that is, if the coefficients a_{ix} and b_{ij} are such that the overall system of equations (1), (2) and (3) is nonsingular), the $(n-m) \times (n - m)$ matrix $B_2 W^{(p)}$ is nonsingular, and (15) can be solved to give

$$u_*^{(n)} = (B_2 W^{(p)})^{-1} (h_2 - B_2 y^{(p)}) \quad .$$

This equation provides the values $u_1, u_2, \ldots, u_{n-m}$, and if we denote by $w_{x1}, w_{x2}, \ldots, w_{x, \, n - m}$ the elements of the final row of $W^{(x)}$ (or the x th row of $W^{(n)}$ for $x \leq n$), (14) gives

$$(16) \qquad u_x = y_x + \sum_{i=1}^{n-m} u_i w_{xi} \qquad (x = 1, \, 2, \, \ldots, \, p) \quad .$$

At this point the question may arise in the mind of the reader whether it is possible, in the case of constant coefficients, to retain the expedient of obtaining additional solutions of the homogeneous equation by merely shifting the argument and also utilize the equations (2) to reduce the number of simultaneous equations to be solved in the final step. In other words, is it possible by appropriate choice of the starting vectors $y^{(n)}$ and $w^{(n)}$ to reduce the upper limit of the summation in (9) from n to $n - m$?

It will be shown that the answer is negative, except in unusual cases. Substitution of the modified form of (9) into (2) gives, in matrix notation,

$$B_1 u^{(n)} = B_1 y^{(n)} + B_1 W^{(n)} K = h_1 .$$

This must be an identity in the K_i, since these quantities cannot be evaluated until the final step. Therefore we must have

$$(17) \qquad B_1 y^{(n)} = h_1 ,$$

$$(18) \qquad B_1 W^{(n)} = O .$$

As it is assumed that the m equations (2) are independent, and therefore B_1 is of rank m, a vector $y^{(n)}$ can be found which satisfies (17). The requirement (18), however, is less easily met. As it is being assumed that the $W^{(n)}$ matrix is based on a single w-sequence, the jth column being $w^{(n+j-1)}$, the quantities w_1, w_2, ..., w_{2n-m-1} (which are the elements appearing in $W^{(n)}$) must satisfy not only the difference equation (8) but also m further homogeneous linear difference equations with constant coefficients whose auxiliary polynomials have as coefficients the elements of the individual rows of B (where reading from left to right gives coefficients of ascending powers of the variable). These w's must therefore satisfy the difference equation whose auxiliary polynomial is the greatest common

divisor of the $m + 1$ polynomials. Unless this greatest common divisor is of degree at least $n - m$ (which, in practice, would be unusual), there would be a linear relation among the columns of $W^{(n)}$, and it would not be a permissible starting matrix.

It should be pointed out, however, that when $m = n - 1$ the method described above for the general case is preferable even in the case of constant coefficients, because the starting matrix has only one column in any event, and for the method of the general case the final system of simultaneous equations reduces to one equation in one unknown. If $m = 1$, it is possible to gain the same advantage by reversing the order of indexing and working backwards. Even when $m = n - 2$ (or $m = 2$) the method of the general case may be preferred if p is not large.

In the general case the reversal of order mentioned in the preceding paragraph is clearly advantageous whenever $n - m > m$: that is, when

$$m < \frac{1}{2} n.$$

4. EXAMPLES.

Example 1. Solve the difference equation

(19) $$u_x = 2u_{x-1} - 2u_{x-2} + 2u_{x-3} - u_{x-4} + g_x$$

for $u_1, u_2, \ldots, u_{20}$, subject to the end conditions:

(20)
$$u_1 - 2u_2 = 1$$
$$u_1 + u_2 - 6u_3 = -2$$
$$3u_{18} - u_{19} - u_{20} = 645$$
$$u_{19} - u_{20} = -412,$$

where

$$g_x = x^2 - 20x + 120 - 4(-1)^x .$$

SOLUTION. Table 1 shows, in the first four columns, the values of g_x required, and the values of y_x and w_x developed (from the starting values indicated for $x = 1, 2, 3, 4$) by successive application, in the respective cases, of (19) and its homogeneous counterpart

$$u_x = 2u_{x-1} - 2u_{x-2} + 2u_{x-3} - u_{x-4} .$$

Equation (9) gives

$$u_x = y_x + \sum_{i=1}^{4} K_i w_{x+i-1} \qquad (x = 1, 2, \ldots 20) .$$

Substituting this expression (for the appropriate values of x and using the calculated values of y_x and w_{x+i-1}) in the conditions (20) gives

$$K_1 + 2K_4 = 1$$

$$K_1 + 6K_3 + 11K_4 = -2$$

$$8K_1 + 7K_2 + 5K_3 + 7K_4 = 191 .$$

$$K_2 + K_3 = 8.$$

TABLE 1

x	g_x	y_x	w_x	u_x
1		0	1	43
2		0	0	21
3		0	0	11
4		0	0	3
5	49	49	-1	32
6	32	130	-2	91
7	33	195	-2	146
8	20	248	-2	191
9	25	342	-3	265
10	16	464	-4	365
11	25	570	-4	461
12	20	668	-4	551
13	33	815	-5	678
14	32	1002	-6	843
15	49	1189	-6	1020
16	52	1388	-6	1211
17	73	1660	-7	1463
18	80	2000	-8	1781

TABLE 1 (Cont.)

x	g_x	y_x	w_x	u_x
19	105	2372	-8	2143
20	116	2792	-8	2555
21			-9	
22			-10	
23			-10	

Solution of these equations yields the values: $K_1 = 43$, $K_2 = -23$, $K_3 = 31$, $K_4 = -21$, and therefore,

$$u_x = y_x + 43w_x - 23w_{x+1} + 31w_{x+2} - 21w_{x+3} .$$

From this equation the values of u_x in the final column of Table 1 were calculated.

EXAMPLE 2.   Solve the difference equation

$$xu_x = (x + 1) u_{x-1} + (x - 1)u_{x-2} - xu_{x-3} + 24,$$

for $u_1, u_2, \ldots, u_8$, subject to the end conditions:

$$2u_1 + u_2 - u_3 = -4$$

$$u_1 - 2u_2 + u_3 = 10$$

$$9u_7 - 8u_8 = -124 .$$

SOLUTION. Upon solving the first two equations (21) to give u_2 and u_3 in terms of u_1, we have

$$u_1 = u_1 + 0$$

$$u_2 = 3u_1 - 6$$

$$u_3 = 5u_1 - 2 .$$

The trivial equation which appears first has been included in order to exhibit clearly the starting vectors for calculating y_x and w_{x1}. These are given, respectively, by the constant terms and the coefficients of u_1 in the right members of the above equations. The resulting values of y_x and w_{x1} appear in the second and third columns of Table 2.

Now (16) gives, in this case

$$u_x = y_x + u_1 w_{x1} \qquad (x = 1, 2, \ldots, 8) ,$$

and, in particular,

$$u_7 = 95/6 u_1 + 195/7$$

$$u_8 = (1835/96)u_1 + 4371/112.$$

Substitution of these expressions in the third equation (21) yields $u_1 = 6$, and we have

$$u_x = y_x + 6w_{x1},$$

from which the final column of Table 2 was calculated.

TABLE 2

x	y_x	w_x	u_x
1	0	1	6
2	-6	3	12
3	-2	5	28
4	-1	15/2	44
5	8	10	68
6	29/2	155/12	92
7	195/7	95/6	122 6/7
8	4371/112	1835/96	153 5/7

REFERENCES

1. L. M. Milne-Thomson, The Calculus of Finite Differences, Macmillan and Co., Ltd., London, 1933.

2. C. H. Richardson, An Introduction to the Calculus of Finite Differences, D. Van Nostrand Co., Inc., New York, 1954.

3. A. C. Aitken, Determinants and Matrices (8th ed.), Interscience Publishers, Inc., New York, 1954.

4. R. W. Wagner, "A note on linear difference equations," Amer. Math. Monthly, 65, 351-353, 1958.

5. B. Friedman, Principles and Techniques of Applied Mathematics, John Wiley and Sons, Inc., New York, 1956.

6. R. R. Stoll, Linear Algebra and Matrix Theory, McGraw-Hill Book Co., Inc., New York, 1952.

7. F. R. Gantmacher, The Theory of Matrices, Vol. 1, Chelsea Publishing Co., New York, 1959.

STEADY-STATE TEMPERATURES IN A SLAB CONTAINING

A PLANE INSULATING FILAMENT,

PART I: FORMULATION AND SOLUTION BY CONFORMAL MAPPING

J. E. Zweig, M.J. Pascual and S. D. Beck
Watervliet Arsenal, Watervliet, New York

__INTRODUCTION__ . When microflakes are imbedded in a heat conducting medium subjected to a temperature gradient, the heat flow will be disturbed compared to the flow in the homogeneous medium. The problem discussed in this note was suggested by this phenomenon, but the model described should not be construed as an accurate representation of an actual situation. Instead, the problem is considered for its mathematical interest and as a possible indication of the analytic difficulties that can by anticipated in examining similar models.

__FORMULATION OF THE MODEL__ .   Consider an infinite slab contained between the planes y = -1 and y = 1. A semi-infinite filament is imbedded parallel to the surfaces. We take the positive x direction in the plane of the filament and outwardly normal to the edge. The faces y = -1 and y = 1 maintained at uniform temperatures T = 1 and T = 0, respectively. The filament is a perfect insulator. The model is two dimensional. The region is shown in Figure 1.

Figure 1.

Original

Slab
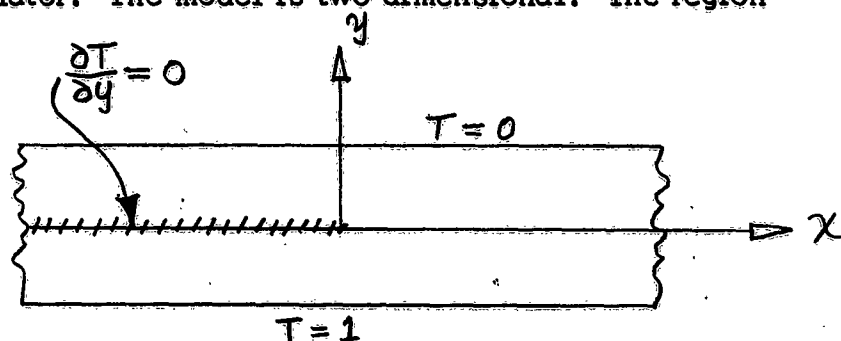
We seek the temperature field T = T (x, y) which satisfies Laplace's equation

$$(1) \qquad \frac{\partial^2 T}{\partial x^2} \quad + \quad \frac{\partial^2 T}{\partial y^2} \quad = \quad 0.$$

subject to the condition that T is finite and that

(2) $T(x, 1) = 0$, $T(x, -1) = 1$,

(3) $\dfrac{\partial T(x, 0)}{\partial y} = 0$,   for $x < 0$.

Two methods are used to investigate the problem: separation of variables and conformal mapping. The first of these methods leads to a series solution and the second to a solution in closed form. Numerical results from the two methods are in precise agreement, as expected.

SOLUTION BY SEPARATION OF VARIABLES[1].   It is convenient to divide the region into three subregions:

Region (1): $-\infty < x < 0$, $0 < y \leq 1$;

Region (2): $-\infty < x < 0$, $-1 \leq y < 0$;

Region (3): $0 < x < \infty$, $-1 \leq y \leq 1$.

A different expression for the temperature will be sought for each region, with the stipulation that these match at $x = 0$. Designate as T_i the temperature in the i th region. Let

(4) $T_i = X_i Y_i$.

Substitution into Eq. (1) leads to

(5) $\dfrac{X_i{}''}{X_i} = -\dfrac{Y_i{}''}{Y_i} = \left[k^{(i)}\right]^2$,

where $k^{(i)}$ is an eigenvalue for the i th region. This leads to a solution of the form

(6)
$$T_i = \left[A^{(i)} \exp(k^{(i)}x) + B^{(i)} \exp(-k^{(i)}x)\right]\left[C^{(i)} \sin(k^{(i)}y) + D^{(i)} \cos(k^{(i)}y)\right] .$$

(1) Churchill, R.V., "Fourier Series and Boundary Value Problems, "McGraw-Hill, N.Y. (1941)

Consider region (1), for which the boundary conditions become

(7) $\qquad Y_1'(0) = 0$, $\qquad\qquad\qquad Y_1(1) = 0$.

These, and the requirement that T be finite imply

(8) $T_1 = \displaystyle\sum_{n=1}^{\infty} K_n^{(1)} \exp\left[(2n-1)\pi x/2\right] \cos\left[(2n-1)\pi y/2\right]$ '

where

(9) $\qquad\qquad\qquad\qquad K_n^{(1)} = A_n^{(1)} D_n^{(1)}$.

The boundary conditions in region (2) can be made homogeneous by defining

(10) $\qquad\qquad\qquad\qquad \widetilde{T}_2 = T_2 - 1$,

subject to boundary conditions

(11) $\qquad \dfrac{\partial \widetilde{T}_2(x, 0)}{\partial y} = 0$, $\qquad\qquad \widetilde{T}_2(x, -1) = 0$.

The solution for $\widetilde{T}_2$ is the same as that for T_1, therefore

(12) $\qquad T_2 = 1 + \displaystyle\sum_{n=1}^{\infty} K_n^{(2)} \exp\left[\frac{(2n-1)\pi x}{2}\right] \cos\left[\frac{(2n-1)\pi y}{2}\right]$.

In region (3) an auxiliary function $\widetilde{T}_3$ is defined

(13) $\qquad\qquad\qquad\qquad \widetilde{T}_3 = T_3 - \left(\frac{1-y}{2}\right)$,

with boundary conditions

(14) $\qquad\qquad\qquad\qquad \widetilde{T}_3(x, 1) = \widetilde{T}_3(x, -1) = 0$.

$A^{(3)}$ must vanish for T to remain finite. Eq (14) is satisfied by $\sin(k)$ when k is an integral multiple of π, and by $\cos(k)$ when k is an odd multiple of $\pi/2$. Terms of both types are required, giving

$$(15) \qquad T_3 = \frac{1-y}{2} + \sum_{n=1}^{\infty} \left\{ K_n^{(3)} \exp\left[-\frac{(2n-1)\pi x}{2}\right] \cos\frac{(2n-1)\pi y}{2} \right.$$

$$\left. + L_n \exp(-n\pi x) \sin(n\pi y) \right\} ,$$

and where

$$(16) \qquad K_n^{(3)} = B_n^{(3)} D_n^{(3)} , \qquad L_n = B_n^{(3)} C_n^{(3)} .$$

It now remains to satisfy the matching conditions at $x = 0$. Consider first the segment $y > 0$, for which

$$(17) \qquad T_1(0, y) = T_3(0, y) , \qquad \frac{\partial T_1(0, y)}{\partial x} = \frac{\partial T_3(0, y)}{\partial x} .$$

Equations (8) and (15) imply

$$(18) \qquad \sum_{n=1}^{\infty} K_n^{(1)} \cos\frac{(2n-1)\pi y}{2}$$

$$= \frac{1-y}{2} + \sum_{n=1}^{\infty} \left\{ K_n^{(3)} \cos\left[\frac{(2n-1)\pi y}{2}\right] + L_n \sin(n\pi y) \right\} ,$$

$$(19) \qquad \sum_{n=1}^{\infty} \left(\frac{2n-1}{2}\right) K_n^{(1)} \cdot \cos\left[\frac{(2n-1)\pi y}{2}\right]$$

$$= - \sum_{n=1}^{\infty} \left\{ \left(\frac{2n-1}{2}\right) K_n^{(3)} \cdot \cos\left[\frac{(2n-1)\pi y}{2}\right] + n L_n \sin(n\pi y) \right\} .$$

Relations similar to Equations (18) for $y < 0$ give us, with equations (12) and (15)

$$(20) \qquad 1 + \sum_{n=1}^{\infty} K_n^{(2)} \cos\left[\frac{(2n-1)\pi y}{2}\right]$$

$$= \frac{1-y}{2} + \sum_{n=1}^{\infty} \left\{ K_n^{(3)} \cos\left[\frac{(2n-1)\pi y}{2}\right] + L_n \sin(n\pi y)\right\} \; .$$

$$(21) \qquad \sum_{n=1}^{\infty} \left(\frac{2n-1}{2}\right) K_n^{(2)} \cdot \cos\left[\frac{(2n-1)\pi y}{2}\right]$$

$$= \div \sum_{n=1}^{\infty} \left\{ \left(\frac{2n-1}{2}\right) K_n^{(3)} \cdot \cos\left[\frac{(2n-1)\pi y}{2}\right] + n L_n \sin(n\pi y)\right\} \; .$$

In equations (20) and (21) replace y by $-y$. The modified equations are then valid for $y > 0$ since in their original form they held for $y < 0$. Add Equation (18) and the modified Equation (20). This gives

$$(22) \qquad \sum_{n=1}^{\infty} \left(K_n^{(1)} + K_n^{(2)} - 2 K_n^{(3)}\right) \cos\left[\frac{(2n-1)\pi y}{2}\right] = 0 \; .$$

Add equation (19) and the modified Equation (21). Then

$$(23) \qquad \sum_{n=1}^{\infty} \frac{2n-1}{2} \left(K_n^{(1)} + K_n^{(2)} + 2 K_n^{(3)}\right) \cos\left[\frac{(2n-1)\pi y}{2}\right] = 0 \; .$$

Since Equations (22) and (23) must hold for arbitrary values of y

$$(24) \qquad K_n^{(1)} + K_n^{(2)} - 2 K_n^{(3)} = 0,$$
$$K_n^{(1)} + K_n^{(2)} + 2 K_n^{(3)} = 0.$$

Therefore

$$(25) \qquad\qquad K_n^{(3)} = 0$$

$$(26) \qquad\qquad K_n^{(1)} = - K_n^{(2)} = K_n \qquad .$$

The determination of the temperatures is dependent now on two series expressions with the unknown amplitudes K_n and L_n. Equations (18) and (19) remain for their determination. These reduce to

$$(27) \qquad \sum_{n=1}^{\infty} K_n \cos\left[\frac{(2n-1)\pi y}{2}\right] = \frac{1-y}{2} + \sum_{n=1}^{\infty} L_n \sin(n\pi y) \, ,$$

$$(28) \qquad \sum_{n=1}^{\infty} \frac{2n-1}{2} K_n \cos\left[\frac{(2n-1)\pi y}{2}\right] = - \sum_{n=1}^{\infty} n L_n \sin(n\pi y) \quad .$$

Multiply Equations (27) and (28) by $\sin(m\pi y)$ and integrate from zero to one. This gives

$$(29) \qquad \sum_{n=1}^{\infty} \frac{4m\, K_n}{\pi\left[(2m)^2 - (2n-1)^2\right]} = \frac{1}{2\pi m} + \frac{L_m}{2} \quad ,$$

$$(30) \qquad \sum_{n=1}^{\infty} \frac{4m\,(2n-1)\, K_n}{\pi\left[(2m)^2 - (2n-1)^2\right]} = - m L_m \quad .$$

Elimination of L_m from Equations (29) and (30) gives

$$(31) \qquad \sum_{n=1}^{\infty} \frac{K_n}{2m - 2n + 1} = \frac{1}{4m} \quad .$$

Multiply Equations (27) and (28) by $\cos\left[(2m - 1)\,\pi y/2\right]$ and integrate from zero to one, getting

(32)
$$\frac{K_m}{2} = \frac{2}{(2m - 1)^2\,\pi^2} + \sum_{n=1}^{\infty} \frac{4n\,L_n}{\pi\left[(2n)^2 - (2m - 1)^2\right]} \quad,$$

(33)
$$\frac{(2m - 1)\,K_m}{4} = -\sum_{n=1}^{\infty} \frac{4\,n^2\,L_n}{\pi\left[(2n)^2 - (2m - 1)^2\right]} \quad.$$

Elimination of K_m from equations (32) and (33) gives

(34)
$$\sum_{n=1}^{\infty} \frac{2n\,L_n}{2n - 2m + 1} = -\left[\frac{1}{(2m - 1)\,\pi}\right] \quad.$$

Equations (31) and (34) each represents an infinite system of equations from which L_n and K_n can be found. These are related, moreover, by equations (30) and (33). In the companion paper it will be shown that K_n and L_n can be expressed in closed form as

(35)
$$K_n = \frac{(2n - 1)!}{\pi\left[2^{n-1}\,(2n - 1)\,(n - 1)!\right]^2} \quad,$$

(36)
$$L_n = \frac{(2n - 1)!}{\pi\left[2^n\,n!\right]^2} \quad.$$

SOLUTION BY CONFORMAL MAPPING [2].   The region under consideration can be transformed by routine conformal mapping procedures to yield results in closed form. The symmetry about the mid-plane $(y = 0)$ enables us to consider only the lower half of the slab. The mapping is performed in two steps. We first map from the z plane to the w plane by

(37)
$$w = \frac{1}{2} + \exp\left[\pi(z + i)\right] \quad,$$

(2) Churchill, R. V., "Introduction to Complex Variables and Applications," McGraw-Hill, N.Y. (1948)

$$(38) \qquad u = \frac{1}{2} - \exp(\pi x)\cos(\pi y),$$

$$v = -\exp(\pi x)\sin(\pi y).$$

This transformation is illustrated in Figure 2.
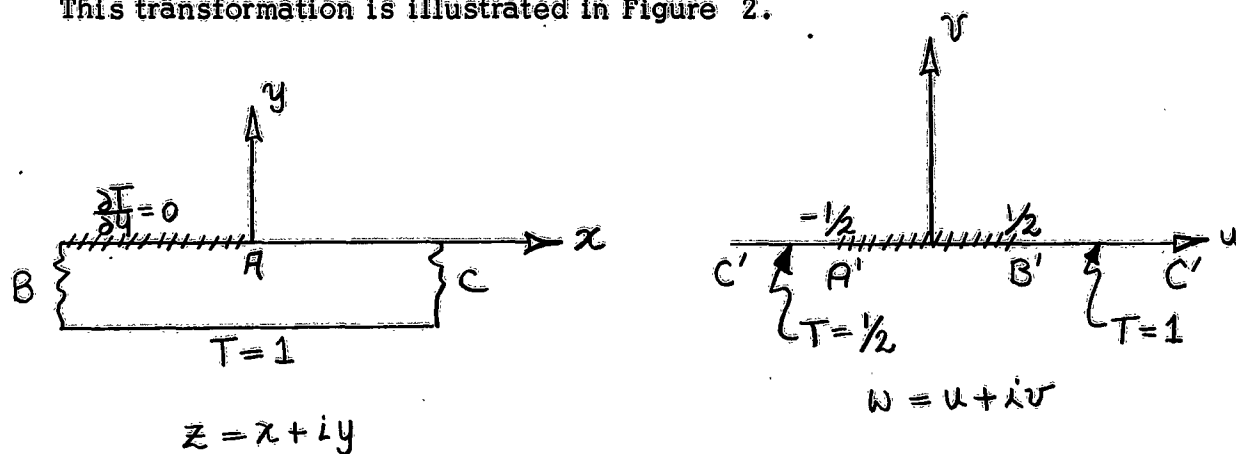
Figure 2.

Transformation $\omega = \frac{1}{2} + \exp\{\pi(z+i)\}$

It becomes immediately apparent from the symmetry in the w plane that the line u = 0 and therefore its image in the z plane

$$\exp(\pi x)\cos(\pi y) = \frac{1}{2}$$

is an isotherm at temperature T = 3/4

A second tramsformation

$$(39) \qquad w = \frac{1}{2}\cosh\zeta$$

or

$$(39a) \qquad u = \frac{1}{2}\cosh\xi\cos\eta$$

$$v = \frac{1}{2}\sinh\xi\sin\eta ,$$

maps the w plane into the ζ plane, as shown in Figure 3.

Figure 3.

Transformation

$w = \frac{1}{2} \cosh \zeta$

$\zeta = \xi + i\eta$
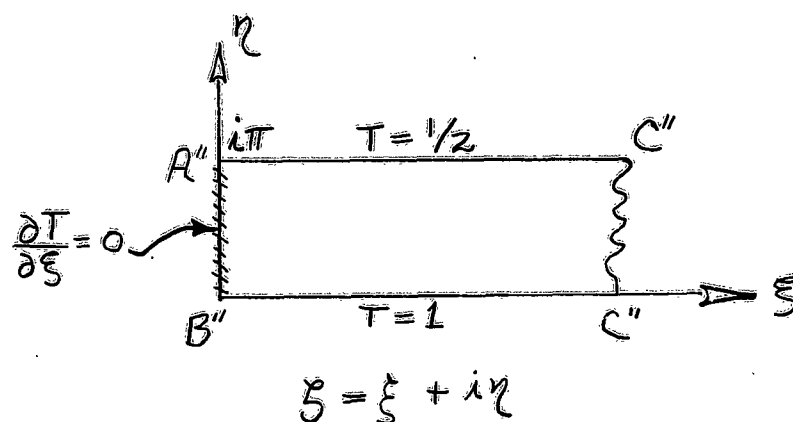
In order to assure that the mapping is one to one we are restricted to the interval

$$0 \leqslant \eta < 2\pi.$$

The original infinite strip shown in Figure 2 has thus been mapped into the semi-infinite strip of Figure 3.

The solution to Laplace's equation for this region is

(40) $$T = 1 - \frac{\eta}{2\pi}$$

Elimination of w from Equations (37) and (39) gives

(41) $$\frac{1}{2} + \exp\left[\pi(z + i)\right] = \frac{1}{2} \cosh \zeta$$

or

(41a) $$\frac{1}{2} - \exp(\pi x) \cos(\pi y) = \frac{1}{2} \cosh \xi \cos \eta,$$

$$- \exp(\pi x) \sin(\pi y) = \frac{1}{2} \sinh \xi \sin \eta .$$

We note the following correspondence between regions of the ζ and z planes.

(42)

$$0 \leqslant \eta \leqslant \frac{\pi}{2} \quad \longleftrightarrow \quad -\infty < \exp(\pi x) \cos(\pi y) \leqslant \frac{1}{2},$$

$$\frac{\pi}{2} \leqslant \eta \leqslant \pi \quad \longleftrightarrow \quad \frac{1}{2} \leqslant \exp(\pi x) \cos(\pi y) < \infty.$$

If we eliminate ξ from Equation (39a) we obtain

$$(43) \qquad \cos^2 \eta = \frac{1}{2} \left[1 + 4u^2 + 4v^2 \pm R \right],$$

where

$$(44) \quad R = \sqrt{(4u^2 + 4v^2 + 1)^2 - 16u^2} = \sqrt{[(2u-1)^2 + 4v^2][(2u+1)^2 + 4v^2]}.$$

Consideration of temperatures on the boundaries indicates that the minus sign must be taken in Equation (43).

It is convenient to write

$$(45) \qquad \tan^2 \eta = \frac{1-P}{1+P},$$

where

$$(46) \qquad P = 4u^2 + 4v^2 - R.$$

Then

$$(47) \quad \eta = \begin{cases} \arctan \sqrt{\dfrac{1-P}{1+P}} & \text{, for} \quad \exp(\pi x)\cos(\pi y) \leq \dfrac{1}{2} \ , \\[3ex] \pi - \arctan \sqrt{\dfrac{1-P}{1+P}} & \text{, for} \quad \exp(\pi x)\cos(\pi y) \geq \dfrac{1}{2} \ , \end{cases}$$

where the arctangent is taken in the interval $(0, \pi/2)$.

As an incidental result, equation (40) also gives the temperature field for the w plane, as indicated in Figure 2.

NUMERICAL RESULTS. The temperature in the slab is given by equation (40) where η, P, u and v are obtained in terms of x and y, by making use of equations (47), (46), (44) and (37a). Therefore, for any prescribed point in the lower half of the slab ($y \leq 0$), the temperature can be obtained by a direct calculation. In the upper half of the slab temperature values are found immediately from

$$T(x, -y) = 1 - T(x, y).$$

For many purposes it may be desireable to examine the isotherms, that is, to determine the curves along which the temperature is constant. In order to do this it is more convenient to express the coordinates of the points along the contours in terms of ξ and η. The curves $\eta =$ constant are the isotherms while those on which $\xi =$ constant are their orthogonal trajectories, the flow lines.

If we solve equations (41a) for x and y we find

$$(49) \qquad x = \frac{1}{\pi} \log \left[\frac{\cosh \xi - \cos \eta}{2} \right] ,$$

$$(50) \qquad \tan(\pi y) = \frac{\sinh \xi \, \sin \eta}{\cosh \xi \, \cos \eta - 1} = S.$$

If we take the usual principal value of the inverse tangent (that is, between $-\pi/2$ and $\pi/2$ we may write

(51) $\qquad y = \begin{cases} \dfrac{1}{\pi}\arctan S\ , & \text{for} \qquad S < 0\ , \\[2em] \dfrac{1}{\pi}\arctan S - 1\ , & \text{for} \qquad S < 0\ \cdot\ \cdot \end{cases}$

When $S = 0$, $y = -1$ or 0, make the first choice for $\eta = 0$, the second for either or $\eta = \pi$ or $\xi = 0$.

Figure 4 shows a few isotherms and flow lines in the lower half of the slab. Those in the upper half are simply reflections about the x axis.

Figure 4
Temperature Field in an Infinite Slab with a Semi-Infinite Insulator
——— Isotherms ---- Flow Lines
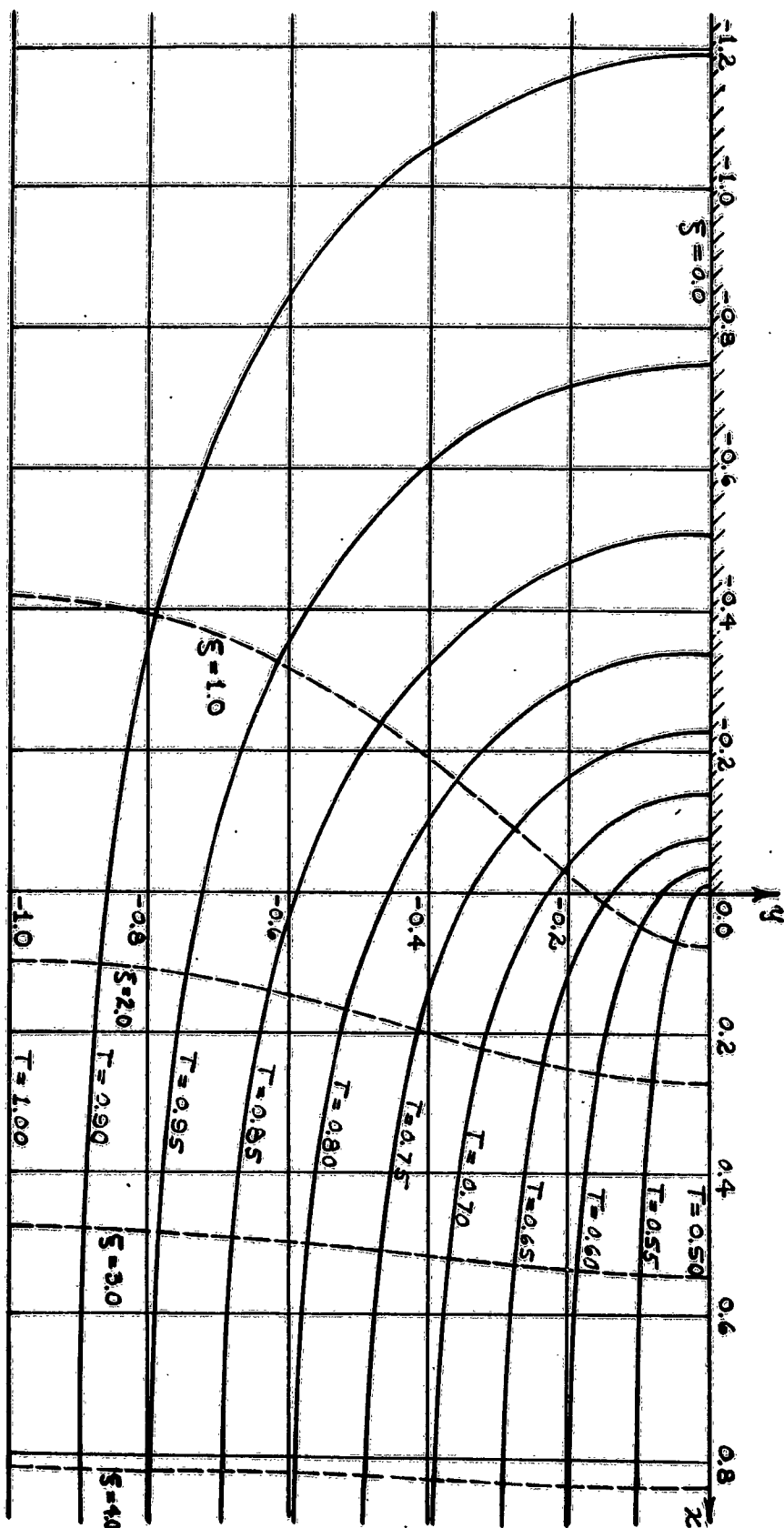
PART II

SOLUTION TO THE INFINITE SYSTEMS

BY NUMERICAL INDUCTION*

M. J. Pascual and J. E. Zweig
Watervliet Arsenal, Watervliet, New York

The infinite systems which had to be solved to obtain the coefficients of the Fourier expansion for the Temperature function were:

$$(1) \quad \sum_{n=1}^{\infty} \frac{K_n}{2m - 2n + 1} = \frac{1}{4m}, \quad m = 1, 2, \ldots,$$

and

$$(2) \quad \sum_{n=1}^{\infty} \frac{2n \ L_n}{2n - 2m + 1} = - \frac{1}{(2m - 1)\pi}, \quad m = 1, 2, \ldots,$$

The unknowns K_n and L_n are also related through the equation:

$$(3) \quad L_m = \sum_{n=1}^{\infty} \frac{-4 (2n - 1) \ K_n}{\pi(2m - 2n + 1) \ (2m + 2n - 1)}$$

In matrix form (1) appears as follows:

$$(4) \quad A \begin{pmatrix} K_1 \\ K_2 \\ \cdot \\ \cdot \\ \cdot \\ K_n \\ \cdot \\ \cdot \end{pmatrix} = \frac{1}{4} \begin{pmatrix} 1 \\ \frac{1}{2} \\ \cdot \\ \cdot \\ \cdot \\ \frac{1}{n} \\ \cdot \\ \cdot \end{pmatrix}$$

We first considered the finite case of (4) namely:

---

*This is Part II of the paper entitled "Steady - State Temperatures in a Slab Containing a Plane Insulating Filament".

$$(5) \qquad A_n \cdot \begin{pmatrix} K_1 \\ K_2 \\ \vdots \\ K_n \end{pmatrix} = \frac{1}{4} \cdot \begin{pmatrix} 1 \\ \frac{1}{2} \\ \vdots \\ \frac{1}{n} \end{pmatrix}$$

in which

$$(6) \qquad A_n = \left\| \left[\frac{1}{2i - 2j + 1} \right] \right\| \qquad \begin{array}{l} i = 1, 2, \ldots, n, \\[4pt] j = 1, 2, \ldots, n. \end{array}$$

We examined A_2^{-1}, A_3^{-1}, A_4^{-1}, A_5^{-1} and the first entry of A_6^{-1} in an effort to make a conjecture as to what A_n^{-1} might be. The clues appeared as follows:

$$A_2^{-1} = \frac{1}{2^2} \begin{bmatrix} 3 & 3 \\ -1 & 3 \end{bmatrix}, \qquad A_3^{-1} = \begin{bmatrix} 45 & 15 & 45 \\ -9 & 9 & 15 \\ -3 & -9 & 45 \end{bmatrix} \cdot \frac{1}{2^6},$$

$$A_4^{-1} = \frac{1}{2^8} \cdot \begin{bmatrix} 175 & 105 & 105 & 175 \\ -75 & 135 & 75 & 105 \\ -15 & -18 & 135 & 105 \\ -5 & -15 & -75 & 175 \end{bmatrix}$$

$$A_5^{-1} = \frac{1}{2^{14}} \begin{bmatrix} 3 \cdot 5^2 \cdot 7^2 & 2^2 \cdot 3^2 \cdot 5^2 \cdot 7 & 2 \cdot 3 \cdot 5^4 \cdot 7 & 2^2 \cdot 3 \cdot 5^2 \cdot 7 & 3 \cdot 5^2 \cdot 7^2 \\ -2^2 \cdot 5^2 \cdot 7^2 & 2^4 \cdot 3 \cdot 5^2 \cdot 7 & 2^3 \cdot 3 \cdot 5^2 \cdot 7 & 2^4 \cdot 5^2 \cdot 7^2 & 2^2 \cdot 3^2 \cdot 5^2 \cdot 7 \\ -2 \cdot 3 \cdot 5^2 \cdot 7 & -2^3 \cdot 3^3 \cdot 5^2 & 2^2 \cdot 3 \cdot 4^2 \cdot 5^2 & 2^3 \cdot 3 \cdot 5^2 \cdot 7 & 2 \cdot 3 \cdot 5^4 \cdot 7 \\ -2^2 \cdot 3 \cdot 5 \cdot 7 & -2^4 \cdot 3 \cdot 5^2 & -2^3 \cdot 3^3 \cdot 5^2 & 2^4 \cdot 3 \cdot 5^2 \cdot 7 & 2^2 \cdot 3^2 \cdot 5^2 \cdot 7 \\ -5^2 \cdot 7 & -2^2 \cdot 3 \cdot 5 \cdot 7 & -2 \cdot 3 \cdot 5^2 \cdot 7 & -2^2 \cdot 5^2 \cdot 7^2 & 3^2 \cdot 5^2 \cdot 7^2 \end{bmatrix}$$

$$A_6^{-1} = \frac{1}{2^{16}} \begin{bmatrix} 7^2 \cdot 9^2 \cdot 11 & \cdots \\ \vdots & \ddots & \ddots \\ \vdots & & \ddots \end{bmatrix}$$

We guessed the first entry of A_n^{-1} as being

$$(7) \qquad a_{11}^1(n) = \frac{\left[(2n-2)!\right]^2 (2n-1)}{2^{4(n-1)} \left[(n-1)!\right]^4} \qquad ,$$

after which we proceeded to factor out the first entry of each inverse found in (6), and then guessed at the first row of A_n^{-1} obtaining for $j \geq 2$

$$(8) \qquad a_{1j}^1(n) = a_{11}^1(n) \; \frac{(2j-3)!}{2^{j-2}(j-1)!\,(j-2)!} \; \frac{(n-1)(n-2)\cdots(n-j+1)}{(2n-3)(2n-5)\cdots(2n-2j+1)} \; .$$

Next came the first column of A_n^{-1}.

$$(9) \qquad a_{i1}^1(n) = a_{11}^1(n) \; \frac{(2i-4)!}{2^{i-2}(i-1)!\,(i-2)!} \; \frac{(n-1)(n-2)\cdots(n-i+1)}{(2n-1)(2n-2)\cdots(2n-2i+3)}$$

where $i \geq 2$.

Finally by multiplying $a_{1j}^1(n)$ by $a_{i1}^1(n)$ and supplying the proper factor we conjectured that

$$(10) \qquad a_{ij}^1(n) = \frac{(2i-2)!\,(2j-1)!\,(2n-2i+1)!\,(2n-2j)!}{2^{4(n-1)}(2j-2i+1)\left[(i-1)!\,(j-1)!\,(n-i)!\,(n-j)!\right]^2} \; .$$

Letting $n \longrightarrow \infty$ we find that

$$(11) \qquad \lim_{n \to \infty} a_{ij}^1(n) = \frac{(2i-2)!\,(2j-1)!}{\pi \, 2^{2(i+j)-5}(2j-2i+1)\left[(i-1)!\,(j-1)!\right]^2} \; .$$

Multiplying (4) on the left by $A_\infty^{-1} = \left\| \left[\lim_{\eta \to \infty} a_{ij}^1 (n) \right] \right\|$ we obtained (under the assumption that $A_\infty^{-1} = A^{-1}$) that

$$(12) \qquad K_n = \frac{(2n-2)!}{\pi \, 2^{2n-3} \left[(n-1)! \right]^2} \sum_{j=1}^{\infty} \frac{(2j-1)!}{2^{2j} (2j-2n+1) j \left[(j-1)! \right]^2}$$

The series representing K_n was found to converge very slowly, consequently we used asymptotic expansions to evaluate K_1, K_2, K_3, K_4, with the following results:

$$K_1 = .31830989 \approx \frac{1}{\pi} \quad ,$$

$$(13) \qquad K_2 = .53051661 \approx \frac{1}{6\pi} \quad ,$$

$$K_3 = .23873248 \approx \frac{3}{40\pi}$$

$$K_4 = .14210267 \approx \frac{5}{112\pi} \quad .$$

From these we conjectured that

$$(14) \qquad K_n = \frac{(2n-1)!}{\pi \left[2^{n-1} (2n-1)(n-1)! \right]^2}$$

A similar evaluation of L_1, L_2, L_3, and L_4 led us to the conjecture

$$(15) \qquad L_n = - \frac{(2n-1)!}{2^{2n} \pi (n!)^2}$$

To establish (14), we used the expansion for $\csc^{-1}x$ which gave us:

$$(16) \qquad \sum_{n=1}^{\infty} \frac{(2n-1)! \quad x^{2m-2n}}{\left[2^{n-1}(2n-1)(n-1)!\right]^2} = x^{2m-1}\csc^{-1}x ,$$

where $|x| \geqslant 1$. Integrating (16) we found for m a positive integer that

$$(17) \qquad \sum_{n=1}^{\infty} \frac{(2n-1)! \quad x^{2m-2n+1}}{\left[2^{n-1}(2n-1)(n-1)!\right]^2 (2m-2n+1)} = \frac{x^{2m}}{2m}\csc^{-1}x$$

$$+ \frac{\sqrt{x^2-1}}{2m} \left\{ \frac{x^{2m-2}}{2m-1} + \frac{(2m-2)\,x^{2m-4}}{(2m-1)(2m-3)} + \cdots \right.$$

$$\left. + \frac{(2m-2)(2m-4)\ldots 2}{(2m-1)(2m-3)\ldots 3.1} \right\} + C.$$

To determine C we substituted 1 and -1 for x in (17) and added obtaining

$$(18) \qquad\qquad 2C = 0 \qquad \text{or} \qquad C = 0 .$$

Equation (14) was established by setting $x = 1$, giving

$$(19) \qquad \sum_{n=1}^{\infty} \frac{(2n-1)!}{\left[2^{n-1}(2n-1)(n-1)!\right]^2 (2m-2n+1)} = \frac{\pi}{4m} ,$$

which is equation (1) with K_n given by (14).

To establish conjecture (15) we must show that (2) is satisfied by L_n as given in (15). From the expansion for $(1-x^2)^{-1/2}$ we obtain the following:

$$(20) \qquad \sum_{n=1}^{\infty} \frac{(2n)!\; x^{2n-2m}}{2^{2n}\,(n!)^2} = \frac{1}{x^{2m}} \left\{ \frac{1}{\sqrt{1-x^2}} - 1 \right\},$$

where $0 < |x| < 1$. Integrating (20) we get

$$(21) \qquad \sum_{n=1}^{\infty} \frac{(2n)!\; x^{2n-2m+1}}{2^{2n}\,(n!)^2\,(2n-2m+1)} = \frac{1}{(2m-1)x^{2m-1}} - \phi(x)\sqrt{1-x^2} + C,$$

in which $\phi(x)$ is an odd function of x. Setting $x = 1/2$ and $x = -1/2$ in (21) then adding gives us

$$(22) \qquad\qquad 2C = 0, \qquad C = 0.$$

By Abel's limit theorem if the left side of (21) is convergent for $x = 1$, then its value there must be the limit of the right side as $x \longrightarrow 1-$. To show that

$$(23) \qquad \sum_{n=1}^{\infty} \frac{(2n)!}{2^{2n}\,(n!)^2\,(2n-2m+1)}$$

is convergent we have for $0 < x < 1$ that

$$(24) \qquad \sum_{n=1}^{k} \frac{(2n)!\; x^{2n-2m+1}}{2^{2n}\,(n!)^2\,(2n-2m+1)} < \frac{1}{(2m-1)\,x^{2m-1}} - \sqrt{1-x^2}\,\phi(x) ,$$

and taking limits as $x \longrightarrow 1-$

$$(25) \qquad \sum_{n=1}^{k} \frac{(2n)!}{2^{2n} (n!)^2 (2n-2m+1)} \leqslant \frac{1}{2m-1} \quad .$$

Hence the partial sums of series (23) are bounded and increasing (since its' terms are all positive), and therfore (23) is convergent. Taking the limit as $x \rightarrow 1-$ of the right side of (21) we find by Abel's theorem that

$$(26) \qquad \sum_{n=1}^{\infty} \frac{(2n)!}{2^{2n} (n!)^2 (2n-2m+1)} = \frac{1}{2m-1} \quad ,$$

which is (2) with L_n as in (15).

Finally we establish as true the conjecture $A_{\infty}^{-1} = A^{-1}$ which is to say that $A_{\infty}^{-1} A = I$ where I is the infinite identity matrix. Explicitly this states that

$$(27) \qquad \sum_{j=1}^{\infty} \frac{(2i-2)! \, (2j-1)!}{\pi \cdot 2^{2(i+j)-5} \left[(2j-2i+1) (i-1)! \, (j-1)! \right]^2} = 1$$

for every positive integer i, and that

$$(28) \qquad \sum_{j=1}^{\infty} \frac{(2i-2)! \, (2j-1)!}{\pi \, 2^{2(i+j)-5} (2j-2i+1)(2j-2k+1) \left[(i-1)! \, (j-1)! \right]^2} = 0$$

for all positive integers i, k with $i \neq k$.

Now (27) can be written in the form

$$(29) \qquad \sum_{j=1}^{\infty} \frac{(2j-1)!}{2^{2j-2} \left[(2j-2i+1)(j-1)! \right]^2} \quad = \quad \frac{\pi}{2} \cdot \left(\frac{\left[(i-1)! \right]^2 2^{2i-2}}{(2i-2)!} \right),$$

and the case $i = 1$ is easily verified from (16) by substituting 1 for x. To establish (29) for any positive integer i we start with

$$(30) \qquad \sum_{j=1}^{\infty} \frac{(2j-1)! \, y^{2j-1}}{\left[2^{j-1}(j-1)! \right]^2 (2j-1)^2} \quad = \quad \sin^{-1} y, \qquad |y| \le 1.$$

Differentiating (30) gives

$$(31) \qquad \sum_{j=1}^{\infty} \frac{(2j-1)! \, y^{2j-2}}{\left[2^{j-1}(j-1)! \right]^2 (2j-1)} \quad = \quad \frac{1}{\sqrt{1-y^2}}, \qquad |y| < 1,$$

multiplying this equation through by y and differentiating again gives

$$(32) \qquad \sum_{j=1}^{\infty} \frac{(2j-1)! \, y^{2j-2}}{\left[2^{j-1}(j-1)! \right]^2} \quad = \quad \frac{y^2}{(1-y^2)^{3/2}} \quad + \quad \frac{1}{(1-y^2)^{1/2}};$$

multiplying through by y^{2-2i} and integrating

(33) $\displaystyle\sum_{j=1}^{\infty} \frac{(2j-1)! \; y^{2j-2i+1}}{\left[2^{j-1}(j-1)!\right]^2 (2j-2i+1)} = \frac{y^{3-2i}}{\sqrt{1-y^2}} - \frac{(2i-2)\sqrt{1-y^2}}{(2i-3)\; y^{2i-3}} \left\{ 1 + \right.$

$\displaystyle \frac{2i-4}{2i-5} \; y^2 + \cdots + \frac{(2i-4)(2i-6)\cdots 2}{(2i-5)(2i-7)\cdots 1} \; y^{2i-4} \left.\right\} + C_1 ;$

multiplying through by $\dfrac{1}{y}$ and integrating

(34) $\displaystyle\sum_{j=1}^{\infty} \frac{(2j-1)! \; y^{2j-2i+1}}{\left[2^{j-1}(j-1)!\right]^2 (2j-2i+1)^2} = \sqrt{1-y^2} \; \psi(y) + (1-y^2)^{3/2} \phi(y)$

$\displaystyle + \frac{\left[(i-1)!\right]^2 2^{2i-2}}{(2i-2)!} \; \sin^{-1} y + C_1 \ln |y| + C_2 \quad ,$

in which $\psi(y)$ and $\phi(y)$ are odd functions of y. All equations from (31) on hold for $|y| < 1$. Substituting $1/2$, $-1/2$, $1/3$, $-1/3$ successively into (34) for y and adding we obtain

(35) $\qquad 2C_1 \ln\dfrac{1}{2} + C_2 = 0 \quad$ and $\quad 2C_1 \ln\dfrac{1}{3} + C_2 = 0,$

from which we conclude that $C_1 = C_2 = 0$.

Letting $y \longrightarrow 1-$ in (34) and applying Abel's theorem we get

(36) $\displaystyle\sum_{j=1}^{\infty} \frac{(2j-1)!}{\left[2^{j-1}(j-1)! \; (2j-2i+1)\right]^2} = \frac{\pi}{2} \cdot \frac{\left[2^{i-1}(i-1)!\right]^2}{(2i-2)!} \quad ,$

which is the same as (29).

To establish (28) the steps are the same up to (33) which we now multiply through by $y^{2i-2k-1}$ obtaining (since $C_1 = 0$) upon integrating

$$(37) \qquad \sum_{j=1}^{\infty} \frac{(2j-1)! \; y^{2j-2k+1}}{\left[2^{j-1}(j-1)!\right]^2 (2j-2i+1)(2j-2k+1)} = \sqrt{1-y^2} \; \Psi(y)$$

$$+ (1-y^2)^{3/2} \; \phi(y) + C ,$$

$$|y| < 1.$$

where Ψ and ϕ are odd functions of y so that $C = 0$. Letting $y \longrightarrow 1-$ we find that

$$(38) \qquad \sum_{j=1}^{\infty} \frac{(2j-1)!}{\left[2^{j-1}(j-1)!\right]^2 (2j-2i+1)(2j-2k+1)} = 0,$$

which is equivalent to (28).

The conjecture (10) regarding the inverse of the finite matrix A_n is equivalent to

$$(39) \qquad \sum_{j=1}^{n} \frac{(2j-1)!(2n-2j)!}{\left[(2j-2i+1)(j-1)!(n-j)!\right]^2} = \frac{\left[2^{2(n-1)}(n-i)!(i-1)!\right]^2}{(2i-2)! \; (2n-2i+1)!} ,$$

for all positive integers i and n with $1 \leqslant i \leqslant n$, and

$$(40) \qquad \sum_{j=1}^{n} \frac{(2j-1)! \; (2n-2j)!}{(2j-2i+1)(2j-2k+1) \cdot \left[(j-1)!(n-j)!\right]^2} = 0,$$

for all positive integers i, k, n with $1 \leqslant i, k \leqslant n$ and $i \neq k$. (39) corresponds to the fact that the main diagonal elements of the product of A_n by it's inverse must be ones, and (40) corresponds to the fact that the off diagonal elements must be zeros.

IMPROVED TARGET MODEL FOR LETHAL AREAS PRODUCED

BY CYLINDRICAL AND SPHERICAL ROUNDS

Sherman L. Gerhard

Engineering Sciences Laboratory, Feltman Research Laboratories
Picatinny Arsenal, Dover, New Jersey

SUMMARY. A more realistic target model has been described which takes into account the fact that part of a target may not be exposed to fragments from rounds ejecting fragments in a limited angular range.

The speeds and directions of fragments ejected by cylindrical rounds have been derived; the equation for the density distribution of these fragments at any field point has been obtained. Flow charts and computer programs to compute A_L have been compiled for both cylinders and spheres. Curves plotted for fragment densities vs. height at four ranges for cylinders and spheres having equal numbers of fragments and side-spray angles show that for a sphere the density is practically constant whereas for a cylinder the density rises toward the edge of the side-spray, and is especially high for the 3-caliber cylinder.

Lethal areas for these same charges are greater for the .5-caliber cylinder than for the corresponding sphere, but are less for the 3-caliber cylinder than for the corresponding sphere.

FRACTIONAL EXPOSURE OF EXTENDED TARGETS

Heretofore it has been assumed that the presented area of a target, A_p, is entirely exposed to the beam of fragments from a burst. This assumption is adequate for full-spray rounds and for side-spray rounds at a great distance, but for low burst heights and narrow spray angles the results are unreasonable.

The improved target model is assumed to be a vertical plane area enclosed by the body outline of a human target, like the cardboards used in target practice. These targets may stand in random orientations everywhere in the field.

LIST OF SYMBOLS

H	= burst height
T	= target height
HU	= upper fragment beam
HL	= lower fragment beam
TU	= upper limit of exposed part of target
TL	= lower limit of exposed part of target
f	= fraction of target exposed
$\bar{n}$	= fragment density at the target
N	= number of fragments in round
θ_1	= angle to lower edge of side-spray
θ_2	= angle to upper edge of side-spray
R	= horizontal range
ρ	= slant range
V_o	= initial fragment velocity
V_c	= cut-off velocity
m	= fragment weight, in grains
Ap	= average target presented area
EH	= expected number of hits
EK	= expected number of lethal hits
CK	= form factor
CD_{02}	= drag coefficient
W	= total weight of all fragments, in pounds

Vulnerability. The vulnerabilities of different parts of the human body are obviously not alike. Relative numerical values for these quantities have been derived by BRL, (Reference 1) for six different parts of the body, and have been incorporated by Picatinny Arsenal into a new computer program described in Reference 2.

Exposed Area as a Fraction of A_p. For practical reasons the A_p figures compiled by ORO and BRL will continue to be used as the basis for calculating E_H. The target is assumed vertical, as shown in Figure 1, and subtends the angle between TU and TB as seen from the burst point, whereas the rays of fragments may be limited to a side spray between HU and HL. The points TU, TL and TB are always on the target, whereas HU and HL are elevations at any range, independent of the target height and position. In this illustration only the upper part of the target would be exposed to fragments. The exposed part is AB, and the fractional part of the whole target exposed is f = AB/AC, if the target is the same width for its entire height. If the width is not constant the fraction exposed can still be calculated if the width is known as a function of height.

The next step in the derivation is to show how the A_p cover function data are used. The slant range vector ρ is defined as the bisector of the angle between TU and TL drawn from the burst point. At the intersection P of ρ and the target a plane C'D' is erected perpendicular to ρ, as shown in the figure. The area A'C' enclosed between TU and TB represents the presented area A_p as given by the cover functions, i.e., an area normal to the radius vector from the source. In this plane the ratio of exposed to total target area is A'B'/A'C', which is for all practical purposes assumed equal to f.

The fragments striking the exposed part of the target AB are the same ones that pass through A'B' and therefore the number striking the target is

$$E_H = n \, f \cdot A_p,$$

where n is the density at P and

$$f = AB/AC \cong A'B'/A'C'.$$
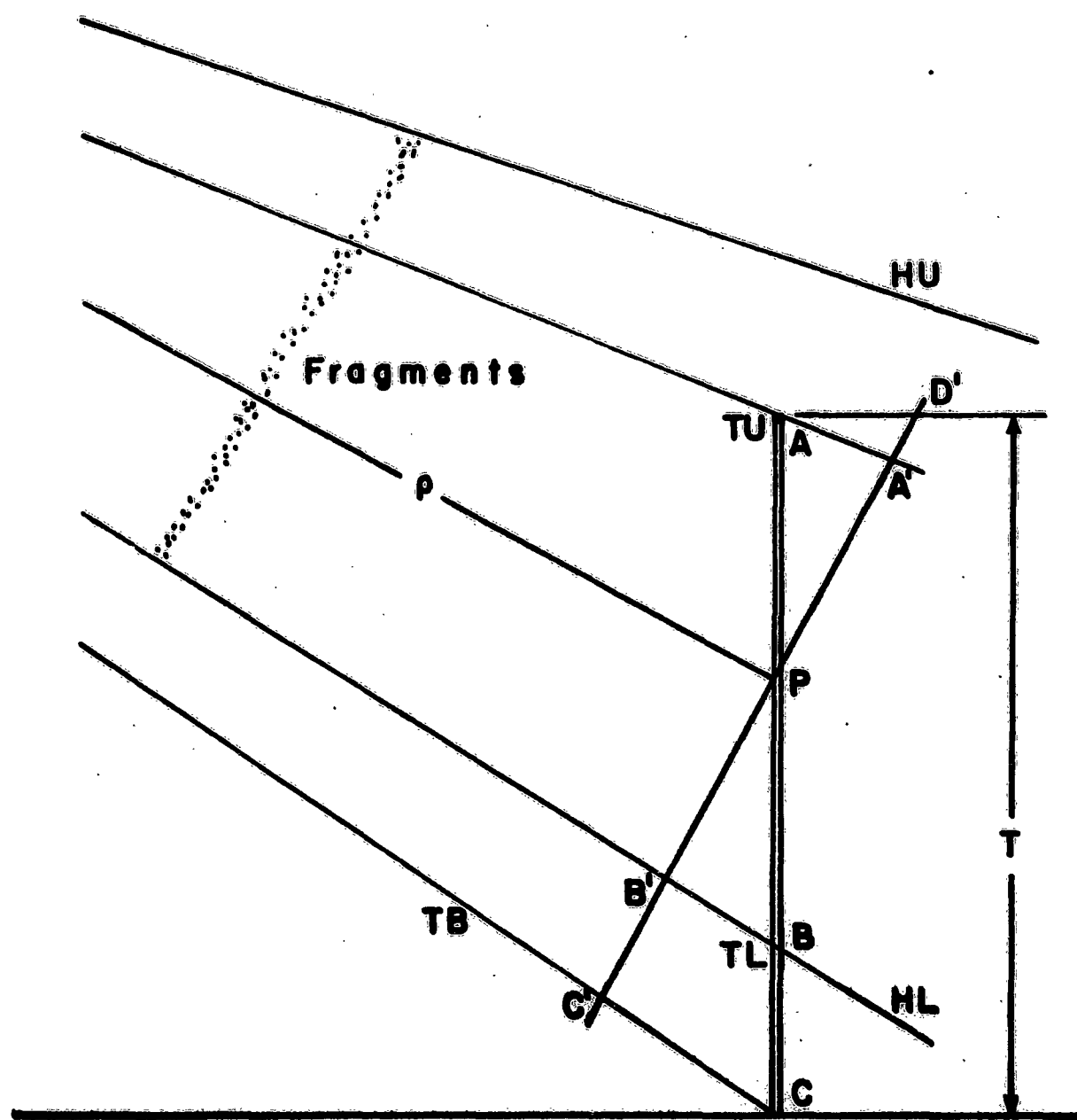
Figure 1. Partially Exposed Target

It is also assumed that the slant range ρ is the same for all points on A'B'.

The calculation of f may be pursued further at this point, if we assume that we know the equations for the lines HU and HL. The values for TU and TL are then given in general by the relations:

If
(1)

	HU	$\leq$	0	TU	=	0
	HL	$\leq$	0	TL	=	0 .

If
(2)

	T	$\leq$	HL	f	=	0
	T	$>$	HL	TL	=	HL
	T	$\leq$	HU	TU	=	T
	T	$>$	HU	TU	=	HU,

where HU and HL are evaluated at whatever range the target happens to stand. In the computer programs $f = (TU - TL)/T$.

CYLINDRICAL ROUNDS

A round of this type consists of a cylinder of high explosive encased in a hollow metal cylinder or liner. The fragmentation of the liner may be controlled or random. If random fragmentation occurs the mass distribution will be governed by some probability function, such as Mott's law; this kind of performance is not included in the present study. Instead, we assume controlled fragmentation, where all the fragments are of the same mass and are distributed uniformly throughout the liner. The ends of the round are assumed plane, and end effects are neglected. The fuze may be placed anywhere along the axis of the round, although certain places may be preferred for convenience in fabrication. Its position is taken as +j if above the c. g. , and negative if below, as shown in Figure 2. It is important to note that its position determines the location of minimum fragment density in the field, as will be seen later.

The performance of fragmenting rounds, including spherical as well as cylindrical ones, is described by two well-established formulae. The speed of fragments ejected is approximated by Gurney's formula

(3)
$$V_o = 8800 \, (M/C + k)^{-1/2}$$
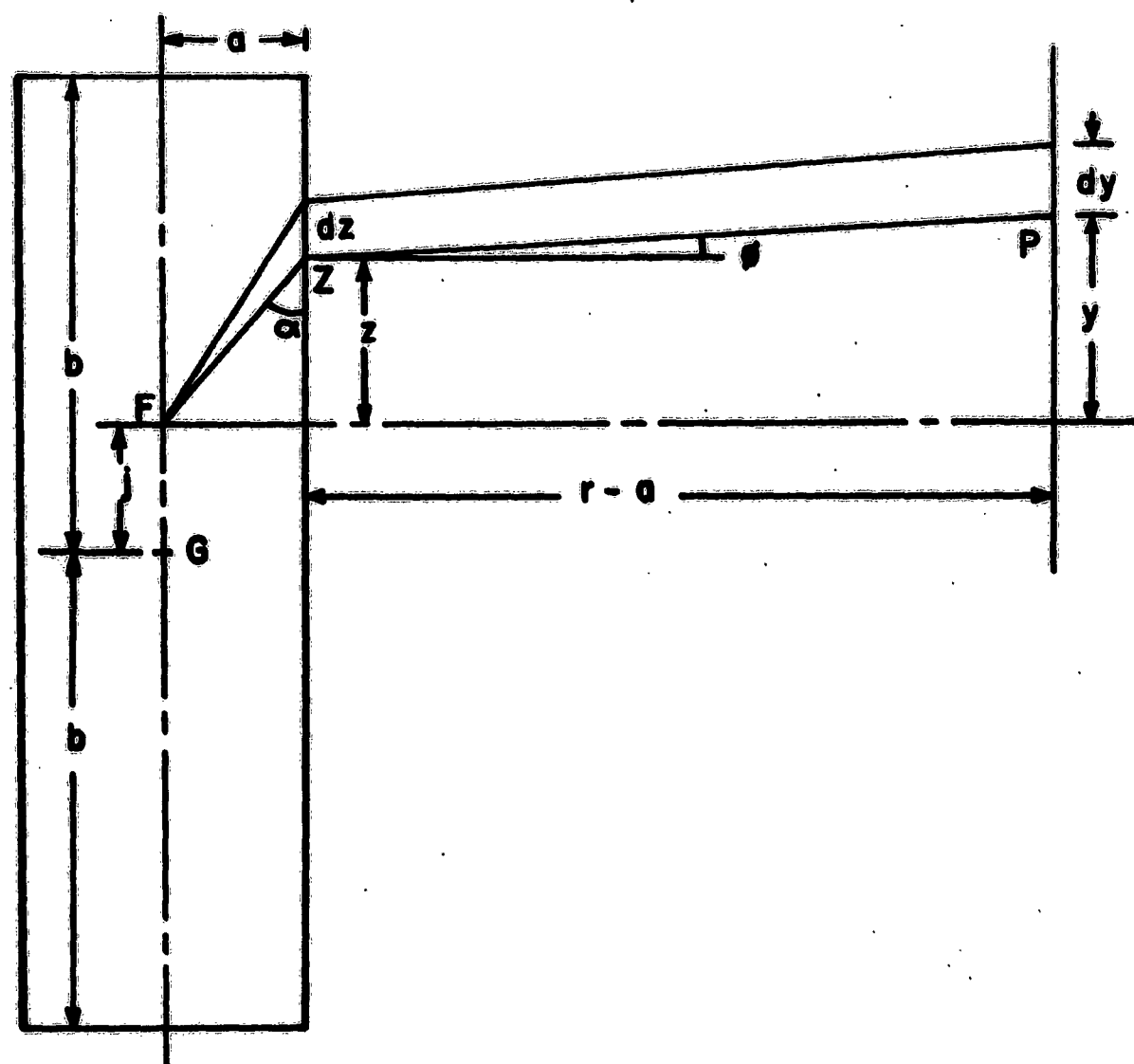
Figure 2. Cylindrical Round

where V_O is in ft/sec and the parameter 8800 is appropriate when Comp. B is the explosive. C/M is the charge-to-mass ratio, and k is 0.5 for cylinders and 0.6 for spheres. This formula checks with experimental results for C/M between 0.5 and 5.6 and limits V_O to values less than 10,000 ft/sec.

The direction in which fragments are ejected is given by Taylor's formula:

$$(4) \qquad\qquad\qquad \sin\phi = (V_O/2d)\cos\alpha$$

where V_O is the initial speed as given by (3) and d is the rate of detonation of the explosive. The definitions of the angles are shown in Figure 2. From the fuze at F the detonation wave expands spherically, intersecting the liner at z, from whence the fragment is ejected in a direction making the (small) angle ϕ with the normal to the surface. (For spherical rounds centrally initiated all fragments leave radially and there is no need to consider Taylor's formula.) Experimental values for d are about 25,000 ft/sec so that $V_O/2d$ is always less than 0.2, thus limiting ϕ to 9° or 10°, even at an infinitely great distance from the fuze, where $\alpha = 0°$. As a result of this directional characteristic, a cylindrical round ejects fragments in a side-spray with an angular divergence of no more than 18° or 20°.

Fragment Distribution in the Field. The choice of a coordinate system for this calculation is dictated by the fairly obvious fact that the rays of fragments are symmetrical about the point of initiation F, which is taken as the origin. The transverse plane through F, perpendicular to the axis, is the reference for measurements parallel to the axis at any field point whose coordinates are (r, y). The equations of motion for a missile give the location of G, the center of gravity, and the orientation of the axis. Since the fuze is usually not at G, this fact must be taken into account in solving numerical problems; it will not affect the calculations based on F as origin.

The fragment distribution at any field point depends upon the distribution in the shell wall. To show clearly the distribution at a field point we split the distribution on the surface of the shell into two linear distributions. Let the circumferential density be n_c and the lengthwise or axial be n_x fragments per foot. The circumferential density at a distance r is

equal to $n'_c = n_c(a/r)$, since the fragments are ejected uniformly in all directions in the reference plane through F.

The axial density at the target requires some detailed calculations, but we can say that n'_x at (r, y) is equal to n_x times some function of r and y, thus $n'_x = n_x f(r, y)$.

To derive $f(r, y)$ we consider the paths of fragments, as shown in Figure 2. A fragment arriving at P came from a corresponding point Z on the shell wall, a distance z from the reference plane. And all the fragments arriving within dy came from a corresponding infinitesimal segment dz on the shell wall. From the figure it is fairly evident that

$$(5) \qquad\qquad\qquad y = z + \phi (r - a)$$

where the approximation $\tan \phi = \phi$ is accurate to within 0.2%/o for $\phi < 10^\circ$. The next step is to find the relation between dy and dz. In (5) we substitute $\phi = D \cos\alpha$, where $D = V_0/2d$ from Taylor's formula, and express $\cos\alpha$ in terms of a and z, giving

$$y = z + (r-a) Dz/(a^2 + z^2)^{1/2}$$

and

$$dy/dz = 1 + (r-a) Da^2/(a^2 + z^2)^{3/2}.$$

Since the fragments in the differential segment dy came from the differential segment dz in which density is n_x, we have the equality

$$n_x dz = n'_x dy \text{ or } n_x' = n_x dz/dy$$

thus

$$n'_x = n_x/(1 + D(r/a - 1) \sin^3\alpha)$$

where we have used the relation $a/(a^2 + z^2)^{1/2} = \sin \alpha$.

At this stage we can combine the results for n'_c and n'_x, obtaining

$$(6) \qquad\qquad n = n_1(a/r)^2/(a/r + D(1-a/r) \sin^3\alpha)$$

where $n_1 = n_c n_x$ = number of fragments per unit area on the shell.

This result is correct but it is inconvenient because it contains the angle   and not the y coordinate of the field point, which is the desired independent variable. To derive the desired result we go back to (5) and express y as a function of α :

(7) $y = a \cot \alpha + D(r-a)\cos \alpha$.

Previous analysis of this problem has shown that a new variable $x = \sin \alpha$ is a preferable choice. No matter what variable is chosen (z or α) on the right side, a quartic equation ensues, which has to be solved for the chosen variable as a function of y, to be inserted into the distribution function (6). Making the indicated substitution, equation (7) yields the equation

(8) $x^4 + x^3 P + x^2 \left[(P/2)^2 (1 + (y/a)^2) - 1 \right] - xP - (P/2)^2 = 0$,

where $P = 2/(D(r/a-1))$ and is always positive for $r \geq a$.

The roots x_i of this equation are the numbers to be inserted in (6) for $\sin^3 \alpha$ to get the fragment distribution as a function of y and r. Examination of the coefficients in (8) provides clues to the solution of the equation. As y appears only as y^2 the signs of the roots are unaffected by the sign of y, thus satisfying the obvious symmetry of the fragment distribution. Descartes' rule of signs predicts that there can be only one positive real root. The coefficient of x^2 may be either plus or minus, but in either case there is still only one change of sign. The geometry in Figure 2 shows that the angle α ranges from $0°$ to $180°$, and its sine is always plus. On the basis of these considerations it is fairly safe to conclude that the single positive root of (8) is the one to be used as the value of $\sin \alpha$, regardless of the sign of y.

The shape of the distribution function (6) will be described to provide a more complete understanding of the performance of cylindrical rounds. In general the value of the function must be known at each point of the

target, especially when the different vulnerabilities of separate parts of the target are taken into account. However, for the special application treated here this information is not required, as will be explained later.

Curves for $n(r, y)$ are shown in Figures 3 and 4 for an infinite cylinder with 10,000 fragments per sq. ft., which is approximately the density for 64 1/8" cubes per sq. in. The value 0.164 is used for the parameter $V_o/2d$. The density at the target decreases as r increased (Fig. 3), but it increases as y increases (Fig. 4).

For finite cylinders the surface terminates at the vertical lines shown in Figure 4 for three different cylinders. One cylinder has a caliber $(b/a) = 3$ and is initiated at the center, shown in the figure by the number 3. The other cylinders both have calibers = 1. One of these is initiated at the center, shown by 1 in the figure. For central initiation the surface is symmetrical about the origin; only the left edge is labeled in the figure. The third cylinder is initiated at end, shown by 1e; for this position of the fuze one edge of the surface is always at the center, as shown in the figure. Shifting the fuze toward one end of the cylinder shortens the surface at this end, and lengthens slightly the other end.

The maximum densities represented by the high plateaus in Figure 4 are attained only by very long cylinders, about 30 calibers.

LETHAL AREA CALCULATIONS FOR CYLINDRICAL ROUNDS

The first steps are the evaluation of parameters dependent only on the round. The slant range ρ is sufficiently well approximated by r itself because $\rho = r \sec \phi \cong 1$ for vertical incidence of the charge, which is the case considered here.

Two other parameters are the angles ϕ_U and ϕ_L which limit the fragment beam at the upper and lower ends of the cylinder. These angles, as shown in Figures 2 and 5, are given by

(9)
$$\phi_U = D (b-j) / (a^2 + (b-j)^2)^{1/2}$$

$$\phi_L = D(b+j) / (a^2 + (b+j)^2)^{1/2}$$
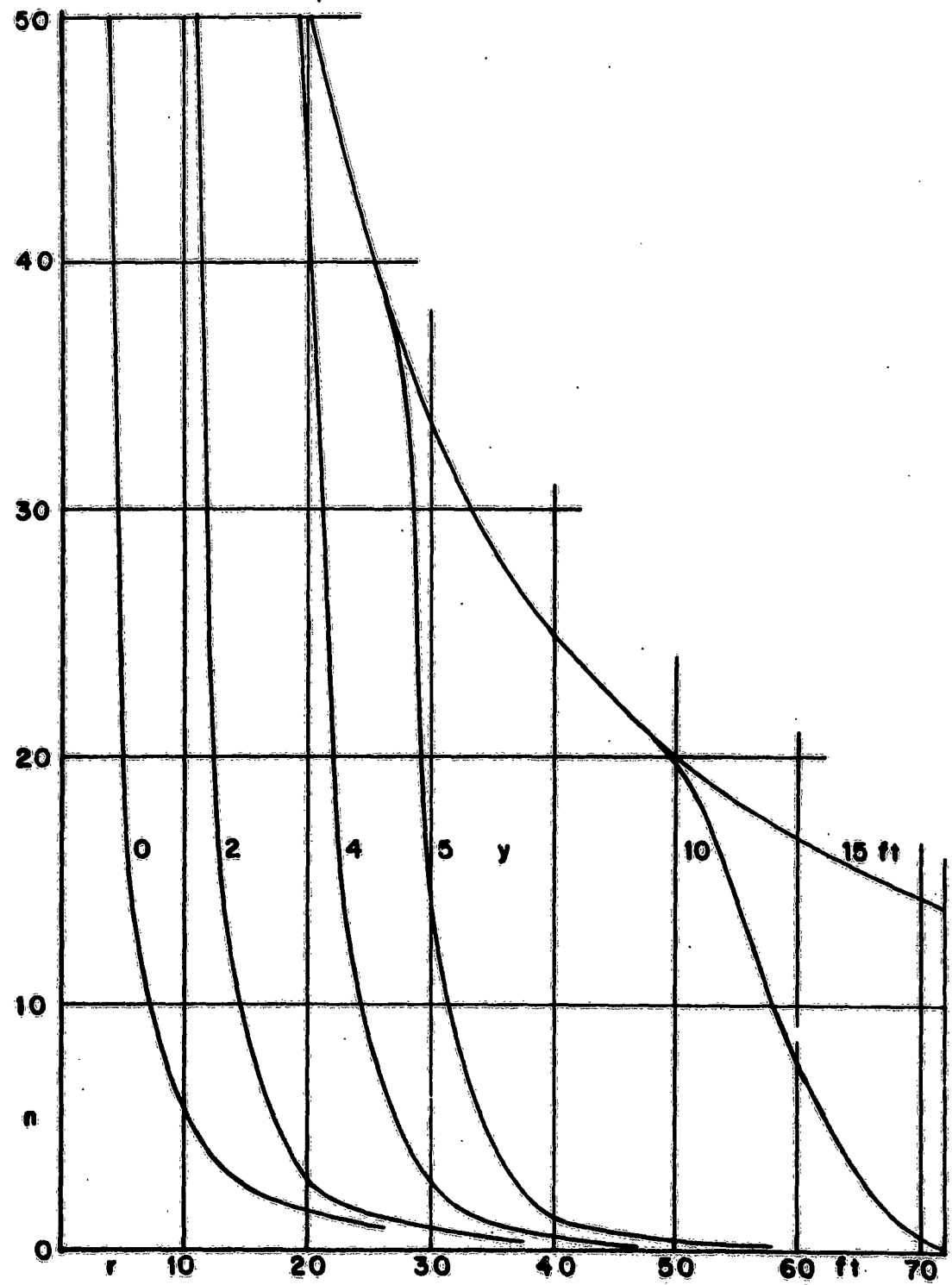
Figure 3. Fragment Density vs. Range
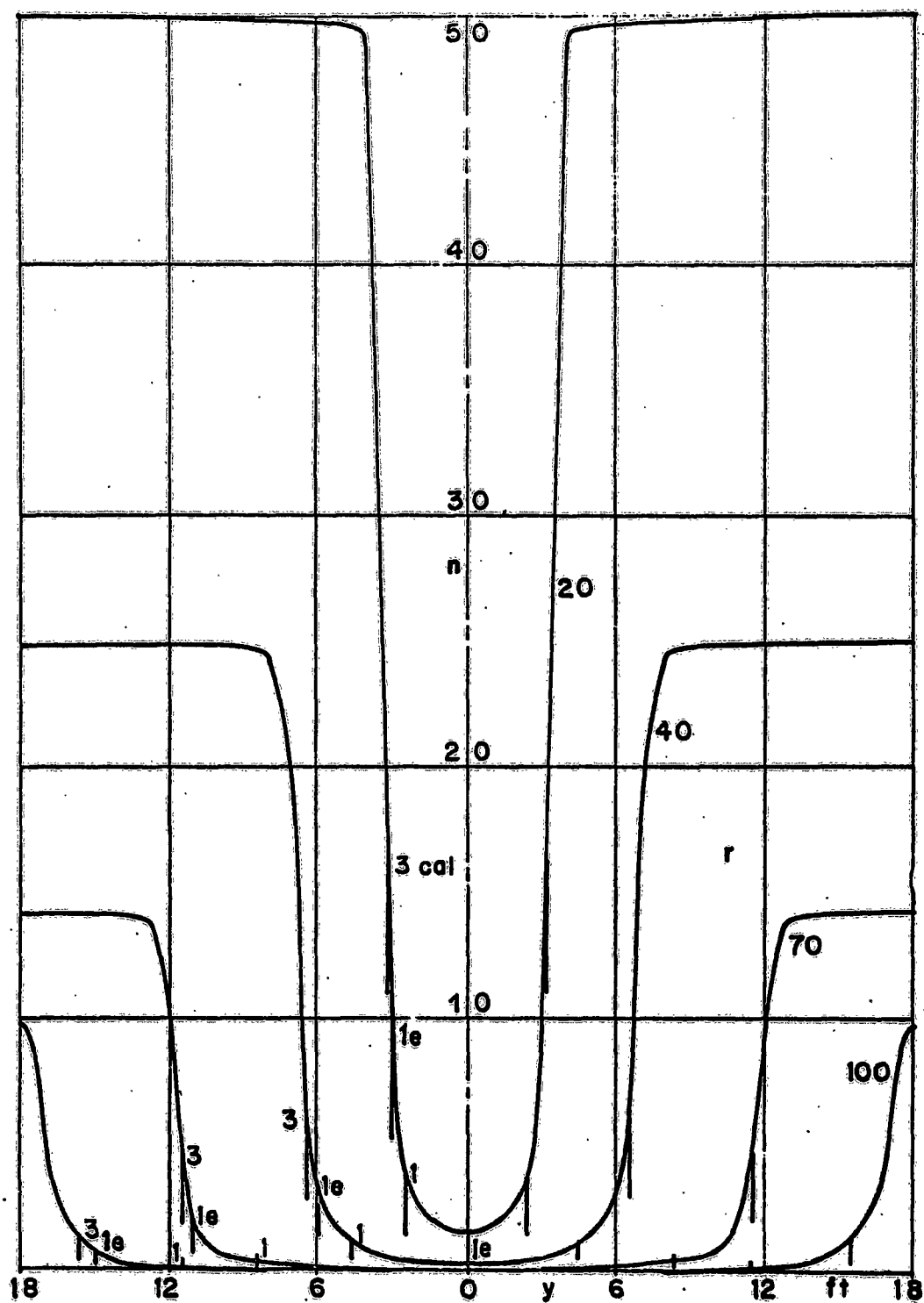
Figure 4. Fragment Density vs. Axial Extent
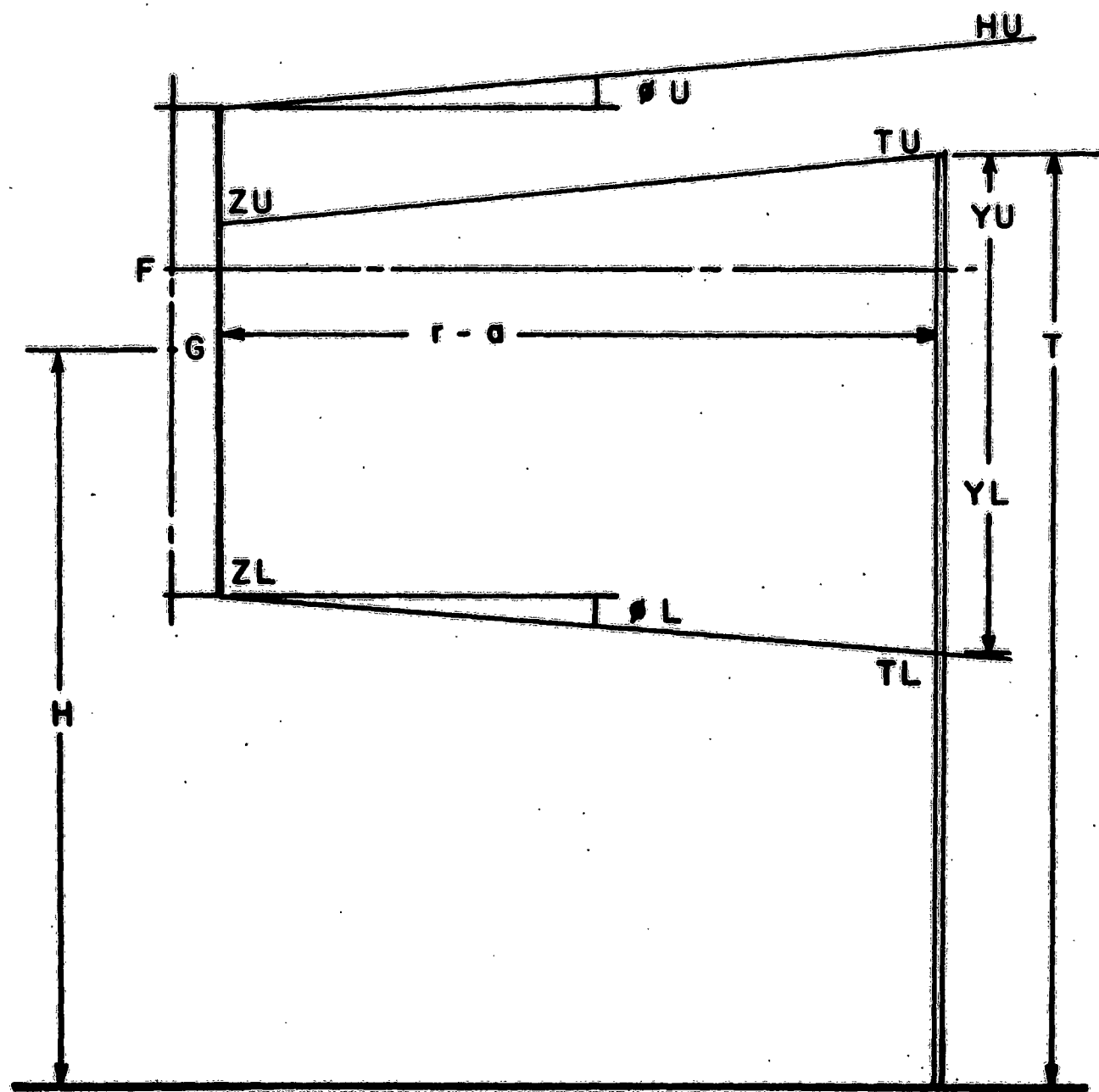
Figure 5. Extended Target and Cylindrical Round

Another parameter is the interval of r over which lethality may occur. There are two possible values for the upper limit. For given values of all other parameters r will have a maximum value beyond which $P_K = 0$.

$$(10) \qquad R_2 = (m^{1/3}/1.5q)\ln(mV_o^{3/2}/B)$$

where B is a lethality parameter. If a cut-off velocity V_c is specified, below which P_K is arbitrarily set equal to zero, another maximum value of r is obtained:

$$(11) \qquad R_2 = (m^{1/3}/q)\ln(V_o/V_c)$$

where q is the product of three aerodynamic factors in the velocity decay formula

$$(12) \qquad V = V_o \exp(-q\, r\, m^{-1/3})$$

The smaller of the two values (10) or (11) is taken as the upper limit.

The lower limit must be taken as at least twice the radius $\underline{a}$, because smaller values would produce irrelevant roots for the quartic equation (8).

$$(13) \qquad R_1 = 2a$$

The other one occurs when the bottom of the round is above the top of the target

$$(14) \qquad R_1 = (H-b-T)\,/\,\phi_{L}.$$

and the target is entirely unexposed at shorter ranges. The larger of
the two values (13) or (14) is taken as the lower limit.

The range of r is $R_2 - R_1$. Anticipating the calculation of A_L in the
last part of the computation, this interval $R_2 - R_1$ is divided into a suit-
able number of panels, say 40, for numerical integration by Simpson's
rule. At each of these 40 values of r, the following factors are calculated.

Elevations of HU, HL, TU and TL. The elevations of the edges of the
fragment beam are given by the equations

(15)
$$HU = H + b + r\phi_U$$

$$HL = H - b - r\phi_L.$$

The values of TU and TL are obtained by using (15) in conjunction
with the conditions (1) and (2). To calculate the number of fragments
striking the target we need the distances from the horizontal reference
plane $y = 0$ to the edges of the exposed part of the target, given by

(16)
$$YU = TU - (H + j)$$

$$YL = TL - (H + j).$$

These y values may be positive or negative. The number of fragments
striking a strip one foot wide between YU and YL is the integral

(17)
$$N' = \int_{YL}^{YU} n\,(r, y)\, dy.$$

If YU and YL have the same sign they are both on the same side of
the reference plane. Since n is an even function of y, the signs of YU and
YL are in this case immaterial. But if YU and YL have opposite signs
the integration straddles the origin, hence it is necessary to keep track
of the signs of YU and YL, and to integrate accordingly.

Keeping in mind these precautions we can now preceed to the numerical
calculation. At first glance it would seem that we would have to integrate

the distribution function (6), which would be quite a task. But if we go back to the derivation of this function we are reminded that the fragments reaching dy on the target are the same ones that left the segment dz on the liner.

Therefore

$$(18) \qquad \int_{YL}^{YU} n\,(r,y)\,dy \quad = \quad \int_{ZL}^{ZU} n_1\,dz = n_1\,\triangle\,Z$$

which is a much simpler task. But we still need to solve the quartic equation (8) to obtain ZU and ZL corresponding to the two y limits, and the signs of the z limits must be the same as the signs of the corresponding y limits.

Since the point-to-point variation in density of fragments on the exposed part of the target is of no interest here, the density distributions n_1 and n are best discarded and the total number of fragments N" = 7000 W/m will be used instead.

If we imagine the target to be a cylinder completely surrounding the ground zero of the burst point, then

$$N = N''\,\triangle\,Z/2b$$

is the number of fragments striking the target. The average number per square foot is the above value divided by the lateral area of the target cylinder of radius r and height T:

$$(19) \qquad \overline{N} = N''\,\triangle Z/(4\pi\,br\,T).$$

The remainder of the calculation is routine:

$$E_K = \bar{\bar{N}} A_p \, P_{HK}$$

(20) $$P_K = 1 - \exp(-E_K)$$

$$A_L = 2\pi \int_{R_1}^{R_2} P_K \, r \, dr.$$

The element of area is $2\pi r \, dr$ because for vertical incidence the contours of constant P_K are circles.

A flow chart indicating the principal steps in the computation is shown in Figure 7.

LETHAL AREA CALCULATIONS FOR SPHERICAL ROUNDS

The procedure follows the same general steps as used for cylindrical rounds. The two upper limits for r given in (10) and (11) now become

(21) $$R'_2 = (R^2 - (H - T)^2)^{1/2}$$

when the burst is above the target.

An additional upper limit must be considered here, when $0_2 < 90^\circ$, as shown in Figure 6.

(22) $$R''_2 = H \tan \theta_2$$

The lower limit for r is zero except when the burst is above the target and $\theta_1 > 0$, then

(23) $$R_1 = (H-T) \tan \theta_1$$

The range of r is $R_2 - R_1$ and this is divided into a suitable number of panels, as for the cylinder. At each of these intermediate r values, the following factors are calculated:
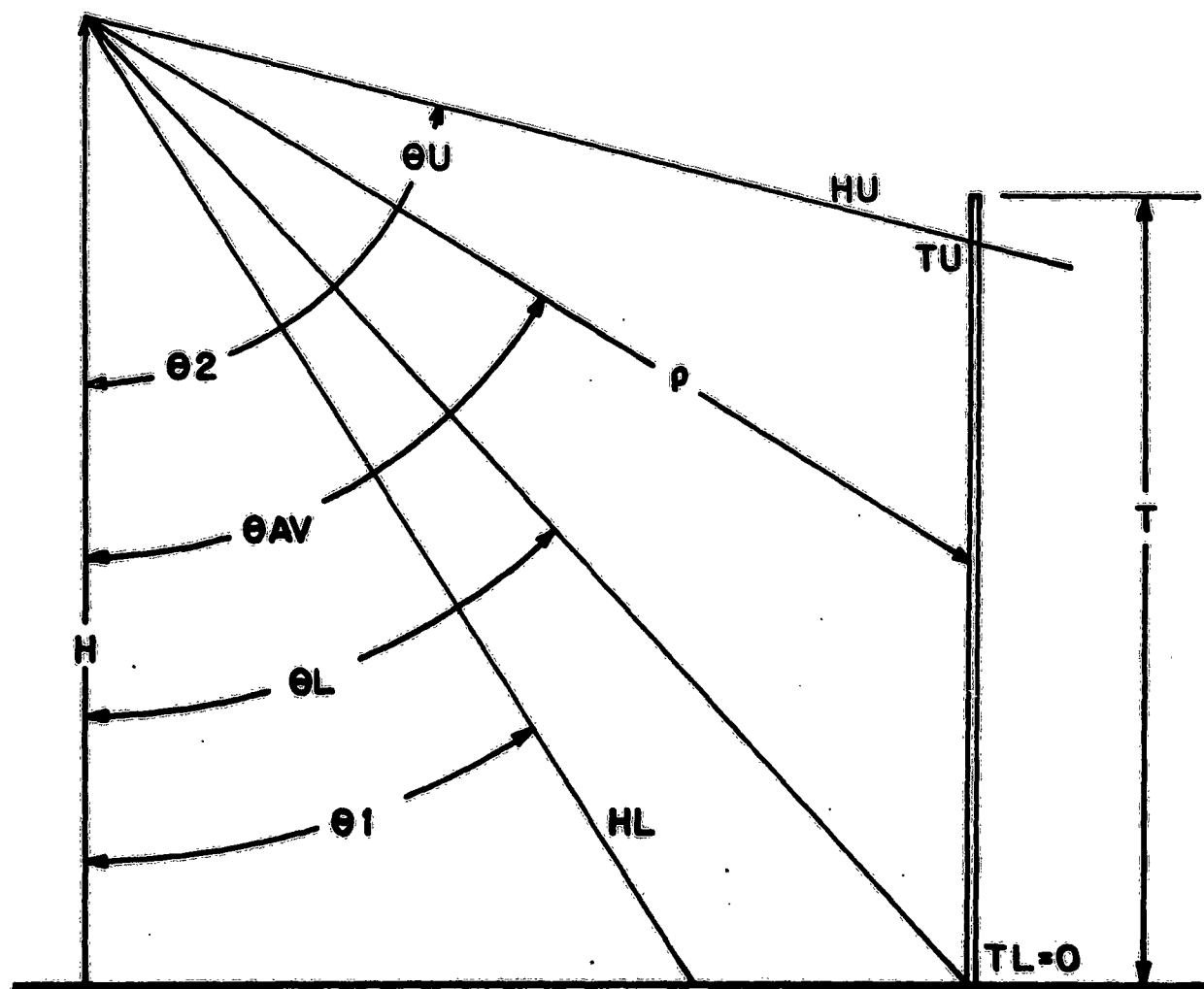
Figure 6. Extended Target and Spherical Round

$$HU = H - r \cot \theta_2$$

(24)

$$HL = H - r \cot \theta_1$$

From (24) and the conditions (1) and (2)

(25) $$f = (TU - TL)/T.$$

The average slant range, from the definition given earlier, is obtained after the following steps:

$$\tan \theta_U = r/(H - TU)$$

$$\tan \theta_L = r/(H - TL)$$

(26)

$$\theta_{AV} = (\theta_U + \theta_L)/2$$

$$\rho = r/\sin \theta_{AV}.$$

This value of ρ is used to calculate P_{HK} as well as the density of fragments at the target.

The fragment density on the target is

$$n = N/(2\pi \rho^2 (\cos \theta_1 - \cos \theta_2))$$

where

$$N = 7000 \ W/m.$$

The next step is to obtain

$$E_K = n \times f \times A_p \times P_{HK}$$

and the other final steps are the same as (20) for the cylinder.

The flow chart for the sphere resembles in many respects the flow chart for the cylinder, as shown in Figure 7.

SIMPLIFIED FLOW CHARTS
for Lethal Areas of
Cylindrical and Spherical Charges
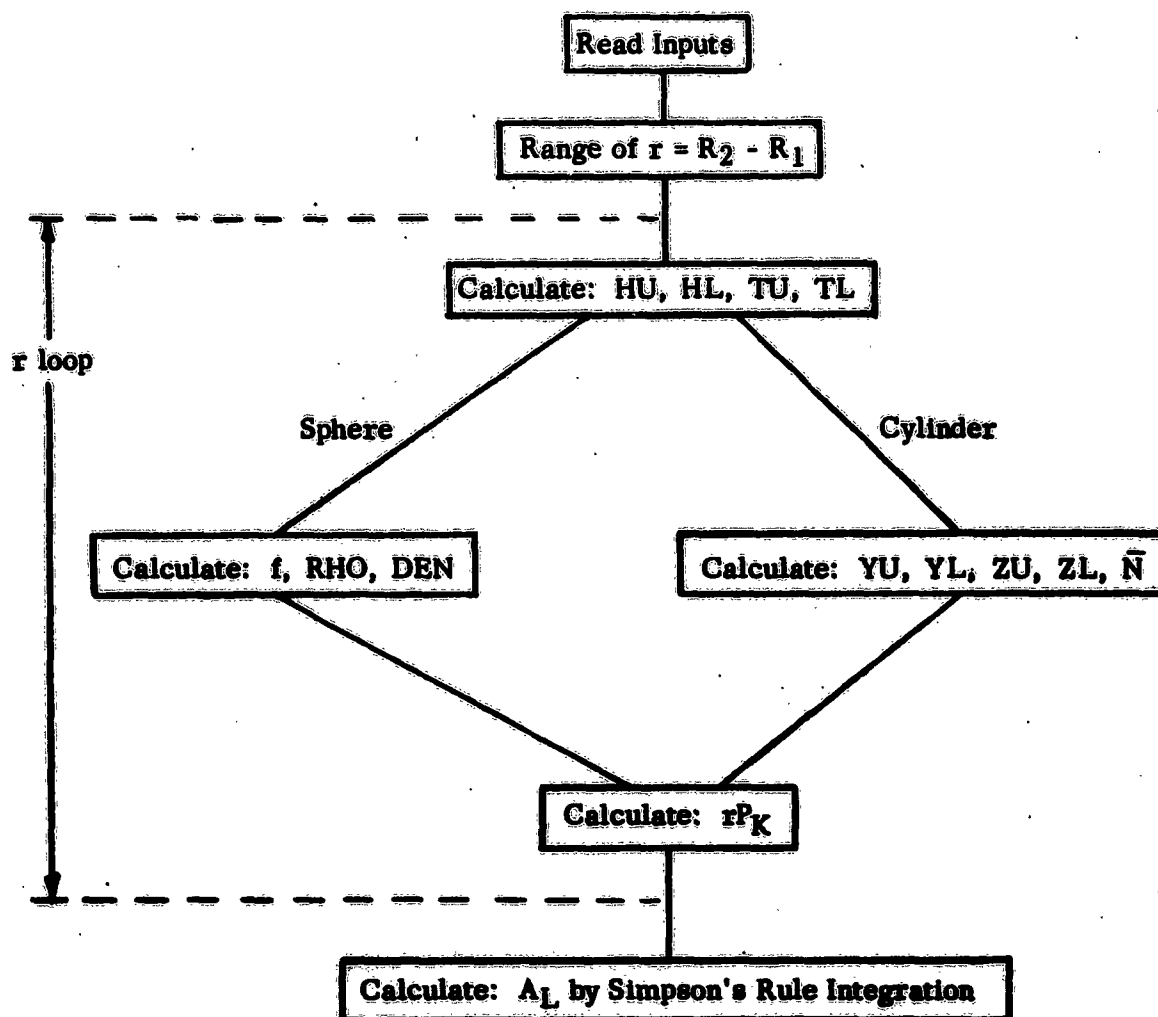
Figure 7. Flow Charts for Cylinders and Spheres

COMPARISON OF CYLINDERS AND SPHERES

In making this comparison all rounds are assumed to produce 2000 fragments, all with the same initial velocity, the same individual mass, and uniformly distributed. To examine the effect of the shapes of cylindrical charges, three calibers were chosen: 3.0, 1.0 and 0.5, each one initiated at the c.g. (mid point of the length). Corresponding to each of these cylinders, a particular sphere was designed. The limiting angle ϕ_e at the end of the cylinder was used to determine the side-spray angle for the sphere. Since the beam of fragments from the cylinder is symmetrical above and below the fuze, the same symmetrical orientation was used on the sphere, i.e., $\theta_1 = 90° - \phi_e$ and $\theta_2 = 90° + \phi_e$. The numerical values of the parameters thus obtained for the six rounds are shown in Table I.

The field densities were calculated for ranges of 10, 20, 40, and 70 ft. and for a series of y values ending at the edges of the beams in each case, as shown in Figures 8 to 11.

To provide a basis for understanding the shape of the curves shown for spherical rounds, it may be instructive to mention that the spherical round has a distribution function analogous to the one for a cylindrical round, namely

$$(27) \qquad n_s(r, y) = n_1 a^2 /(y^2 + r^2)$$

where a is the radius of the sphere and r is a parameter. This function is seldom noticed in going through lethal area calculations because it is so easily computed. Written in the form

$$n_s = kr^3 /(y^2 + r^2)$$

where

$$k = n_1 a^2/r^3,$$

it is the equation of the "Witch of Agnesi" (Ref. 3), first constructed and described by Maria Gaetana Agnesi in Milan in the 18th Century. This is a cubic curve having a maximum at $y = 0$, and decreasing asymptotically to zero for large y values, just the opposite trend from the density function (6)

for the cylinder. The points of inflection for (27) are at $y = \pm r / \sqrt{3} = \pm .5774\ r$, and at these points the function is 75°/o of its maximum value.

To obtain some idea of the range of (27) encountered in the above examples chosen for comparison, it can be shown that the edges of the fragment beams come at about one-fourth the distance to the inflection point. Hence the curves for the spheres are practically straight lines with very slight negative slopes. They are actually curves with a horizontal tangent at $y = 0$, and a negative curvature imperceptible in the region of interest here.

This design of spherical rounds produced probably the fairest possible comparison but it is not quite perfect because the edges of the side sprays from the sphere are inside those from the cylinder, by an amount equal to half the cylinder length at top and bottom. But the difference is relatively slight at short ranges, as is evident in Figures 8 and 9, and is almost imperceptible at longer ranges. In all cases, the cylinder fires the same number of fragments at the target but they spread over a slightly greater vertical expanse.

This slight imperfection in comparison cannot be corrected by placing the sphere farther from any one particular target so that the edges of its side spray coincide with those of the cylinder in that particular direction, because to obtain A_L by integration over all other targets around ground zero, the two rounds will not have the same point for ground zero.

The lethal areas shown in the last two lines of the table were calculated for target heights of 5.5 ft. (standing men) and .75 ft. (prone men), the burst height in each case being half the target height. This burst height was chosen to exploit the symmetry of the side sprays. Many other situations might be used to compare cylinders and spheres, but they will be reserved for the optimization studies to be described in later reports.

DISCUSSION. The fragment densities at field points shown in Figures 8 to 11 indicate that the sphere produces practically constant density in the y direction, whereas the cylinder produces a lower density at $y = 0$, which rises above that for the sphere somewhere in the last third of the y range to the edge of the fragment beam. The 3-caliber cylinder ends
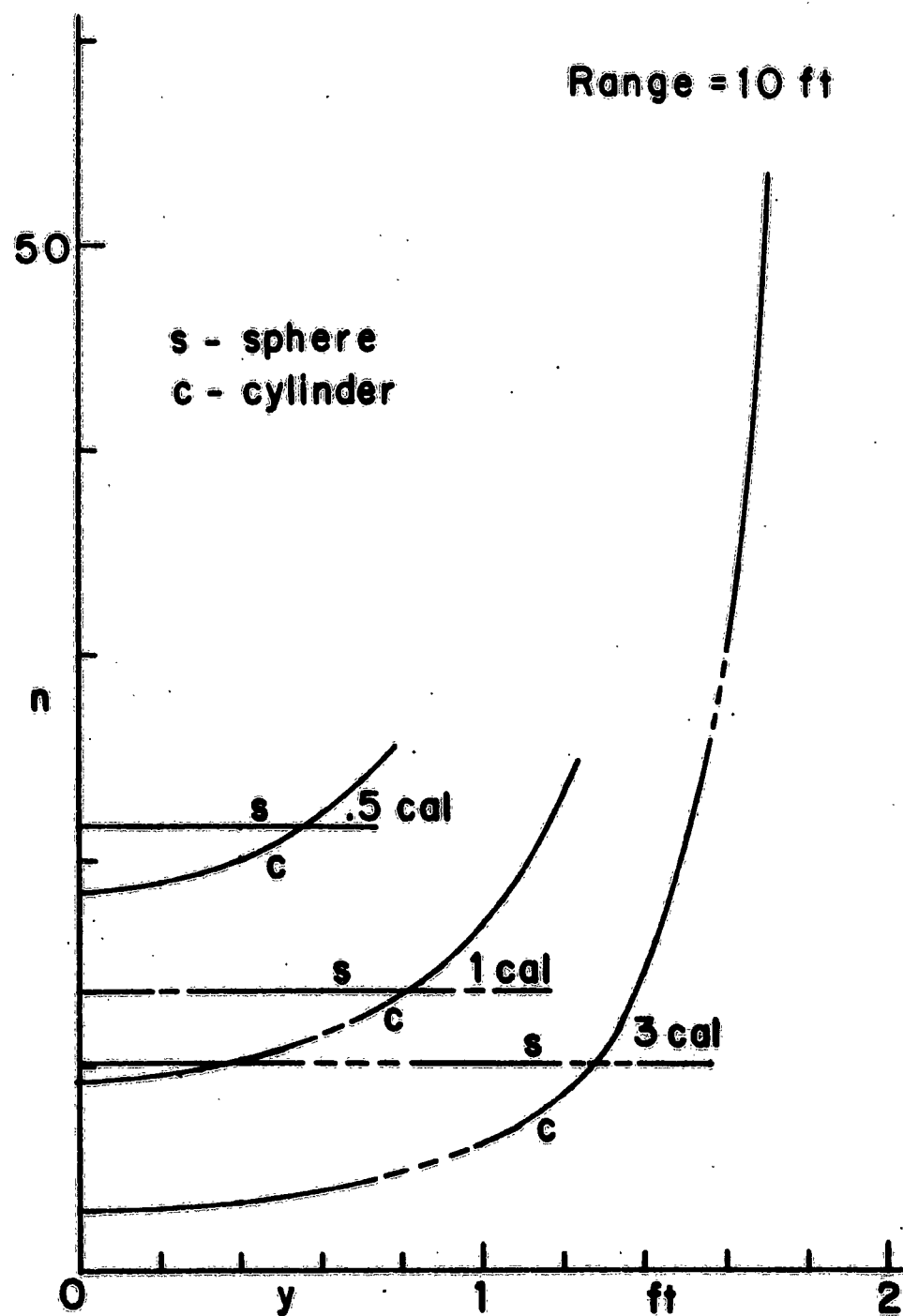
Figure 8. Fragment Density vs. Height for Cylinders and Spheres at 10 ft.
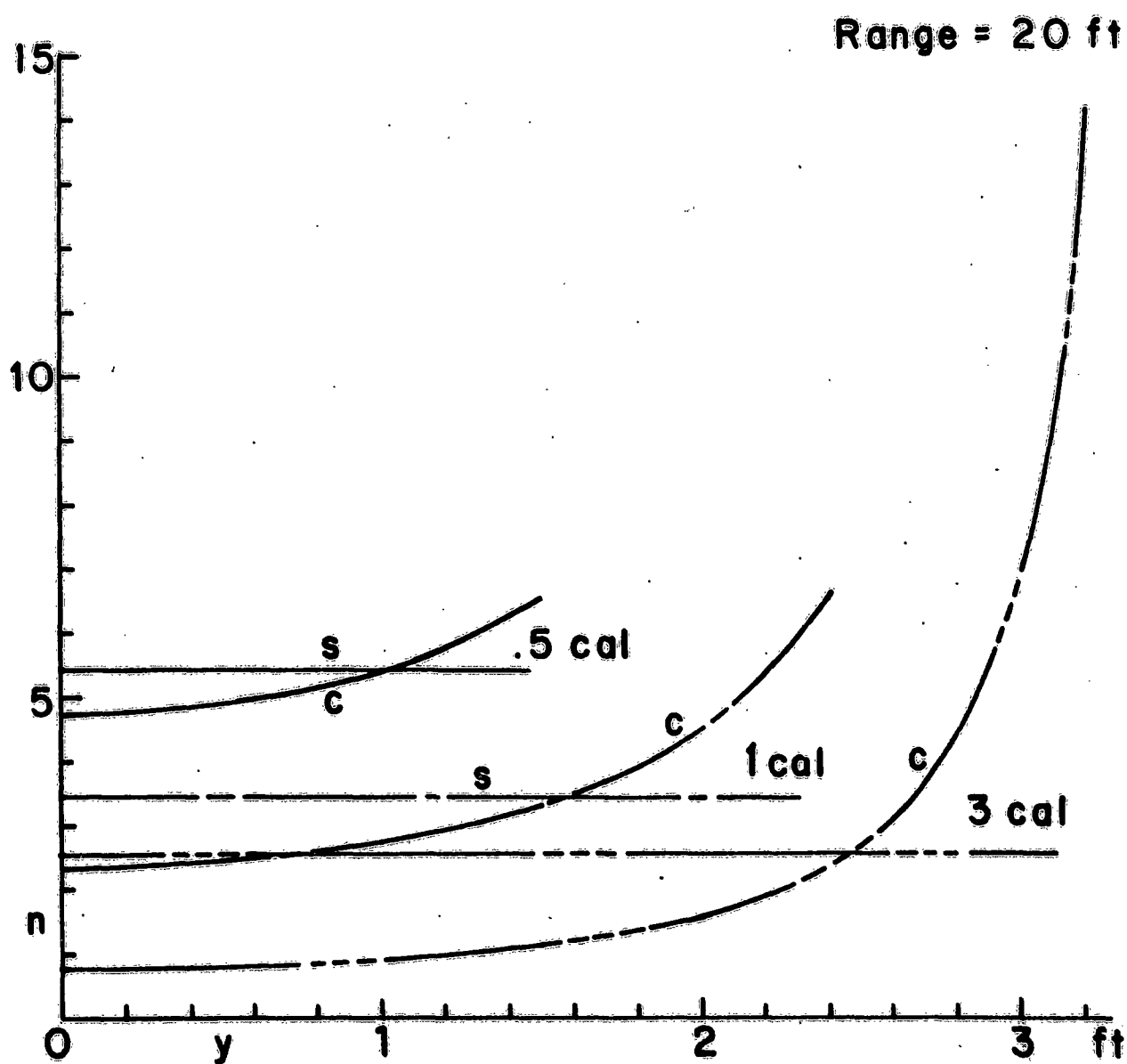
Figure 9. Fragment Density vs. Height for Cylinders and Spheres at 20 ft.
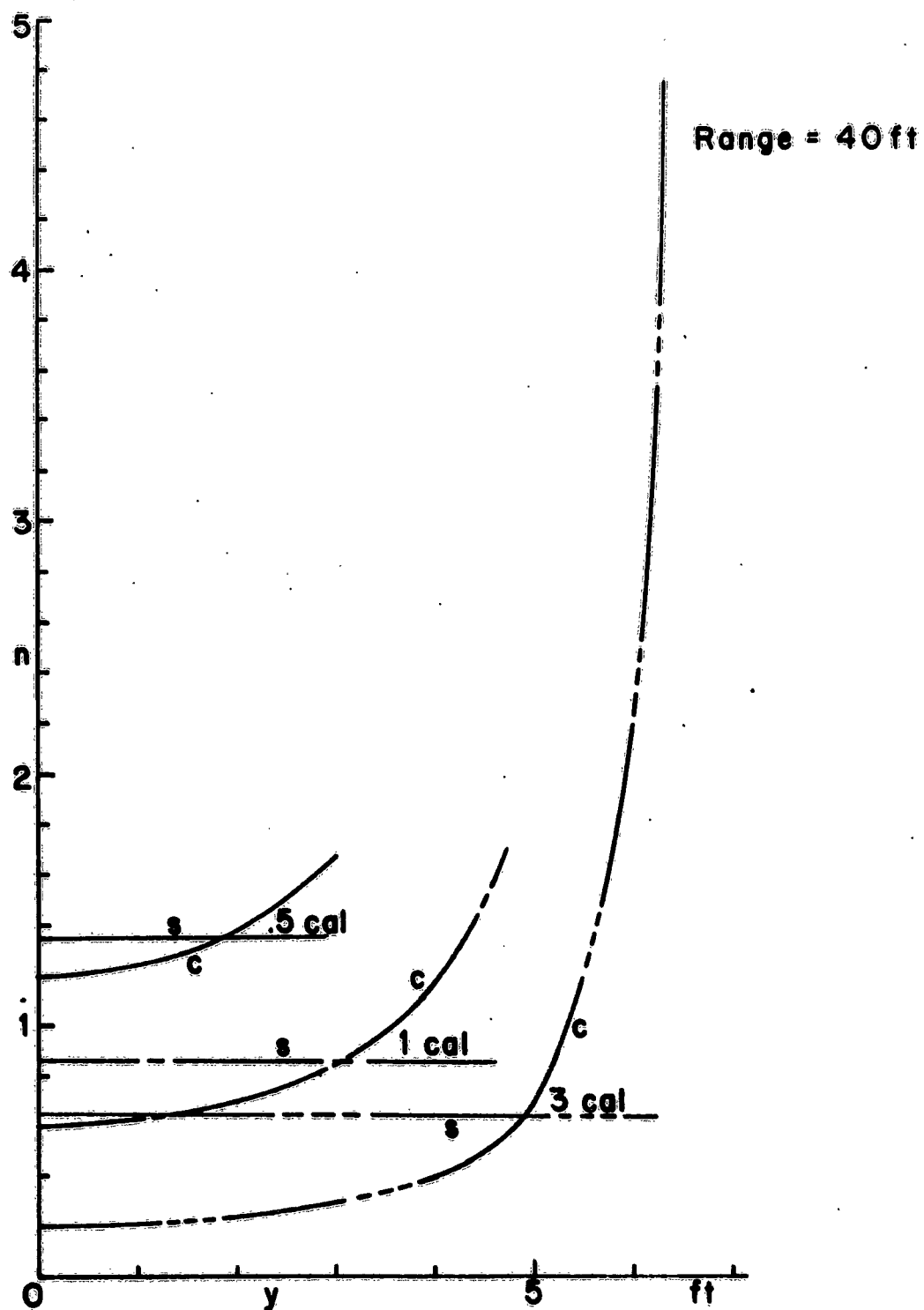
Figure 10. Fragment Density vs. Height for Cylinders and Spheres at 40 ft.
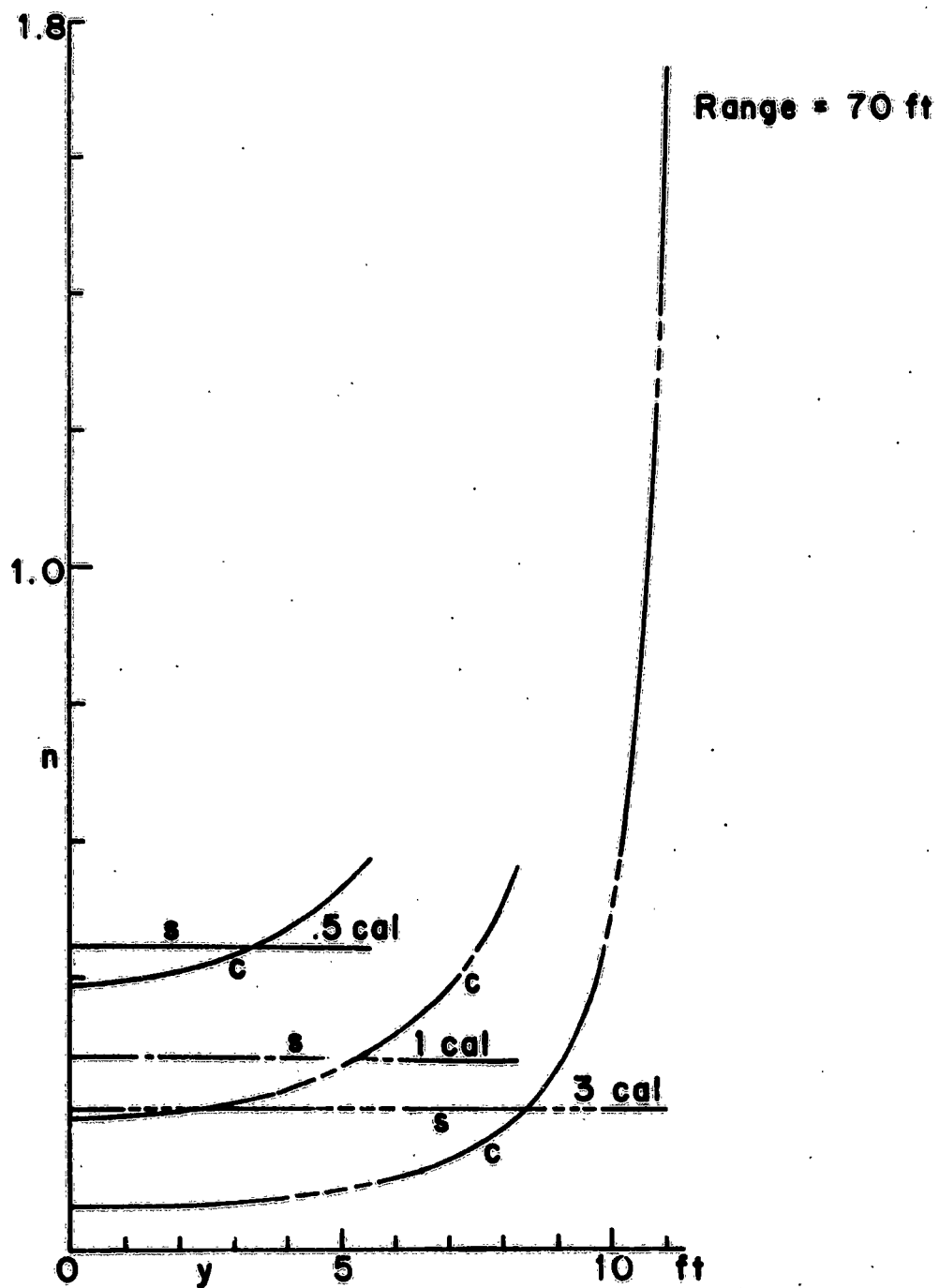
Figure 11. Fragment Density vs. Height for Cylinders and Spheres at 70 ft.

with a density at the edge of the beam which is five or more times greater than the sphere density. This ratio seems to increase as the range r increases. The two shorter cylinders chosen for this study just happen to end with nearly equal densities at the edges of their beams. For the cylinders the increase in fragment density as y increases is to be expected from the curves shown in Figure 4.

The lethal areas shown in Table I for these six rounds are less for prone targets than for standing targets.

The sphere has a larger lethal area than the long cylinder, but a smaller area than the short cylinder for both stances of the target, whereas for the intermediate 1-caliber rounds the sphere is slightly superior for prone targets while the cylinder is definitely superior for standing.

The very high densities at the edge of the beam for the 3-caliber cylinder shown in Figures 8 to 11 seems to act as a disadvantage in comparison with the nearly constant density for the sphere, inasmuch as the 3-caliber cylinder has definitely less lethal area than the sphere for both stances of the target.

REFERENCES

1. Letter, dated 26 February 1960, from E. E. Minor, Terminal
    Ballistics Laboratory, BRL, to Chief of Ordnance; Subject, "Wound
    Ballistic Vulnerablity of Human Body Components".

2. Picatinny Arsenal Technical Memorandum No. 1215, "A New Lethality
    Model and Associated Optimum Fragmentation Characteristics",
    (1963)

3. Granville and Smith "Elements of the Differential and Integral Calculus",
    (Ginn and Co., Boston, 1911) Page 271.

A QUADRATURE FORMULA FOR CERTAIN

FUNCTIONS OF MORE THAN ONE VARIABLE

Joseph S. Tyler

U. S. Army Chemical Research and Development Laboratories
Edgewood Arsenal, Maryland

INTRODUCTION. This paper is concerned with a technique for evaluating multiple integrals numerically when the integrands satisfy certain conditions which are to be specified in the paper. The general idea is to reduce the problem of n-fold integrations to a problem of solving n equations for a particular set of parameters.

The integration of a single integral is discussed first and the technique is then extended to multiple cases. Formulas treating the general n-fold integration problem are finally included.

Case 1 The One-Fold Integral. Let it be required to perform the following integration:

$$(1.0) \qquad I_1 = \int_0^1 f(x)\, dx.$$

In order to evaluate this integral, an auxiliary integral is introduced:

$$(1.1) \qquad J = \int_0^1 \frac{d}{dx}\left[x\, f(x)\right] \cdot dx = f(1) - 0\, f(0).$$

Assuming that $\left[0 \cdot f(0)\right] = 0$, equation (1.1) is simply

$$(1.2) \qquad J = \int_0^1 f(x)\, dx + \int_0^1 x\, f_x(x)\, dx = f(1).$$

On applying the Gaussian-Legendre one-point quadrature formula to both integrals of equation (1.2), one obtains the following.

$$(1.3) \qquad \int_0^1 f(x) \, dx \doteq f(1/2) + \frac{1}{24} f_{xx}(\lambda)$$

$$(1.4) \qquad \int_0^1 x f_x \, dx = \frac{1}{2} f_x(1/2) + \frac{1}{24} \left[\lambda f_{xxx}(\lambda) + 2 f_{xx}(\lambda), \right]$$

$$0 \leq \lambda \leq 1,$$

so that equation (1.2) can be expressed as:

$$(1.5) \qquad J = f(1/2) + \frac{1}{24} f_{xx}(\lambda) + (1/2) f_x(1/2) + \frac{1}{24} \cdot$$

$$\left[\lambda f_{xxx}(\lambda) + 2 f_{xx}(\lambda) \right] = f(1)$$

or

$$(1.6) \qquad \lambda f_{xxx}(\lambda) + 3 f_{xx}(\lambda) = 24 \cdot \left[f(1) - f(1/2) - \frac{1}{2} f_x(1/2) \right] \quad .$$

The numerical solution of the required integral can be expressed as follows:

$$I_1 = \int_0^1 f(x) \, dx = f(1/2) + \frac{1}{24} f_{xx}(\lambda), \quad 0 \leq \lambda \leq 1,$$

where the number λ is obtained by solving the following expression:

$$(1.6) \qquad \lambda f_{xxx}(\lambda) + 3 f_{xx}(\lambda) = 24 \left[f(1) - f(1/2) - 1/2 f_x(1/2) \right] \quad .$$

provided that:

(1) There is one and only one number λ, $(0 \leq \lambda \leq 1)$, that satisfies Equation (1.6).

(2) $f(x)$ is of class C_3 on the closed domain $[0, 1]$.

(3) $0 \cdot f(0) = 0$.

[Example No. 1] : Let $f(x) = x e^x$,

then

$$I_1 = \int_0^1 x \ e^x \ dx = 1$$

By Formulas

$f(x) = x e^x$

$f_x(x) = (x + 1) e^x$

$f_{xx}(x) = (x + 2) e^x$

$f_{xxx}(x) = (x + 3) e^x$

$I_1 = f(1/2) + \frac{1}{24} f_{xx}(\lambda)$

$I_1 = \frac{1}{2} e^{\frac{1}{2}} + \frac{1}{24} [2 + \lambda] \ e^\lambda$

$\lambda f_{xxx}(\lambda) + 3 f_{xx}(\lambda) = 24 \left[f(1) - f(\frac{1}{2}) - \frac{1}{2} f_x(\frac{1}{2}) \right]$

$[\lambda^2 + 6\lambda + 6] \cdot e^\lambda = 24 \left[e - \frac{5}{4} e^{\frac{1}{2}} \right] \longrightarrow \lambda \simeq 0.5186,1$

$I_1 \simeq 0.82435 + \frac{1}{24} \cdot \left[(2.51861)(1.6820) \right] \simeq 1.000,86.$

$\left[\text{Example No. 2}\right]$ Let $f(x) = x^n$ for $n \neq -1$.

then,

$$I_1 = \int_0^1 x^n \, dx = 1/(n+1) .$$

By Formulas:

$f(x) = x^n$

$f_x(x) = n \, x^{n-1}$

$f_{xx}(x) = n \, (n-1) \, x^{n-2}$

$f_{xxx}(x) = n \, (n-1) \, (n-2) \, x^{n-3}$

$I_1 = f(1/2) + \dfrac{1}{24} \, f_{xx}(\lambda)$

$I_1 = \left(\dfrac{1}{2}\right)^n + \dfrac{1}{24} \cdot \left[(n) \cdot (n-1) \, \lambda^{n-2}\right]$

$\lambda f_{xxx}(\lambda) + 3 f_{xx}(\lambda) = 24 \left[f(1) - f\left(\dfrac{1}{2}\right) - \dfrac{1}{2} f_x\left(\dfrac{1}{2}\right)\right]$

or $(n) \, (n-1) \, \lambda^{n-2} = \dfrac{24}{(n+1)} \cdot \left[1 - \left(\dfrac{1}{2}\right)^n - n \left(\dfrac{1}{2}\right)^n\right]$.

Hence:

$$I_1 = \left(\dfrac{1}{2}\right)^n + \dfrac{1}{24} \, \dfrac{24}{(n+1)} \cdot \left[1 - \left(\dfrac{1}{2}\right)^n = n \left(\dfrac{1}{2}\right)^n\right] = \dfrac{1}{n+1} .$$

Case 2:   The Two-Fold Integral .   Let

$$(2.0) \qquad I_2 = \int_0^1 \int_0^1 f(x, y) \, dx \, dy.$$

Utilizing the results for Case 1, (the one-fold integral).

$$(2.1) \qquad I_2 = \int_0^1 f(1/2, y) \, dy + \frac{1}{24} \int_0^1 f_{xx}(a, y) \, dy, \quad 0 \le a \le 1,$$

or

$$(2.2) \qquad I_2 = \int_0^1 f(x, \tfrac{1}{2}) \, dx + \frac{1}{24} \int_0^1 f_{yy}(x, b) \, dx, \quad 0 \le b \le 1.$$

Apply the results for Case 1 a second time, first to Equation (2.1) and next to Equation (2.2) one obtains:

$$(2.3) \qquad I_2 = f(\tfrac{1}{2}, \tfrac{1}{2}) + \frac{1}{24} f_{yy}(\tfrac{1}{2}, c) + \frac{1}{24} f_{xx}(a, \tfrac{1}{2}) + \left[\frac{1}{24}\right]^2 \cdot$$

$$f_{xxyy}(a, d),$$

and

$$(2.4) \qquad I_2 = f(\tfrac{1}{2}, \tfrac{1}{2}) + \frac{1}{24} f_{xx}(g, \tfrac{1}{2}) + \frac{1}{24} f_{yy}(\tfrac{1}{2}, b)$$

$$+ \left[\frac{1}{24}\right]^2 \cdot f_{yyxx}(h, b),$$

$$0 \le a \le 1, \ 0 \le b \le 1, \ 0 \le c \le 1, \ 0 \le d \le 1, \ 0 \le g \le 1, \ 0 \le h \le 1.$$

It is obvious that equations (2.3) and (2.4) are equal; moreover f_{xx} (·) and f_{yy} (·) are continuous functions, on the domain of definition; hence,

$$a = g = h, \quad b = c = d \ .$$

In conclusion, the two-fold integral can be evaluated as follows:

$$I_2 = \int_0^1 \int_0^1 f(x, y) \ dx \ dy$$

$$I_2 \simeq f(\tfrac{1}{2}, \tfrac{1}{2}) + \tfrac{1}{24} \cdot \left[f_{xx}(a, \tfrac{1}{2}) + f_{yy}(\tfrac{1}{2}, b) \right]$$

$$+ \left[\tfrac{1}{24} \right]^2 \cdot f_{xxyy}(a, b), \quad 0 \leq a \leq 1, \ 0 \leq b \leq 1 \ ,$$

where the numbers a and b are obtained by solving the equations:

$$a \ f_{xxx}(a, \tfrac{1}{2}) + 3 f_{xx}(a, \tfrac{1}{2}) = 24 \left[f(1, \tfrac{1}{2}) - f(\tfrac{1}{2}, \tfrac{1}{2}) - \tfrac{1}{2} f_y(\tfrac{1}{2}, \tfrac{1}{2}) \right].$$

$$b \ f_{yyy}(\tfrac{1}{2}, b) + 3 f_{yy}(\tfrac{1}{2}, b) = 24 \left[f(\tfrac{1}{2}, 1) - f(\tfrac{1}{2}, \tfrac{1}{2}) - \tfrac{1}{2} f_y(\tfrac{1}{2}, \tfrac{1}{2}) \right].$$

provided that:

(1) There is one and only one real root

  a, $\left[0 \leq a \leq 1 \right]$, and b, $\left[0 \leq b \leq 1 \right]$.

(2) f(x, y), $f_{xxx}(x, y)$, $f_{yyy}(x, y)$ are real valued

continuous functions defined on the closed sets $\left[0 \leq x \leq 1, \right.$

$\left. 0 \leq y \leq 1 \right]$.

$$(3) \quad \left[0 \cdot f \quad (0, y) \right] \quad = \quad \left[0 \cdot f \quad (x, 0) \right] \quad = 0.$$

Case 3: The Three-Fold Integral.

$$I_3 = \int_0^1 \int_0^1 \int_0^1 f(x, y, z) \, dx \, dy \, dz$$

$$I_3 = f\left(\frac{1}{2}, \frac{1}{2}, \frac{1}{2}\right) + \frac{1}{24} \left[f_{xx}\left(a, \frac{1}{2}, \frac{1}{2}\right) + f_{yy}\left(\frac{1}{2}, b, \frac{1}{2}\right) + f_{zz}\left(\frac{1}{2}, \frac{1}{2}, c\right) \right]$$

$$+ \left[\frac{1}{24}\right]^2 \cdot \left[f_{xxyy}(a, b, 1/2) + f_{xxzz}(a, 1/2, c) + f_{yyzz}(1/2, b, c) \right]$$

$$+ \left[\frac{1}{24}\right]^3 \cdot \left[f_{xxyyzz}(a, b, c) \right] ,$$

$$0 \leq a \leq 1, \; 0 \leq b \leq 1, \; 0 \leq c \leq 1 ,$$

$$a f_{xxx}(a, 1/2, 1/2) + 3 f_{xx}(a, 1/2, 1/2) = 24 \left[f(1, 1/2, 1/2) \right.$$
$$\left. - f(1/2, 1/2, 1/2) - \frac{1}{2} f_x(1/2, 1/2, 1/2) \right] ,$$

$$b f_{yyy}(1/2, b, 1/2) + 3 f_{yy}(1/2, b, 1/2) = 24 \left[f(1/2, 1, 1/2) - f(1/2, 1/2, 1/2) \right.$$
$$\left. - \frac{1}{2} f_y(1/2, 1/2, 1/2) \right] ,$$

$$c f_{zzz}(1/2, 1/2, c) + 3 f_{zz}(1/2, 1/2, c) = 24 \left[f(1/2, 1/2, 1) - f(1/2, 1/2, 1/2) \right.$$
$$\left. - \frac{1}{2} f_z(1/2, 1/2, 1/2) \right] .$$

Case 4: The Four-Fold Integral

$$I_4 = \int_0^1 \int_0^1 \int_0^1 \int_0^1 f(x, y, z, t) \, dx \, dy \, dz \, dt$$

$$I_4 = f(1/2, 1/2, 1/2, 1/2)$$

$$+ \frac{1}{24} \left[f_{xx}(a, 1/2, 1/2, 1/2) + f_{yy}(1/2, b, 1/2, 1/2) \right.$$

$$\left. + f_{zz}(1/2, 1/2, c, 1/2) + f_{tt}(1/2, 1/2, 1/2, d) \right]$$

$$+ \left[\frac{1}{24} \right]^2 \left[f_{xxyy}(a, b, 1/2, 1/2) + f_{xxzz}(a, 1/2, c, 1/2) + f_{xxtt}(a, 1/2, 1/2, d) \right.$$

$$\left. + f_{yyzz}(1/2, b, c, 1/2) + f_{yytt}(1/2, b, 1/2, d) + f_{zztt}(1/2, 1/2, c, d) \right]$$

$$+ \left[\frac{1}{24} \right]^3 \left[f_{xxyyzz}(a, b, c, 1/2) + f_{xxyytt}(a, b, 1/2, d) + f_{xxzztt}(a, 1/2, c, d) \right.$$

$$\left. + f_{yyzztt}(1/2, b, c, d) \right]$$

$$+ \left[\frac{1}{24} \right]^4 \cdot \left[f_{xxyyzztt}(a, b, c, d) \right] ,$$

$$0 \leq a \leq 1, \quad 0 \leq b \leq 1, \quad 0 \leq c \leq 1, \quad 0 \leq d \leq 1 .$$

$$a\, f_{xxx}(a, 1/2, 1/2, 1/2) + 3\, f_{xx}(a, 1/2, 1/2, 1/2) = 24 \cdot$$

$$\left[f(1, 1/2, 1/2, 1/2) - f(1/2, 1/2, 1/2, 1/2) - \frac{1}{2} f_x(1/2, 1/2, 1/2, 1/2) \right] ,$$

$$b\, f_{yyy}(1/2, b, 1/2, 1/2) + 3\, f_{yy}(1/2, b, 1/2, 1/2) = 24 \cdot \left[f(1/2, 1, 1/2, 1/2) \right.$$

$$\left. - f(1/2, 1/2, 1/2, 1/2) - \frac{1}{2} f_y(1/2, 1/2, 1/2, 1/2) \right] ,$$

$$c\, f_{zzz}(1/2, 1/2, c, 1/2) + 3\, f_{zz}(1/2, 1/2, c, 1/2) = 24 \left[f(1/2, 1/2, 1, 1/2) \right.$$

$$\left. - f(1/2, 1/2, 1/2, 1/2) - \frac{1}{2} f_z(1/2, 1/2, 1/2, 1/2) \right] ,$$

$$d\, f_{ttt}(1/2, 1/2, 1/2, d) + 3\, f_{tt}(1/2, 1/2, 1/2, d) = 24 \left[f(1/2, 1/2, 1/2, 1) \right.$$

$$\left. - f(1/2, 1/2, 1/2, 1/2) - \frac{1}{2} f_t(1/2, 1/2, 1/2, 1/2) \right] .$$

Example No. 1   Let $f(x, y, z, t) = x y z t^5$

Then

$$I_4 = \int_0^1 \int_0^1 \int_0^1 \int_0^1 x y z t^5 \; dx \; dy \; dz \; dt = 1/48.$$

By Formulas:

$f_x = y z t^5$	$f_y = x z t^5$	$f_z = x y t^5$
$f_{xx} = 0$	$f_{yy} = 0$	$f_{zz} = 0$
$f_{xxx} = 0$	$f_{yyy} = 0$	$f_{zzz} = 0$

$f_t = 5 x y z t^4$	$f_{xxyy} = f_{xxzz} = f_{xxtt} = f_{yyzz} = f_{yytt} = f_{zztt} = 0$
$f_{tt} = 20 x y z t^3$	$f_{xxyyzz} = f_{xxyytt} = f_{xxzztt} = f_{yyzztt} = 0$
$f_{ttt} = 60 x y z t^2$	$f_{xxyyzztt} = 0$

Moreover; $a = b = c = 0$, and

$$d \, f_{ttt} (1/2, 1/2, 1/2, d) + 3 f_{tt} (1/2, 1/2, 1/2, d) =$$

$$24 \left[f (1/2, 1/2, 1/2, 1) - f(1/2, 1/2, 1/2, 1/2) - \frac{1}{2} f_t (1/2, 1/2, 1/2, 1/2) \right]$$

$$\frac{15}{2} \, d^3 + \frac{15}{2} \, d^3 = 39/16$$

$$d^3 = \frac{13}{80} \; ;$$

so that

$$I_4 = (1/2)^8 + \frac{1}{24} \cdot \frac{5}{2} d^3 = (1/2)^8 + \frac{13}{768}$$

$$I_4 = 1/48 \,.$$

The N-Fold Integral:

$$I_n = \int_0^1 \cdots \int_0^1 f(x_1, x_2, \ldots, x_n) \, dx_1 \, dx_2 \cdots dx_n$$

$$I_n = f(1/2, \ldots, 1/2)$$

$$+ \frac{1}{24} \sum_{i=1}^n f_{x_i x_i}(a_i, 1/2, \ldots, 1/2)$$

$$+ \left[\frac{1}{24}\right]^2 \cdot \sum_{i < j}^n f_{x_i x_i x_j x_j}(a_i, a_j, \frac{1}{2}, \ldots, 1/2)$$

$$+ \left[\frac{1}{24}\right]^3 \cdot \sum_{i < j < k}^n f_{x_i x_i x_j x_j x_k x_k}(a_i, a_j, a_k, \frac{1}{2}, \ldots, \frac{1}{2}) + \cdots$$

$$+ \left[\frac{1}{24}\right]^n f_{x_1 x_1 x_2 x_2 \ldots x_n x_n}(a_1, a_2, \ldots a_n)\,,$$

$$0 \le a_\lambda \le 1, \quad \lambda = 1, 2, \ldots, n \,.$$

The parameters, $(a_1, a_2, \ldots, a_n)$ are solutions of the following equations.

$$a_\lambda f_{x_\lambda x_\lambda x_\lambda}(a_\lambda, 1/2, \ldots, 1/2) + 3 f_{x_\lambda x_\lambda}(a_\lambda, 1/2, \ldots, 1/2) =$$

$$24 \cdot \left[f(x_\lambda = 1, 1/2, \ldots, 1/2) - f(1/2, \ldots, 1/2) \right]$$

$$= \frac{1}{2} f_{x_\lambda}(1/2, \ldots, 1/2), \qquad \lambda = 1, 2, \ldots, n;$$

provided that

1) There is one and only one real root a_λ, $\left[0 \leq a_\lambda \leq 1 \right]$, for each subscript λ of the above differential equations,

2) $f(x_1, \ldots, x_n)$, $f_{x_\lambda x_\lambda x_\lambda}(x_1, \ldots, x_n)$, are real valued continuous functions defined on the closed sets $\left[0 \leq x_\lambda \leq 1 \right]$,

3) $0 \cdot f(0, \left\{ x_\lambda \right\},) = 0$.

THE DUFFING PROBLEM COMPLETED

Raimond A. Struble

North Carolina State College, Raleigh, North Carolina

Today I should like to discuss some theoretical and practical implications relating to the general solution of the Duffing equation

(1) $$\ddot{x} + n^2 x - \beta x^3 = \beta F_o \cos \lambda t$$

(n, F_o, λ, β constant, $|\beta|$ small).

For some time now we have been applying a formal expansion procedure in the study of oscillation problems. The techniques were originally developed during an investigation of the resonant motion of artificial satellites and the Duffing equation furnished us with one of our first textbook-type applications of these techniques. There have been others, some more interesting and some less interesting, and certainly the last chapter on this work has not yet been written. However, it is not my intent here to discuss these formal techniques nor their future in this business but, rather, it is my intent to illustrate with this familiar Duffing problem some interesting results which stem from rigorous considerations. Coupled with the extensive formal results you may or may not agree with my suggestion that the Duffing problem is now, perhaps, completed.

The formal expansion obtained previously suggests that the general solution of (1) should be either a combination oscillation which exhibits two basic frequencies or a mono-frequency oscillation with a long-period beat. Two noteworthy special cases are (i) a stable periodic solution corresponding to a beat of vanishing amplitude and (ii) a transient solution characterized by an envelope which is the limit of a beat with least period tending to infinity. The limit envelope is unstable and consists of separatrices departing from and returning to a stationary envelope. The latter, in turn, corresponds to an unstable periodic solution of (1). The periodic solutions are well-known and have been uncovered by rigorous

methods. It is, of course, always reassuring to find that particular known behavior is properly embedded within results inferred from formal procedures. I intend to show that in this case at least, the suggested general behavior of (1) is, in fact, correct as $\beta \to 0$. In doing so, I shall introduce an artifice for extending the application of the method of averaging to distinctly new problem areas. I'm referring here to rigorous applications of the averaging method and not to the intuitive or formal applications which are very popular. This work will appear in a short paper scheduled for publication in the Journal of the Society for Industrial and Applied Mathematics.

First we introduce the van der Pol variables (a, b) by equations

(2)
$$x = a \cos \lambda t + b \sin \lambda t$$

$$\dot{x} = -\lambda a \sin \lambda t + \lambda b \cos \lambda t$$

and slow time s by the equation

$$s = \frac{\beta}{2\lambda} t,$$

then (1) is equivalent to the variational system

$$\frac{da}{ds} = - \left[\eta + \frac{3}{4} A^2 \right] b - f_1(a, b, s)$$

(3)

$$\frac{db}{ds} = \left[\eta + \frac{3}{4} A^2 \right] a + F_o + f_2(a, b, s),$$

where

$$A^2 = a^2 + b^2, \qquad \eta = \frac{\lambda^2 - n^2}{\beta}$$

$$f_1(a, b, s) = \left[\eta + \frac{3}{4} A^2 + \frac{3}{4} (b^2 - \frac{a^2}{3}) + \frac{F_o}{a} \right] a \sin 4\lambda \frac{2s}{\beta}$$

$$-\left[\eta + \frac{3}{4}A^2 + \frac{3}{4}(\frac{b^2}{3} - a^2)\right] b \cos 4\lambda^2\frac{s}{\beta}$$

$$+ \frac{3}{4}(\frac{a^2}{3} - b^2) a \sin 8\lambda^2\frac{s}{\beta} + \frac{3}{4}(\frac{b^2}{3} - a^2) b \cos 8\lambda^2\frac{s}{\beta},$$

$$f_2(a, b, s) = \left[\eta + \frac{3}{4}A^2 + \frac{3}{4}(a^2 - \frac{b^2}{3})\right] b \sin 4\lambda^2\frac{s}{\beta}$$

$$+ \left[\eta + \frac{3}{4}A^2 + \frac{3}{4}(\frac{a^2}{3} - b^2) + \frac{F_o}{a}\right] a \cos 4\lambda^2\frac{s}{\beta}$$

$$+ \frac{3}{4}(\frac{a^2}{3} - b^2) a \cos 8\lambda^2\frac{s}{\beta} + \frac{3}{4}(a^2 - \frac{b^2}{3}) b \sin 8\lambda^2\frac{s}{\beta}.$$

This is the traditional variation of parameters method and there are no approximations involved here. In slow time s, f_1 and f_2 are rapidly varying terms of zero mean value and the averaged equations associated with (3) are simply

(4)
$$\frac{da}{ds} = -\left[\eta + \frac{3}{4}A^2\right] b$$

$$\frac{db}{ds} = \left[\eta + \frac{3}{4}A^2\right] a + F_o.$$

One might suspect that some aspects of the true behavior of the Duffing oscillator might be reflected in these simple equations. We shall return to this question presently.

The solutions of (4), the averaged system, have been discussed in detail in a paper which appeared in the Archive of Rational Mechanics and Analysis last year. Trajectories for typical cases are illustrated in Figs. 1 and 2. Nearly all of the solutions of (4) are periodic (actually elliptic functions) and these would depict long-period beats of the motion. In slow time, the least periods are independent of β, as is (4), if the detuning is held constant. The averaged system possesses the integral

(5)
$$(\eta + \frac{3}{8}A^2) A^2 + 2F_o a = c,$$

where c is a constant. The various trajectories, of course, correspond
to particular choices of the integration constant c, as indicated in Fig. 1.
The centers correspond to stationary oscillations and are located so as
to give the known values for the amplitudes of the stable periodic solu-
tions of (1). The saddle point in Fig. 2 corresponds to the unstable
periodic solution of (1).

For a permissible value of c, we let Γ_c denote the locus defined by
(5) along which the motion given by (4) is periodic of least period P_c.
For later considerations, it is convenient now to picture the trajectory
as being wound about a cylinder in (a, b, s)-space which has for its
crossection, Γ_c. (See Fig. 3.) Actually, the cylinder is composed
entirely of trajectories since the phase is arbitrary. The cylinder is
then referred to as an integral manifold. Since there exists an integral,
the equation of first variation of (4) with respect to a periodic solution
will of necessity admit two zero characteristic exponents and the method
of averaging does not apply. Hence, we look for a similar but more
amenable system. What is desired is a system which will permit a
rigorous application of the method of averaging and at the same time will
not be totally unlike the one we have. In order to apply the method of
averaging we shall make the Γ_c-cylinder rather special. We shall force
the neighboring trajectories to move toward the cylinder without altering
the cylinder itself. In the original circumstance this is not the case
since all neighboring solutions also lie on similar cylinders. The transient
behavior of neighboring solutions is a characteristic requirement for the
mathematical theory of averaging. One seems to get nowhere without
it!

Let us introduce the function

$$(6) \qquad I(a, b, c) \equiv \left(\eta + \frac{3}{8} A^2\right) A^2 + 2F_o a - c,$$

and then consider the auxiliary system

$$(7) \qquad \frac{da}{ds} = -\left[\eta + bI(a, b, c) + \frac{3}{4} A^2\right] b - f_1(a, b, s)$$

$$\frac{db}{ds} = \left[\eta + bI(a, b, c) + \frac{3}{4} A^2\right] a + F_o + f_2(a, b, s).$$

The averaged equations associated with (7) are

(8)
$$\frac{da}{ds} = -\left[\eta + bI(a, b, c) + \frac{3}{4} A^2\right] b$$

$$\frac{db}{ds} = \left[\eta + bI(a, b, c) + \frac{3}{4} A^2\right] a + F_o$$

and retain the particular periodic solution along Γ_c since the auxiliary term $bI(a, b, c)$ vanishes every where on Γ_c. However, the equation of first variations of (8) with respect to the periodic solution along Γ_c now possesses but one zero characteristic exponent. Indeed, since (8) is autonomus, one characteristic exponent is zero and the second is given by the well-known expression

$$\frac{1}{P_c} \int_0^{P_c} \text{trace } H \, ds',$$

where H is the coefficient matrix of the equation of first variation evaluated along Γ_c. Since the contribution of the original terms in (4) to this definite integral is zero, one need only compute the contribution of the auxiliary terms in (8). These are readily found to give

$$\frac{1}{P_c} \int_0^{P_c} \text{trace } H \, ds = -\frac{2F_o}{P_c} \int_0^{P_c} b^2 \, ds < 0.$$

Thus, the periodic solution along Γ_c is now asymptotically (orbitally) stable. The neighboring solutions tend to the Γ_c-cylinder. Accordingly, for each sufficiently small $|\beta|$, there will be an asymptotically stable integral manifold M_c of the auxiliary system (7) lying near the corresponding Γ_c-cylinder. This manifold will not be a cylinder but will vary slightly in crossection. (See Fig. 4.) However, throughout its entire length it will lie near the Γ_c-cylinder. More specifically, there exists functions $a*(s, \theta, \beta)$, and $b^*(s, \theta, \beta)$, periodic in s and θ of periods $\beta\pi/\lambda$ and P_c respectively, which satisfy the inequality

(9) $\left| a^*(s, \theta, \beta) - a_c(\theta) \right| + \left| b^*(s, \theta, \beta) - b_c(\theta) \right| \leq \delta(\beta)$

for all s and θ, with $\delta(\beta) \to 0$ as $\beta \to 0$. Here a_c and b_c denote solution functions for the periodic motion along Γ_c. On the manifold the system (7) is equivalent to a differential equation of the form

$$\frac{d\theta}{ds} = 1 + F(s, \theta, \beta), \qquad \text{where} \quad \left| F(s, \theta, \beta) \right| \leq \delta(\beta).$$

This describes how a particular trajectory is wound about the manifold. Thus, not only is the manifold near the Γ_c-cylinder for small $\left| \beta \right|$, but the motion on the manifold is nearly the same as that along Γ_c. We note in passing that for a suitable constant k, the inequality

(10) $\left| I(a, b, c) \right| \leq k\, \delta(\beta)$

is satisfied everywhere on M_c.

Suppose now that $a(s)$, $b(s)$ is a solution of the original variational system (3) with initial point on Γ_c and $a^*(s) = a^*(s, \theta(s), \beta)$, $b^*(s) = b^*(s, \theta(s), \beta)$ is a particular solution of (7) lying on the manifold M_c with initial point within $\delta(\beta)$ of $a(0)$, $b(0)$. We may express each of (3) and (7) in integral equation form. For example (3) may be written

$$a(s) = a(0) - \int_0^s \left\{ \left[\eta + \frac{3}{4} A^2 \right] b - f_1(a, b, \sigma) \right\} d\sigma$$

$$b(s) = b(0) + \int_0^s \left\{ \left[\eta + \frac{3}{4} A^2 \right] a + F_0 + f_2(a, b, \sigma) \right\} d\sigma$$

When similar equations are written for (7) all terms correspond except the initial values and the auxiliary terms proportional to bI. If these equations are subtracted from the above, one readily derives the inequality

$$\left| a(s) - a^*(s) \right| + \left| b(s) - b^*(s) \right| \le K \int_0^s \left[\left| a(\sigma) - a^*(\sigma) \right| + \left| b(\sigma) - b^*(o) \right| + \delta(\beta) \right] d\sigma + \delta(\beta)$$

where K is a suitable positive constant. We have used the inequality (10) here for the additional bl-terms and this accounts for the $\delta(\beta)$ term inside the integral. The $\delta(\beta)$ term outside accounts for the slightly different initial values. Using a familiar argument of Bellman this, in turn, leads to the inequality

(11) $$\left| a(s) - a^*(s) \right| + \left| b(s) - b^*(s) \right| \le 2\delta(\beta) \ e^{Ks}.$$

The inequality (11) furnishes a bound on the growth of the difference between the unknown exact solution and a known approximate solution lying on the manifold M_c. Now if $\varepsilon > 0$, we may define, for small $|\beta|$, the positive number

(12) $$R(\beta) = \frac{1}{K} \ \ln \frac{\varepsilon}{2\delta(\beta)} \ .$$

Then, implies that

(13) $$\left| a(s) - a^*(s) \right| + \left| b(s) - b^*(s) \right| \le \varepsilon$$

for $0 \le s \le R(\beta)$. Clearly, (12) implies that $R(\beta) \to \infty$ as $\beta \to 0$.

This, together with the inequality (9), establishes the following theorem.

APPROXIMATION THEOREM. Let $a(s)$, $b(s)$ be a solution of (3) with initial values lying on a locus Γ_c corresponding to a nontrivial periodic solution $a_c(s)$, $b_c(s)$ of the averaged system (4). If $\Delta > 0$, then there exist for $|\beta|$ small, two functions $\delta(\beta)$ and $R(\beta) > 0$ such that

(14)   (i) $$\left| a(s) - a_c(\theta(s)) \right| + \left| b(s) - b_c(\theta(s)) \right| \le \Delta$$

is satisfied for $0 \le s \le R(\beta)$.

(ii) The function $\theta(s)$ satisfies a differential equation of the form

$$\frac{d\theta}{ds} = 1 + F(s, \theta, \beta)$$

for which $|F(s, \theta, \beta)| \le \delta(\beta)$ for all s and θ. Furthermore, $\delta(\beta) \to 0$ and $R(\beta) \to \infty$ as $\beta \to 0$.

It is important to notice that while the beat period P_c in slow time s is fixed, the approximation (14) is valid throughout an interval tending to infinity as β tends to zero. Thus the basic long-period beat phenomena is most certainly a true characteristic of the exact solution.

I would now like to touch on some interpretations and implications. It is clear from (7) that the auxiliary bI-terms may be lumped into the detuning parameter η to form an equivalent (non constant) detuning parameter

$$\eta_* = \eta + bI.$$

Recalling that

$$\eta = \frac{\lambda^2 - n^2}{\beta}$$

the effect may be visualized as a change of either imput frequency or of natural frequency. For instance, if we let $a^*(s)$, $b^*(s)$ be a solution of (7) lying on the manifold M_c and define λ_* by the equation

(15) $\lambda_*^2(t) = \lambda^2 + \beta b^* I = \lambda^2 + \beta b^*(\frac{\beta t}{2\lambda}) \cdot I(a^*(\frac{\beta t}{2\lambda}), b^*(\frac{\beta t}{2\lambda}), c),$

then we conclude from (10) that there exists a constant k_1 such that

(16) $|\lambda_*(t) - \lambda| \le k_1 \beta \delta(\beta)$

for all t. The auxiliary system (7) then becomes the exact variational system for the equation

(17) $\ddot{x} + n^2 x - \beta x^3 = \beta F_o \cos \lambda_* t,$

where the exciting frequency λ_* is sensibly constant. In fact, according to (16), the difference between λ_* and the constant λ is small even when compared to β . In many applications, there may be no practical difference between (17) and (1). But perhaps even more significant is the fact that with similar small variations in the exciting frequency the envelope of the oscillation could vary rather arbitrarily. Indeed, if $c(s)$ is any continuous function wity values corresponding to periodic trajectories of (4), then the auxiliary system (7) with c replaced by $c(s)$ will possess a "variable" manifold $M_{c(s)}$. Since the region near $M_{c(s)}$ is always one of attraction, $M_{c(s)}$ will "drag along" neighboring solutions. If the movement is sufficiently slow, a particular solution will remain close of order $\delta(\beta)$ for all s. The imput frequency modulations as computed above will then be small of order $\beta\delta(\beta)$. There is, therefore, an uncertainty in the ultimate behavior of practical systems described by (1) and a precise characterization of the solutions of (1) beyond that given here is likely to be of limited practical interest. Only very minor fluctuations in exciting frequency may induce large changes in the response.

Alternatively one might use the identities

$$a = x \cos \lambda t - \frac{\dot{x}}{\lambda} \sin \lambda t$$

$$b = x \sin \lambda t + \frac{\dot{x}}{\lambda} \cos \lambda t,$$

which are obtained by inverting the transformation (2), and define a nonconstant frequency n_* by the equation

$$n_*^2 (x, \dot{x}, t) = n^2 - \beta b I(a, b, c).$$

The auxiliary system (7) then becomes the exact variational system for the equation

(19) $$x + n_*^2 x - \beta x^3 = \beta F_o \cos \lambda t.$$

Again, with initial values near Γ_c , the difference between n_* and the constant n is small like $\beta\delta(\beta)$. If c is changed slowly, a solution of (19) will trail along accordingly.

Finally I should like to mention a recent result obtained by Jürgen Moser which relates to this problem. He has shown that for nearly all values of the input frequency λ the solutions of (1) are almost-periodic with exactly two basic frequencies. The exceptions are just the nearly resonant cases, one of which we have concentrated on here. His result applied here coincides with our view of those trajectories which are far removed from the origin in Figs. 1 and 2. Thus we have the rather fascinating situation where the periodic responses emerge in the very heart of the resonance region while the almost periodic responses emerge in the far removed regions. Evidentally, these special solutions are linked together by curious beating-type responses which up to now have escaped rigorous detection.
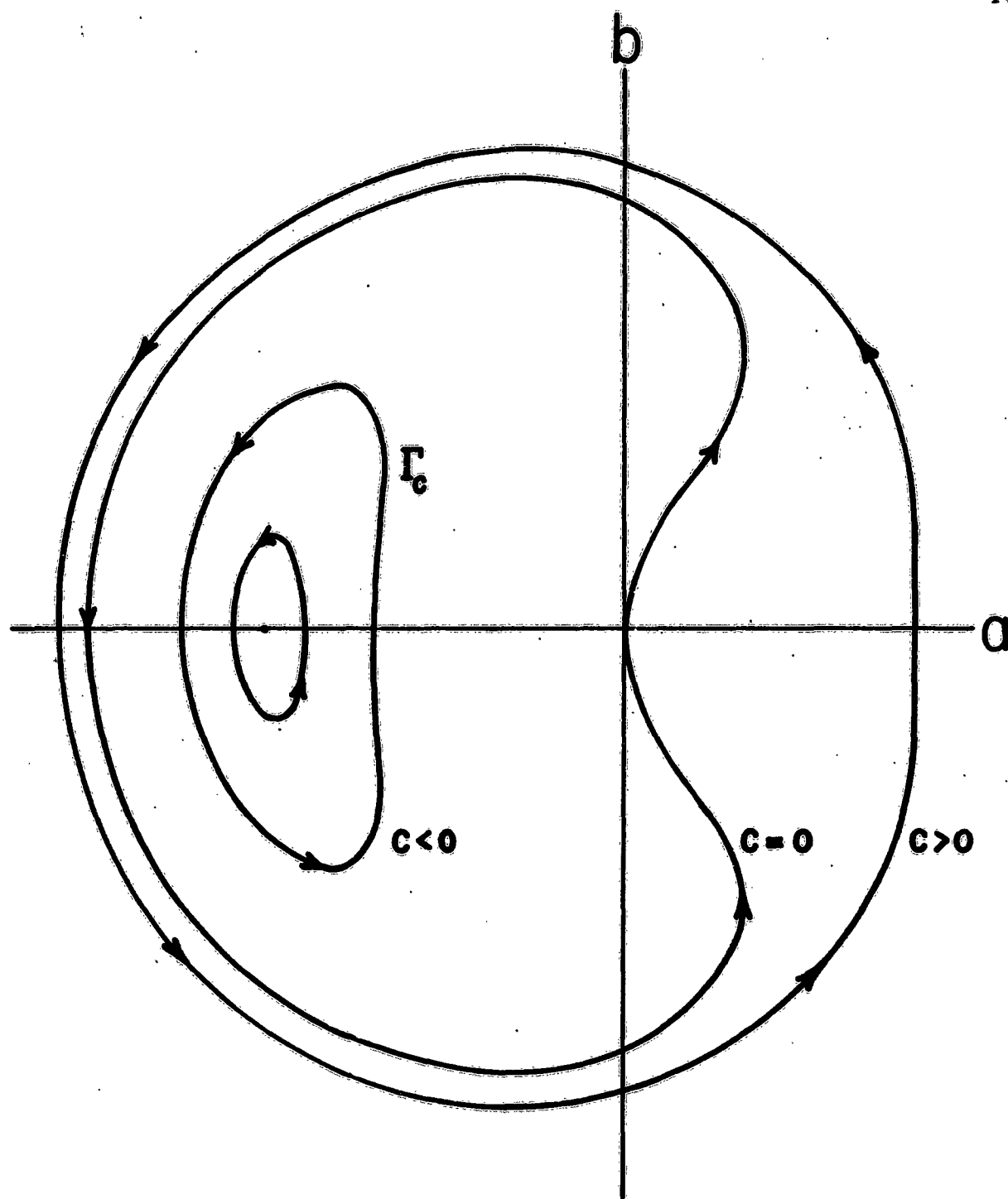
Figure 1
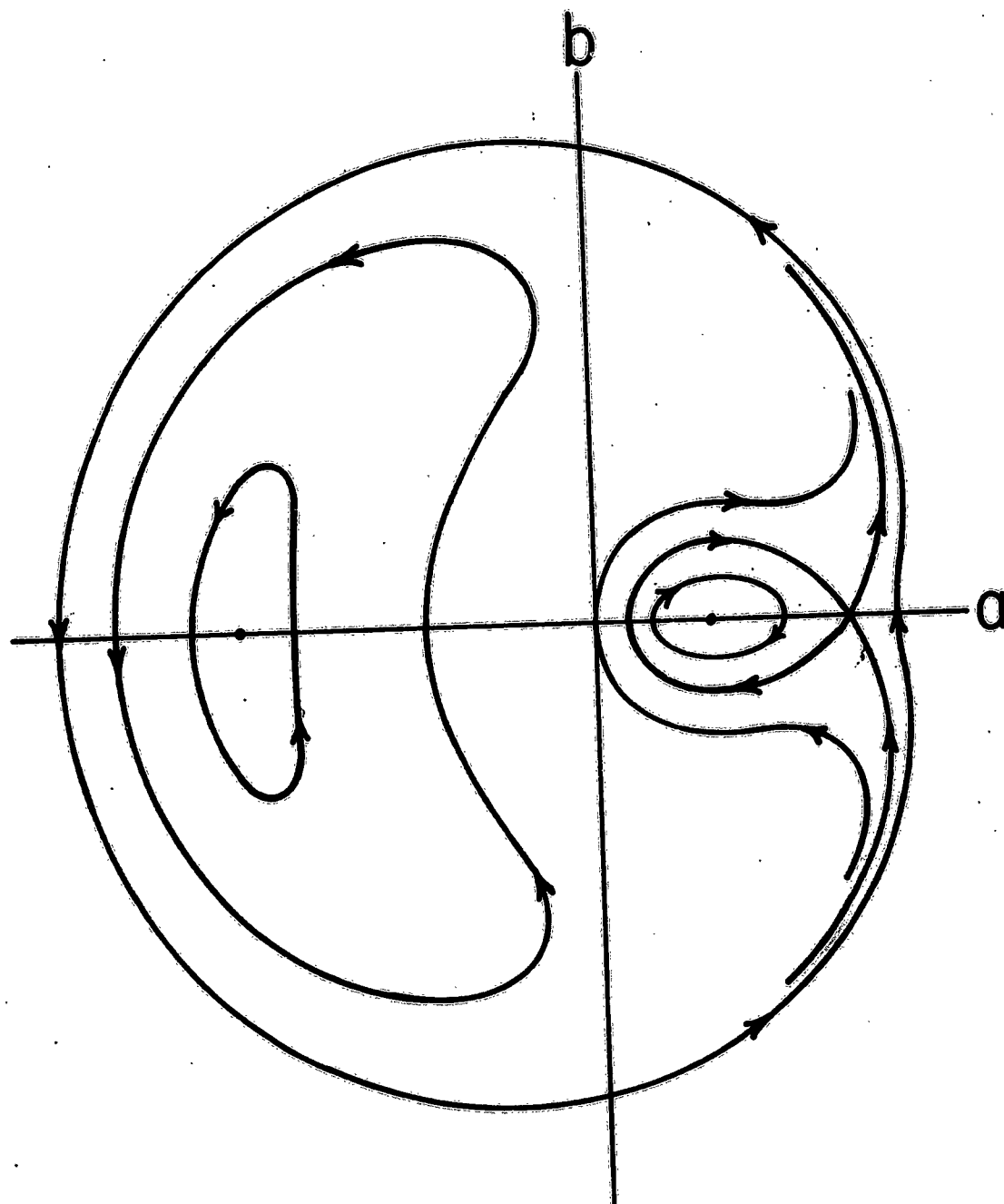
Figure 2
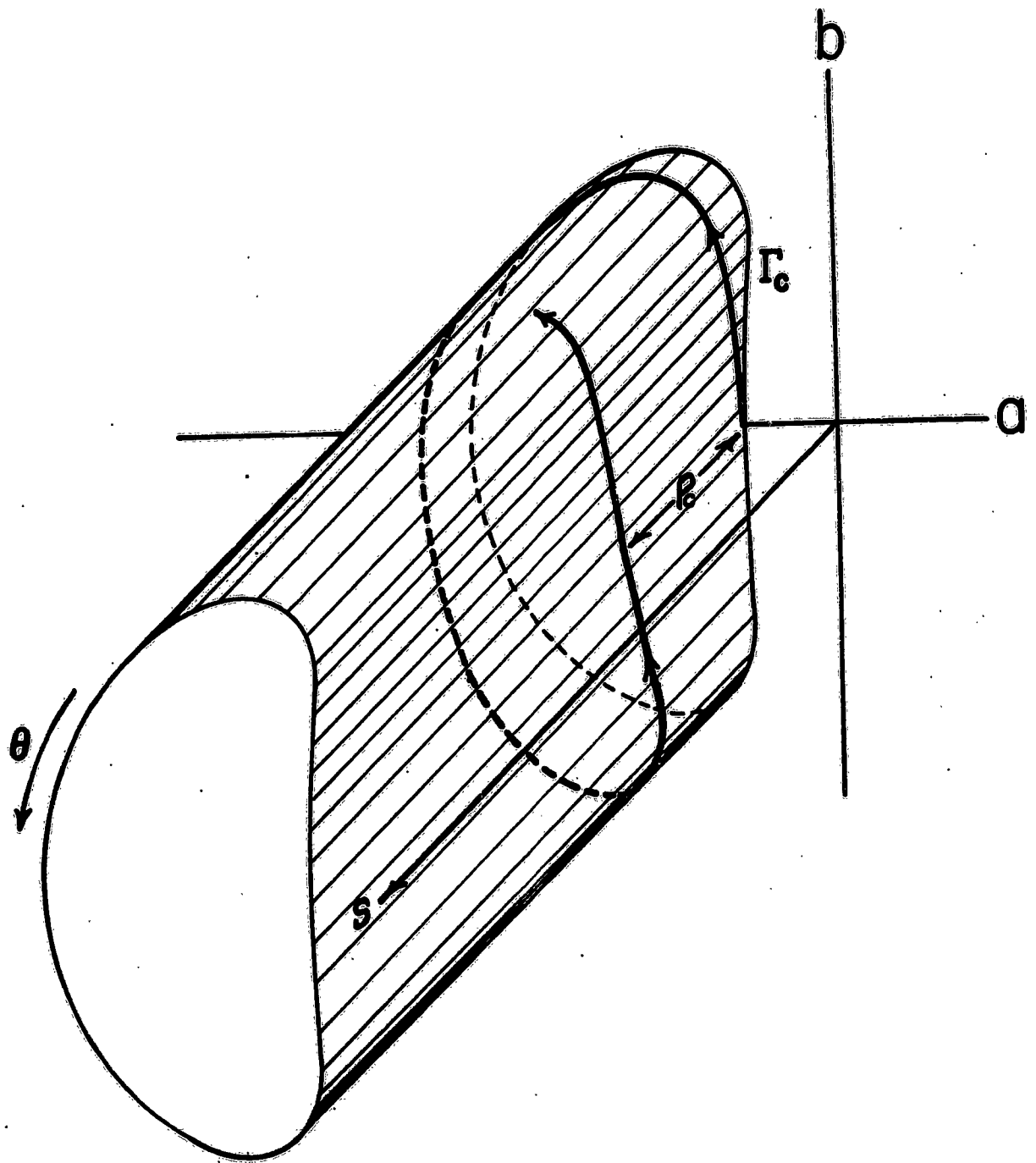
Figure 3
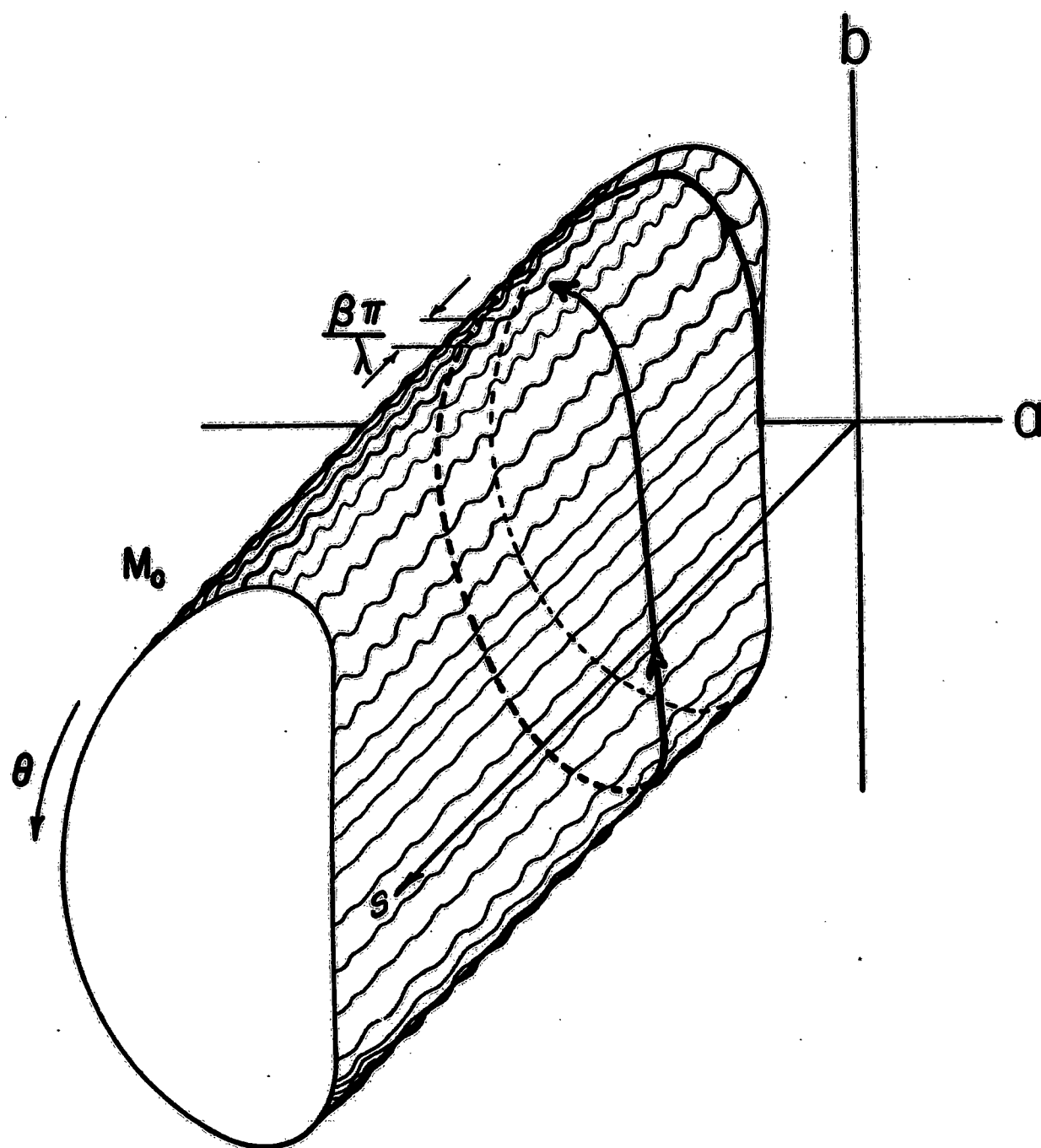
Figure 4

SOME ASPECTS OF NONLINEAR VISCOELASTICITY

Julian L. Davis
Explosive and Propellant Laboratory
Picatinny Arsenal, Dover, New Jersey

I. <u>INTRODUCTION</u>. This work was motivated by the need to attempt to understand the response of viscoelastic media to dynamic loads in the non-linear range. A variety of military problems in the plastics and packaging area involve the response of viscoelastic media to finite amplitude oscillatory deformations and stresses applied on the boundaries. The classical linear theory of viscoelasticity is unable to adequately explain some experimental results for such finite amplitude boundary conditions which destroy the linearity of the response of the elastic and viscous elements of the medium. We have therefore sought to formulate a nonlinear theory for dynamic loading that would keep the essential features of the medium and yet be simple enough to lend itself to mathematical analysis using elementary techniques.

We restrict ourselves here to a one-dimensional discrete viscoelastic medium including mass. Perhaps the most natural way to introduce small nonlinearities in the medium is in the elastic element through the elastic modulus and in the viscous element through the viscosity coefficient. (This will be explained in Section 2 "Nonlinear Hypothesis". We apply the method to single Voigt and Maxwell models with and without mass and then to coupled models, restricting ourselves, in this paper, to first order nonlinearities. The main results are that the response of a nonlinear Voigt model to a sinusoidally applied stress is governed by a "nonlinear complex compliance", and the response of a nonlinear Maxwell model to a sinusoidally applied strain is governed by a "nonlinear complex modulus". The extension to coupled systems involves complex compliances or moduli that are the sums of the moduli of the individual elements.

2. <u>NONLINEAR HYPOTHESIS</u>. We shall characterize a single Voigt and Maxwell model by the following parameters: m-mass, a positive constant; E-nonlinear elastic coefficient, η -nonlinear viscosity coefficient. For a coupled system let E_i, η_i be the parameters of the i th element of the system (Voigt or Maxwell). Let the positive constant E_0 be the linear elastic coefficient

(Young's Modulus for compression or tension), and η_o be the linear viscosity coefficient. Let ϵ_E be the strain on the elastic element and ϵ_η the strain on the viscous element. Our hypothesis of nonlinearity is as follows: Assume we can approximate E by an Nth degree polynomial in ϵ_E whose leading term is E_o and η by an Nth degree polynomial in $\dot\epsilon^*_\eta$ whose leading term is η_o, restricting ourselves to a first order nonlinear theory. Specifically:

(1) $$E = E_o + \gamma_E f(\epsilon_E), \quad \eta = \eta_o + \gamma_\eta g(\dot\epsilon_\eta)$$

(2) $$f(\epsilon_E) = \sum_{j=1}^{N} a_{1j}\, \epsilon_E^{j}, \quad g(\dot\epsilon_\eta) = \sum_{j=1}^{N} a_{2j}\, \dot\epsilon_\eta^{j}.$$

γ_E, (γ_η) are dimensionless constants that give a measure of nonlinearity in the spring, (dashpot). The set of constants $\{a_{1j}\}$ are considered to be known functions of E_o and $\{a_{2j}\}$ known functions of η_o. We further specialize (2) to two cases: (a) $N = 1$ which we call "quadratic nonlinearity"; (b) $N = 2$, "cubic nonlinearity."

3. <u>SINGLE VOIGT MODEL</u>. Consider a single Voigt model with mass. It is composed of an inertial element (mass), an elastic element (spring), and a viscous element (dashpot) coupled in parallel. The model is defined by the following conditions:

(3) $$\epsilon_\eta = \epsilon_E = \epsilon_m = \epsilon$$

(4) $$\sigma_m + \sigma_\eta + \sigma_E = \sigma,$$

where $(\epsilon_\eta, \epsilon_E, \epsilon_m)$ represents the strain on the viscous, elastic, and inertial elements, respectively, and $(\sigma_\eta, \sigma_E, \sigma_m)$ represents the stress on those elements. The boundary condition is given by σ, the applied time varying stress. In this paper σ will be a given sinusoidal function of time. The following constitutive equations are assumed for each of the

---

* We use the notation $\dot f = \dfrac{df}{dt}$

elements:

(5) $\quad \sigma_m = m\ddot{\epsilon}, \; \sigma_\eta = \eta\dot{\epsilon}, \; \sigma_E = E\epsilon \, ,$

where m is the mass per unit length. E and η are governed by (1) and (2).
The system of equations (1) . . . (5) completely defines our model for a
prescribed set of internal parameters $\left\{ \delta_E, \delta_\eta ; \, a_{1j}, \, a_{2j} \right\}$ and boundary
condition $\sigma(t)$. Inserting (5) into (4) and using (1) yields the following
nonlinear ordinary differential equation governing the response of the model
to a prescribed $\sigma(t)$:

(6)
$$\ddot{\epsilon} + 2\zeta\dot{\epsilon} + \omega_0^2\epsilon + \delta_E f(\epsilon)\epsilon + \delta_\eta g(\dot{\epsilon})\dot{\epsilon} = \sigma/m \, ,$$
$$\omega_0^2 = \frac{E_0}{m}, \quad 2\zeta = \frac{\eta_0}{m} \, ,$$

where ω_0 is the natural frequency of vibration and ζ is called the "damping
coefficient." It is thus seen that the problem of finding the response of our
nonlinear Voigt model with mass to a prescribed $\sigma(t)$ is transformed to that
of solving a nonlinear ordinary differential equation for ϵ. But (6) is a
well-known type of equation occurring in the theory of nonlinear vibrations
and is called (under certain circumstances) Duffing's equation [1, 2]. One
point worth mentioning here: We do not make the restriction that $\sigma(t)$ is of
the order of δ_E or δ_η which appears to be made in the standard works on
nonlinear mechanics. Summarizing thus far: We have transformed the
problem into that of solving a problem in nonlinear vibrations.

We now seek periodic solutions of (6) for a prescribed periodic $\sigma(t)$
by the following perturbation method: Expand ϵ in a power series in δ_E
and δ_η where the coefficients are functions of time to be determined.

(7) $\quad \epsilon = \epsilon_0 + \sum_{m=1}^{\infty} \delta_E^m \epsilon_\eta + \sum_{n=1}^{\infty} \delta_\eta^n e_m \, ,$

where $\epsilon_1, \epsilon_2, \ldots e_1, e_2, \ldots$ are unknown functions of t which
are determined by an infinite set of <u>linear</u> nonhomogeneous differential

equations obtained by inserting (7) into (6), using (2), and setting the coefficient of each power of δ_E and δ_η separately equal to zero (since δ_E and δ_η are independent parameters). We get:

$$\ddot{\epsilon}_0 + 2\zeta\dot{\epsilon}_0 + \omega_0^2\epsilon_0 = \frac{\sigma(t)}{m}$$

(8)
$$\ddot{\epsilon}_i + 2\zeta\dot{\epsilon}_i + \omega_0^2\epsilon_i = F_i(\epsilon_0, \epsilon_1, \ldots, \epsilon_{i-1}, e_1, e_2, \ldots, e_{i-1})$$

$$\ddot{e}_i + 2\zeta\dot{e}_i + \omega_0^2 e_i = G_i(\epsilon_0, \epsilon_1, \ldots, \epsilon_{i-1}, e_1, e_2, \ldots, e_{i-1})$$

where the forcing functions $\{F_i, G_i\}$ are known functions of their arguments. In practice, of course, a finite number of equations in (8) are used where the number of terms of the M th partial sums approximating the right hand side of (7) depends on the rapidity of the convergence of these series which in turn depends on the magnitude of the parameters that control the nonlinearity. M is called the order of nonlinearity. Since we consider in this paper only first order nonlinearity M = 1 and (7) becomes

(9)
$$\epsilon = \epsilon_0 + \delta_E\epsilon_1 + \delta_\eta e_1$$

ϵ_1, e_1 , are the first order perturbing functions. We now consider special cases.

3-a. <u>VOIGT WITHOUT MASS - QUADRATIC NONLINEARITY</u>. Specializing (2) to the case of quadratic nonlinearity by setting $N = 1, a_{1j} = E_0\delta_{ij}, a_{2j} = \frac{E_0}{\lambda^2}\delta_{2j}$; $\delta_{ij} = \begin{cases} 1 & i = j \\ 0 & i \neq j \end{cases}$, we get

(10) $f(\epsilon_E) = E_0\epsilon, \quad g(\dot{\epsilon}_\eta) = \frac{E_0\dot{\epsilon}}{\lambda^2}, \quad \lambda = \frac{E_0}{\eta_0}$,

since $\epsilon_E = \epsilon_\eta$ for a Voigt model. λ is called the retardation time for a linear Voigt model without mass. Specializing (6) to the case of zero mass we get

(11) $\dot{\epsilon} + \lambda\epsilon + \delta_E\lambda\epsilon^2 + \delta_\eta\dot{\epsilon}^2 = \frac{\bar{\sigma}e^{i\omega t}}{\eta_0}$,

where $\bar{\sigma}$ is the amplitude and ω is the frequency of the applied stress.

Note that the order of the differential equation is reduced by one so that an initial condition is lost. We are not concerned with this point here since we are only interested in the steady state solution. This case of zero mass was solved [3]. The solution is

$$(12) \qquad \epsilon = J^* \bar{\sigma} ,$$

where J^* is called the "nonlinear complex compliance" and is given by

$$(13) \quad J^* = J_0^* + \left(\delta_E - \frac{\delta \eta}{\mu^2} \right) J_1^* ; \qquad \mu = \frac{\lambda}{\omega} = \frac{E_0}{\eta_0 \omega} ,$$

where μ is a dimensionless frequency and J_0^* and J_1^* are complex valued functions of μ given by

$$(14) \quad J_0^* = J_0' + i J_0'' ; \quad J_0' = \frac{\mu^2}{E_0(1+\mu^2)} , \quad J_0'' = -\frac{\mu}{E_0(1+\mu^2)} ,$$

$$J_1^* = J_1' + i J_1'' = \frac{w\, e^{i\omega t}}{\bar{\sigma}} , \quad w = u + i v , \quad u = \frac{\mu(5-\mu^2)}{(\mu^2+4)(\mu^2+1)^2} ,$$

$$(15)$$
$$v = -\frac{2\mu^2(1-2\mu^2)}{(\mu^2+4)(\mu^2+1)^2} , \quad J_1' = \bar{\sigma}(u\cos\omega t - v\sin\omega t),$$

$$J_1'' = \bar{\sigma}(v\cos\omega t + u\sin\omega t) .$$

J_0^* is the standard complex modulus for a single linear Voigt model without mass. J_1^* represents the first order nonlinear contribution to J^*. Note that J_1^* is a sinusoidal function of t whose amplitude $\frac{w}{\bar{\sigma}}$ is frequency dependent according to the expressions for u and v.

3-b VOIGT WITH MASS – CUBIC NONLINEARITY. Consider the nonlinear differential equation (6) representing the Voigt model with mass. For cubic nonlinearity N=2 in (2) so that

$$(16) \quad f(\epsilon) = a_{11}\epsilon + a_{12}\epsilon^2, \quad g(\dot{\epsilon}) = a_{21}\dot{\epsilon} + a_{22}\dot{\epsilon}^2$$

Putting (16) into (6) and using (9), the perturbation method yields the following

system of linear differential equations (setting $\sigma = \bar{\sigma} \cos \omega t$) :

$$\ddot{\epsilon}_0 + 2\zeta\dot{\epsilon}_0 + \omega_0^2\epsilon_0 = F\cos\omega t, \quad \ddot{\epsilon}_1 + 2\zeta\dot{\epsilon}_1 + \omega_0^2\epsilon_1 = C \ ,$$

(17)

$$\ddot{e}_1 + 2\zeta\dot{e}_1 + \omega_0^2 e_1 = D$$

where

(18) $-C = a_{11}\epsilon_0^2 + a_{12}\epsilon_0^3 \ , \quad -D = a_{21}\dot{\epsilon}_0^2 + a_{22}\dot{\epsilon}_0^3 \ , \quad F = \dfrac{\bar{\sigma}}{m}$

the solution for ϵ_0 is

$$\epsilon_0 = A\cos\omega t + B\sin\omega t$$

(19)

$$A = \frac{Fx}{\Delta} \ , \quad B = \frac{Fy}{\Delta} \ , \quad x = \omega_0^2 - \omega^2, \quad y = 2\zeta\omega, \quad \Delta = x^2 + y^2$$

The forcing functions C and D are given by

$$C = \sum_{n=1}^{3} (c_n \cos n\omega t + \bar{c}_n \sin n\omega t)$$

(20)

$$D = \sum_{n=1}^{3} (d_n \cos n\omega t + \bar{d}_n \sin n\omega t) \ ,$$

(21)

$$c_1 = -\frac{3\,a_{11}x F^3}{4\Delta^2} \ , \quad c_2 = \frac{a_{11}(y^2 - x^2) F^2}{2\Delta^2} \ , \quad c_3 = \frac{a_{12}x(3y^2 - x^2) F^3}{4\Delta^3}$$

$$\bar{c}_1 = -\frac{3\,a_{12}y F^3}{4\Delta^2} \ , \quad \bar{c}_2 = -\frac{a_{11}xy F^2}{\Delta^2} \ , \quad \bar{c}_3 = \frac{a_{12}y(y^2 - 3x^2) F^3}{4\Delta^3}$$

$$d_1 = -\frac{3\,a_{22}\,\omega^3\,y\,F^3}{4\Delta^2}\ , \quad d_2 = \frac{a_{21}\,\omega^2(y^2 - x^2)\,F^2}{2\Delta^2}\ ,$$

(21)

$$d_3 = \frac{a_{22}\,\omega^3\,y\,(3x^2 - y^2)\,F^3}{4\Delta^3}\ , \quad \bar{d}_1 = \frac{3\,a_{22}\,\omega^3 + F^3}{4\Delta^2}$$

$$\bar{d}_2 = \frac{a_{21}\,\omega^2\,x\,y\,F^2}{\Delta^2}\ , \quad \bar{d}_3 = \frac{a_{22}\,\omega^3\,x\,(3y^2 - x^2)\,F^3}{4\Delta^3}$$

The solution for ϵ_1 and e_1 is given by

$$(22)\ \epsilon_1 = \sum_{n=1}^{3} (f_n \cos n\omega t + \bar{f}_n \sin n\omega t),\ e_1 = \sum_{n=1}^{3} (g_n \cos n\omega t + \bar{g}_n \sin n\omega t).$$

Putting (22) into (17-b, c), using (20) for C and D, and equating coefficients of like harmonics of $\cos n\omega t$ and $\sin n\omega t$, we get

$$f_n = \frac{x_n c_n - y_n \bar{c}_n}{\Delta_n}\ , \quad \bar{f}_n = \frac{x_n \bar{c}_n + y_n c_n}{\Delta_n}\ ; \quad \Delta_n = x_n^2 + y_n^2\ , \ \Delta_1 = \Delta,$$

(23)

$$g_n = \frac{x_n d_n - y_n \bar{d}_n}{\Delta_n}\ , \quad \bar{g}_n = \frac{x_n \bar{d}_n + y_n d_n}{\Delta_n}\ ; \quad x_n = \omega_o^2 - n^2\omega^2,\ y_n = 2n\zeta\omega$$

Now consider only the fundamental mode. This is obtained by setting $f_n = \bar{f}_n = g_n = \bar{g}_n = 0$ for $n = 2, 3$. The perturbing functions ϵ_1 and e_1 become

$$\epsilon_1 = f_1 \cos \omega t + \bar{f}_1 \sin \omega t,\ e_1 = g_1 \cos \omega t + \bar{g}_1 \sin \omega t;\ f_1 = \frac{3\,a_{12}(y^2 - x^2)\,F^3}{4\Delta^3}\ ,$$

(24)

$$\bar{f}_1 = -\frac{3\,a_{12}\,x\,y\,F^3}{2\Delta^3}\ , \quad g_1 = -\frac{3\,a_{22}\,\omega^3\,x\,y\,F^3}{2\Delta^3}\ , \quad \bar{g}_1 = \frac{3\,a_{22}\,\omega^3(x^2 - y^2)\,F^3}{4\Delta^3}$$

We observe that f_1, $\bar{f}_1$ are functions of ω that depend only on the ϵ^2 term in $f(\epsilon)$ and g_1, g_2 depend only on the $\dot{e}^2$ term in $g(\dot{e})$, i.e. $f_1, \ldots, \bar{g}_1$, depend only on the "cubic" part of the nonlinearity (see (16)). This means: for the case of "quadratic" nonlinearity where $a_{12} = a_{22} = 0$ in (16),

$$f_1 = \bar{f}_1 = g_1 = g_1 = 0 \qquad\qquad \text{so that the fundamental}$$

mode does not appear in the nonlinear part of the solution. The same is true for the Voigt model without mass. That is why the nonlinear part of the solution for in SECTION 3.-a does not involved the fundamental mode.

Gathering the above results the nonlinear complex compliance becomes

$$J^* = J' + iJ'' = J_0' + J_1' + i(J_0'' + J_1''),$$

(25) $J_0' = A, \quad J_0'' = -B; \quad J_1' = \delta_E f_1 + \delta_\eta \bar{f}_1, \quad -J_1'' = \delta_E g_1 + \delta_\eta \bar{g}_1.$

A, B are given by (19) and $f_1, \ldots, \bar{g}$, are given by (24).

4. **SINGLE MAXWELL MODEL.** Consider a single Maxwell model with mass. It consists of a mass, spring and dashpot in series, and is defined by the following conditions:

(26) $\sigma_E = \sigma_\eta = \sigma_m = \sigma$

(27) $\epsilon_E + \epsilon_\eta + \epsilon_m = \epsilon$

where ϵ is the applied strain and is a given sinusoidal function of time. The constitutive equations are

(28) $\epsilon_E = \dfrac{\sigma}{E}, \quad \dot{\epsilon}_\eta = \dfrac{\sigma}{\eta}, \quad \ddot{\epsilon}_m = \dfrac{\sigma}{m},$

where E and η are given by (1). For the case of cubic nonlinearity N = 2 in (2) so that*

(29)
$$E = E_0 + \delta_E (a_{11} \epsilon_E + a_{12} \epsilon_E^2)$$

$$\eta = \eta_0 + \delta_\eta (a_{21} \dot{\epsilon}_\eta + a_{22} \dot{\epsilon}_\eta^2).$$

---

* We use the same notation as for the Voigt model.
    There is no ambiguity.

Inserting (29) into (28) and keeping only first order terms in γ_E and γ_η we get for ϵ_E and $\dot{\epsilon}_\eta$:

(30)
$$\epsilon_E = \frac{\sigma}{E_o} - \gamma_E \left(\frac{a_{11}\sigma^2}{E_o^3} + \frac{a_{12}\sigma^3}{E_o^4} \right)$$

$$\dot{\epsilon}_\eta = \frac{\sigma}{\eta_o} - \gamma_\eta \left(\frac{a_{21}\sigma^2}{\eta_o^3} + \frac{a_{22}\sigma^3}{\eta_o^4} \right)$$

ϵ_E and $\dot{\epsilon}_\eta$ are cubic polynomials in σ, the linear term occurring for $\gamma_E = \gamma_\eta = 0$. From the above we derive the following nonlinear differential equation which governs the response of the model for the case of cubic non-linearity:

(31)
$$\ddot{\sigma} + \lambda \dot{\sigma} + \omega_o^2 \sigma - \gamma_E \left[\left(\frac{2a_{11}\sigma}{E_o^2} + \frac{3a_{12}\sigma^2}{E_o^3} \right) \ddot{\sigma} + \left(\frac{2a_{11}}{E_o^2} + \frac{6a_{12}\sigma}{E_c^3} \right) \dot{\sigma}^2 \right]$$

$$- \gamma_\eta \lambda \left(\frac{2a_{21}\sigma}{\eta_o^2} + \frac{3a_{22}\sigma^2}{\eta_c^3} \right) \dot{\sigma} = E_o \ddot{\epsilon} .$$

4.-a MAXWELL WITHOUT MASS - QUADRATIC NONLINEARITY. For quadratic nonlinearity $f(\epsilon_E)$, $g(\dot{\epsilon}_\eta)$ are given by

(32)
$$f(\epsilon_E) = E_o \epsilon_E , \quad g(\dot{\epsilon}_\eta) = \frac{E_o}{\lambda^2} \dot{\epsilon}_\eta .$$

The case of the Maxwell model without mass corresponds to letting $\omega_o \rightarrow \infty$ in (31) which becomes:

(33) $\dot{\sigma} + \lambda\sigma - \frac{2\gamma_E \sigma \dot{\sigma}}{E_o} - \frac{\gamma_\eta \sigma^2}{\eta_o} = E_o \dot{\epsilon} = i\omega E_o \bar{\epsilon} e^{i\omega t} ,$

---

* We use the same notation as for the Voigt model.
  There is no ambiguity

for the case $\epsilon = \bar{\epsilon} e^{i\omega t}$. Again the order of the differential equation is reduced by one. This case was solved[3] by the first order perturbation method. The solution is

(34)
$$\sigma = E^* \epsilon ,$$

where the "nonlinear complex modulus" E^* is given by

(35) $E^* = E' + i E''$; $E' = u_0 + u_1 \epsilon$, $E'' = v_0 + v_1 \epsilon$.

The classical complex modulus for a linear Maxwell model without mass is given by

(36)
$$E_0^* = u_0 + i v_0 ; \quad u_0 = \frac{E_0}{1 + \mu^2} , \quad v_0 = \mu u_0 , \quad \mu = \frac{\lambda}{w} ,$$

and the nonlinear portion of E^* is given by

$$Du_1 = 4\delta_E (1 - 2\mu^2) + \delta_\eta \mu^2 (5 - \mu^2) , \quad Dv_1 = 4\delta_E (5 - \mu^2)\mu - 2\delta_\eta (1 - 2\mu^2)$$

(37)
$$E_0 D = (4 + \mu^2)(1 + \mu^2) .$$

(35) shows that the nonlinear portion of E^* depends linearly on ϵ, the coefficients u_1 and v_1, both depending on δ_E, δ_η and μ. Clearly for the linear case $\delta_E = \delta_\eta = 0$ and $E^* = E_0^*$.

4.-b MAXWELL WITH MASS - CUBIC NONLINEARITY. Consider (31) which governs the response of the Maxwell model for this case. The first order perturbation method involves setting

$$(38) \qquad \sigma = \sigma_0 + \delta_E \sigma_1 + \delta_\eta S_1 .$$

Inserting (38) into (31) and keeping only first order terms in δ_E and δ_η we get the following system of linear differential equations for σ_0 and the perturbing functions σ_1, and S_1,:

$$(39) \quad \ddot{\sigma}_0 + \lambda \dot{\sigma}_0 + \omega_0^2 \sigma_0 = G \cos \omega t, \quad \ddot{\sigma}_1 + \lambda \dot{\sigma}_1 + \omega_0^2 \sigma_1 = F, \quad \ddot{S}_1 + \lambda \dot{S}_1 + \omega_0^2 S_1 = G.$$

Note that σ_0 is the solution of the linearized (31) obtained by setting $\delta_E = \delta_\eta = 0$, and setting $\epsilon = \bar{\epsilon} \cos \omega t$. We obtain for the forcing functions

$$(40) \quad G = -\omega_0^2 E_0 \bar{\epsilon}, \quad F = (A_1 \sigma_0 + A_2 \sigma_0^2)\ddot{\sigma}_0 + (A_1 + 2A_2 \sigma_0)\dot{\sigma}_0, \quad G = 2B_1 \sigma_0 + 3B_2 \sigma_0^2,$$

$$A_1 = -\frac{2 a_{11}}{E_0^2}, \quad A_2 = -\frac{3 a_{12}}{E_0^3}, \quad B_1 = -\frac{a_{21} \lambda}{\eta_0^2}, \quad B_2 = -\frac{a_{22} \lambda}{\eta_0^3}$$

The solution for σ_0 is

$$(41) \quad \sigma_0 = A \cos \omega t + B \sin \omega t; \quad A = \frac{Gx}{\Delta}, \quad B = \frac{Gy}{\Delta}, \quad x = \omega_0^2 - \omega^2,$$

$$y = 2 \zeta \omega, \qquad \lambda = \frac{\omega_0^2}{2 \zeta}, \qquad \Delta = x^2 + y^2 .$$

Considering only the fundamental frequency in the steady state solution of G_1 and S_1 the forcing functions become

$$(42) \qquad F = c_1 \cos \omega t + \bar{c}_1 \sin \omega t, \quad G = d_1 \cos \omega t + \bar{d}_1 \sin \omega t,$$

where

$$c_1 = \omega B A_1 - \frac{3\omega^2}{4} A(A^2 + B^2) A_2 , \quad \bar{c}_1 = \omega A A_1 - \frac{3\omega^2}{4} B(A^2 + B^2) A_2$$

(43)

$$d_1 = 2B_1 A , \quad \bar{d}_1 = 2B_2 A , \quad A^2 + B^2 = \frac{\bar{F}^2}{\triangle} \quad .$$

σ_1 and S_1 are then given by

$$\sigma_1 = f_1 \cos \omega t + \bar{f}_1 \sin \omega t , \quad s_1 = g_1 \cos \omega t + \bar{g}_1 \sin \omega t; \quad f_1 = \frac{x c_1 - y \bar{c}_1}{\triangle} ,$$

(44)

$$\bar{f}_1 = \frac{x \bar{c}_1 + y c_1}{\triangle} , \quad g_1 = \frac{x d_1 - y \bar{d}_1}{\triangle} , \quad \bar{g}_1 = \frac{x \bar{d}_1 + y d_1}{\triangle} .$$

The nonlinear complex modulus for this case becomes

$$(45) \quad E^* = E' + i E'' ; \quad E' = A + \delta_E f_1 + \delta_\eta g_1 , \quad -E'' = B + \delta_E \bar{f}_1 + \delta_\eta \bar{g}_1 .$$

For the linear case $E^* = E_o^* = A - iB, \delta_E = \delta_\eta = 0$.

The nonlinear contribution to E^* is given by $\delta_E (f_1 - i\bar{f}_1) + \delta_\eta (g_1 - i\bar{g}_1)$.

5. COUPLED VOIGT MODEL . Consider N nonlinear Voigt elements with mass coupled in series. We make the following assumptions concerning the coupling: (a) The internal strain of the model equals the sum of the internal strains of each element: $\epsilon = \sum_{\lambda=1}^{N} \epsilon_\lambda$. ϵ_λ is the strain on the i th element. (b) The stress on each element is the same and equals the applied stress $\sigma(t)$.   (c) The i th element is governed by the internal parameters $E_{oi}, \eta_{oi}, \delta_{E_i}, \delta_{\eta_i}$, and $\delta_{E_i} = \delta_{E_j} = \delta_E, \delta_{\eta_i} = \delta_{\eta_j} = \delta_\eta$, i, j = 1, 2, ... , N.

From this it follows that the nonlinear complex compliance J^* is given by

$$J^* = \sum_{i=1}^{N} J_i^*, \qquad J_i^* = J_{oi}^* + J_{1i}^*,$$

where J_{oi}^* and J_{1i}^* are given by (25), using an appropriate subscript i for the i th element. Thus we have an additivity principle for the nonlinear portion of the complex compliance. For the linear case $J^* = \sum_{i=1}^{N} J_{oi}^*$ which is the classical result for a coupled linear Voigt model with mass. For the massless case this reduces to the classical result given in Ref. (4) p. 13.

6. **COUPLED MAXWELL MODEL** . Consider N nonlinear Maxwell elements with mass coupled in parallel under the assumptions: (a) The stress on the model equals the sum of the internal stresses of each element:

$\sigma = \sum_{i=1}^{N} \sigma_i$ where σ_i is the stress on the i th element. (b) The strain on each element is the same. (c) $\delta_{E_i} = \delta_{E_j} = \delta_E$, $\delta_{\eta_i} = \delta_{\eta_j} = \delta_\eta$. It follows that the nonlinear complex modulus E^* is the sum of the non-linear complex moduli of each element: $E^* = \sum_{i=1}^{N} E_i^*$. E_i^* is given by (45) substituting i for the i th element.

REFERENCES

1. Minorsky, N. "Introduction to Non-Linear Mechanics" J. W. Edwards (1947) Part II.

2. Stoker, J. J. "Nonlinear Vibrations" Interscience Publishers, N.Y. (1950) Ch. IV App. I.

3. Davis, J. L. "An Elementary Theory of Nonlinear Viscoelasticity" J. Polymer Sci., in press

4. Bland, D. R. "The Theory of Linear Viscoelasticity" Pergamon Press (1960)

PLANE PLASTIC DEFORMATION OF SOILS*

Shunsuke Takagi, [1] M. ASCE
Materials Research Branch
Research Division
U. S. Army Cold Regions Research and Engineering Lab.

SYNOPSIS

A consistent theory of plane plastic deformation of soil is formulated by assuming soil as an ideal material that has constant cohesion and frictional angle. Such an ideal soil is an extension of the ideal metal that has, in the terminology of soil mechanics, cohesion only.

After a review of the existing theories from which the present theory has emerged, the mathematical expression referred to as the "compression characteristic" is developed. Then the system of differential equations describing the plasticity of the material is devised. Consistency of the system of equation is shown by the theory of characteristic lines.

Many mathematical and physical difficulties remain to be solved before the perfect explanation of the plasticity of ideal soil will be attained.

INTRODUCTION

The mathematical study of the plasticity of an ideal soil having constant cohesion and frictional angle, which, for convenience, will be called $c\phi$-material, has not yet been extensively developed. The objective herein is to

---

There is an errata sheet at the end of this paper.

present a consistent mathematical basis for the plastic deformation of $c\phi$-material with motion limited to in-plane motion.

The theory is developed using only the mathematical requirements that are mandatory to make the strain-rate tensor consistent with the stress tensor. Introduction of these mathematical requirements permits the assignment of suitable characteristics to $c\phi$-material. These characteristics are: (1) Although the directions of principal stress and principal strain rate are coincident for a plastic metal (Saint-Venant's postulation[2]), this is not necessarily so for a $c\phi$-material; (2) a $c\phi$-material, depending on its mode of deformation, has either compressibility or dilatancy, which causes change of density; (3) the relationship between stress and strain rate is not determined a priori but in accordance with boundary and initial conditions; (4) it is expected that the three dimensional yield criterion of $c\phi$-material may be the form suggested by D. C. Drucker and W. Prager;[3] and (5) it is also expected that limitation of the mode of motion will give various forms of yield criterion.

The differential equations formulated on these bases are confirmed to be consistent by the theory of characteristic lines. They include nonlinear terms caused by local acceleration that, when treated with the theory of characteristic lines, demonstrate that a $c\phi$-material assumes the motion of a liquid when, under realization of slip lines, a certain velocity is surpassed. This phenomenon is evidenced by the transfer of two of the three characteristic lines from the real to the imaginary. Moreover, these equations include non-steady terms. Therefore, when adequately developed, they have sufficient generality to become effective eventually in analyzing any type of plane plastic motion of $c\phi$-material. Two simple examples—vibration under the Rankine state and one-dimensional secondary consolidation—are treated in the text.

Limitations for the practical application of the present theory are: (1) There is no concise experimental method that will provide numerical values of both cohesion and frictional angle because the three-dimensional theory remains so obscure that the effect of boundary and initial conditions on plastic behavior during customary tests on soils is uncertain; (2) such deformation of $c\phi$-material that precedes the plastic deformation, corresponding to elastic deformation in metal, is not combined with the plastic deformation (therefore, we do not know exactly what actual deformation corresponds to the deformation considered herein); and (3) the mathematical proof for existence and uniqueness of the solution is not yet known. These limitations must be removed in the future by enlarging the properties of $c\phi$-material to make it an idealization of the actual soil.

Notation.—The letter symbols adopted for use in this paper are defined where they first appear and are listed alphabetically in Appendix V.

REVIEW OF THE EXISTING THEORIES

After scrutinizing two apparently irreconcilable approaches for formulating the plasticity of $c\phi$-material, the author was able to form a general theory of plane deformation of $c\phi$-material. One successful method was the extended

[2] "The Mathematical Theory of Plasticity," by R. Hill, Oxford Univ. Press, New York, N. Y., 1956, p. 38.

[3] "Soil Mechanics and Plastic Analysis or Limit Design," by D. C. Drucker and W. Prager, Quarterly of Applied Mathematics, Vol. 2, 1952, pp. 157-165.

use of the concept of the pole on the Mohr circle.[4] If the stress point of a plane through a given point in the ground is known on the Mohr circle, another intersection with the Mohr circle of the line drawn through the stress point parallel to the plane is a fixed point called the pole. Conversely, the line drawn from the pole parallel to a plane that passes through the given point in the ground, when it intersects the Mohr circle again, gives the stress point of that plane. However, because the use of this concept largely depends on the location of the stress point, the sign convention for tangential stress must be clearly defined.

If major and minor principal stresses, σ_I and σ_{II}, respectively, are located as shown in Fig. 1, tangential stresses τ on slopes PQ are directed as shown,

$\theta > 0;$ $\theta < 0;$

$m > 0, \ i < 0;$ $m < 0, \ i < 0;$

$\tau < 0.$ $\tau > 0.$
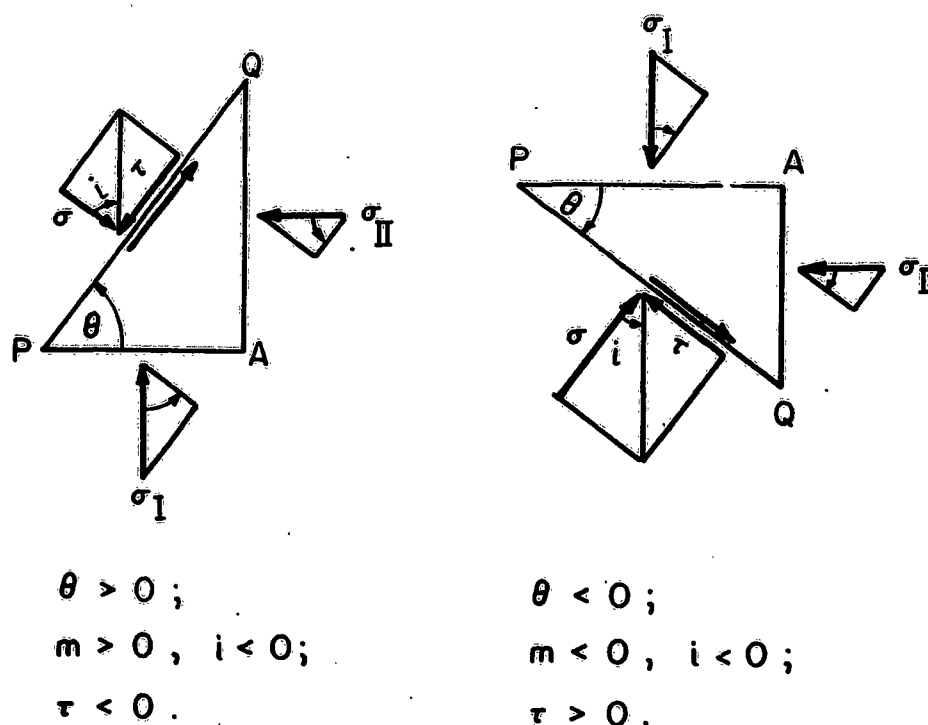
FIG. 1.—SIGN OF TANGENTIAL STRESS

in which slopes PQ in the left and right figures are rotated by θ counterclockwise and clockwise, respectively, from the plane PA of major principal stress.

In order to express the direction of τ, Karl Terzaghi,[5] Hon. M. ASCE, uses the angle of inclination, i, of compound stress, which, however, is seldom utilized in the application. The better choice is to use the rotational direction of the fictitious moment that is formed by a pair of tangential stresses, τ,

[4] "Lectures on Theories in Soil Mechanics," Parts I-VIII, by Shunsuke Takagi, Journal, Agric. Engrg. Soc. of Japan, Tokyo, Japan, Part I: Vol. 26, No. 4, 1958, pp. 58-63; Part II: Vol. 26, No. 5, 1958, pp. 41-45; Part III: Vol. 26, No. 6, 1959, pp. 50-55; Part IV: Vol. 27, No. 1, 1959, pp. 44-49; Part V: Vol. 27, No. 2, 1959, pp. 49-54; Part VI: Vol. 27, No. 3, 1959, pp. 38-44; Part VII: Vol. 27, No. 4, 1959, pp. 43-50; Part VIII: Vol. 27, No. 6, 1960, pp. 37-44 (in Japanese).

[5] "Theoretical Soil Mechanics," by Karl Terzaghi, John Wiley and Sons, Inc., New York, N. Y., 1951, p. 16.

located on opposite sides of the same slope because its direction is easily determined as a result of agreement with the rotational direction of θ. Moreover, this choice is helpful in visualizing the direction of motion on the slope under consideration because τ on the slope may be considered as the component of motion that brings τ into action. The fictitious rotational direction was termed sign m by the author[4] in order to express the sign of tangential stress. Sign m is positive when θ is positive.

The application of this concept on the Mohr circle will now be described. In Fig. 2, x and y are the coordinate axes of the physical plane. The right-hand and left-hand coordinate systems are shown in Fig. 2. The angle θ in the stress plane is directed in the same manner as θ in the physical plane. Therefore, θ is positive in both of the stress planes; and accordingly sign m of τ at

RIGHT - HAND
COORDINATE

LEFT - HAND
COORDINATE
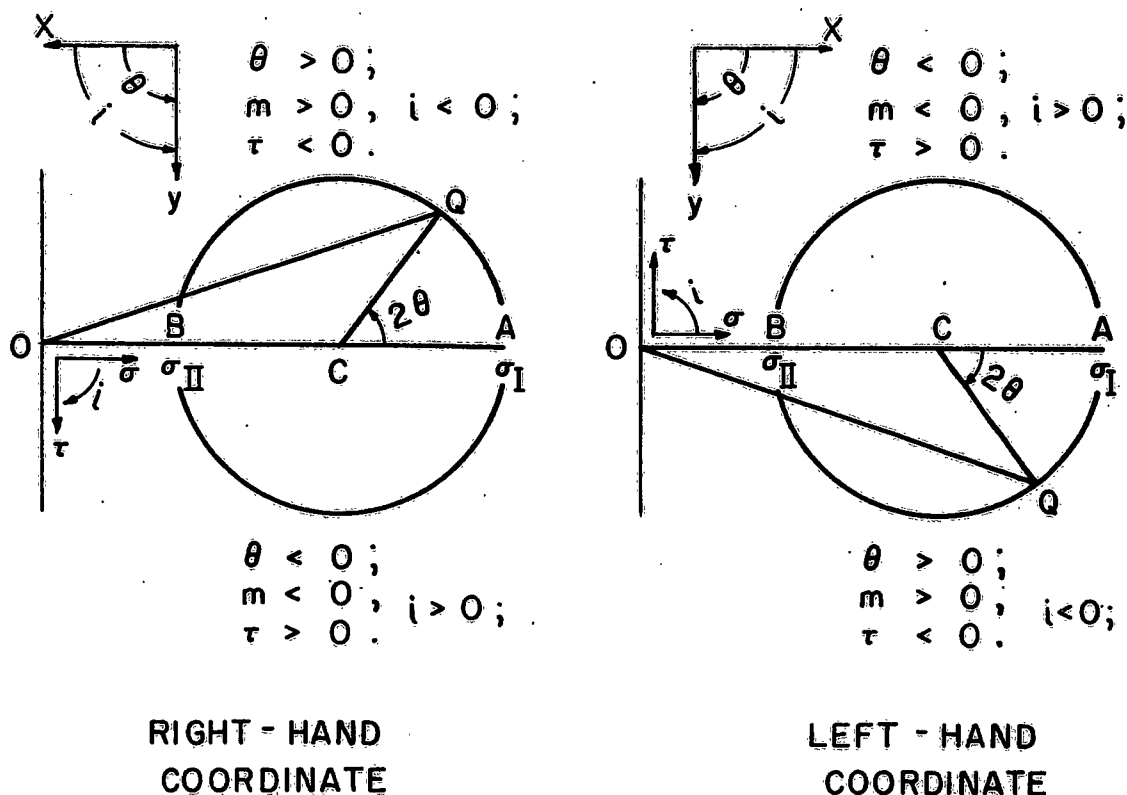
FIG. 2.—SIGN OF TANGENTIAL STRESS ON THE MOHR CIRCLE

Q in both figures is positive by definition. Angle QOC in Fig. 2, however, is apparently opposite in direction to i in Fig. 1, although both should be the same. This discrepancy can be resolved only by directing the τ axis as shown in Fig. 2. Then, the σ, τ coordinate system obtains the opposite sense from the x, y coordinate system. The following equation is obtained in this manner:

$$\tau = -\textcircled{\sigma} \sin 2\theta \quad \dots\dots\dots\dots\dots(1)$$

in which $\textcircled{\sigma}$ is the radius of the Mohr circle. The relations established so far are shown collectively in Fig. 2.

Once the pole is located on the Mohr circle, the directions of the slip lines, which for consistency will be called stress characteristic directions, are easily determined by the geometric method (Fig. 3).

The pole will be located by assuming that the location of the stress point V of the vertical plane has the central angle 2θ measured from the point A of major principal stress. The next step is to introduce δ, defined by

$$2\ \delta = \frac{\pi}{2} - \rho \quad \dots \dots \dots \dots \dots \dots \dots (2)$$

in which ρ is the frictional angle. Then, from the geometry in Fig. 3,

$$< DPH = \theta + \delta \quad \dots \dots \dots \dots \dots \dots (3a)$$

and

$$< EPH = - \theta + \delta \quad \dots \dots \dots \dots \dots \dots (3b)$$

in which D and E are the +m and -m stress points, respectively, on the limiting lines, and H is the stress point of the horizontal plane. Stress characteristic directions PD and PE are therefore given as

$$dy = - \tan \left(\theta \pm \delta \right) dx \quad \dots \dots \dots \dots \dots (4)$$

in which the upper and lower of the double signs indicate the +m and -m directions, respectively. This convention of double signs will be used throughout this paper unless otherwise stated.

Eq. 4 has been derived using the right-hand coordinate system with the y axis directed vertically downward. It is also valid (if the convention shown in Fig. 2 is followed) not only for the right-hand coordinate system with the y axis directed vertically upward, but also for the left-hand coordinate system with the y direction either vertically downward or upward. It should be noted that the σ axis does not have to be horizontal in order to apply the geometry of the Mohr circle; however, slight complications must be disposed of if the σ axis is not horizontal.

When the sense of the σ, τ coordinate system is observed, the theory of characteristic lines provides the same stress characteristic direction as given by the geometric method. This may be verified by using Sokolovski's method,[6] or by using the method presented subsequently herein. The negative sign in front of $\tan \left(\theta \pm \delta \right)$ does not appear in Sokolovski's equations because of the different definition for θ (see Eqs. 1.15 and 1.16[6]). If it is desired to remove the negative sign, θ should be defined as one-half the central angle of the pole, or as the angle from the horizontal to the line of action of σ_I. This choice, however, is not convenient for manipulating the geometry of the Mohr circle.

The basic assumption for plastic deformation adopted in the general theory of plasticity is that the strain rate, or, if not referring to time, the strain

6 "Statics of Soil Media," by V. V. Sokolovski, Butterworth, London, 1960.

increment, is determined by the stress, whereas in elastic deformation the strain itself is related to stress.[7,8,9]

In the case of a metal obeying the Mises criterion of yielding (in which J_2 is equal to a constant) the relation between a component of strain rate $\dot{\epsilon}_{ij}$ and components of stress σ_{ij} is found by differentiating the yield function J_2 in respect to σ_{ij}, that is,

$$\dot{\epsilon}_{ij} = f \frac{\partial J_2}{\partial \sigma_{ij}} \quad \ldots\ldots\ldots\ldots\ldots\ldots (5)$$

in which J_2 is the second invariant of the deviatoric stress tensor,

$$J_2 = \frac{1}{6}\left[\left(\sigma_1 - \sigma_2\right)^2 + \left(\sigma_2 - \sigma_3\right)^2 + \left(\sigma_3 - \sigma_1\right)^2\right] \ldots\ldots (6)$$

in which σ_1, σ_2, and σ_3 are the principal stresses, arranged in an arbitrary order; f is a positive constant; and the dot on $\dot{\epsilon}_{ij}$ signifies differentiation with

FIG. 3.—STRESS CHARACTERISTIC DIRECTIONS

[7] "Meta-Theory of Mechanics of Continua Subject to Deformations of Arbitrary Magnitudes (Duality of Definitions of Strain, Strain Increment and Stress for Elastic and Plastic Finite Deformations)," Y. Yoshimura, Report No. 343, Aeronautical Research Inst., Univ. of Tokyo, Tokyo, Japan, 1959.

[8] "Sosei-Rikigaku," by Y. Yoshimura, Kyoritsu Publishing Co., Tokyo, Japan, 1959 (in Japanese).

[9] "Theoretical Elasticity," by A. E. Green and W. Zerna, Oxford Univ. Press, New York, N. Y., 1954.

respect to time. When regarded as a function of the state of stress, J_2 is called plastic potential. It must be noted, however, that in deriving Eq. 5 Saint-Venant's postulation[2] is presumed.

Drucker and Prager[3] extended the concept of plastic potential to the three-dimensional deformation of cϕ-material, showing that

$$J_2^{1/2} - \lambda \, J_1 = k \ldots \ldots \ldots (7)$$

is a proper generalization of the Mises criterion of yielding,[10] and

$$\Psi_d = \bar{J}_2^{1/2} - \lambda \, \bar{J}_1 \ldots \ldots \ldots (8)$$

is the plastic potential for this case, in which λ and k are positive constants and $\bar{J}_1$ is the first invariant,

$$J_1 = \sigma_1 + \sigma_2 + \sigma_3 \ldots \ldots \ldots (9)$$

It should be noted that a positive sign is used to indicate compressive stress herein. In the case of plane strain, the yield criterion (Eq. 7) is reduced to the Mohr criterion of yielding. It is noted that Saint-Venant's postulation[2] is still maintained.

Drucker and Prager's theory was advanced further by Drucker[10] and Shield[11] for the case of plane deformation, but could not be widely accepted by researchers in soil mechanics. The reason may be that it was not clear whether Drucker and Prager's derivation from the three-dimensional extension of the yield criterion was adequate for the plane deformation of cϕ-material (Brinch Hansen[12]). H. Yamaguchi[13] almost succeeded in indicating that, if Saint-Venant's postulation[2] is presumed, the Drucker and Prager extension of the Mohr criterion of yielding is the only possible yield criterion for the three-dimensional deformation of cϕ-material (see Appendixes III and IV).

G. A. Geniev[14] developed another theory of plane deformation. Geniev's fundamental concept is most easily explained geometrically, as shown in Fig. 4. If both the scale and the position of the $\dot{\epsilon}$, $\dot{\gamma}$ axes are adequately selected, in which $\dot{\gamma}$ is shear strain rate, the Mohr circle of strain rate may be superimposed on the Mohr circle of stress with the poles of both circles fixed at the same point (for example, P) so that the geometric interpretation is feasible. The stress point at which the plastic deformation is operative is, as is well recognized, either D or E where the limiting lines touch the Mohr

[10] "Limit Analysis of Two and Three Dimensional Soil Mechanics Problems," by D. C. Drucker, Journal of the Mechanics and Physics of Solids, Vol. 1, 1953, pp. 217-226.

[11] "Mixed Boundary Value Problems in Soil Mechanics," by R. T. Shield, Quarterly of Applied Mathematics, Vol. 11, 1953, pp. 61-75.

[12] "Earth Pressure Calculation," by Brinch Hansen, The Institutions of Danish Civ. Engrs., Copenhagen, 1953.

[13] "A Theory on the Velocity Field in the Plastic Flow of Granular Materials," by H. Yamaguchi, Transactions, J. S. C. E., No. 63, 1959, pp. 8-16 (in Japanese).

[14] "Voprosy Dinamiki Sypuchei Sredy," by G. A. Geniev, Akademiia Stroitel'stva i Arkhitektury SSSR, Moscow, 1958.

circle, whereas the strain-rate point at which the plastic deformation is operative, called the operative strain-rate point, is not known. However, Geniev arbitrarily assumed (1) that the operative strain-rate point would be the maximum shear strain-rate point, and (2) that the operative strain-rate point would fall on the stress point of the same sign m on one of the limiting lines. Then, either PD or PE is the common characteristic direction. The $\dot{\epsilon}$ axis appears on either $A'_\epsilon B'_\epsilon$ or $A''_\epsilon B''_\epsilon$, which are rotated by ρ counterclockwise and clockwise, respectively, from the σ axis. Thus, as was suggested by de Josselin de Jong,[15] Geniev deviated from Saint-Venant's postulation[2] adopted for metallurgy.

Although Geniev's first assumption is arbitrary, the second assumption is mandatory. If two distinct characteristic directions exist, one from stress
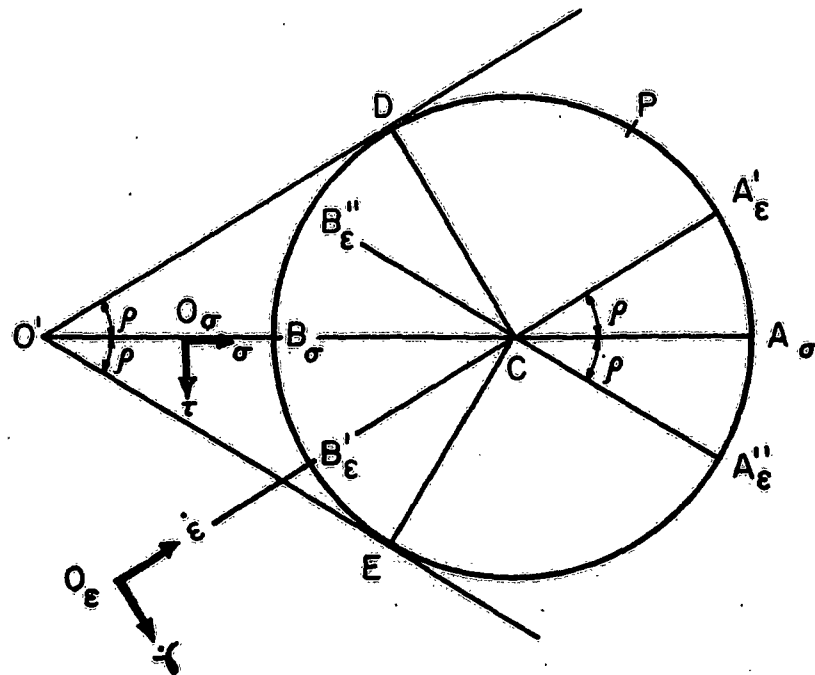
FIG. 4.—FUNDAMENTALS OF THE GENIEV DEFORMATION

and one from strain rate, it is not possible to satisfy conditions on boundary lines, or to connect two discontinuous solutions across a line. Coincidence of both strain-rate characteristic directions with the stress characteristic direction of the same sign m, as in the Drucker and Prager deformation, is not necessary.

In order to formulate the general deformation, Geniev's second assumption is adopted as the first basic assumption herein. The arbitrary location of the operative strain-rate point on the strain-rate Mohr circle is replaced by the following principle, which Yamaguchi[13] inductively adopted in deriving the Drucker and Prager plane deformation, although not in a perfect form, from

[15] "The Undefiniteness in Kinematics for Friction Material," by G. de Josselin de Jong, Brussels Conf. on Earth Pressure Problems, Belgian Group of Internatl. Soc., S.M.F.E., Vol. I, 1958, pp. 56–70.
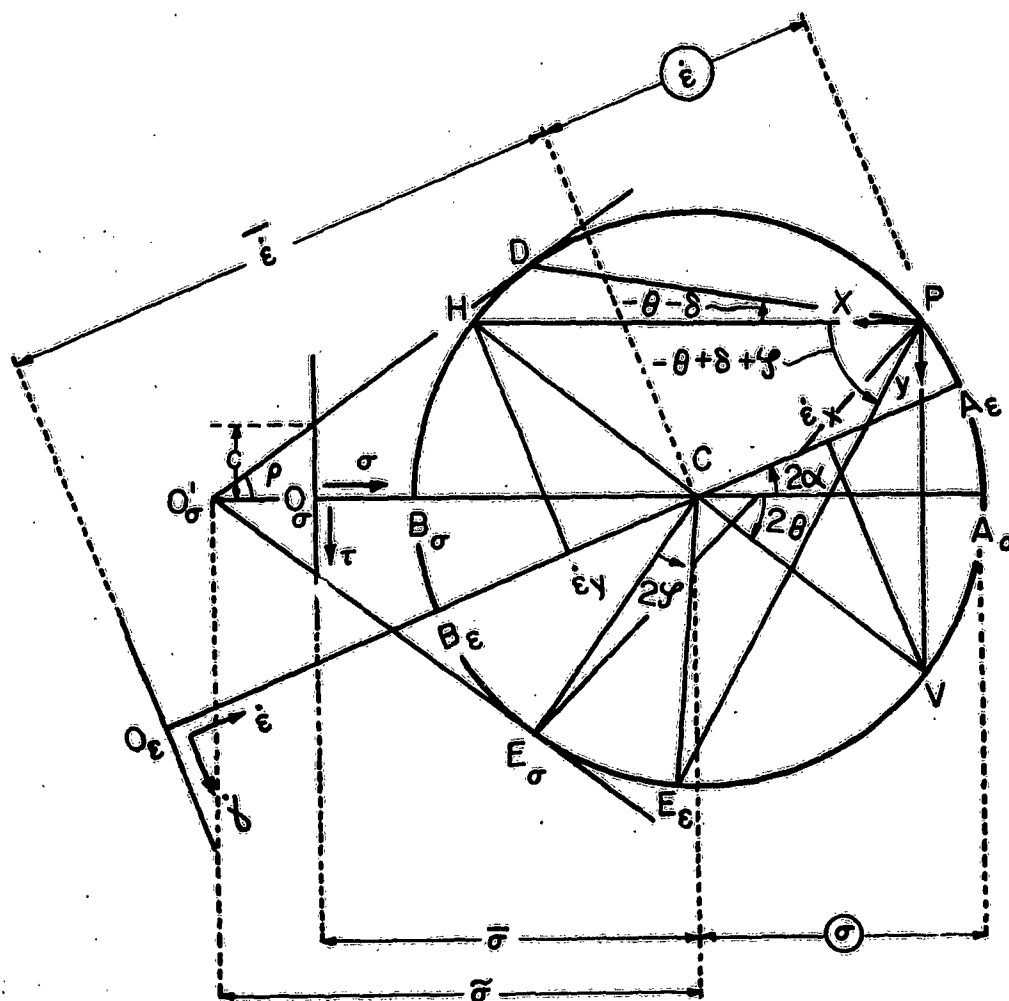
FIG. 5.—ACTIVATION OF THE +m STRESS POINT

the Mohr criterion of yielding on the basis of Saint-Venant's postulation: The transformation of a set of first-order partial differential equations to a coordinate system in which the coordinates are the characteristic lines of the given equations is simplification of the set of equations into a set in which each equation contains directional differentials in only one coordinate. The set of transformed equations may be expressed as a set of total differential equations each of which is valid along a characteristic direction. This is a mathematical fact (Appendix I), and is adopted herein as the second basic assumption.

THE COMPRESSION CHARACTERISTIC

Let us suppose that the strain-rate Mohr circle and the stress Mohr circle are superimposed with their poles at the same point P (Figs. 5 and 6). Then, according to the first basic assumption, the operative strain-rate point must appear on either D in Fig. 5 or E in Fig. 6, which (since the x, y coordinate system is assumed here to be the right-hand coordinate system) is either the

+m or the -m stress point, respectively. The stress point on which the operative strain-rate point occurs will be termed activated.

The location of the inoperative strain-rate point (for example, E_ϵ in Fig. 5 or D_ϵ in Fig. 6), however, is not known a priori. It is assumed that the central angle of E_ϵ or D_ϵ is larger by 2ϕ than that of the -m or the +m stress point on the limiting lines (E_σ in Fig. 5 or D_σ in Fig. 6). It is also assumed that the central angle of the point A_ϵ of major principal strain rate is larger by 2α than that of the point A_σ of major principal stress. The immediate ob-

FIG. 6.—ACTIVATION OF THE -m STRESS POINT

jective of the following analysis is to determine what relationship must exist between ϕ and α in order that the strain-rate characteristics conform to the stress characteristics.

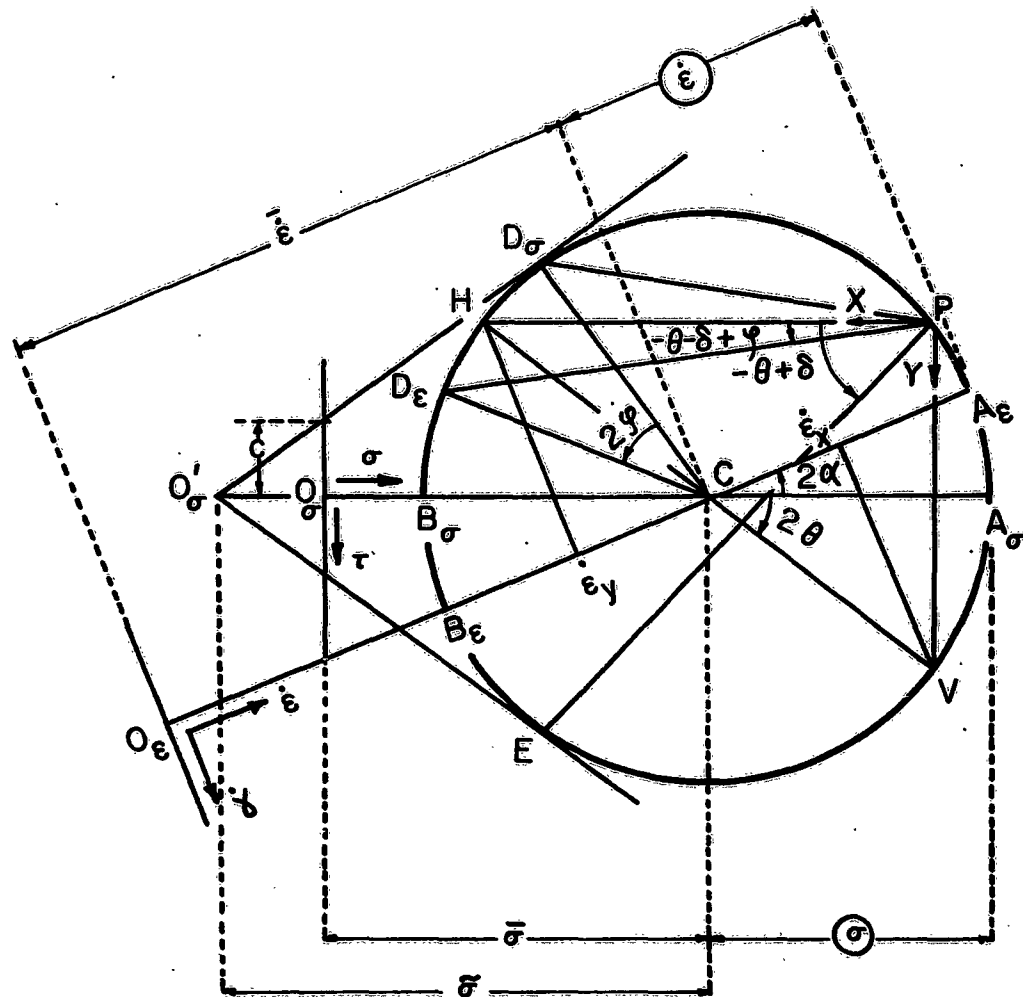From the geometry of Figs. 5 and 6,

$$\dot{\epsilon}_x = \bar{\dot{\epsilon}} + \textcircled{$\dot{\epsilon}$} \cos (2\theta - 2\alpha) \dots\dots\dots\dots (10)$$

$$\dot{\varepsilon}_y = \bar{\varepsilon} - \textcircled{ε} \cos\,(2\theta - 2\alpha) \dots\dots\dots\dots (11)$$

and

$$\dot{\gamma}_{xy} = - \textcircled{ε} \sin\,(2\theta - 2\alpha) \dots\dots\dots\dots (12)$$

in which $\textcircled{$\varepsilon$}$ and $\bar{\varepsilon}$ are the radius and the $\bar{\varepsilon}$ coordinate of the center of the strain-rate Mohr circle, and the negative sign in the right-hand side of Eq. 12 is used in accordance with the sign convention for τ_{xy}.

Components of strain rate are assumed to be positive when they are compressive. Components of velocity are positive in the positive x or y directions, and are connected by the relations,

$$\dot{\varepsilon}_x = - \frac{\partial\,v_x}{\partial\,x} \dots\dots\dots\dots\dots (13)$$

$$\dot{\varepsilon}_y = - \frac{\partial\,v_y}{\partial\,y} \dots\dots\dots\dots\dots (14)$$

and

$$\dot{\gamma}_{xy} = - \frac{1}{2}\left(\frac{\partial\,v_x}{\partial\,y} + \frac{\partial\,v_y}{\partial\,x}\right) \dots\dots\dots\dots (15)$$

Eliminating $\bar{\varepsilon}$ and $\textcircled{$\varepsilon$}$ in Eqs. 10, 11, and 12 and using Eqs. 13, 14, and 15, yields the following:

$$\left(\frac{\partial\,v_x}{\partial\,x} - \frac{\partial\,v_y}{\partial\,y}\right)\sin\,(2\theta - 2\alpha) + \left(\frac{\partial\,v_x}{\partial\,y} - \frac{\partial\,v_y}{\partial\,x}\right)\cos\,(2\theta - 2\alpha) = 0 \dots (16)$$

Eq. 16 is the only equation that connects components of velocity and, by Yamaguchi's principle, (at the top of p. 115) it must become total differential equations when expressed in terms of strain-rate characteristic directions.

For a consistent analysis, reference is made to the vector field determined by the strain-rate characteristic directions, schematically represented in Fig. 7, in which $\vec{s}_0$ and $\vec{s}_1$ are the operative and the inoperative directions, respectively. The angles that these strain-rate characteristics make with the x direction are easily determined from the geometry in Fig. 5 or Fig. 6, in which the operative direction is PD or PE and the inoperative direction is PE_ε or PD_ε, respectively. The result is summarized as $- \theta \textcircled{$\mp$} \delta$ for the operative and $- \theta \textcircled{$\pm$} \delta + \phi$ for the inoperative, in which the upper or the lower of the double signs in the circle corresponds to the activation of the +m or the −m stress characteristic direction, respectively, and the circle surrounding the double signs signifies that only one of the double signs is actually used.

The relationship between the vectors (dx, dy) and $\left(ds_0,\ ds_1\right)$ gives the relationship between the directional differentiations,

$$\sin \left(\phi \oplus 2 \, \delta\right) \frac{\partial}{\partial \, x} = - \sin \left(\theta \ominus \delta - \phi\right) \frac{\partial}{\partial \, s_0} + \sin \left(\theta \oplus \delta\right) \frac{\partial}{\partial \, s_1} \; \dots \; (17)$$

$$\sin \left(\phi \oplus 2 \, \delta\right) \frac{\partial}{\partial \, y} = - \cos \left(\theta \ominus \delta - \phi\right) \frac{\partial}{\partial \, s_0} + \cos \left(\theta \oplus \delta\right) \frac{\partial}{\partial \, s_1} \; \dots \; (18)$$

It should be noted that the differentiation with respect to s_0 and s_1 does not indicate that the quantity to be differentiated is expressible as a function of
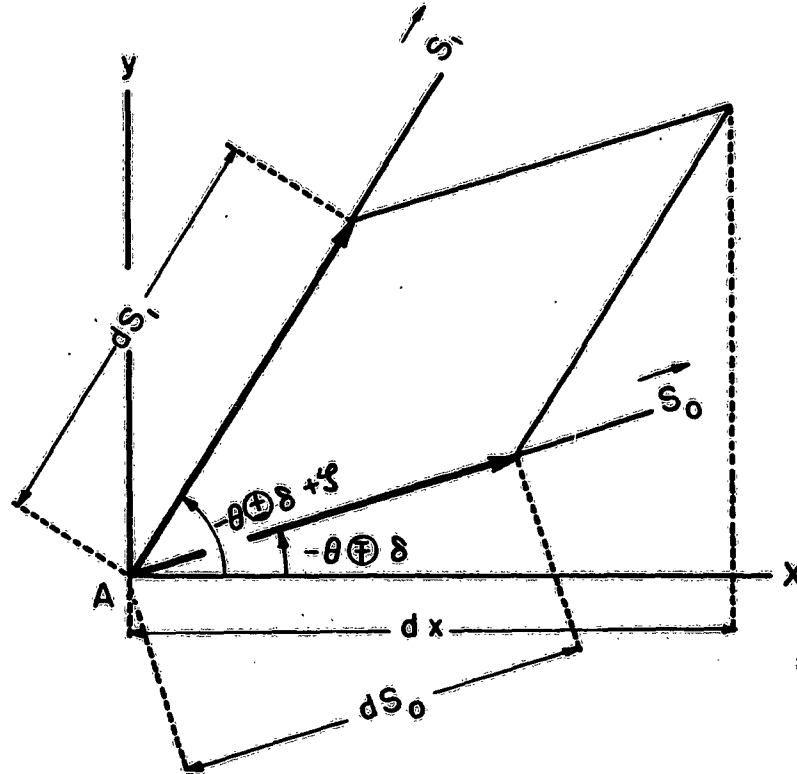
FIG. 7.—VECTOR FIELD DETERMINED BY THE STRAIN-
RATE CHARACTERISTIC DIRECTIONS

s_0 and s_1. This is evident from the fact that the order of differentiation in $\partial^2 / \partial s_0 \, \partial s_1$ usually cannot be reversed. The differentiation with respect to s_0 and s_1 shall be understood to signify the rate of change of quantity in the respective directions.

Substitution of relationships 17 and 18 into Eq. 16 yields

$$- \left[\frac{\partial \, v_x}{\partial \, s_0} \cos \left(\theta \oplus \delta - 2\alpha + \phi\right) - \frac{\partial \, v_y}{\partial \, s_0} \sin \left(\theta \ominus \delta - 2\alpha + \phi\right) \right] +$$

$$+ \left[\frac{\partial \, v_x}{\partial \, s_1} \cos \left(\theta \oplus \delta - 2\alpha\right) - \frac{\partial \, v_y}{\partial \, s_1} \sin \left(\theta \ominus \delta - 2\alpha\right) \right] = 0 \; \dots \; (19)$$

Eq. 19 is not a total differential equation, and the sums of the terms within each set of brackets must be zero in order to yield two total differential equations. The two total differential equations thus obtained may be written in the following forms:

$$dv_x \cos \left(\theta \pm \delta - 2\alpha + \phi\right) - dv_y \sin \left(\theta \pm \delta - 2\alpha + \phi\right) = 0 \quad \ldots \ldots (20)$$

along the operative strain-rate characteristic directions, in which,

$$\frac{dx}{\cos \left(\theta \pm \delta\right)} = \frac{dy}{- \sin \left(\theta \pm \delta\right)} = ds_0 \quad \ldots \ldots \ldots \ldots (21)$$

and

$$dv_x \cos \left(\theta \mp \delta - 2\alpha\right) - dv_y \sin \left(\theta \mp \delta - 2\alpha\right) = 0 \quad \ldots \ldots (22)$$

along the inoperative strain-rate characteristic direction, in which,

$$\frac{dx}{\cos \left(\theta \mp \delta - \phi\right)} = \frac{dy}{- \sin \left(\theta \mp \delta - \phi\right)} = ds_1 \quad \ldots \ldots \ldots (23)$$

Thus, two conditions have been obtained beginning from one relationship (Eq. 16) and the existence of another relationship should be expected. To write this other relationship, substitute

$$dv_x = \frac{\partial v_x}{\partial x} dx + \frac{\partial v_x}{\partial y} dy \quad \ldots \ldots \ldots \ldots \ldots (24a)$$

$$dv_y = \frac{\partial v_y}{\partial x} dx + \frac{\partial v_y}{\partial y} dy \quad \ldots \ldots \ldots \ldots \ldots (24b)$$

into Eqs. 20 and 22 and use Eqs. 21 and 23 to eliminate dy/dx. Solving the two equations thus obtained simultaneously for $\partial v_x / \partial x$ and $\partial v_y / \partial y$, and adding the resultant two equations, the following is obtained:

$$\left(\frac{\partial v_x}{\partial x} + \frac{\partial v_y}{\partial y}\right) \cos (2\alpha - \phi) \sin (2\theta - 2\alpha)$$

$$= \cos \left(\phi \pm 2 \delta\right) \left(\frac{\partial v_x}{\partial y} + \frac{\partial v_y}{\partial x}\right)$$

$$+ \sin (2\theta - 2\alpha) \sin (\phi - 2\alpha) \left(\frac{\partial v_y}{\partial x} - \frac{\partial v_x}{\partial y}\right) \quad \ldots \ldots (25)$$

This relationship must be an invariant of strain-rate tensor, and the second term in the right-hand member must vanish. This requirement is fulfilled by setting

$$\phi = 2 \alpha \quad \dots\dots\dots\dots\dots\dots \quad (26)$$

Then, Eq. 25 changes to

$$\bar{\varepsilon} = - \textcircled{\varepsilon} \cos \left(2\alpha \textcircled{\pm} 2\delta\right) \quad \dots\dots\dots\dots\dots \quad (27)$$

using the expressions of $\dot{\gamma}_{xy}$ in Eqs. 12 and 15. This relationship will provide a systematic treatment for the plasticity of $c\phi$-material and henceforth will be referred to as the compression characteristic.

Because $\bar{\varepsilon}$ indicates the rate of volume decrease and $\textcircled{\varepsilon}$ is positive, either dilatancy or compression must accompany the plastic deformation of $c\phi$-material in accordance with $\cos\left(2\alpha \textcircled{\pm} 2\delta\right)$ > or < 0, respectively. For the particular case of $2\alpha = \textcircled{\pm}\rho$, a change in volume does not occur; this is the deformation described by G. A. Geniev.[14] In the case of the Drucker and Prager plane deformation, in which $2\alpha = 0$, dilatancy always occurs, as Drucker and Prager have stated.

Eq. 26 stipulates the following geometric interpretation: the inoperative strain-rate point is symmetric with the operative strain-rate point in regard to the $\dot{\varepsilon}$ axis on the strain-rate Mohr circle.

Eq. 26 simplifies Eqs. 20 and 22 to the same form,

$$dv_x \, dx + dv_y \, dy = 0 \quad \dots\dots\dots\dots\dots \quad (28)$$

in which Eq. 21 is valid along the operative strain-rate characteristic directions, and

$$\frac{dx}{\cos\left(\theta \textcircled{\mp} \delta - 2\alpha\right)} = \frac{dy}{- \sin\left(\theta \textcircled{\mp} \delta - 2\alpha\right)} = ds_1 \quad \dots\dots \quad (29)$$

is valid along the inoperative strain-rate characteristic directions. Reduction to the simple form of Eq. 28 results in the following interpretations: (1) The increment of velocity, of which the components are dv_x and dv_y, along each of the strain-rate characteristic directions is normal to the respective strain-rate characteristic direction, of which the components are dx and dy; and (2) the unit compression rates $\dot{\varepsilon}_0$ and $\dot{\varepsilon}_1$ in the operative and the inoperative directions, respectively, are both zero, as may be verified by substitution of Eqs. 24a and 24b into Eq. 28. However, the shear strain rate $\dot{\gamma}_{01}$ in the coordinates of the strain-rate characteristic line is not zero (see Appendix II) and therefore $\bar{\varepsilon}$ is not zero.

The following theorem can be presented in a manner similar to the derivation of Eq. 25. If Eq. 28 is assumed to be valid in both the operative and the inoperative directions, both Eqs. 16 and 27 must be valid. Therefore, Eq. 28 is equivalent to Eqs. 16 and 27.

CHARACTERISTIC DIRECTIONS

Fundamental equations governing the plastic deformation of $c\phi$-material are as follows:

Writing $\overline{O'\ C} = \tilde{\sigma}$ in Fig. 3, and from the geometry of the stress Mohr circle, the following is obtained:

$$\sigma_x = \tilde{\sigma}\ (1 + \sin \rho \cos 2\theta) - c \cot \rho \ \ldots\ldots\ldots\ (30)$$

$$\sigma_y = \tilde{\sigma}\ (1 - \sin \rho \cos 2\theta) - c \cot \rho \ \ldots\ldots\ldots\ (31)$$

and

$$\tau_{xy} = - \tilde{\sigma} \sin \rho \sin 2\theta \ \ldots\ldots\ldots\ldots\ldots\ (32)$$

in which c denotes cohesion. The stress, strain-rate relationship is obtained by eliminating $\tilde{\sigma}$, θ, and $\bar{\bar{\epsilon}}$ in Eqs. 30, 31, 32, 10, 11, 12, and 27 (see Appendix III). It is noted that α is generally a function of location and time, and that the variability of α leads to particular attributes of cϕ-n. iterial.

The equations of motion are

$$\frac{1}{\gamma}\left(\frac{\partial \sigma_x}{\partial x} + \frac{\partial \tau_{xy}}{\partial y}\right) + v_x \frac{\partial v_x}{\partial x} + v_y \frac{\partial v_x}{\partial y} + \frac{\partial v_x}{\partial t} = X \ \ldots\ldots\ (33)$$

$$\frac{1}{\gamma}\left(\frac{\partial \tau_{xy}}{\partial x} + \frac{\partial \sigma_y}{\partial y}\right) + v_x \frac{\partial v_y}{\partial x} + v_y \frac{\partial v_y}{\partial y} + \frac{\partial v_y}{\partial t} = Y \ \ldots\ldots\ (34)$$

and the equation of continuity is

$$\frac{\partial \gamma}{\partial t} + \frac{\partial\left(\gamma\ v_x\right)}{\partial x} + \frac{\partial\left(\gamma\ v_y\right)}{\partial y} = 0 \ \ldots\ldots\ldots\ldots\ (35)$$

in which (since either dilatancy or compression always occurs) the unit density γ is a function of the variables x, y, and t; and X and Y are the external forces on the unit mass in the x and y directions, respectively.

The plastic work rate

$$\dot{W} = \sigma_x \dot{\epsilon}_x + 2 \tau_{xy} \dot{\gamma}_{xy} + \sigma_y \dot{\epsilon}_y \ \ldots\ldots\ldots\ldots\ (36)$$

must remain non-negative during the plastic deformation of cϕ-material if no irreversible changes other than the plastic deformation are concurrent. Upon substitution of Eqs. 30, 31, 32, 10, 11, 12, and 27 and the equation,

$$\textcircled{\sigma} = \tilde{\sigma} \sin \rho \ \ldots\ldots\ldots\ldots\ldots\ldots\ (37)$$

$\dot{W}$ is found to be

$$\dot{W} = 2\ \textcircled{\dot{\epsilon}}\ \cot\ \rho\ \left[c\ \cos\ \left(2\alpha \oplus 2\delta\right) \oplus \textcircled{\sigma} \sin\ 2\alpha\right] \ \ldots\ldots\ (38)$$

in which $\widetilde{\sigma}$ is the radius of the stress Mohr circle. Therefore, the inequality condition

$$\widetilde{c} \left[c \, \cos \, \left(2\alpha \pm 2\delta \right) \pm \widetilde{\sigma} \, \sin \, 2\alpha \right] \geqq 0 \, \ldots \ldots \ldots \, (39)$$

must be satisfied. The consistency of this system of equations is shown in the following analysis: Inserting Eqs. 30, 31, and 32 into Eqs. 33 and 34 yields

$$P_1 \frac{1}{\gamma} \frac{\partial \widetilde{\sigma}}{\partial x} + Q_1 \frac{1}{\gamma} \frac{\partial \widetilde{\sigma}}{\partial y} + R_1 \frac{1}{\gamma} 2 \, \widetilde{\sigma} \, \sin \rho \, \frac{\partial \theta}{\partial x} + S_1 \frac{1}{\gamma} 2 \, \widetilde{\sigma} \, \sin \rho \, \frac{\partial \theta}{\partial y} +$$

$$+ v_x \frac{\partial v_x}{\partial x} + v_y \frac{\partial v_x}{\partial y} = X - \frac{\partial v_x}{\partial t} \, \ldots \ldots \ldots \ldots \, (40)$$

and

$$P_2 \frac{1}{\gamma} \frac{\partial \widetilde{\sigma}}{\partial x} + Q_2 \frac{1}{\gamma} \frac{\partial \widetilde{\sigma}}{\partial y} + R_2 \frac{1}{\gamma} 2 \, \widetilde{\sigma} \, \sin \rho \, \frac{\partial \theta}{\partial x} + S_2 \frac{1}{\gamma} 2 \, \widetilde{\sigma} \, \sin \rho \, \frac{\partial \theta}{\partial y} +$$

$$+ v_x \frac{\partial v_y}{\partial x} + v_y \frac{\partial v_y}{\partial y} = Y - \frac{\partial v_y}{\partial t} \, \ldots \ldots \ldots \ldots \, (41)$$

in which

$$P_1 = 1 + \sin \rho \, \cos \, 2\theta \ldots \ldots \ldots \ldots \ldots \, (42)$$

$$Q_1 = - \sin \rho \, \sin \, 2\theta \ldots \ldots \ldots \ldots \ldots \, (43)$$

$$R_1 = - \sin \, 2\theta \ldots \ldots \ldots \ldots \ldots \ldots \, (44)$$

$$S_1 = - \cos \, 2\theta \ldots \ldots \ldots \ldots \ldots \ldots \, (45)$$

$$P_2 = - \sin \rho \, \sin \, 2\theta \ldots \ldots \ldots \ldots \ldots \, (46)$$

$$Q_2 = 1 - \sin \rho \, \cos \, 2\theta \ldots \ldots \ldots \ldots \ldots \, (47)$$

$$R_2 = - \cos \, 2\theta \ldots \ldots \ldots \ldots \ldots \ldots \, (48)$$

and

$$S_2 = \sin \, 2\theta \ldots \ldots \ldots \ldots \ldots \ldots \, (49)$$

Eliminating $\bar{\epsilon}$ and $(\tilde{\epsilon})$ in Eqs. 10, 11, and 12, and using Eqs. 13, 14, and 15 yields

$$A_1 \frac{\partial v_x}{\partial x} + B_1 \frac{\partial v_x}{\partial y} + C_1 \frac{\partial v_y}{\partial x} + D_1 \frac{\partial v_y}{\partial y} = 0 \quad \ldots \ldots (50)$$

By eliminating $(\tilde{\epsilon})$ and using the expression for $\tilde{\gamma}_{xy}$ in Eq. 12, Eq. 27 changes to

$$A_2 \frac{\partial v_x}{\partial x} + B_2 \frac{\partial v_x}{\partial y} + C_2 \frac{\partial v_y}{\partial x} + D_2 \frac{\partial v_y}{\partial y} = 0 \quad \ldots \ldots (51)$$

in which

$$A_1 = \sin (2\theta - 2\alpha) \ldots \ldots \ldots \ldots (52)$$

$$B_1 = \cos (2\theta - 2\alpha) \ldots \ldots \ldots \ldots (53)$$

$$C_1 = \cos (2\theta - 2\alpha) \ldots \ldots \ldots \ldots (54)$$

$$D_1 = - \sin (2\theta - 2\alpha) \ldots \ldots \ldots \ldots (55)$$

$$A_2 = \sin (2\theta - 2\alpha) \ldots \ldots \ldots \ldots (56)$$

$$B_2 = - \cos (2\alpha \oplus 2\delta) \ldots \ldots \ldots \ldots (57)$$

$$C_2 = - \cos (2\alpha \oplus 2\delta) \ldots \ldots \ldots \ldots (58)$$

and

$$D_2 = \sin (2\theta - 2\alpha) \ldots \ldots \ldots \ldots (59)$$

In addition, the conditions of one-valuedness for the unknowns, $\tilde{\sigma}$, θ, v_x, v_y, and γ must be satisfied:

$$d\tilde{\sigma} = \frac{\partial \tilde{\sigma}}{\partial x} dx + \frac{\partial \tilde{\sigma}}{\partial y} dy \ldots \ldots \ldots \ldots (60)$$

$$d\theta = \frac{\partial \theta}{\partial x} dx + \frac{\partial \theta}{\partial y} dy \ldots \ldots \ldots \ldots (61)$$

$$dv_x = \frac{\partial v_x}{\partial x} dx + \frac{\partial v_x}{\partial y} dy \ldots \ldots \ldots \ldots (62)$$

$$dv_y = \frac{\partial v_y}{\partial x} dx + \frac{\partial v_y}{\partial y} dy \ldots \ldots \ldots \ldots (63)$$

and

$$dy = \frac{\partial \gamma}{\partial x}\ dx + \frac{\partial \gamma}{\partial y}\ dy \dots \dots \dots (64)$$

The ten equations in Eqs. 35, 40, 41, 50, 51, and 60 through 64 contain ten local partial derivatives of σ, θ, v_x, v_y, and γ with respect to x and y. The determinant of coefficients (Δ) of the ten simultaneous (algebraic) linear equations with the ten local derivatives as unknowns is calculated and found to be equal to

$$\Delta = \Delta_\sigma\ \Delta_\epsilon\ \left(v_x\ dy - v_y\ dx\right)$$

in which

$$\Delta_\sigma = \begin{vmatrix} P_1 & Q_1 & R_1 & S_1 \\ P_2 & Q_2 & R_2 & S_2 \\ dx & dy & 0 & 0 \\ 0 & 0 & dx & dy \end{vmatrix} \quad \text{and} \quad \Delta_\epsilon = \begin{vmatrix} A_1 & B_1 & C_1 & D_1 \\ A_2 & B_2 & C_2 & D_2 \\ dx & dy & 0 & 0 \\ 0 & 0 & dx & dy \end{vmatrix}$$

Characteristic directions are determined by placing Δ equal to zero. One of the characteristic directions is the stream line, in which $dx/v_x = dy/v_y$. From $\Delta_\sigma = 0$, the stress-characteristic directions already given by Eq. 4 are determined. From $\Delta_\epsilon = 0$, the operative and the inoperative strain-rate characteristic directions already given by Eqs. 21 and 29, respectively, are determined. It is then obvious that Eq. 28 is also valid for this case in which the change of both stress and density is concurrent with the change of velocity.

For purposes of consistency in the following paragraphs, a transformation of Eq. 28 is added here by placing

$$v_x = v \cos \omega \dots \dots \dots \dots (65)$$

and

$$v_y = v \sin \omega \dots \dots \dots \dots (66)$$

in which v is the magnitude of compound velocity and ω denotes the angle measured from the x axis to the direction of velocity. Eq. 28 then changes to

$$dv/v = \tan\left(\theta \oplus \delta + \omega\right)\ d\omega \dots \dots \dots \dots (67)$$

along the operative strain-rate characteristic direction, expressed by Eq. 21, and to

$$dv/v = \tan\left(\theta \oplus \delta - 2\alpha + \omega\right) d\omega \quad\dots\dots\dots\dots (68)$$

along the inoperative strain-rate characteristic direction, expressed by Eq. 29.

One of the most interesting subjects in the plastic motion of $c\phi$-material is the realization of slip lines, in which a particular phenomenon may occur that cannot be seen in the plastic motion described in previous paragraphs. A slip line is a flow line of the material that is realized when the direction of velocity coincides with the activated stress characteristic direction, or, in other words, with the operative strain-rate characteristic direction.

When the slip line is realized,

$$\omega = -\theta \oplus \delta + n\pi \quad\dots\dots\dots\dots\dots\dots (69)$$

Then, from Eq. 67,

$$dv = 0 \quad\dots\dots\dots\dots\dots\dots\dots (70)$$

on the slip line, of which the direction is given by Eq. 21. In other words, velocity is constant along the slip line, which is a remarkable feature of $c\phi$-material. From Eq. 68,

$$dv/v = \tan\left(2\alpha \oplus 2\delta\right) d\theta \quad\dots\dots\dots\dots (71)$$

in the inoperative strain-rate characteristic direction, given by Eq. 29. Particularly in the Geniev deformation (in which $2\alpha = \oplus \rho$) the inoperative is the equi-θ direction, because $d\theta$ must be zero to maintain the right side of Eq. 71 at a finite value. For the realization of slip lines, the strain-rate characteristic directions and the total differential equations along these directions are obtained in this manner as a particular case of the plastic motion in general.

Characteristic directions for realization of slip lines other than those previously mentioned are obtained by writing

$$v_x = v \cos\left(\theta \oplus \delta\right) \quad\dots\dots\dots\dots\dots (72)$$

and

$$v_y = -v \sin\left(\theta \oplus \delta\right) \quad\dots\dots\dots\dots\dots (73)$$

allowing v to be either positive or negative. By substituting Eqs. 72 and 73 into Eqs. 33 and 34, the following is obtained:

$$P_1 \frac{\partial \tilde{\sigma}}{\partial x} + Q_1 \frac{\partial \tilde{\sigma}}{\partial y} + R_1 \, 2 \, \tilde{\sigma} \sin \rho \, \frac{\partial \theta}{\partial x} + S_1 \, 2 \, \tilde{\sigma} \sin \rho \, \frac{\partial \theta}{\partial y}$$

$$= \gamma \left(X - \frac{\partial v_x}{\partial t} + 2 \, \bar{\epsilon} \, v_x \right) \dots \dots \dots \dots \dots (74)$$

and

$$P_2 \frac{\partial \tilde{\sigma}}{\partial x} + Q_2 \frac{\partial \tilde{\sigma}}{\partial y} + R_2 \, 2 \, \tilde{\sigma} \sin \rho \, \frac{\partial \theta}{\partial x} + S_2 \, 2 \, \tilde{\sigma} \sin \rho \, \frac{\partial \theta}{\partial y}$$

$$= \gamma \left(Y - \frac{\partial v_y}{\partial t} + 2 \, \bar{\epsilon} \, v_y \right) \dots \dots \dots \dots \dots (75)$$

in which

$$P_1 = 1 + \sin \rho \cos 2\theta \dots \dots \dots \dots \dots (76)$$

$$Q_1 = - \sin \rho \sin 2\theta \dots \dots \dots \dots \dots (77)$$

$$R_1 = - \sin 2\theta \dots \dots \dots \dots \dots (78)$$

$$S_1 = - \cos 2\theta + \nu^2 \dots \dots \dots \dots \dots (79)$$

$$P_2 = - \sin \rho \sin 2\theta \dots \dots \dots \dots \dots (80)$$

$$Q_2 = 1 - \sin \rho \cos 2\theta \dots \dots \dots \dots \dots (81)$$

$$R_2 = - \cos 2\theta - \nu^2 \dots \dots \dots \dots \dots (82)$$

$$S_2 = \sin 2\theta \dots \dots \dots \dots \dots (83)$$

$$\nu^2 = \frac{\gamma \, v^2}{2 \, \tilde{\sigma} \sin \rho} \dots \dots \dots \dots \dots (84)$$

and

$$\bar{\epsilon} = - \frac{1}{2} \left(\frac{\partial v_x}{\partial x} + \frac{\partial v_y}{\partial y} \right) \dots \dots \dots \dots \dots (85)$$

In deriving Eqs. 74 and 75, the relationships

$$\bar{v}_x \frac{\partial v_x}{\partial x} + \bar{v}_y \frac{\partial v_x}{\partial y} + 2 \bar{\bar{\epsilon}} \, v_x = v^2 \frac{\partial \theta}{\partial y} \dots \dots \dots (86)$$

and

$$v_x \frac{\partial v_y}{\partial x} + v_y \frac{\partial v_y}{\partial y} + 2 \bar{\bar{\epsilon}} \, v_y = - v^2 \frac{\partial \theta}{\partial x} \dots \dots \dots (87)$$

which are easily verified by the use of Eqs. 72, 73, and 85, are used to calculate the nonlinear local acceleration terms in Eqs. 33 and 34. It should be noted that S_1 and R_2 include velocity terms that are derived from the nonlinear local acceleration terms. This inclusion causes a resonance, as derived in the following.

Because Eqs. 74 and 75 contain $\bar{\bar{\epsilon}}$, Eq. 85 must be considered. By substituting Eqs. 72 and 73 into Eq. 85, the following is obtained:

$$A_3 \frac{\partial v}{\partial x} + B_3 \frac{\partial v}{\partial y} + C_3 \, v \frac{\partial \theta}{\partial x} + D_3 \, v \frac{\partial \theta}{\partial y} = - 2 \bar{\bar{\epsilon}} \dots \dots (88)$$

in which

$$A_3 = \cos \left(\theta \oplus \delta \right) \dots \dots \dots \dots (89)$$

$$B_3 = - \sin \left(\theta \oplus \delta \right) \dots \dots \dots \dots (90)$$

$$C_3 = - \sin \left(\theta \oplus \delta \right) \dots \dots \dots \dots (91)$$

and

$$D_3 = - \cos \left(\theta \oplus \delta \right) \dots \dots \dots \dots (92)$$

Combining the conditions of one-valuedness for $\tilde{\sigma}$, θ, and v with Eqs. 74, 75, and 88, six simultaneous (algebraic) linear equations with six unknowns are obtained, that are the local partial derivatives of $\tilde{\sigma}$, θ, and v with respect to x and y. Eq. 35, the condition of continuity, may not be considered in the present analysis because the fact that the characteristic direction to which Eq. 35 is related is the stream line, is already recognized in the preceding analysis.

Calculating the determinant of coefficients of the six simultaneous (algebraic) linear equations yields

$$\Delta = \Delta_v \, \Delta_\sigma \dots \dots \dots \dots \dots (93)$$

in which

$$\Delta_v = \begin{vmatrix} A_3 & B_3 \\ dx & dy \end{vmatrix} \quad \text{and} \quad \Delta_\sigma = \begin{vmatrix} P_1 & Q_1 & R_1 & S_1 \\ P_2 & Q_2 & R_2 & S_2 \\ dx & dy & 0 & 0 \\ 0 & 0 & dx & dy \end{vmatrix}$$

From $\Delta_v = 0$, the activated stress characteristic direction is obtained, which, in this case, is the direction of slip line. From $\Delta_\sigma = 0$,

$$\frac{dy}{dx} = \frac{-\sin 2\theta \left(1 + \nu^2 \sin \rho\right) \mp \cos \rho \sqrt{1 - \nu^4}}{\cos 2\theta \left(1 + \nu^2 \sin \rho\right) + \left(\nu^2 + \sin \rho\right)} \quad \ldots \ldots (94)$$

This transforms to

$$dy = -\tan \left(\theta \pm \bar{\delta}\right) dx \quad \ldots \ldots \ldots \ldots (95)$$

by placing

$$2\,\bar{\delta} = \frac{\pi}{2} - \bar{\rho} \left(0 \leqq \rho \leqq \frac{\pi}{2}\right) \quad \ldots \ldots \ldots \ldots (96)$$

$$\cos \bar{\rho} = \frac{\cos \rho \sqrt{1 - \nu^4}}{1 + \nu^2 \sin \rho} \quad \ldots \ldots \ldots \ldots (97)$$

and

$$\sin \rho = \frac{\nu^2 + \sin \rho}{1 + \nu^2 \sin \rho} \quad \ldots \ldots \ldots \ldots (98)$$

or summarizing Eqs. 96, 97, and 98

$$\tan \bar{\delta} = \sqrt{\frac{1 - \nu^2}{1 + \nu^2}} \tan \delta \quad \ldots \ldots \ldots \ldots (99)$$

The directions given by Eq. 95 will be called resonance characteristic directions. These were derived by Geniev[14] as a particular case of his deformation, but they are still valid, even for the general deformation.

When $v = 0$, or when $\nu^2 = 0$, $\bar{\delta}$ and $\bar{\rho}$ become δ and ρ, respectively, and the resonance characteristic directions coincide with those given by Eq. 4.

When $\nu^2 \leqq 1$, or when $(1/2)\gamma\, v^2 < \bar{\sigma}\sin\rho$, $\bar{\delta}$ is real, and the resonance characteristic directions are real. However, when $\nu^2 > 1$, or when $(1/2)\gamma\, v^2 > \bar{\sigma}$ $\sin\rho$, $\bar{\delta}$ is imaginary, and the resonance characteristic directions disappear. The only remaining characteristic direction is the stream line. In other words, the system of Eqs. 74, 75, and 85 transfers from the hyperbolic to the quasi-elliptic when v increases beyond the critical velocity, $(2\ \bar{\sigma}\sin\rho/\gamma)^{1/2}$. This mathematical statement may be restated in physical terms as follows: When v in the realization of slip lines becomes larger than the critical velocity, the motion of $c\phi$-material gains likeness to that of a liquid.

Because the consistency of the system of the fundamental Eqs. 10, 11, 12, 27, 30, 31, 32, 33, 34, and 35 has been shown, it is now possible to analyze the plastic motion of $c\phi$-material; however, one difficulty still remains and that is the lack of a general method for determining α. In fact, as may be seen from the following examples, α must be determined in such a manner that the solution exists under given boundary and initial conditions. Therefore, the stress and strain-rate relationship, which is a system of functions of α, is also dependent on the boundary and initial conditions. However, the mathematics for this type of problem is not yet known. The following examples are presented with the intention of illustrating the general method for determining α by citing particular cases.

*Example 1—Vibration Under the Rankine State.—*The velocity field in a ground will be analyzed assuming that the ground surface is horizontal and that all the properties of the ground are functions of depth and time maintaining the same values in the horizontal planes. This is an extension of the Rankine state of stress for inclusion of the velocity field.

For simplicity, only the active state will be considered, in which the horizontal plane is the plane of major principal stress. Then, in the lower part of Fig. 8, A is the stress point of a horizontal plane under consideration and B is the pole. Moreover, if the right-hand coordinate system is assumed, then

$$2\theta = \pi \dotfill (100)$$

The +m and -m stress characteristic directions are BD and BE, in which D and E are the +m and -m stress points in contact with the respective limiting lines. Then, as may be recognized from the geometry in Fig. 8, the +m and -m stress characteristic lines, which are shown in the upper part of Fig. 8 as $\overline{bd}$ and $\overline{be}$, form angles of $-\delta$ and $+\delta$ with the vertical, respectively.

Because all the quantities are functions of y and t,

$$\dot{\epsilon}_x = 0 \dotfill (101)$$

Eq. 101 is equivalent to

$$\bar{\epsilon} = \textcircled{$\dot{\epsilon}$}\cos 2\alpha \dotfill (102)$$

as may be recognized from the expression for $\dot{\epsilon}_x$ in Eq. 10. Assuming the activation of the -m stress characteristic direction for this case, then

$$\bar{\epsilon} = -\textcircled{$\dot{\epsilon}$}\cos(2\alpha - 2\delta) \dotfill (103)$$

from Eq. 27. In order to make Eqs. 102 and 103 compatible, α is determined as

$$2\alpha = \delta \mp \frac{\pi}{2} \quad \dots\dots\dots\dots\dots\dots (104)$$

which reduces Eqs. 102 and 103 to the same form

$$\bar{\epsilon} = \pm \textcircled{\epsilon} \sin \delta \quad \dots\dots\dots\dots\dots\dots (105)$$

The double sign of Eq. 105, which is not referred to sign m, signifies compression for the upper sign and dilatancy for the lower sign, because $\textcircled{\epsilon}$ is a positive number and $\bar{\epsilon}$, by definition, is positive when compressive.
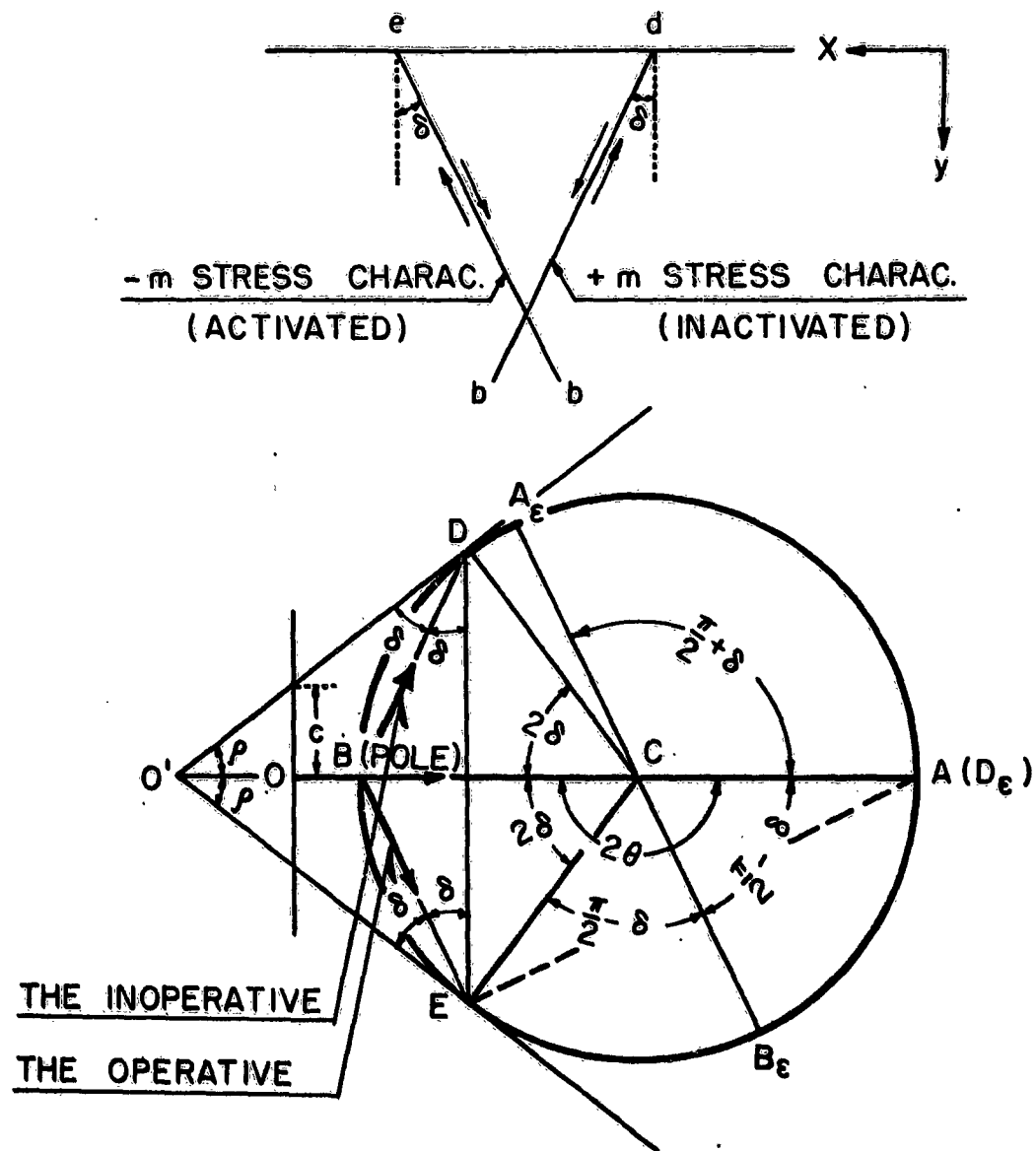

FIG. 8.—THE RANKINE STATE UNDER HORIZONTAL GROUND SURFACE

The plastic work rate, $\dot{W}$, for this case, is found to be

$$\dot{W} = \pm\, 2\, \textcircled{\dot{\epsilon}}\, \cot\rho\, \left[\textcircled{\sigma}\, \cos\delta - c\, \sin\delta\right] \dotfill (106)$$

in which the double sign is in the same order as in Eq. 105. Therefore, if c is sufficiently small, dilatancy cannot take place since $\dot{W}$ must be positive.

Eq. 28, the total differential equation along the strain-rate characteristic directions, is for this case

$$\left(\frac{\partial v_x}{\partial y}\, dx + \frac{\partial v_y}{\partial y}\, dy\right) dy = 0 \dotfill (107)$$

in which the operative strain-rate characteristic direction is

$$dy = -\cot\delta\, dx \dotfill (108)$$

as shown from Eq. 21, and the inoperative strain-rate characteristic direction is

$$dy = 0 \dotfill (109)$$

as shown from Eq. 29.

By substituting Eq. 108 into Eq. 107, it is found that

$$V = v_y\, \cos\delta - v_x\, \sin\delta \dotfill (110)$$

is a function of t alone. V is the component of velocity along the operative strain-rate characteristic direction, the positive direction being downward to the right, as may be recognized from the upper part of Fig. 8. Since Eq. 109 satisfies Eq. 107, another component of velocity is indeterminate in this case, because the equivalence of Eq. 28 with Eqs. 16 and 27, as presented at the bottom of p. 120, does not allow the existence of any other relationship.

The difficulty of determining the component of velocity normal to the operative strain-rate characteristic direction may be avoided by assuming the realization of slip line, in which case

$$v_x = -V(t)\, \sin\delta \dotfill (111)$$

and

$$V = V(t)\, \cos\delta \dotfill (112)$$

Reducing v_x and v_y to functions of t alone causes the strain-rate Mohr circle to dwindle to a point, and neither compression nor dilatancy occur in this case.

Eq. 109 may be determined from the geometry in Fig. 8, in which, for simplicity, the location of A_ϵ is shown for the lower sign of Eq. 104 only. By the geometric interpretation of Eq. 26, D_ϵ must appear at a point in symmetry

with E in respect to A_ϵ B_ϵ and must coincide with A, showing that the inoperative strain-rate characteristic direction is horizontal.

The stress, strain-rate relationships obtained thus far provide equations for determining the distributions of stress and velocity. By substituting the value of θ given by Eq. 100, the Eqs. 30, 31, and 32 change to

$$\sigma_x = \tilde{\sigma}\, 2\, \sin^2 \delta - c \cot \rho \quad \dots \dots \dots \dots \quad (113)$$

$$\sigma_y = \tilde{\sigma}\, 2\, \cos^2 \delta - c \cot \rho \quad \dots \dots \dots \dots \quad (114)$$

and

$$\tau_{xy} = 0 \dots \dots \dots \dots \dots \dots \quad (115)$$

The equations of motion (Eqs. 33 and 34) then become

$$-\frac{dV}{dt} \sin \delta = X \quad \dots \dots \dots \dots \dots \quad (116)$$

and

$$\frac{1}{\gamma} \frac{\partial \tilde{\sigma}}{\partial y}\, 2\, \cos^2 \delta + \frac{dV}{dt} \cos \delta = Y \quad \dots \dots \dots \quad (117)$$

on substitution of Eqs. 111 through 115. The equation of continuity (Eq. 35) becomes

$$\frac{\partial \gamma}{\partial t} + V(t)\, \cos \delta\, \frac{\partial \gamma}{\partial y} = 0 \dots \dots \dots \dots \quad (118)$$

on substitution of Eqs. 111 and 112. Moreover, it is assumed herein that the external force is vibrational:

$$X = a \sin \omega t \quad \dots \dots \dots \dots \dots \quad (119)$$

and

$$Y = g \quad \dots \dots \dots \dots \dots \dots \quad (120)$$

in which a and ω are constants, and g is the acceleration due to gravity.

Then, integration of Eq. 116 yields

$$V(t) = \frac{a}{\omega \sin \delta} \cos \omega t + A \dots \dots \dots \dots \quad (121)$$

in which A is a constant. Eq. 118 is integrated to yield

$$\gamma = C \exp\left[B\left(- y \sec \delta + \frac{a}{\omega^2 \sin \delta} \sin \omega t + A t \right) \right] \dots (122)$$

in which B and C are constants. Then, Eq. 117 is integrated to yield

$$\tilde{\sigma} = - \frac{C}{2 B \cos \delta} (g + a \cot \delta \sin \omega t) \exp\left[B\left(- y \sec \delta \right.\right.$$

$$\left.\left. + \frac{a}{\omega^2 \sin \delta} \sin \omega t + A t \right) \right] +$$

$$+ F(t) \dots (123)$$

on the condition that B is not zero, in which F(t) is a function dependent on t alone.

F(t), in Eq. 123, is determined from the boundary condition that $\sigma_y = 0$ at $y = 0$. The constant A may be determined from the initial condition of the plastic motion, if it is known, such as $V = 0$ at $t = 0$. However, deficiencies in the present knowledge of $c\phi$-material are such that no appropriate method for determining B and C is available.

According to the limitation imposed herein, Eq. 106 shows the value of the plastic work rate for the -m activation in the active state (the +m or -m activation refers to the activation of the +m or -m stress characteristic direction). It may be shown that Eq. 106 is also valid for the +m activation in the active state. In the passive state,

$$\dot{W} = \pm 2 \, \text{\textcircled{$\dot{\epsilon}$}} \, \cot \rho \, \left[\text{\textcircled{σ}} \sin \delta - c \cos \delta \right] \dots (124)$$

for both the +m and -m activation, in which the upper and lower parts of the double sign correspond to cases of compression and dilatancy, respectively. Therefore, if c is sufficiently small, dilatancy can never occur in any of the cases of the Rankine state.

Before advancing the general theory for practical application, several difficulties must be solved. One of the problems is the theorization of the so-called progressive failure, which is an enlargement of the region of plastic motion or elongation of slip lines, or, in the terms of plasticity of metal, elasto-plastic deformation. It is expected that the progressive failure is related to the particular role of time as a parameter, not as an explicit unknown, in the total differential equations for plastic deformation. The total differential equations are not shown, except for Eq. 28, because of space limitation. However, since time derivatives are not considered as unknowns in the simultaneous (algebraic) linear equations for deriving characteristic directions, it is clear that any resulting total differential equations do not contain total differentials in regard to time (see Appendix I).

Example 2—One-Dimensional Secondary Consolidation.—The effect of the flow of water on the two-dimensional motion of $c\phi$-material with the pores filled with water is easily formulated by considering the well-established

empirical fact that the intergranular stress alone is responsible for the motion of $c\phi$-material. Eqs. 10, 11, 12, 27, 30, 31, 32, and 35 may be used with the convention that σ_x, σ_y, and τ_{xy} are the components of intergranular stress, and γ is the submerged unit density of $c\phi$-material. The equations of motion for this case are subject to modification and are obtained by replacing σ_x, σ_y, and τ_{xy} in Eqs. 33 and 34 with $\sigma_x + p$, $\sigma_y + p$, and τ_{xy}, respectively, as follows:

$$\frac{1}{\gamma}\left(\frac{\partial \sigma_x}{\partial x} + \frac{\partial \tau_{xy}}{\partial y}\right) + v_x \frac{\partial v_x}{\partial x} + v_y \frac{\partial v_x}{\partial y} + \frac{\partial v_x}{\partial t} = X - \frac{1}{\gamma}\frac{\partial p}{\partial x} \ldots \quad (125)$$

and

$$\frac{1}{\gamma}\left(\frac{\partial \tau_{xy}}{\partial x} + \frac{\partial \sigma_y}{\partial y}\right) + v_x \frac{\partial v_y}{\partial x} + v_y \frac{\partial v_y}{\partial y} + \frac{\partial v_y}{\partial t} = Y - \frac{1}{\gamma}\frac{\partial p}{\partial y} \ldots \quad (126)$$

in which p represents the water pressure. The characteristic directions determined by these equations are the same as those presented previously since, in obtaining the characteristic directions, p may be assumed to be a function of x, y, and t.

In order to complete the formulation, the assumption in the theory of three-dimensional consolidation[16,17] that the rate of volume decrease of $c\phi$-material is equal to the discharge of water out of the volume under consideration will be introduced. Then,

$$2 \bar{\epsilon} = \text{div } V_w \quad \ldots\ldots\ldots\ldots\ldots\ldots \quad (127)$$

in which V_w is the flux of water through a unit area including sections of soil particles and water. V_w is given by the Darcy law as

$$V_w = - k \text{ grad } \phi \quad \ldots\ldots\ldots\ldots\ldots\ldots \quad (128)$$

in which k is the hydraulic coefficient and ϕ is the velocity potential. Combining Eqs. 127 and 128 yields

$$2 \bar{\epsilon} = - \text{div}(k \text{ grad } \phi) \ldots\ldots\ldots\ldots\ldots \quad (129)$$

In Eq. 129, k is a function of γ and must be considered as a function of x, y, and t.

Consider a layer of $c\phi$-material lying on an impermeable bed, extending infinitely in the horizontal direction and filled with water to the surface, that is being consolidated under a uniform load (q per unit area) on the horizontal

[16] "General Theory of Three-dimensional Consolidation," by M. A. Biot, Journal of Applied Physics, Vol. 12, 1941, p. 155.

[17] "Physics of Consolidation," by Shunsuke Takagi, Report of the Inst. of Science and Tech., Univ. of Tokyo, Tokyo, Japan, Vol. 8, 1954, pp. 221-234.

ground surface. The subject of this analysis is the plastic deformation of the layer, which is known as secondary consolidation. The origin of the x and y axes will be placed on the impermeable bed, the y direction being upward.

The motion of the $c\phi$-material, in this case, must be vertically downward. Therefore, it is assumed that

$$v_x = 0 \dots\dots\dots\dots\dots\dots (130)$$

and that v_y is a function of y and t. Then,

$$\dot{\epsilon}_x = 0 \dots\dots\dots\dots\dots\dots (131)$$

and

$$\dot{\gamma}_{xy} = 0 \dots\dots\dots\dots\dots\dots (132)$$

which are equivalent to

$$\bar{\dot{\epsilon}} + \widehat{\dot{\epsilon}} \cos (2\theta - 2\alpha) = 0 \dots\dots\dots\dots (133)$$

and,

$$- \widehat{\dot{\epsilon}} \sin (2\theta - 2\alpha) = 0 \dots\dots\dots\dots (134)$$

respectively, as may be seen from Eqs. 10, 11, and 12. By making Eqs. 133 and 134 compatible, and considering that compression alone occurs in this case, the following is obtained:

$$2\theta - 2\alpha = \pi \dots\dots\dots\dots\dots (135)$$

and

$$\bar{\dot{\epsilon}} = \widehat{\dot{\epsilon}} \dots\dots\dots\dots\dots\dots (136)$$

By substituting Eq. 136 into Eq. 27, α is determined as

$$2\alpha = \pi \overset{+}{\underset{-}{\ominus}} 2\delta \dots\dots\dots\dots\dots (137)$$

Then, θ in Eq. 135 is determined:

$$2\theta = \overset{+}{\underset{-}{\ominus}} 2\delta \dots\dots\dots\dots\dots (138)$$

The plastic work rate for this case is

$$\dot{W} = 2 \widehat{\dot{\epsilon}} \cot \rho \left[- c + \widehat{\sigma} \cos \rho \right] \dots\dots\dots\dots (139)$$

The flow of water causes another kind of energy dissipation—the frictional loss—and the inequality condition for this case is

$$\dot{W} + k \left(\frac{\partial \, p}{\partial \, y} \right)^2 \gtreqless 0 \ldots \ldots \ldots \ldots \ldots (140)$$

The stress, strain-rate relationship obtained above is summarized and shown in Fig. 9. In accordance with the +m (or the -m) activation, A_+ (or A_-) is the major principal strain-rate point, B_+ (or B_-) is the minor principal strain-rate point, and the pole P_+ (or P_-) coincides with B_- (or B_+). P_+ (or P_-) is shown as the origin of the respective $\dot{\epsilon}$, $\dot{\gamma}$ axes.

Substituting the values of α and θ, thus obtained, into Eqs. 21 and 29, it is found that the operative and the inoperative directions are coincident and horizontal, which is the same as Eq. 109. This fact is also illustrated in Fig. 9, in which two strain-rate characteristic directions are coincident, $P_+ A_+$ (or
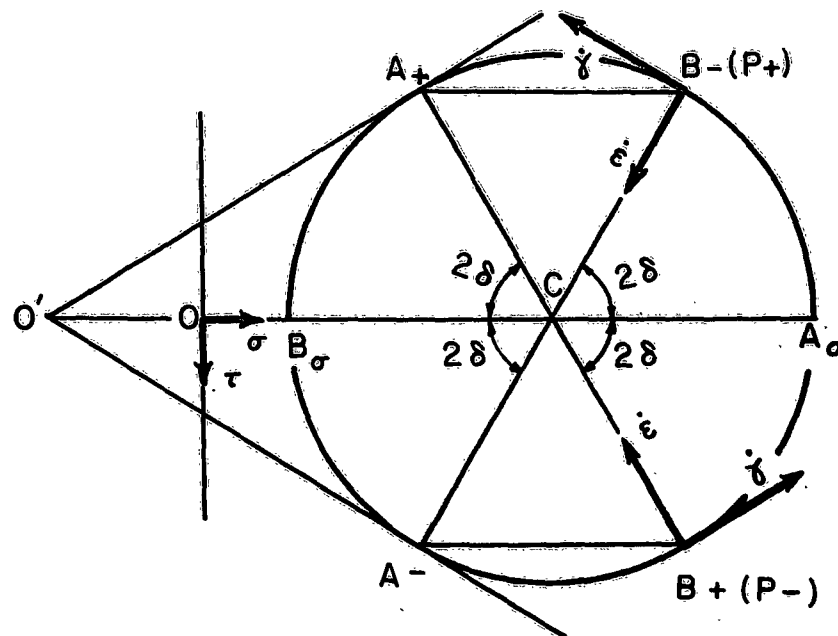

FIG. 9.—STRESS STRAIN-RATE RELATIONSHIP IN THE ONE-
DIMENSIONAL SECONDARY CONSOLIDATION

$P_- A_-$) in accordance with the +m (or -m) activation. Slip lines cannot be developed in this case.

Substituting Eq. 138 into Eqs. 30, 31, and 32 yields

$$\sigma_x = \tilde{\sigma} \left(1 + \sin^2 \rho \right) - c \cot \rho \ldots \ldots \ldots \ldots (141)$$

$$\sigma_y = \tilde{\sigma} \cos^2 \rho - c \cot \rho \ldots \ldots \ldots \ldots \ldots (142)$$

and

$$\tau_{xy} = \oplus \, \tilde{\sigma} \sin \rho \cos \rho \ldots \ldots \ldots \ldots \ldots (143)$$

The state of stress given by Eqs. 141, 142, and 143 is essentially different from the state of stress assumed in the primary consolidation.[17]

For simplicity, it is assumed that no body force is working on the system. Then, substituting Eqs. 141, 142, and 143 into Eqs. 125 and 126 yields

$$\widetilde{\sigma} = F(t) \dotfill (144)$$

and

$$\frac{\partial v_y}{\partial t} = -\frac{1}{\gamma} \frac{\partial p}{\partial y} \dotfill (145)$$

in which $F(t)$ is a function of t alone. The nonlinear local partial derivative is neglected in order to obtain Eq. 145. $F(t)$ will be determined from the boundary condition at the ground surface that

$$\sigma_y + p = q \dotfill (146)$$

if p is known on the boundary.

From Eq. 35,

$$\frac{\partial \gamma}{\partial t} + \frac{\partial (\gamma v_y)}{\partial y} = 0 \dotfill (147)$$

Eq. 129, under the present assumptions, becomes

$$-\frac{\partial v_y}{\partial y} = -\frac{\partial}{\partial y}\left(\frac{k}{\gamma_w} \frac{\partial p}{\partial y}\right) \dotfill (148)$$

which, on integration, yields

$$v_y = \frac{k}{\gamma_w} \frac{\partial p}{\partial y} + G(t) \dotfill (149)$$

in which $G(t)$ is a function of t alone. Using the boundary conditions at the impermeable bed,

$$v_y = 0 \dotfill (150)$$

and

$$\frac{\partial p}{\partial y} = 0 \dotfill (151)$$

$G(t)$ is found to be equal to zero, and

$$v_y = \frac{k}{\gamma_w} \frac{\partial p}{\partial y} \dotfill (152)$$

Combining Eqs. 145 and 152 yields

$$v = -\frac{1}{\gamma_w} k \gamma \frac{\partial v_y}{\partial t} \quad \ldots\ldots\ldots\ldots\ldots\ldots (153)$$

Solution of the simultaneous differential equations (Eqs. 147 and 153) for γ and v_y will give the solution of this problem. The equations can be solved numerically, provided the functional relationship between k and γ is given.

It is interesting to note from Eq. 152 that, in this case, the velocity of $c\phi$-material, which is directed downward, equals the velocity of water, which is directed upward.

It is well known that the pore pressure in secondary consolidation is almost constant throughout the sample in a consolidometer, but it is the writer's opinion that this empirical fact cannot be used in the analysis. To explain this, the form of water surrounding the particles must be considered. The free water that is not affected by the adsorption force of particles flows first under the pressure of the overburden load. When the free water has disappeared, the outermost part of the adsorbed water will begin to move. Successive initiation of motion of the films of adsorbed water, first the outer films, then those closer to the particle, forms the secondary consolidation. But the pressure that causes the motion of these thin water films, surmounting rather high resistance in the adsorbed water, cannot be measured by a piezometer, which indicates the pressure of the stationary free water in the porous stone.

For rigorous treatment, the immovable part of the adsorbed water must be considered as a part of solid particles, and must be included in γ. This necessity arises from the simplification of the complicated flow of adsorbed water in the Darcy law. The Darcy law originally takes into account only the flow of free water that is not affected by the adsorption force of particles. If the Darcy law is extended to cover also the flow of adsorbed water, some modifications of the Darcy law such as mentioned above will be necessary.

Because of these difficulties, a complete explanation of secondary consolidation has not yet been attained. However, the validity of the general theory of plastic deformation herein is manifest also in the analysis for Example 2.

CONCLUSIONS

A consistent mathematical foundation for plane plastic motion of $c\phi$-material is presented herein. However, several problems have yet to be solved.

First, the condition for the existence and uniqueness of the solution under given boundary and initial conditions must be investigated using the proper interpretation of the plastic work rate. It is expected that this condition will provide the general method for determining α.

Second, the theory of three-dimensional plastic motion must be developed in order that the assumption adopted in the theory may be compared with the empirical results. The most essential requisite for this development will be the geometric interpretation of the three-dimensional tensor, with which the strain-rate tensor and stress tensor must be adequately connected in the

same manner as was accomplished herein for the plane plastic motion. The geometry suitable for this objective will be the geometry on a spherical surface or the non-Euclidean elliptic geometry on a plane with suitable geometric interpretation of tensor invariants because these are extensions of the geometry of the Mohr circle used herein.

Third, a theory of pre-plastic deformation, such as that presented by K. Hoshino,[18,19,20] must be connected with this theory in order that the transfer from the pre-plastic to the plastic deformation may be considered.

Fourth, the three-dimensional yield criterion of $c\phi$-material is not known a priori, but may be assumed to be represented by Eq. 7, as was suggested by Drucker and Prager, in accordance with the general theory of plasticity (Appendix IV). It should be noted that the three-dimensional yeild criterion, if established in this form, gives, on limitation of the mode of motion, various specifications of the yield criterion.

An attempt must be made to solve these problems by enlarging the properties of $c\phi$-material to make it an idealization of actual soil. Moreover, if engineers are successful in combining the irreversible thermodynamics with the three-dimensional theory thus developed, then not only soil mechanics but also snow and ice mechanics may come under their command.

APPENDIX I.—PROOF OF YAMAGUCHI'S PRINCIPLE

Consider, for simplicity, a set of only two partial differential equations for only two unknown functions $f(x, y)$ and $g(x, y)$:

$$a_1 \frac{\partial f}{\partial x} + b_1 \frac{\partial f}{\partial y} + c_1 \frac{\partial g}{\partial x} + d_1 \frac{\partial g}{\partial y} = e_1 \quad \ldots \ldots (154)$$

and

$$a_2 \frac{\partial f}{\partial x} + b_2 \frac{\partial f}{\partial y} + c_2 \frac{\partial g}{\partial x} + d_2 \frac{\partial g}{\partial y} = e_2 \quad \ldots \ldots (155)$$

in which a_1 through e_1 and a_2 through e_2 are given functions of x, y, and, in some cases, other parameters. In addition to Eqs. 154 and 155, the conditions of one-valuedness for f and g must be taken into account:

$$df = \frac{\partial f}{\partial x} dx + \frac{\partial f}{\partial y} dy \quad \ldots \ldots \ldots \ldots (156)$$

[18] "A Basic Theory of Plasticity in Soil Mechanics and its Application to Triaxial Test Results," by K. Hoshino, Transactions, J.S.C.E., No. 21, 1954 (in Japanese).

[19] "A General Theory of Mechanics of Soils," by K. Hoshino, Proceedings, 4th Internatl. Conf., S.M.F.E., 1957, London, pp. 160-166.

[20] "An Analysis of the Volume Change, Distortional Deformation and Induced Pore Pressure of Soils Under Triaxial Loading," by K. Hoshino, presented at the 5th Internatl. Conf., Paris, S.M.F.E., 1961.

and

$$dg = \frac{\partial g}{\partial x} dx + \frac{\partial g}{\partial y} dy \dots\dots\dots\dots\dots\, . \ (157)$$

Eqs. 154 through 157 may be considered to form four simultaneous (algebraic) linear equations to determine four unknowns, that is, four partial derivatives of f and g with respect to x and y. By placing the determinant, Δ, of the simultaneous equations equal to zero, the characteristic directions of the partial differential equations, Eqs. 154 and 155, are determined.

When dx : dy represents one of the characteristic directions, the following simultaneous linear equations are solvable, determining the ratio $\lambda : \mu : p : q$.

$$\lambda a_1 + \mu a_2 = p \ dx \ \dots\dots\dots\dots\dots \ (158)$$

$$\lambda b_1 + \mu b_2 = p \ dy \ \dots\dots\dots\dots\dots \ (159)$$

$$\lambda c_1 + \mu c_2 = q \ dx \ \dots\dots\dots\dots\dots \ (160)$$

and

$$\lambda d_1 + \mu d_2 = q \ dy \ \dots\dots\dots\dots\dots \ (161)$$

The existence of the solution is assured since Δ is zero along the characteristic direction. Eqs. 158 through 161 are constructed by multiplying the rows of Δ with λ, μ, p, and q and adding the results.

Multiply Eqs. 154 and 155 by λ and μ, respectively, and add the two equations thus obtained. Then,

$$p \ df + q \ dy = \lambda e_1 + \mu e_2 \ \dots\dots\dots\dots\dots \ (162)$$

Eq. 162 is the total differential equation along the given characteristic direction. This proves Yamaguchi's principle (at the top of p. 115).

This method of finding a total differential equation will be conveniently used to determine the total differential equations along the characteristic directions for the general plastic deformation of cϕ-material. These are not presented herein because of space limitations.

APPENDIX II.—STRAIN-RATE TENSOR IN THE STRAIN-RATE CHARACTERISTIC LINE COORDINATES

The angle of intersection of a pair of conjugate strain-rate characteristic lines is $2\alpha \oplus 2\delta$ (Fig. 7 with substitution of 2α for ϕ) and varies with loca-

tion and time. The analysis of strain-rate tensor under this variable angle of intersection becomes considerably easier and more systematic with the formulation of invariability of tensors and vectors under coordinate transformation. In this section, the notation of tensor analysis will be used for systematic treatment.

Unit vectors are designated at an arbitrary point under consideration in the operative and the inoperative strain-rate characteristic directions, respectively, by e_0 and e_1, and those in the x and y directions, respectively, by e_x and e_y. Then,

$$e_0 = e_x \cos\left(\theta \oplus \delta\right) - e_y \sin\left(\theta \oplus \delta\right) \quad\dots\dots\dots (163)$$

and

$$e_1 = e_x \cos\left(\theta \ominus \delta - 2\alpha\right) - e_y \sin\left(\theta \ominus \delta - 2\alpha\right) \quad\dots (164)$$

in which e_0 and e_1 are covariant basic vectors.

Introduce, in addition to e_0 and e_1, the contravariant basic vectors, e^0 and e^1, which are defined by

$$e_j \cdot e^i = \delta_j^{\,i} \quad\dots\dots\dots\dots\dots\dots (165)$$

in which i and j are indexes expressing 0 or 1, and $\delta_j^{\,i}$ is a Kronecker delta.

The dot indicates a scalar product. e^0 and e^1 are at right angles with e_1 and e_0, respectively, but are not unit vectors. The symbols e^0 and e^1 are expressed easily in terms of e_x and e_y as follows:

$$e^0 \sin\left(2\alpha \oplus 2\delta\right) = - e_x \sin\left(\theta \oplus \delta - 2\alpha\right)$$

$$- e_y \cos\left(\theta \ominus \delta - 2\alpha\right) \dots\dots\dots\dots (166)$$

and

$$e^1 \sin\left(2\alpha \oplus 2\delta\right) = e_x \sin\left(\theta \oplus \delta\right) + e_y \cos\left(\theta \oplus \delta\right) \dots (167)$$

Or simultaneously solving Eqs. 166 and 167 for e_x and e_y:

$$e_x = e^0 \cos\left(\theta \oplus \delta\right) + e^1 \cos\left(\theta \ominus \delta - 2\alpha\right) \dots\dots (168)$$

and

$$e_y = - e^0 \sin\left(\theta \oplus \delta\right) - e^1 \sin\left(\theta \oplus \delta - 2\alpha\right) \dots\dots (169)$$

Quantities such as $T_{ij}\, e^i\, e^j$, $T_i^{\,j}\, e^i\, e_j$, $T^i_{\,j}\, e_i\, e^j$, and $T^{ij}\, e_i\, e_j$ are called tensors of the second degree, provided they are invariant under coordinate transformation. It is customary to write a vector as $V^i\, e_i$ or $V_i e^i$, combining

components with basic vectors. But this is not true for a tensor. The writer is indebted to Y. Yoshimura[7,8] for this manner of expressing tensors. In the preceding equations, $e^i e^j$, and so forth, do not signify any kind of product, but merely indicate sequences of two basic vectors. It should be noted that the convention of the dummy index in the tensor analysis is observed. Therefore, $T_{ij} e^i e^j$, for example, is the sum of four terms. A tensor of the second degree may be expressed by any one of the above four forms. When expressed in the first or the fourth form, a set of four terms, T_{ij} or T^{ij}, respectively, is called a set of covariant or contravariant components of a tensor of the second degree. The components of strain-rate tensor with physical meaning must be covariant, because other forms cannot give the well-established law of transformation.

Designating the indexes expressing x or y by λ and μ, the invariability of the strain-rate tensor under coordinate transformation is expressed as

$$\dot{\epsilon}_{ij} \, e^i \, e^j = \dot{\epsilon}_{\lambda\mu} \, e^\lambda \, e^\mu \quad \dots\dots\dots\dots (170)$$

It should be noted that e^λ equals e_λ in the x, y coordinate system, in which the x and y directions are fixed and are orthogonal. Substitute Eqs. 168 and 169 into Eq. 170, and compare the coefficients of $e^0 e^0$, $e^0 e^1$, $e^1 e^0$, and $e^1 e^1$. Then,

$$\dot{\epsilon}_{00} = \dot{\epsilon}_{xx} \cos^2 \left(\theta \pm \delta\right) - \dot{\epsilon}_{xy} \sin \left(2\theta \pm 2\delta\right)$$

$$+ \dot{\epsilon}_{yy} \sin^2 \left(\theta \pm \delta\right) \quad \dots\dots\dots\dots (171)$$

$$\dot{\epsilon}_{01} = \dot{\epsilon}_{10} = \dot{\epsilon}_{xx} \cos \left(\theta \pm \delta\right) \cos \left(\theta \pm \delta - 2\alpha\right) - \dot{\epsilon}_{xy} \sin \left(2\theta - 2\alpha\right)$$

$$+ \dot{\epsilon}_{yy} \sin \left(\theta \pm \delta\right) \sin \left(\theta \pm \delta - 2\alpha\right) \quad \dots\dots\dots (172)$$

and

$$\dot{\epsilon}_{11} = \dot{\epsilon}_{xx} \cos^2 \left(\theta \mp \delta - 2\alpha\right) - \sin \left(2\theta \mp 2\delta - 4\alpha\right)$$

$$+ \dot{\epsilon}_{yy} \sin^2 \left(\theta \mp \delta - 2\alpha\right) \quad \dots\dots\dots\dots (173)$$

in which the property

$$\dot{\epsilon}_{xy} = \dot{\epsilon}_{yx} \quad \dots\dots\dots\dots\dots (174)$$

is used.

Reverting to the original notation, and substituting Eqs. 10, 11, and 12 into Eqs. 171, 172, and 173 yields

$$\dot{\epsilon}_0 = \bar{\bar{\epsilon}} + \textcircled{\dot{\epsilon}} \cos \left(2\alpha \textcircled{\pm} 2\delta\right) \quad \ldots \ldots \ldots \ldots \ldots (175)$$

$$\dot{\epsilon}_1 = \bar{\bar{\epsilon}} + \textcircled{\dot{\epsilon}} \cos \left(2\alpha \textcircled{\pm} 2\delta\right) \quad \ldots \ldots \ldots \ldots \ldots (176)$$

and

$$\dot{\gamma}_{01} = \bar{\bar{\epsilon}} \cos \left(2\alpha \textcircled{\pm} 2\delta\right) + \textcircled{\dot{\epsilon}} \quad \ldots \ldots \ldots \ldots (177)$$

When the compression characteristic, Eq. 27, is used, Eqs. 175, 176, and 177 reduce to

$$\dot{\epsilon}_0 = 0 \quad \ldots \ldots \ldots \ldots \ldots \ldots \ldots \ldots (178)$$

$$\dot{\epsilon}_1 = 0 \quad \ldots \ldots \ldots \ldots \ldots \ldots \ldots \ldots (179)$$

and

$$\dot{\gamma}_{01} = \textcircled{\dot{\epsilon}} \sin^2 \left(2\alpha \textcircled{\pm} 2\delta\right) \ldots \ldots \ldots \ldots \ldots (180)$$

The following equation defines $\bar{\bar{\epsilon}}$:

$$2 \bar{\bar{\epsilon}} = g^{ij} \dot{\epsilon}_{ij} \quad \ldots \ldots \ldots \ldots \ldots \ldots \ldots (181)$$

in which g^{ij} is given[7,8,9] by $\mathbf{e}^i \cdot \mathbf{e}^j$. Eq. 181 becomes the compression characteristic when Eqs. 166 and 167 and Eqs. 175, 176, and 177 are substituted in the right-hand side.

The tensor analysis introduced in this manner in the Euclidian geometry is much simpler and more comprehensible than the tensor analysis in the Riemannian geometry, in which the concept of basic vectors cannot be used consistently. The reason for this is that the Riemannian geometry is constructed as a limitation of the Euclidian geometry by omitting an appropriately chosen number of pairs of basic vectors in the latter. As long as algebraic calculation alone is concerned, the basic vectors in both geometries are used consistently. When, however, differentiation of vectors and tensors is introduced, the use of basic vectors must be abandoned in the case of the Riemannian geometry because the derivative of a vector in the Riemannian space, which is a part of the Euclidian space, cannot necessarily be confined in the original Riemannian space. In order to obtain a clear description of the Euclidian geometry, it is advisable to use the combination of components and basic vectors instead of using components alone, as was done in the Riemannian geometry. For example, it will be found that all the formulas for rec-

tangular coordinates are valid intact even for the curvilinear coordinates, if combinations of components and basic vectors are adopted to express vectors and tensors.

APPENDIX III.—STRESS, STRAIN-RATE RELATIONSHIP

Consider $\bigcirc\!\!\!\!\!\sigma$ and $\bar{\sigma}$ to be the radius and the σ coordinate of the center, respectively, of the Mohr circle of stress, as shown in Fig. 3. Then Eqs. 30, 31, and 32 may be written in another form:

$$\sigma_x = \bar{\sigma} + \bigcirc\!\!\!\!\!\sigma \cos 2\theta \quad\ldots\ldots\ldots\ldots\ldots (182)$$

$$\sigma_y = \bar{\sigma} - \bigcirc\!\!\!\!\!\sigma \cos 2\theta \quad\ldots\ldots\ldots\ldots\ldots (183)$$

and

$$\tau_{xy} = -\bigcirc\!\!\!\!\!\sigma \sin 2\theta \quad\ldots\ldots\ldots\ldots\ldots (184)$$

in which

$$\bigcirc\!\!\!\!\!\sigma = \tilde{\sigma} \sin \rho = \bar{\sigma} \sin \rho + c \cos \rho \quad\ldots\ldots\ldots (185)$$

In order to obtain the stress, strain-rate relationship in harmonious form, Eqs. 182, 183, and 184, rather than Eqs. 30, 31, and 32, must be used with Eqs. 10, 11, and 12 and Eq. 27 to eliminate θ, because $\bigcirc\!\!\!\!\!\sigma$ and $\bar{\sigma}$ are the same type of tensor invariants as $\bigcirc\!\!\!\!\!\epsilon$ and $\bar{\epsilon}$.

The following is one of the expressions of the stress, strain-rate relationship:

$$\frac{\bigcirc\!\!\!\!\!\sigma}{\bigcirc\!\!\!\!\!\epsilon} \dot{\epsilon}_x = \frac{\sigma_x}{2} \cos \rho \cos \left(\rho \mp 2\alpha\right) - \frac{\sigma_y}{2} \left[\cos 2\alpha + \sin \rho \sin \left(\rho \mp 2\alpha\right)\right] -$$

$$- \tau_{xy} \sin 2\alpha - c \cos \rho \sin \left(\rho \mp 2\alpha\right) \quad\ldots\ldots\ldots (186)$$

$$\frac{\bigcirc\!\!\!\!\!\sigma}{\bigcirc\!\!\!\!\!\epsilon} \dot{\epsilon}_y = \frac{\sigma_y}{2} \cos \rho \cos \left(\rho \mp 2\alpha\right) - \frac{\sigma_x}{2} \left[\cos 2\alpha + \sin \rho \sin \left(\rho \mp 2\alpha\right)\right] +$$

$$+ \tau_{xy} \sin 2\alpha - c \cos \rho \sin \left(\rho \mp 2\alpha\right) \quad\ldots\ldots\ldots (187)$$

$$\frac{\bigcirc\!\!\!\!\!\sigma}{\bigcirc\!\!\!\!\!\epsilon} \dot{\gamma}_{xy} = \tau_{xy} \cos 2\alpha + \frac{\sigma_x - \sigma_y}{2} \sin 2\alpha \quad\ldots\ldots\ldots (188)$$

However, the most charming of the several possible expressions of the stress, strain-rate relationship may be the following matrix representation with reduction of the tensor to deviatoric:

$$\frac{1}{\dot{\epsilon}}\begin{bmatrix} \dot{\epsilon}'_x & \dot{\gamma}_{xy} \\ \dot{\gamma}_{xy} & \dot{\epsilon}'_y \end{bmatrix} = \frac{1}{\sigma}\begin{bmatrix} \cos 2\alpha & -\sin 2\alpha \\ \sin 2\alpha & \cos 2\alpha \end{bmatrix}\begin{bmatrix} \sigma'_x & \tau_{xy} \\ \tau_{xy} & \sigma'_y \end{bmatrix} \quad \dots \dots (189)$$

in which a prime signifies that the respective quantity is deviatoric. Eq. 189 shows that the two deviatoric tensors are connected by a matrix, as if a cφ-material is an anisotropic material.

When $\alpha = 0$, the following relationships exist:

$$\frac{1}{2\dot{\epsilon}}\dot{\epsilon}_x = \frac{\partial}{\partial \sigma_x}\left(\sigma - \bar{\sigma} \sin \rho\right) \dots \dots \dots (190)$$

$$\frac{1}{2\dot{\epsilon}}\dot{\epsilon}_y = \frac{\partial}{\partial \sigma_y}\left(\sigma - \bar{\sigma} \sin \rho\right) \dots \dots \dots (191)$$

$$\frac{1}{\dot{\epsilon}}\dot{\gamma}_{xy} = \frac{\partial}{\partial \tau_{xy}}\left(\sigma - \bar{\sigma} \sin \rho\right) \dots \dots \dots (192)$$

in which

$$\sigma^2 = \left(\frac{\sigma_x - \sigma_y}{2}\right)^2 + \tau_{xy}^2 \dots \dots \dots \dots (193)$$

and

$$\bar{\sigma} = \frac{\sigma_x + \sigma_y}{2} \dots \dots \dots \dots \dots (194)$$

Therefore,

$$\Psi = \sigma - \bar{\sigma} \sin \rho \dots \dots \dots \dots \dots (195)$$

is a plastic potential in plane deformation for the case in which Saint-Venant's postulation is valid. It should be noted that

$$\Psi = c \cos \rho \dots \dots \dots \dots \dots (196)$$

is the Mohr criterion of yielding. The validity of the concept of plastic potential in the Drucker and Prager plane deformation of cφ-material is manifest in this analysis.

APPENDIX IV.—BEARING ON THE DRUCKER AND PRAGER THREE-DIMENSIONAL DEFORMATION

By placing $\alpha = 0$ in Eqs. 186, 187, and 188, the following is obtained:

$$\frac{\textstyle\bigodot{\sigma}}{\textstyle\bigodot{\epsilon}} \dot{\epsilon}_x = \frac{\cos^2 \rho}{2} \sigma_x - \frac{1 + \sin^2 \rho}{2} \sigma_y - c \sin \rho \cos \rho \dots \dots (197)$$

$$\frac{\textstyle\bigodot{\sigma}}{\textstyle\bigodot{\epsilon}} \dot{\epsilon}_y = \frac{\cos^2 \rho}{2} \sigma_y - \frac{1 + \sin^2 \rho}{2} \sigma_x - c \sin \rho \cos \rho \dots \dots (198)$$

and

$$\frac{\textstyle\bigodot{\sigma}}{\textstyle\bigodot{\epsilon}} \dot{\gamma}_{xy} = \tau_{xy} \dots \dots \dots \dots \dots \dots \dots (199)$$

When x and y are the principal axes, the Eqs. 197, 198, and 199 may be abbreviated as follows:

$$\frac{\textstyle\bigodot{\sigma}}{\textstyle\bigodot{\epsilon}} \dot{\epsilon}_i = \frac{\cos^2 \rho}{2} \sigma_i - \frac{1 + \sin^2 \rho}{2} \sigma_j - c \sin \rho \cos \rho \dots \dots (200)$$

in which a set of indexes, i and j, represents the two sets of cyclic permutations of the indexes 1 and 2 of the principal axes.

The generalization of Eq. 200 to three-dimensional deformation may be:

$$K \dot{\epsilon}_p = \sigma_p - \nu \left(\sigma_q + \sigma_r \right) - A \dots \dots \dots \dots \dots (201)$$

in which K, ν, and A are undetermined constants, and the indexes p, q, and r represent the three sets of cyclic permutations of the indexes 1, 2, and 3 of the principal axes.

In the case of the plane strain, it may be assumed that

$$\dot{\epsilon}_3 = 0 \dots \dots \dots \dots \dots \dots \dots \dots (202)$$

and

$$\sigma_3 = \nu \left(\sigma_1 + \sigma_2 \right) + A \dots \dots \dots \dots \dots \dots (203)$$

Then,

$$K \, \dot{\epsilon}_i = \sigma_i \left(1 - \nu^2\right) - \sigma_j \left(\nu + \nu^2\right) - A \, (1 + \nu) \, \ldots \ldots \quad (204)$$

Comparing Eq. 204 with Eq. 200, it is found that

$$\nu = \frac{1 + \sin^2 \rho}{2} \, \ldots \ldots \ldots \ldots \ldots \quad (205)$$

and

$$A = c \, \sin \rho \, \cos \rho \, \ldots \ldots \ldots \ldots \ldots \quad (206)$$

Determined in this manner, K is referred to as the two-dimensional tensor invariant, and cannot be used in the three-dimensional deformation.

A three-dimensional plastic potential Ψ_3 may be defined by

$$\frac{\partial \, \Psi_3}{\partial \, \sigma_\lambda} = K \, \dot{\epsilon}_\lambda \, \ldots \ldots \ldots \ldots \ldots \quad (207)$$

with $\lambda = 1, 2,$ and 3. Substituting Eqs. 202 and 203 into the right-hand side of Eq. 207 and integrating the three equations thus obtained yields

$$\Psi_3 = \frac{1}{2} \left(\sigma_1^2 + \sigma_2^2 + \sigma_3^2\right) - \nu \left(\sigma_1 \, \sigma_2 + \sigma_2 \, \sigma_3 + \sigma_3 \, \sigma_1\right)$$

$$- A \left(\sigma_1 + \sigma_2 + \sigma_3\right) + B \, \ldots \ldots \ldots \ldots \quad (208)$$

in which B is an integration constant, and ν and A are given by Eqs. 205 and 206. By using the relationships

$$\sigma_1^2 + \sigma_2^2 + \sigma_3^2 = \frac{1}{3} J_1^2 + 2 J_2 \, \ldots \ldots \ldots \ldots \quad (209)$$

and

$$\sigma_1 \, \sigma_2 + \sigma_2 \, \sigma_3 + \sigma_3 \, \sigma_1 = \frac{1}{3} \left(J_1^2 - J_2\right) \ldots \ldots \ldots \quad (210)$$

Ψ_3 changes to

$$\Psi_3 = J_2 \, (1 + \nu) - \frac{\sin^2 \rho}{2} J_1^2 - J_1 \, c \, \sin \rho \, \cos \rho + B \, \ldots \quad (211)$$

Therefore, by placing

$$B = - \frac{3}{2} c^2 \, \cos^2 \rho \, \ldots \ldots \ldots \ldots \ldots \quad (212)$$

172

it follows that

$$\Psi_3 = \frac{1}{2}\left(3 + \sin^2\rho\right)\left[J_2 - \lambda^2\left(J_1 + 3\ c\ \cot\rho\right)^2\right] \quad \ldots\ (213)$$

by introducing λ which is defined by

$$\lambda = \frac{\sin\rho}{\sqrt{3\left(3 + \sin^2\rho\right)}} \quad \ldots\ldots\ldots\ldots\ (214)$$

If it is assumed that $\Psi_3 = 0$ is the yield criterion for the three-dimensional plastic deformation of $c\phi$-material. Then, all of the allowable states of stress must be in the region defined by

$$\Psi_3 \leqq 0 \ldots\ldots\ldots\ldots\ldots\ldots\ (215)$$

because particular sets of the allowable state of stress $\sigma_1 = \sigma_2 = \sigma_3$ are contained in this region. Solving the inequality (Eq. 215), it is found that all the allowable stresses are contained either in the region defined by

$$J_2^{1/2} \leqq \lambda\left(J_1 + 3\ c\ \cot\rho\right) \ldots\ldots\ldots\ldots\ (216)$$

or in the region defined by

$$-J_2^{1/2} \geqq \lambda\left(J_1 + 3\ c\ \cot\rho\right) \ldots\ldots\ldots\ldots\ (217)$$

since the boundary of these regions is the yield criterion. By choosing the one region that contains the allowable state of stress $\sigma_1 = \sigma_2 = \sigma_3 = \infty$, it is found that the region of Eq. 216 is allowable, but the region of Eq. 217 is not allowable. Therefore, it is seen, as proposed by Drucker and Prager,[3] that

$$J_2^{1/2} = \lambda\ J_1 + k \ldots\ldots\ldots\ldots\ldots\ (218)$$

in which

$$k = 3\ c\ \cot\rho \ldots\ldots\ldots\ldots\ldots\ (219)$$

is a yield criterion for three-dimensional deformation, and moreover, it is seen that Eq. 8 represents a plastic potential.

One of the difficulties in formulating the three-dimensional theory of $c\phi$-material is that the three-dimensional extension of the Mohr criterion of yielding is not known a priori. However, Eq. 218 may be assumed to be the three-dimensional yield criterion of $c\phi$-material because, although Saint-Venant's postulation has been assumed, Eq. 218 has been proven to be the three-dimensional extension of the Mohr criterion of yielding. Furthermore, Eq. 218 is the simplest of any possible expressions.

As shown by Hill,[21] the three-dimensional yield criterion of the most general isotropic plastic material is a function of J_1, J_2, and J_3 in which J_3 is the third invariant of stress tensor. Then, if it is assumed that Eq. 218 is the three-dimensional yield criterion, it must be admitted that λ and k can contain J_3. It is evident that the three-dimensional yield criterion thus established will contain the intermediate principal stress σ_{II} in addition to σ_I and σ_{III}.

It must also be assumed, in accordance with the general theory of plasticity, that the effect of work-hardening (the hysteresis effect) is contained in λ and k in order that the implication of cohesion may be explained. It must be noted that when the mode of motion is limited, the three-dimensional yield criterion in this form gives various specifications of the yield criterion. It seems hopeful to assume this form as the three-dimensional yield criterion of $c\phi$-material. An attempt must be made to establish the three-dimensional yield criterion in such a form as an idealization of actual soil.

APPENDIX V.—NOTATION

a	= amplitude of the vibrational external force;
c	= cohesion;
ds_0, ds_1	= infinitesimal lengths along the operative and the inoperative strain-rate characteristic directions (not used as covariant components);
ds^0, ds^1	= contravariant components of infinitesimal displacement vector;
e_0, e_1, e_i, e_j	= covariant basic vectors;
e^0, e^1, e^i, e^j	= contravariant basic vectors;
e_x, e_y, e^λ, e^μ	= basic vectors in rectangular coordinates;
g	= acceleration due to gravity;
i	= angle of inclination of compound stress;
J_1, J_2, J_3	= first, second, and third invariants of stress tensor;
k	= (1) Darcy constant and (2) positive constant in the three-dimensional yield criterion;
$+m$, $-m$	= sign m of tangential stress;
p	= water pressure;

21 "The Mathematical Theory of Plasticity." by R. Hill, Oxford Univ. Press, New York, N. Y., 1956, p. 15.

q	= overburden in one-dimensional consolidation;
t	= time;
v, V	= magnitude of compound velocity;
v_x, v_y	= components of velocity;
V_w	= flux of water as vector;
$\dot{W}$	= plastic work rate;
X, Y	= x, y components of external force;
α	= angle between major principal axes of stress tensor and strain-rate tensor;
γ	= density of cϕ-material;
γ_w	= density of water;
$\dot{\gamma}_{xy}$	= shearing strain-rate in the x, y coordinate system;
$\dot{\gamma}_{01}$	= shearing strain-rate in the coordinates of the strain-rate characteristic line;
δ	= 1/2 < BCD in Fig. 3;
$\bar{\delta}$	= quantity used instead of δ to signify resonance characteristic direction;
$\dot{\epsilon}_x, \dot{\epsilon}_y, \dot{\epsilon}_{ij}$	= components of strain-rate tensor, positive when compressive;
$\textcircled{\dot{\epsilon}}$	= radius of the strain-rate Mohr circle;
$\bar{\dot{\epsilon}}$	= $\dot{\epsilon}$ coordinate of the center of the strain-rate Mohr circle, one-half the rate of volume decrease;
θ	= angle from the plane of major principal stress to the vertical plane;
λ	= positive constant in the three-dimensional yield criterion;
ν	= nondimensional velocity signifying resonance characteristic direction;
ρ	= frictional angle;
$\bar{\rho}$	= quantity used intead of ρ to signify resonance characteristic direction;
$\sigma_x, \sigma_y, \sigma_{ij}$	= components of stress tensor, positive when compressive;
$\textcircled{\sigma}$	= radius of the stress Mohr circle;
$\bar{\sigma}$	= σ coordinate of the center of the stress Mohr circle;
$\tilde{\sigma}$	= $\overline{O' \, C}$ in Fig. 3;

$\sigma_I, \sigma_{II}, \sigma_{III}$ = principal stresses arranged in the order of magnitude;

$\sigma_1, \sigma_2, \sigma_3$ = principal stresses arranged in an arbitrary order;

τ_{xy}, τ = shear stress;

ϕ = (1) $1/2 < E_\sigma CE_\epsilon$ in Fig. 5 or $1/2 < D_\sigma CD_\epsilon$ in Fig. 6 and (2) the velocity potential of the ground water flow;

Ψ, Ψ_d = plastic potential;

ω = (1) angle from the x axis to the direction of velocity and the (2) quantity signifying vibrational force; and

$\pm$ $\mp$ = sign notation used where either the upper or the lower of the double sign should be taken in accordance with the activation of +m or -m stress characteristic direction.

ERRATA

for the paper

PLANE PLASTIC DEFORMATION OF SOILS

by

Shunsuke Takagi
J. Eng. Mech. Div., Vol 88 EM 3
June, 1962, pp. 107 - 151

Page 135 - Eq. 3a. Change "$\theta + \delta$" to read "$-\theta - \delta$".

Page 137 - Line 1. Change "state of stress" to read "components of stress".

Page 138 - 2nd par, lines 5 & 6. Change "direction of the same sign" to read "directions of the same sign".

3rd par, line 1. Change "general deformation" to "plastic deformation".

Page 143 - Line following Eq. 20. Change "characteristic directions" to read "characteristic direction".

Page 149 - Eq. 68. Change "⊕" to read "⊕".

Page 155 - Eq. 112. Change "$V = V$" to read "$v_y = V$".

Page 159 - 3rd line following Eq. 126. Change "to be a function" to read "to be a given function".

Page 162 - Eq. 153. Change "$v = -\dfrac{1}{\gamma_w}$" to read "$v_y = -\dfrac{1}{\gamma_w}$".

Page 164 - Eq. 162. Change "$q\,dy =$" to read "$+ q\,dg =$".

Page 165 - 3rd line following Eq. 165. Change "the symbols e^0" to read "the vectors e^0".

Page 166 - Eq. 173. Change "$-\sin(2\theta\oplus\ldots)$" to read "$-\dot{\epsilon}_{xy}\sin(2\theta\oplus\ldots)$".

Page 171 - Line following Eq. 207. Change "Eqs. 202 and 203" to read "Eq. 201".

Eq. 210. Change "$=1/3\,(J_1^2 - J_2)$" to read "$=1/3\,J_1^2 - J_2$".

Eq. 211. Change "$\dfrac{\sin^2\rho}{2}$" to read "$\dfrac{\sin^2\rho}{6}$".

Page 172 - Eq. 219. Change "$k = 3c$" to read "$k = 3\lambda c$".

A SEMI-INFINITE PLATE ON AN ELASTIC FOUNDATION

Donald E. Nevel
U. S. Army Cold Regions Research and Engineering Laboratory
Hanover, New Hampshire

SUMMARY. The solution of the semi-infinite plate on an elastic foundation is presented. This problem occurs when operating on the edge of a floating ice sheet. The equations are evaluated for an edge load, and the results given in graphical form for the following:

a. The maximum deflection which occurs at the edge under the load,

b. The moment which causes the initial cracking of the plate,

c. The distance from the edge that the circumferential crack will occur,

d. The moment that causes the circumferential crack.

The same method of solution can be applied to an infinite strip on an elastic foundation with any combination of simple, rigid, or free support at the edges.

INTRODUCTION. In 1923 Westergaard solved the semi-infinite plate on an elastic foundation with concentrated loads equally spaced along the free edge. This situation is shown in Figure 1. The solution to this problem is in the form of a series. Westergaard let the distance (L) between the loads approach infinity to obtain the solution of a single concentrated load acting on the free edge of the plate. The solution to this problem is in the form of an integral.

Westergaard also solved the semi-infinite plate on an elastic foundation loaded with concentrated loads equally spaced along a line parallel to the free edge. This situation is shown in Figure 2. This solution was obtained by connecting a semi-infinite plate to a plate of finite width. Westergaard could have let the distance (L) between the loads approach infinity in order to solve the plate with the single concentrated load arbitrarily placed, but he did not.
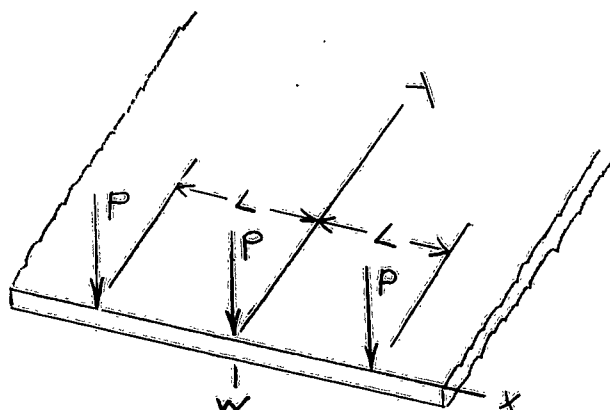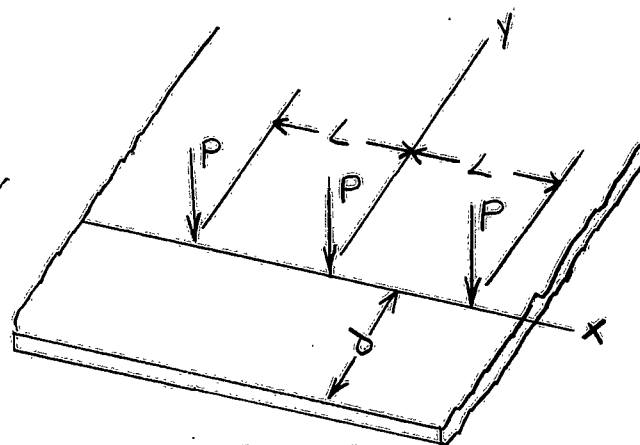
Figure 1   Figure 2

In 1949 Peach used finite differences to solve the semi-infinite plate on an elastic foundation with a concentrated load at the free edge. For Poisson's ratio of 1/3, Peach gave the deflection under the load as $w = 0.351 \ P/k\ell^2$ where k and ℓ are constants that will be defined later. Westergaard had given the correct value of $w = 0.4702 \ P/k\ell^2$ 26 years earlier.

In 1955 Assur translated from Russian a 1943 article by Shapiro. In this article Shapiro states the solution for the semi-infinite plate on an elastic foundation with an arbitrarily placed concentrated load; however, Shapiro did not show the development of the solution.

In 1955 Naghdi, under contract to SIPRE, attempted to solve the semi-infinite plate problem, but was unable to do so. He also could not determine the method of solution used by Shapiro.

Hence, a complete derivation and evaluation of this problem is needed. A practical need occurs in operating on ice sheets floating on water.

The author wishes to thank L. W. Gold of the National Research Council of Canada for a copy of an unpublished manuscript containing a partial solution to the problem. This partial solution did not satisfy all the boundary conditions, but some of the ideas were used in this paper.

A SEMI-INFINITE PLATE ON AN ELASTIC FOUNDATION.   Consider a semi-infinite plate on an elastic foundation, loaded with a concentrated load as shown in Fig. 3.
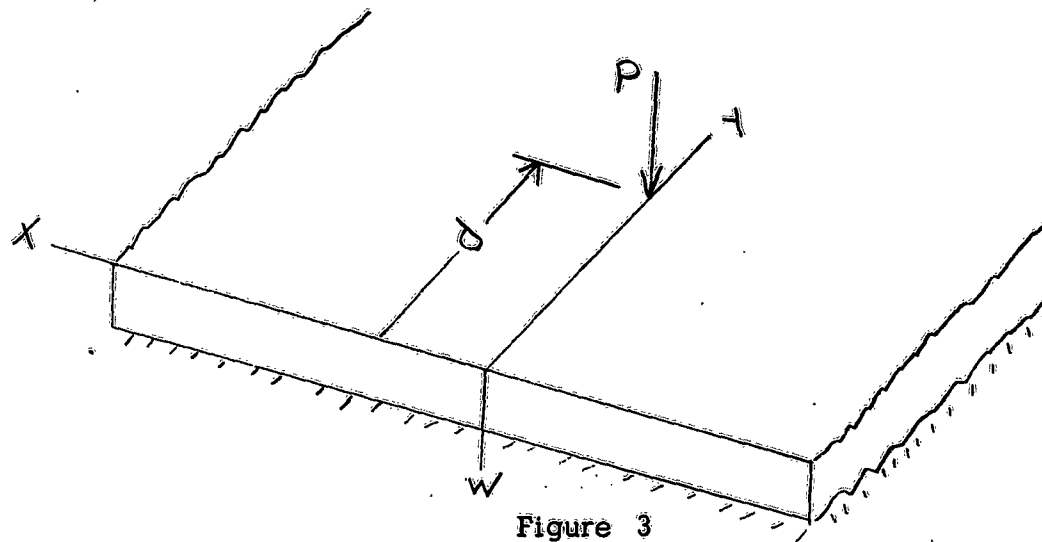
Figure 3

It is assumed that the plate is elastic, homogeneous, and isotropic, and the the edge y=0 is free from forces and constraints. The differential equation of the plate with a concentrated load P at x=0, y=a is

(1) $\dfrac{\partial^4 w}{\partial x^4} + 2 \dfrac{\partial^4 w}{\partial x^2 \partial y^2} + \dfrac{\partial^4 w}{\partial y^4} + \dfrac{k w}{D} = \dfrac{P}{D}\, \delta(y-a)\delta(x)$

where

w = deflection

k = foundation modulus

$D = Eh^3/12(1-\sigma^2)$ = flexural rigidy

E = modulus of elasticity

h = thickness of the plate

σ = Poisson's ratio

δ = Dirac delta function

Letting $\zeta = x/\ell$, $\eta = y/\ell$, $\alpha = a/\ell$, $\omega = wk\,\ell^2/P$ where $\ell^4 = D/k$ the differential equation (1) becomes

(2) $\dfrac{\partial^4 \omega}{\partial \zeta^4} + 2 \dfrac{\partial^4 \omega}{\partial \zeta^2 \partial \eta^2} + \dfrac{\partial^4 \omega}{\partial \eta^4} + \omega = \delta(\eta-\alpha)\,\delta(\zeta)$.

The boundary conditions are

(3) $\quad \omega = \dfrac{\partial^k \omega}{\partial \zeta^k} = 0 \qquad\qquad at \quad \zeta = \pm \infty,$

(4) $\quad \omega = \dfrac{\partial^k \omega}{\partial \eta^k} = 0 \qquad\qquad at \quad \eta = \infty,$

(5) $\quad M_y = \dfrac{D}{\ell^2}\left[\dfrac{\partial^2 \omega}{\partial \eta^2} + \sigma \dfrac{\partial^2 \omega}{\partial \zeta^2}\right] = 0 \quad at \quad \eta = 0,$

(6) $\quad \dfrac{D}{\ell^3}\left[\dfrac{\partial^3 \omega}{\partial \eta^3} + (2-\sigma)\dfrac{\partial^3 \omega}{\partial \eta \partial \zeta^2}\right] = 0 \qquad at \quad \eta = 0,$

where My represents the moment and equation (6) includes the shearing force and twisting moment at the free edge.

Taking the Fourier transform $Y(\phi,\eta) = \displaystyle\int_{-\infty}^{\infty} \omega(\zeta,\eta)\, e^{i\phi\zeta}\, d\zeta$ of equation (2), we obtain

(7) $\quad \dfrac{\partial^4 Y}{\partial \eta^4} - 2\phi^2 \dfrac{\partial^2 Y}{\partial \eta^2} + (1+\phi^4) Y = \delta(\eta - \alpha)$

since equation (3) must be satisfied. The Fourier transform of the other boundary conditions are

(8) $\quad Y = \dfrac{\partial^k Y}{\partial \eta^k} = 0 \qquad at \quad \eta = 0,$

(9) $\quad \dfrac{\partial^2 Y}{\partial \eta^2} - \sigma \phi^2 Y = 0 \qquad at \quad \eta = 0,$

(10) $\quad \dfrac{\partial^3 Y}{\partial \eta^3} - (2-\sigma)\phi^2 \dfrac{\partial Y}{\partial \eta} = 0 \qquad at \quad \eta = 0,$

Taking the Laplace transform $\overline{Y}(\phi,s) = \displaystyle\int_{0}^{\infty} Y(\phi,\eta)\, e^{-s\eta}\, d\eta$ of equation (7), and solving for $\overline{Y}$, we obtain.

(11) $\quad \overline{Y} = \dfrac{(s^3 - 2\phi^2 s) Y(\phi,0) + (s^2 - 2\phi^2) Y'(\phi,0) + s Y''(\phi,0) + Y'''(\phi,0) + e^{-\alpha s}}{s^4 - 2\phi^2 s + 1 + \phi^4}$

where $Y'(\phi,0), Y''(\phi,0), Y'''(\phi,0)$ represent

$$\frac{\partial Y}{\partial \eta}, \quad \frac{\partial^2 Y}{\partial \eta^2}, \quad \frac{\partial^3 Y}{\partial \eta^3} \quad \text{evaluated at } \eta = 0.$$

Using boundary equations (9) and (10) and letting $A = Y(\phi, 0)$, $B = Y'(\phi,0)$, equation (11) becomes the following by means of partial fractions

$$\bar{Y} = \frac{A\epsilon^2\left[1-i\phi^2(1-\sigma)\right]_\Delta + B\left[\epsilon^2(\gamma+i\beta)+\sigma\phi^2(\gamma-i\beta)\right](\beta+i\gamma)-e^{-\alpha\Delta}(\gamma+i\beta)(\beta+i\gamma)}{2\epsilon^2\left[\Delta^2-(\beta+i\gamma)^2\right]}$$

(12)

$$+ \frac{A\epsilon^2\left[1+i\phi^2(1-\sigma)\right]_\Delta + B\left[\epsilon^2(\gamma-i\beta)+\sigma\phi^2(\gamma+i\beta)\right](\beta+i\gamma)-e^{-\alpha\Delta}(\gamma+i\beta)(\beta+i\gamma)}{2\epsilon^2\left[\Delta^2-(\beta+i\gamma)^2\right]}$$

where

$$\epsilon^2 = \sqrt{1+\phi^4}, \quad \beta = \sqrt{\frac{\epsilon^2+\phi^2}{2}} \quad \gamma = \sqrt{\frac{\epsilon^2-\phi^2}{2}}.$$

The inverse Laplace transform of equation (12) is

$$Y = A\left[\cancel{c} - \phi^2(1-\sigma)\,\$s\right]_\eta + \frac{B}{\epsilon^2}\left[\beta(\epsilon^2-\sigma\phi^2)\cancel{c}s + \gamma(\epsilon^2+\sigma\phi^2)\,\$c\right]_\eta$$

(13)
$$+ \frac{H(\eta-\alpha)}{\epsilon^2}\left[\beta\cancel{c}s - \gamma\,\$c\right]_{\eta-\alpha}$$

where $\$ = \sinh\beta p$, $\cancel{c} = \cosh\beta p$, $s = \sin\gamma p$, $c = \cos\gamma p$, p is specified by the subscript, and $H(\eta-\alpha)$ is a unit step function. Applying boundary equation (8) to equation (13) we obtain

(14) $$A = e^{-\beta\alpha} \cdot \frac{\left[\cos\gamma\alpha + \phi^2(1-\sigma)\sin\gamma\alpha\right]}{\gamma\left[4\beta^2\epsilon^2 - (\epsilon^2+\sigma\phi^2)^2\right]}$$

$$B = e^{-\beta\alpha} \frac{\left[\beta(\epsilon^2-\sigma\phi^2)\sin\gamma\alpha - \gamma(\epsilon^2+\sigma\phi^2)\cos\gamma\alpha\right]}{\gamma\left[4\beta^2\epsilon^2 - (\epsilon^2+\sigma\phi^2)^2\right]}.$$

Taking the inverse Fourier transform of equation (13) the solution is

$$(15) \quad W = \frac{P}{2\pi K \ell^2} \int_{-\infty}^{\infty} Y e^{-i\phi\zeta} d\phi = \frac{P}{\pi K \ell^2} \int_0^{\infty} Y \cos\phi\zeta \, d\phi$$

since Y is symmetric with respect to 0. The equations for the moments are

$$(16) \quad M_y = \frac{D}{\ell^2} \left[\frac{\delta^2 W}{\delta\eta^2} + \sigma \frac{\delta^2 W}{\delta\zeta^2} \right] = \frac{P}{\pi} \int_0^{\infty} \left[\frac{\delta^2 Y}{\delta\eta^2} - \sigma\phi^2 Y \cos\phi\zeta \, d\phi \right]$$

$$(17) \quad M_y = \frac{D}{\ell^2} \left[\frac{\delta^2 W}{\delta\zeta^2} + \frac{\delta^2 W}{\delta\eta^2} \right] = \frac{P}{\pi} \int_0^{\infty} \left[-\phi^2 Y + \sigma \frac{\delta^2 Y}{\delta\eta^2} \cos\phi\zeta \, d\phi \right]$$

and

$$(18) \quad \frac{\delta^2 Y}{\delta\eta^2} = A \left[\sigma\phi^2 \Cup c + (\sigma\phi^4 - \epsilon^4) \$s \right]_{\eta} + B \left\{ \beta \left[(2-\sigma)\phi^2 - \epsilon^2 \right] \Cup s \right.$$
$$+ \gamma \left[(2-\sigma)\phi^2 + \epsilon^2 \right] \$c \Big\}_{\eta} + H(\eta - \alpha) \left[\beta \Cup s + \gamma \$c \right]_{\eta = \alpha}.$$

Consider a uniform load from $y = a - m/2$ to $y = a + m/2$ and from $x = -n/2$ to $x = n/2$, as shown in Figure 4. Let $\mu = m/\ell$ and $\nu = n/\ell$.
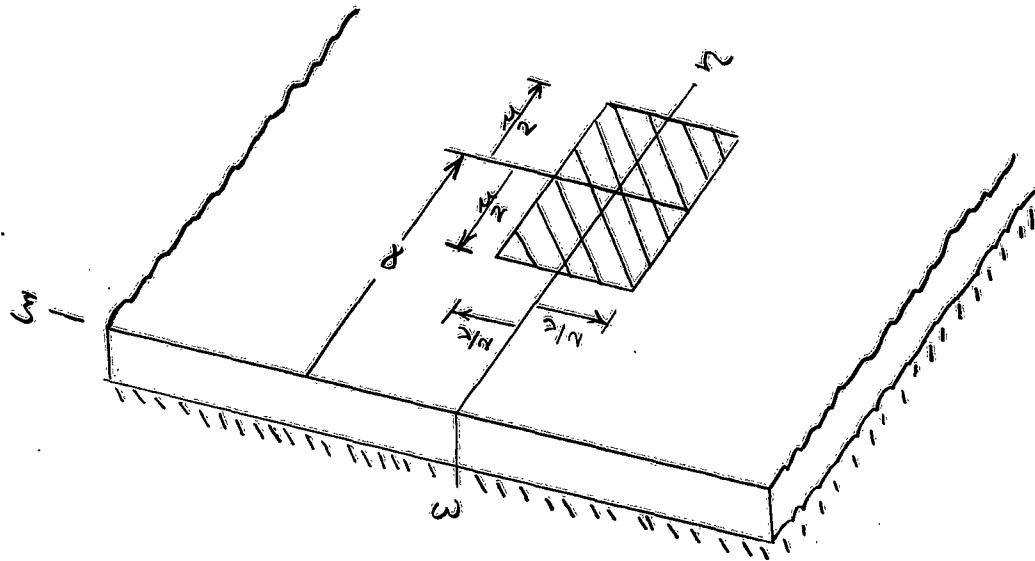
Figure 4.

The solution is obtained by integrating the concentrated load solution, or

$$
(19) \quad W = \frac{P}{\pi k \ell^2 \mu \nu} \int_0^\infty \left[\int_{\alpha - \mu/2}^{\alpha + \mu/2} Y \, d\alpha \right] \left[\int_{-\frac{\nu}{2}}^{\frac{\nu}{2}} \cos \phi \, (\xi - \nu) \, d\nu \right] d\phi ,
$$

where now P is the total load. Integrating,

$$
(20) \quad W = \frac{P}{\pi k \ell^2} \int_0^\infty \frac{Y_1}{\mu} \cdot \frac{2}{\phi \nu} \sin \frac{\phi \nu}{2} \cos \phi \, \xi \, d\phi ,
$$

(21) $Y_1 = \dfrac{A_1}{\epsilon^2}\left[\Phi_c - \phi^2(1-\sigma)\Phi_s\right]_\eta + \dfrac{B_1}{\epsilon^4}\left[\beta(\epsilon^2-\sigma\phi^2)\Phi_s\right.$

$\left. + \delta(\epsilon^2+\sigma\phi^2)\Phi_c\right]_\eta + \dfrac{1}{\epsilon^4}\left[H(\Phi_c - 1 - \phi^2\Phi_s)\right]_{\eta=\alpha+\mu/2}^{\eta=\alpha-\mu/2}$

(22)

$A_1 = 2e^{-\beta\alpha}\dfrac{\beta\left[\epsilon^2-\phi^2(2-\sigma)\right]\left[C_\alpha(\Phi_s)_{\mu/2}-S_\alpha(\Phi_c)_{\mu/2}\right]+\delta\left[\epsilon^2+\phi^2(2-\sigma)\right]\left[S_\alpha(\Phi_s)_{\mu/2}+C_\alpha(\Phi_c)_{\mu/2}\right]}{\delta\left[4\beta^2\epsilon^2-(\epsilon^2+\sigma\phi^2)^2\right]}$

$B_1 = 2e^{-\beta\alpha}\dfrac{(\sigma\phi^4-\epsilon^4)\left[C_\alpha(\Phi_s)_{\mu/2}-S_\alpha(\Phi_c)_{\mu/2}\right]-\sigma\phi^2\left[S_\alpha(\Phi_s)_{\mu/2}+C_\alpha(\Phi_c)_{\mu/2}\right]}{\delta\left[4\beta^2\epsilon^2-(\epsilon^2+\sigma\phi^2)^2\right]}$.

And for determining the moments, we need,

$\dfrac{\delta^2 Y_1}{\delta\eta^2} = \dfrac{A_1}{\epsilon^2}\left[(\sigma\phi^4-\epsilon^4)\Phi_s+\sigma\phi^2\Phi_c\right]_\eta + \dfrac{B_1}{\epsilon^2}\left\{\beta\left[(2-\sigma)\phi^2-\epsilon^2\right]\Phi_s+\delta\left[(2-\sigma)\phi^2+\epsilon^2\right]\Phi_c\right\}_\eta$

(23) $-\left[H\Phi_s\right]_{\eta=\alpha+\mu/2}^{\eta=\alpha-\mu/2}$.

The maximum load capacity of a semi-infinite ice sheet loaded at the edge ($\alpha = \mu/2$), is determined by the maximum deflection and bending moment. The maximum deflection must be less than the depth of ice floating above the water (.084 h > W_{max}), or the plate will become flooded and loose part of its load capacity.

The maximum bending moment must be less than the moment which will crack the ice. For an edge load, the ice will crack as shown in Figure 5. The first crack will occur at the edge under the lead and propagate perpendicular to the edge. A circumferential crack also usually occurs.
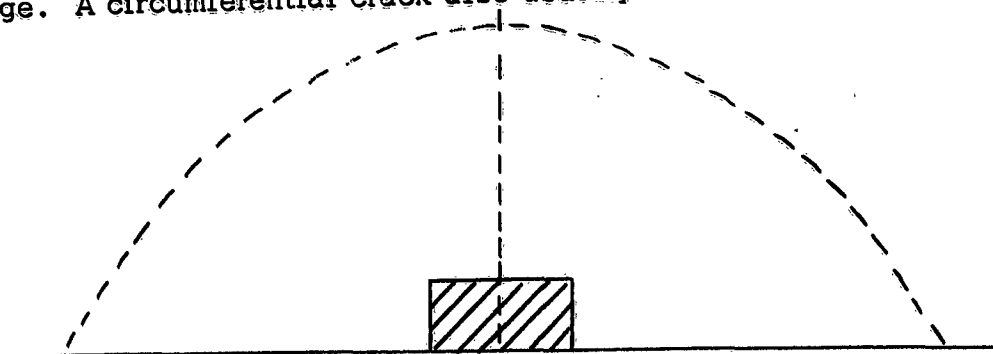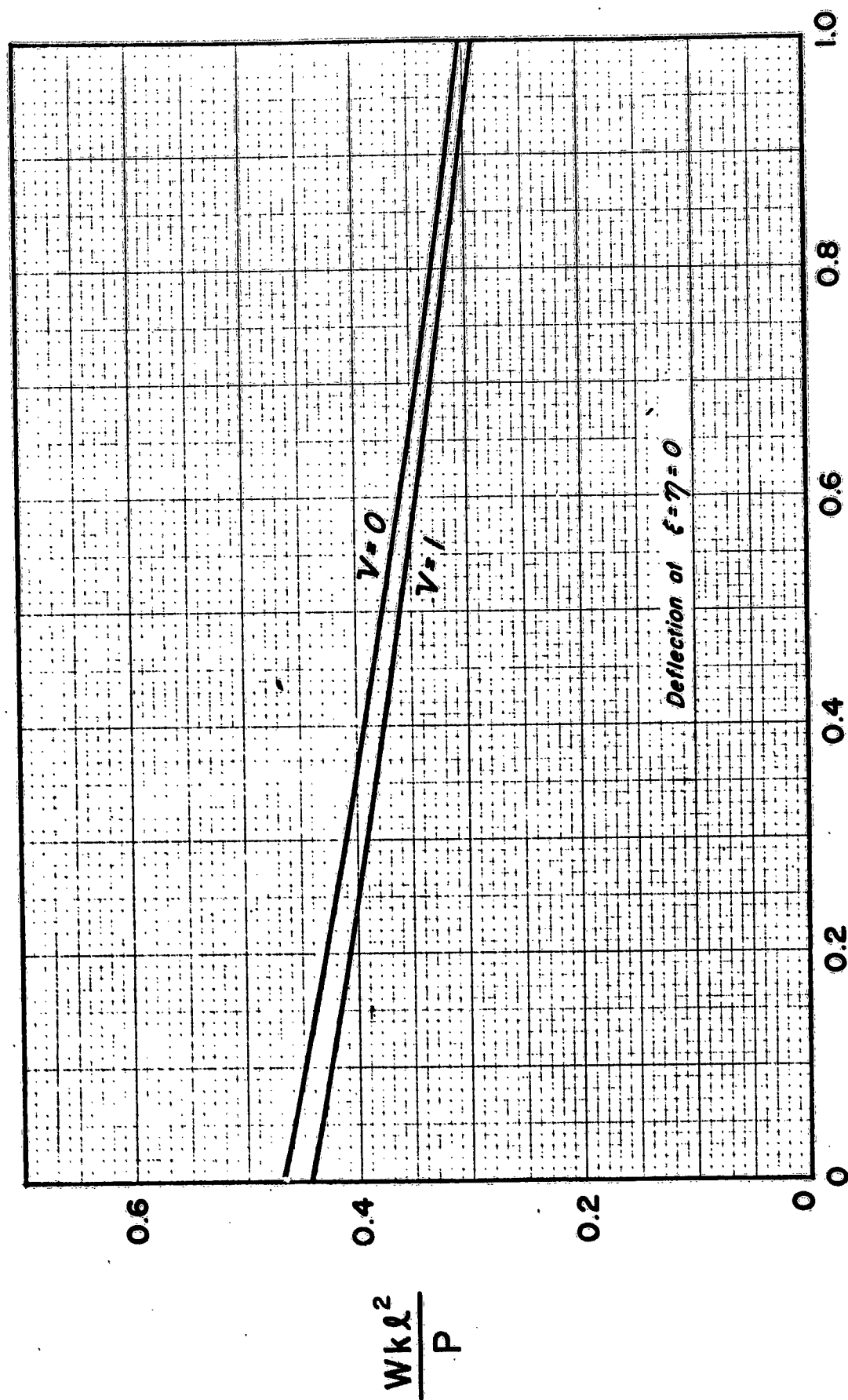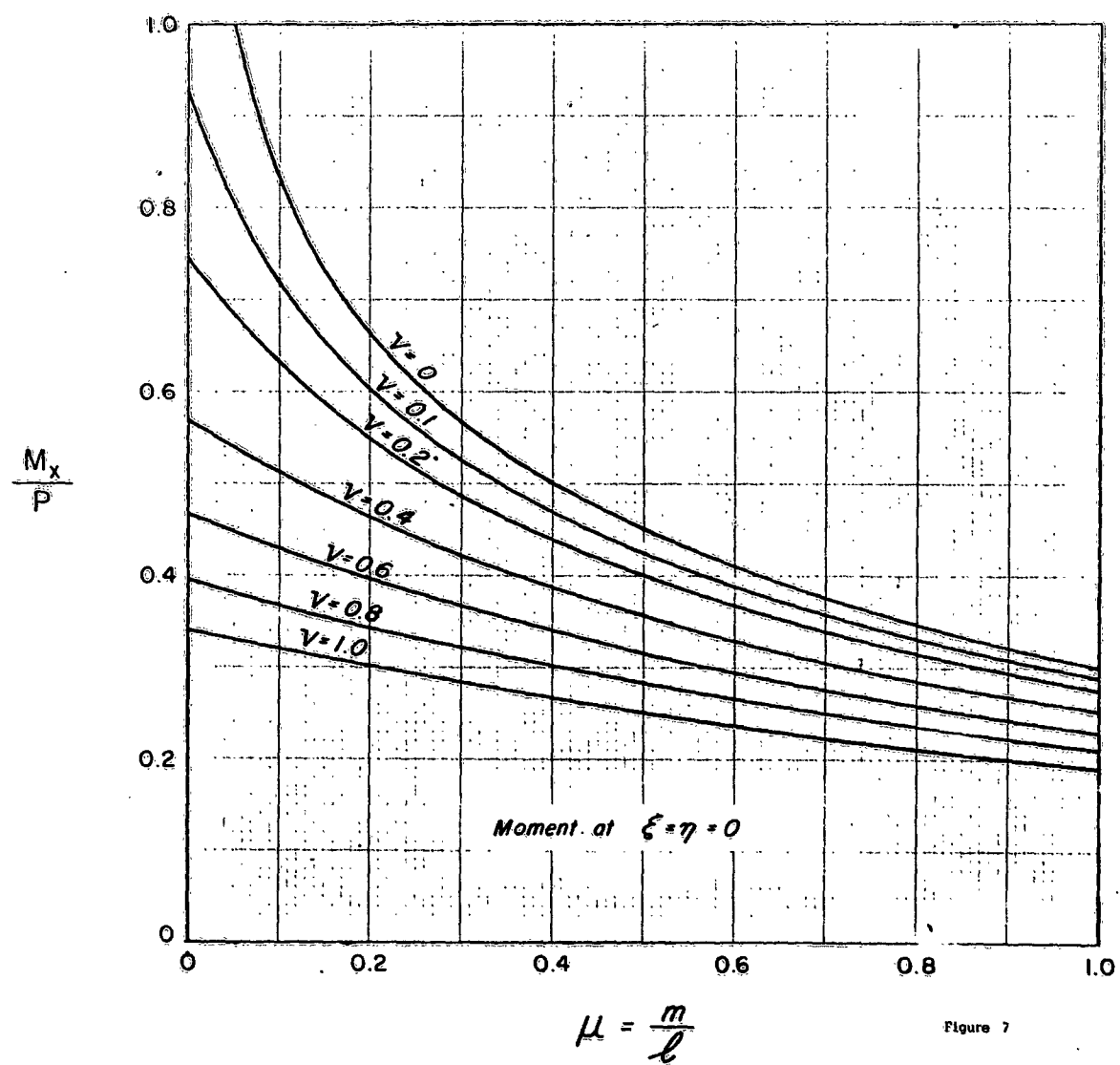

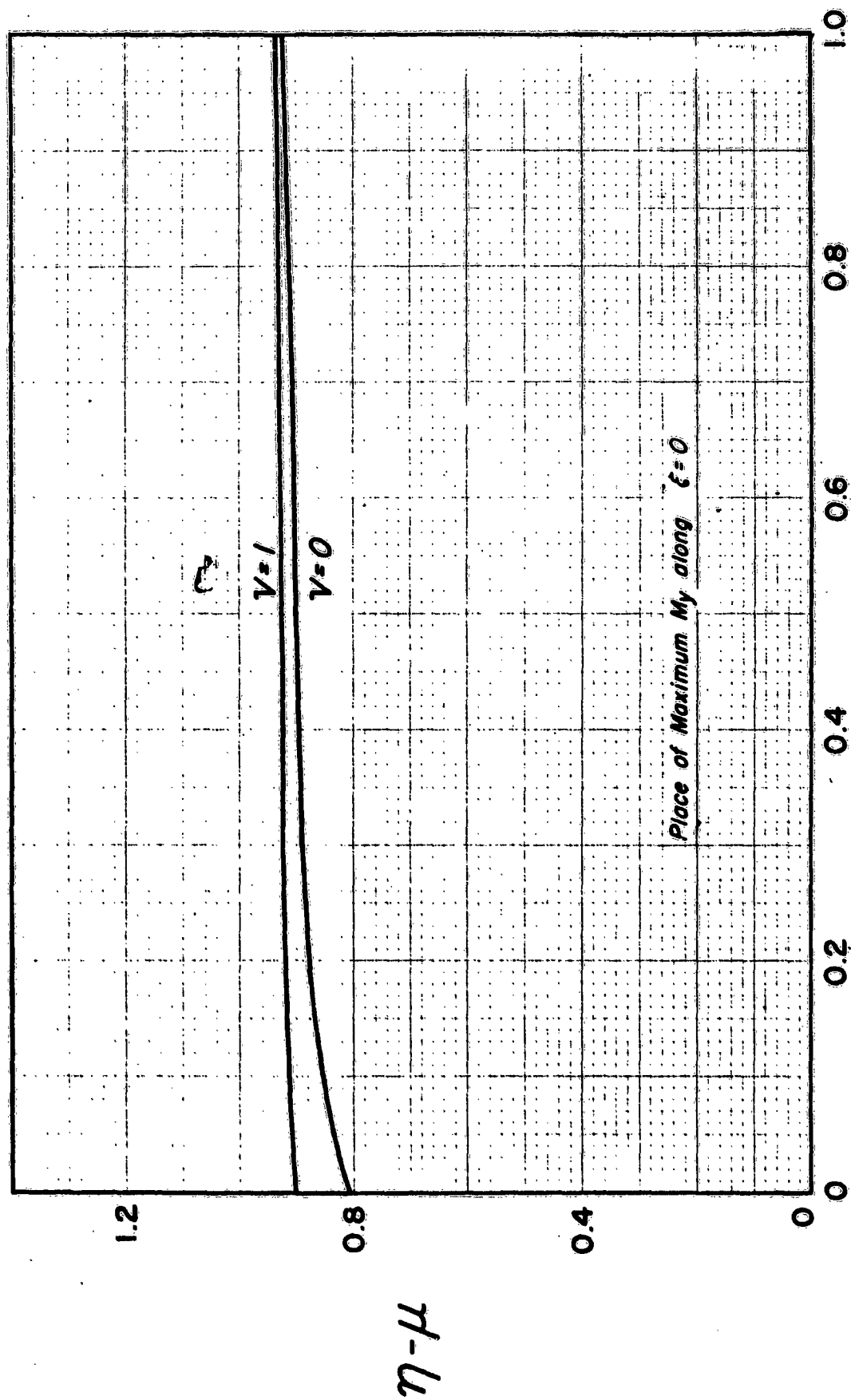Figure 5

Figure 6

$$\mu = \frac{m}{\ell}$$

$$\frac{W k \ell^2}{P}$$

V = 0

V = 1

Deflection at $\xi = \eta = 0$

185

$$\mu = \frac{m}{\ell}$$

Figure 7

Figure 8

For an edge load $a = \mu/2$, letting $\sigma = 1/3$, the following equations were computed and the graphs plotted for various loadings of μ and ν. In each case the integral was divided into two parts. The integral from 0 to 10 was computed by Simpson's rule in increments of $\Delta\phi = 0.1$, and the integral from 10 to ∞ was integrated after making the approximations; $\phi^4 \gg 1$, $\sin\delta\eta = \eta/2\phi$, $\sin\delta\mu = \mu/2\phi$, $\cos\delta\mu = \cos\delta\eta = 1$. The results are accurate to four significant digits.

a) Figure 6 shows the deflection at $x = y = 0$.

$$
(24) \quad \frac{WK\ell^2}{P} = \frac{1}{\pi} \int_0^{10} \frac{A_1}{\mu\epsilon^2} \cdot \frac{2}{\phi\nu} \sin\frac{\phi\nu}{2} \, d\phi
$$

$$
+ \frac{1}{\pi(3+\sigma)} \int_0^{\infty} \left[\frac{(3-\sigma)(1-e^{-\mu\phi})}{(1-\sigma)\mu\phi^4} - \frac{e^{-\mu\phi}}{\phi^3} \right] \frac{2}{\phi\nu} \sin\frac{\phi\nu}{2} \, d\phi.
$$

b) Figure 7 shows the moment M_x at $x = y = 0$. This moment initiates the first crack which is perpendicular to the free edge of the plate.

$$
(25) \quad \frac{M_x}{P} = - \frac{(1-\sigma^2)}{\pi} \int_0^{10} \frac{\phi^2 A_1}{\mu\epsilon^2} \frac{2}{\phi\nu} \sin\frac{\phi\nu}{2} \, d\phi
$$

$$
- \frac{(1-\sigma^2)}{\pi(3+\sigma)} \int_{10}^{\infty} \left[\frac{(3-\sigma)(1-e^{-\mu\phi})}{(1-\sigma)\mu\phi^2} - \frac{e^{-\mu\phi}}{\phi} \right] \frac{2}{\phi\nu} \sin\frac{\phi\nu}{2} \, d\phi.
$$

c) Figure 8 shows the place of the maximum moment M_y along the line $x = 0$.

This moment causes the circumferential crack. Assuming $\eta > \mu$ the equation was solved for η by trial and error.
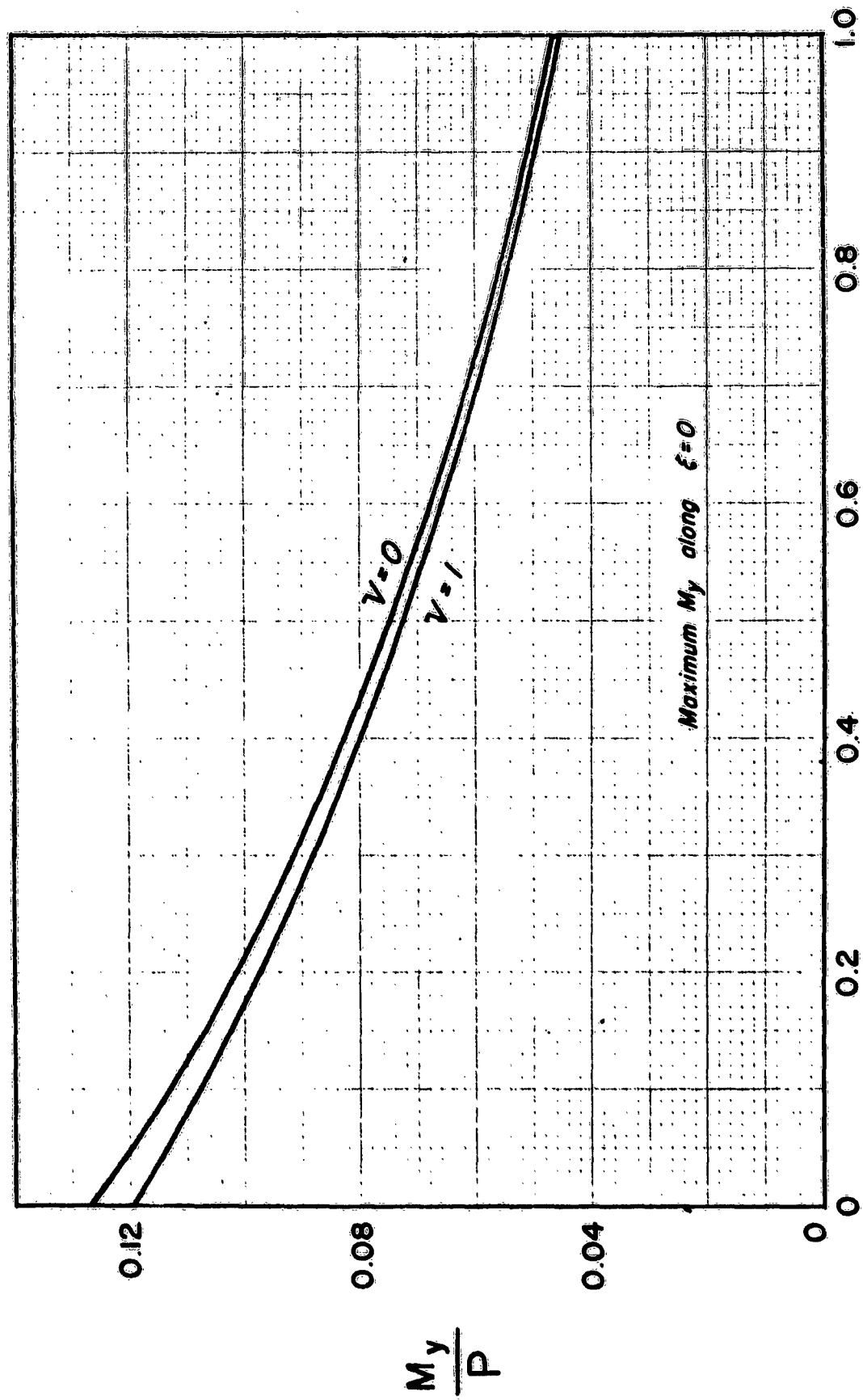
Figure 9

The figure plots $\dfrac{M_y}{P}$ (vertical axis, with values 0.04, 0.08, 0.12) against $\mu = \dfrac{m}{\ell}$ (horizontal axis, from 0 to 1.0). Two curves are shown, labelled $\nu = 0$ and $\nu = 1$. The figure is captioned "Maximum M_y along $\xi = 0$".

$$\frac{\partial}{\partial \eta}\frac{M_y}{P} = \frac{1}{\pi}\int_0^{10}\left\{\left[\left[\epsilon^2\left[1+\phi^4(1-\sigma)^2\right]A_1 + (\sigma\phi^4-\epsilon^4)(1-\phi c)_\mu - \sigma\phi^2(\phi s)_\mu\right](\delta\cos\delta\eta - \beta\sin\delta\eta)\right.\right.$$

(26)

$$-\left[(\sigma\phi^4-\epsilon^4)(\phi s)_\mu + \sigma\phi^2(1-\phi c)_\mu\right](\delta\sin\delta\eta + \beta\cos\delta\eta)\Big\}\frac{e^{-\beta\eta}}{\mu\epsilon^4}\frac{2}{\phi\nu}\sin\frac{\phi\nu}{2}d\phi$$

$$+\frac{(1-\sigma)}{\pi}\int_{10}^{\infty}\left\{\left[\frac{(3-\sigma)(1-e^{-\mu\phi})}{(3+\sigma)\mu}+\frac{(1-\sigma)\phi e^{-\mu\phi}}{(3+\sigma)}\right]\left(\frac{1}{\phi}-\eta\right) + \eta\frac{(1-\cosh\mu\phi)}{\mu}\right.$$

$$\left.-\sinh\mu\phi\right\}e^{-\phi\eta}\frac{2}{\phi\nu}\sin\frac{\phi\nu}{2}d\phi = 0.$$

d) Figure 9 shows the maximum moment M_y along the line x = 0.

$$\frac{M_y}{P} = \frac{1}{\pi}\int_0^{10}\left\{\left[\epsilon^2\left[1+\phi^4(1-\sigma)^2\right]A_1 + (\sigma\phi^4-\epsilon^4)(1-\phi c)_\mu - \sigma\phi^2(\phi s)_\mu\right]\sin\delta\eta\right.$$

(27)

$$\left.+\left[(\sigma\phi^4-\epsilon^4)(\phi s)_\mu + \sigma\phi^2(1-\phi c)_\mu\right]\cos\delta\eta\right\}\frac{e^{-\beta\eta}}{\mu\epsilon^4}\frac{2}{\phi\nu}\sin\frac{\phi\nu}{2}d\phi$$

$$+\frac{(1-\sigma)}{\pi}\int_{10}^{\infty}\left(\left[\frac{(3-\sigma)(1-e^{-\mu\phi})}{(3+\sigma)\mu}+\frac{(1-\sigma)\phi e^{-\mu\phi}}{(3+\sigma)}-\frac{(1-\cosh\mu\phi)}{\mu}-\frac{\sigma\sinh\mu\phi}{2(1-\sigma)\phi^3}\right]\frac{\eta}{2\phi}\right.$$

$$\left.+\frac{\sigma(1-\cosh)\mu\phi)}{(1-\sigma)\phi^2\cdot\mu}-\frac{\sinh\mu\phi}{2\phi}\right\}e^{-\phi\eta}\frac{2}{\phi\nu}\sin\frac{\phi\nu}{2}d\phi.$$

An Infinite Strip on an Elastic Foundation

An infinite strip on an elastic foundation of width 2d is loaded with a concentrated load P as shown in Figure 10. Let $\Delta = d/\ell$.
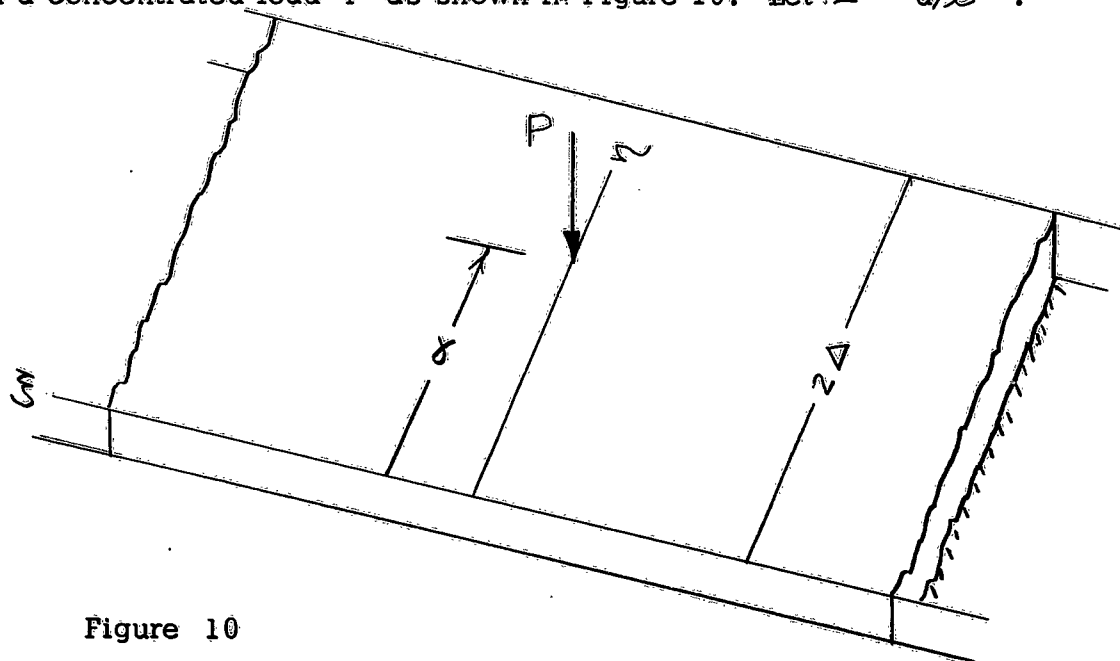

Figure 10

This type of problem with various edge conditions at $\eta = 0$ and $\eta = 2\Delta$ can be solved by the same method as used in the semi-infinite plate. The edge conditions which occur most frequently and their boundary equations are a simple or hinged supported edge,

$$\omega = 0$$

$$\frac{\partial^2 \omega}{\partial \eta^2} + \sigma \frac{\partial^2 \omega}{\partial \zeta^2} = 0$$

a fixed or rigid supported edge,

$$\omega = 0$$

$$\frac{\partial \omega}{\partial \eta} = 0$$

and a free edge.

$$\frac{\partial^2 \omega}{\partial \eta^2} + \sigma \frac{\partial^2 \omega}{\partial \zeta^2} = 0$$

$$\frac{\partial^3 \omega}{\partial \eta^3} + (2-\sigma) \frac{\partial^3 \omega}{\partial \eta \partial \zeta^2} = 0$$

The equations for both edges simply supported and for both edges rigidly supported were derived. Either problem could represent an ice sheet on a river. Numerical evaluation of these equations was not done, since no immediate need was envisioned.

The infinite strip with one edge free and the other simple, fixed, or free differ only in A and B from the semi-infinite plate solution.

The semi-infinite plate problem with either a simple or rigid support at $\eta = 0$, could also have been solved by the same method.

References

1. Westergaard, H. M., Computation of Plates on an elastic foundation with special reference to the problem of tension in concrete roads, Ingenioren, Vol 32 no. 42, 1923.

2. Shapiro, G. S., Design of a plate conceived as an infinite band resting upon an elastic foundation, Comptes Rendus (Doklady) de L Academii des Science de PURSS, Vol XXXVII no. 7-8, 1942.

3. Shapiro, G. S., Deflection of a semi-infinite plate on an elastic foundation, Institut mekhaniki Akademii Nauk SSSR, Prikladnaia mathematika i makhanika, Tom VII, 1943.
SIPRE Translation 48 (1955).

4. Peach, R. W., Bending stresses in a continuous semi-infinite ice field, contained in, Investigation of structural stresses in ice-breaking vessels, edited by J. Ormondroyd, Office of Naval Research, U. S. Navy, Appendix C, Section d, 1950.

5. Naghdi, P., A semi-infinite plate on an elastic foundation with a free edge under concentrated load, contained in, Coupling between moving loads and flexural waves in floating ice sheets, by J. T. Wilson, U. S. Army, Corps of Engineers, SIPRE report 34, 1955.

6. Sneddon, I. N., Fourier transforms, 1951, McGraw-Hill.

OPTIMUM TOLERANCE DESIGN

W. S. Agee
Flight Simulation Laboratory
White Sands Missile Range

INTRODUCTION. The problem of specifying tolerances on the component parts of complex systems has received very little quantative treatment in past system development programs. Almost no methodology has been developed for handling the tolerance design problem. The relative neglect of this problem may be due either to lack of interest or an underestimation of its importance in the system development program. In past programs component tolerances have often been specified in order to meet some tolerance specification on overall subsystem characteristics. However, these subsystem tolerances were set without quantitative consideration of the total system requirements. This procedure can be quite expensive, resulting in either an increase in the cost of building a satisfactory system or the development of an unsatisfactory system. As systems become more and more complex, particularly weapons and space systems with their increasing accuracy requirements, the tolerance design problem becomes increasingly important.

In the tolerance design problem we are given a mathematical model of the system, its inputs and environment, and the performance requirements of the system. We are then required to determine the tolerance of certain random parameters of the system and mathematical model. The tolerance will be defined as some measure of dispersion of the parameter about its nominal value. These tolerances must, of course, be compatible with the specified system performance requirements, and may be optimized on the basis of some desirable criteria. At WSMR we have developed a methodology for the solution of the tolerance design problem which is quite general as far as its area of application is concerned. However, rather than presenting this method abstractly, it will be presented as applied to tolerance design for a guided missile system.

The approach to the tolerance design problem for a guided missile system has been divided into two stages as in Figure 1. The first stage is concerned with the determination of the tolerances for the various subsystems, and the second with the assignment of component tolerances based on the first stage component tolerances. The division of the problem in this manner is for apparent practical reasons.
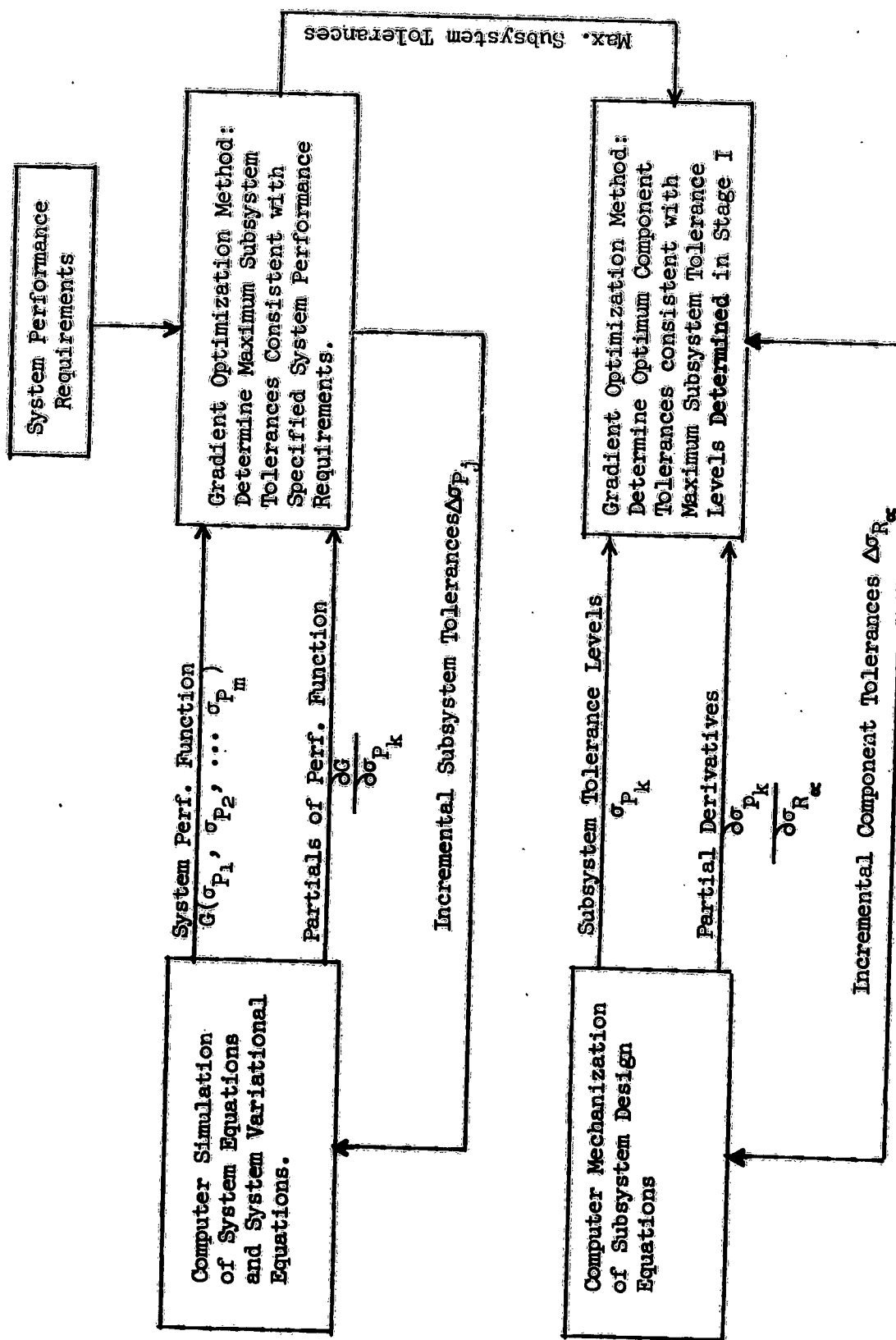
Max. Subsystem Tolerances

System Performance Requirements

Gradient Optimization Method: Determine Maximum Subsystem Tolerances Consistent with Specified System Performance Requirements.

System Perf. Function $G(\sigma_{P_1}, \sigma_{P_2}, \ldots, \sigma_{P_m})$

Partials of Perf. Function $\dfrac{\partial G}{\partial \sigma_{P_k}}$

Incremental Subsystem Tolerances $\Delta\sigma_{P_j}$

Computer Simulation of System Equations and System Variational Equations.

Gradient Optimization Method: Determine Optimum Component Tolerances consistent with Maximum Subsystem Tolerance Levels Determined in Stage I

Subsystem Tolerance Levels σ_{P_k}

Partial Derivatives $\dfrac{\partial \sigma_{P_k}}{\partial \sigma_{R_\alpha}}$

Incremental Component Tolerances $\Delta\sigma_{R_\alpha}$

Computer Mechanization of Subsystem Design Equations

Figure 1

The performance function $G(\sigma_{P_1}, \ldots, \sigma_{P_m})$ for a missile system might be, in the simplest case, the mean square radial miss distance. The subsystem parameters denoted by P_k, $k = 1, \ldots, m$, might be guidance and control parameter, i.e., gains, time constants, etc. Examples of component parameters, R_α, are resistances, capacitances and transistor parameters, of the electronic subsystems.

In the second stage tolerance design the subsystem design equations, i.e., the equations determining the subsystem parameters in terms of the component parameters, will usually be of such complexity to require computer mechanization. From these equations we obtain the subsystem tolerances and their derivatives with respect to the component tolerances. A gradient method is used to increment the component tolerances toward the optimum values.

The use of the two stage method greatly simplifies the complex component tolerance design problem in that it separates the problem into several more tractable tolerance design problems. Another advantage of the two stage method is that design of the subsystem parameter tolerances is possible in the early system design phases, before a concrete design of the subsystems has been established. Before considering explicitly the mathematical formulation of the first stage or subsystem tolerance design problem, we will describe the mathematical representation of the missile system necessary for the formulation and solution of the problem.

SYSTEM REPRESENTATION. The discussion of the system representation will be restricted to continuous dynamic systems, although the methods to be developed will apply to discrete systems as well. The system equations or state equations, i.e., the equations governing the dynamic behavior of the system can be written as

$$\dot{x}_1 (t; P_1, \ldots, P_m) = F_1(x_1, \ldots, x_n; P_1, \ldots, P_m; t) + f_1(t)$$

$$\dot{x}_2 (t; P_1, \ldots, P_m) = F_2(x_1, \ldots, x_n; P_1, \ldots, P_m; t) + f_2(t)$$

$$\dot{x}_n (t; P_1, \ldots, P_m) = F_2(x_1, \ldots, x_n; P_1, \ldots, P_m; t) + f_n(t)$$

where $x_1, \ldots, x_n$ are the state variables of the system, $P_1, \ldots, P_m$ are the subsystem parameters whose tolerances are to be determined, F_i is a known nonlinear function of its arguments, and $f_i(t)$ may be considered as an input to the system. For compactness, the system equations will be written as

$$\dot{x}_i (t; \vec{P}) = F_i(\vec{x}; \vec{P}; t) + f_i(t), \quad i = 1, 2, \ldots, n,$$

where $\vec{x}$ denotes $(x_1, x_2, \ldots, x_n)$ and $\vec{P}$ denotes $(P_1, P_2, \ldots, P_m)$.

Given the values of the state variables at some time, $t = \mathcal{T}$, the functional form of the F_i's, and the system inputs, f_i's, the trajectory of the system is entirely dependent on the values of the subsystem parameters,

P_j. If the system inputs are random functions, an analogous statistical statement can be made. In this case, given the values of the state variables at some time, $t = \mathcal{T}$, the functional form of the F_i 's, the deterministic component of the system input, and the statistical characteristics of the random components of the f_i 's, the statistical characteristics of the trajectory are entirely determined by the values of the subsystem parameters.

VARIATIONAL EQUATIONS. A second set of variables, in addition to the set of state variables, will be useful for the solution of the subsystem tolerance design problem. These variables are the sensitivities of the state variables with respect to the subsystem parameters.

$$\text{Define} \quad w_{ij}(t) = \frac{\partial X_i(t; \vec{P})}{\partial P_j} \quad .$$

The w_{ij} 's are obtainable from the following set of first order, linear differential equations.

$$\dot{w}_{ij}(t) = \sum_{k=1}^{n} \frac{\partial F_i}{\partial x_k} \, w_{kj}(t) + \frac{\partial F_i}{\partial P_j} \, , \quad \begin{array}{l} i = 1, 2, \ldots, n \\[6pt] j = 1, 2, \ldots, m. \end{array}$$

This is easily verified by differentiating the dynamic system equations with respect to the parameter P_j and interchanging the order of differentiation by P_j and t.

Since the state variables are random functions, the sensitivities will also be random functions. We will not consider the possible approaches to

the solution of the variational equations, except to mention that they are usually very complex and must be solved on a computer simultaneously with the nonlinear system equations.

FORMULATION OF THE NONLINEAR PROGRAMMING PROBLEM FOR SUBSYSTEM TOLERANCE DESIGN.

We are now in a position to explicitly formulate and propose a solution of the first stage or subsystem tolerance design problem. Let the m subsystem parameters be random variables denoted by P_j, $j = 1, 2, \ldots, m$. As a measure of the tolerance σ_{P_j} on P_j we choose the RMS deviation of P_j from its nominal or design value. As a system performance function we will choose the mean square radial miss distance, denoted by $G(\vec{\sigma}_p)$

$$ G(\vec{\sigma}_p) = E_{\vec{f}, \vec{P}} \left[x_1^2(\vec{P}; t_f) + x_2^2(\vec{P}; t_f) \right] \quad , $$

where x_1 and x_2 are state variables of the system which we have chosen to be the cartesian components of the miss distance (in two dimensions). The functional form of G is unknown, analytically, however all that will be necessary is that $G(\vec{\sigma}_p)$ and its derivatives be pointwise calculable.

The expectation must be taken over $\vec{f}$, which denotes the random inputs to the system, since the state variables will be subject to random variations even in the absence of random variations in the system parameters. t_f denotes the time of closest approach of missile and target but is not fixed.

Let the performance requirement on the system be

$$ G(\vec{\sigma}_p) \leq R_o^2 \quad . $$

The values of the parameter tolerances must be chosen to satisfy this performance criterion. In general there are many sets of values which will satisfy these specifications. Obviously, we would like to choose each subsystem parameter tolerance as large as possible. In order to

provide a basis for selecting that set of parameter tolerances which best satisfies the criterion of being large, we introduce an objective function as follows. Let the "cost", C_i of a tolerance σ_{p_i} be inversely

proportional to σ_{p_i}. Then the total cost of the subsystem parameter tolerances is

$$C(\vec{\sigma}_p) = \sum_{i=1}^{m} \frac{K_i}{\sigma_{p_i}} \quad ,$$

where K_i is a proportionality constant which provides a relative weighting of the various tolerance costs and also converts each cost to the proper scale of value. In order to keep the discussion simple, we will weigh all tolerance costs equally and choose the value scale which expresses the tolerance as a percentage of nominal value. Then $K_i = p_i^o$

$i = 1, 2, \ldots, m$.

"Cost" of a tolerance as used here is not necessarily to be interpreted in the monetary sense, but rather it provides a measure of the desirability of maintaining a given level of tolerance. This measure of utility possesses the following desirable features which are intuitively associated with a tolerance model.

(1) There is an increasingly severe penalty for the use of small tolerances.

(2) The objective function is a monotonically descreasing function of the tolerance.

(3) The value of a specified increase in tolerance is much greater at lower tolerance levels than at higher ones.

Of course, if a more quantitatively detailed model is desired, the designer is free to incorporate as much detail as available.

In order to specify the subsystem tolerances which satisfy the objective of being largest but yet satisfy the performance requirements of

the missile system, we will minimize the objective function $C(\vec{\sigma}_p)$ subject to the performance constraint. Thus, we have formulated subsystem tolerance design as the nonlinear programming problem

$$\text{Minimize:} \quad C(\vec{\sigma}_p) = \sum_{i=1}^{m} \frac{p_i^o}{\sigma_{p_i}}$$

subject to the constraint $G(\sigma_p) \leqq R_o^2$.

SOLUTION OF THE NONLINEAR PROGRAMMING PROBLEM.

We will now discuss a proposed method of solution for the foregoing program problem, however, since a similar nonlinear programming problem will be formulated for the second stage or component tolerance design problem, the numerical method for solution will be discussed in greater detail later.

The proposed method for the solution of the nonlinear programming problem is a variation of the method described by Charles W. Carroll in JORSA, Mar. 1961, which he calls the "Created Response Surface Technique". This method has proved quite good when applied to the solution of the nonlinear programming problem associated with component tolerance design.

Carroll proposes that, instead of solving the original problem, a sequence of nonlinear programming problems be solved whose final member is the original problem. Specifically, with respect to the problems, under consideration, Carroll's method is to solve the following sequence of problems.

$$\text{Minimize:} \quad H_n(\vec{\sigma}_p) = \sum_{i=1}^{m} \frac{p_i^o}{\sigma_{p_i}} + \frac{\beta_n}{R_o^2 - G(\vec{\sigma}_p)} \quad ,$$

for a finite decreasing sequence of values β_n ending in $\beta_n = 0$ and subject to the constraint $G(\vec{\sigma}_p) \leq R_o^2$. The addition of the weighted reciprocal of the constraint function to the function being minimized imposes an increasingly severe penalty as the constraint boundary is approached. This

has the effect of keeping the solution away from the constraint boundary at every step of the optimization process (except when $\beta_n = 0$). The result of Carroll's method is to arrive at minima for the non-zero values of β_n which are successively closer to the minimum of the original problem, without ever arriving at a constraint boundary. When $\beta_n = 0$, the starting solution should be very close to the desired minimum.

When a gradient method is applied to obtain a numerical solution of the modified nonlinear programming problem, the basic increment in the subsystem parameter values at each step of the solution process is

$$\triangle \sigma_{P_i} = -K_i \frac{\partial H_n}{\partial P_i} = -K_i \left\{ \frac{-P_i}{\sigma_{P_i}^2} + \theta_n \cdot \frac{\frac{\partial G(\vec{\sigma}_p)}{\partial \sigma_{P_i}}}{(R_o - G(\vec{\sigma}_p))^2} \right\},$$

where $K_i > 0$.

In order to complete the discussion of the most significant aspects of the formulation and solution of the subsystem tolerance design problem, we must consider the evaluation of the derivatives $\partial G(\vec{\sigma}_p)/\partial \sigma_{P_i}$ which are necessary for the application of the gradient method.

Let us recall the definition of the system performance function, $G(\vec{\sigma}_p)$.

$$G(\vec{\sigma}_p) = E_{\vec{f}, \vec{P}} \left[x_1^2 (\vec{P}; t_f) + x_2^2 (\vec{P}; t_f) \right] \quad .$$

Taking the derivative of both sides of this expression with respect to σ_{P_i} results in

$$\frac{\partial G(\vec{\sigma}_p)}{\partial \sigma_{P_i}} = \frac{\partial}{\partial \sigma_{P_i}} E_{\vec{f}, \vec{P}} \left[x_1^2 (\vec{P}; t_f) + x_2^2 (\vec{P}; t_f) \right] \quad .$$

Interchanging the order of differentiation and expectation on the right side of this equation (an operation which is valid under rather mild restrictions)

$$\frac{\partial G}{\partial \sigma_{P_i}} = 2E_{\vec{f},\vec{P}} \left[x_1(\vec{P};t_f) \frac{\partial x_1(\vec{P};t_f)}{\partial P_j} \cdot \frac{\partial P_j}{\partial \sigma_{P_j}} + x_2(\vec{P};t_f) \cdot \frac{\partial x_2(\vec{P};t_f)}{\partial P_j} \cdot \frac{\partial P_j}{\partial \sigma_{P_j}} \right]$$

The derivatives $\partial x_i / \partial P_j$ are just the sensitivities which are available from the solution of the variational equations, i.e.,

$$\frac{\partial x_i(\vec{P};t_f)}{\partial P_j} = W_{ij} .$$

The derivatives $\dfrac{\partial P_j}{\partial \sigma_{P_j}}$ may be expressed as

$$\frac{\partial P_j}{\partial \sigma_{P_j}} = \frac{P_j - P_j^O}{\sigma_{P_j}} .$$

Substituting these two relations into the expression for $\partial G / \partial \sigma_{P_j}$

$$\frac{\partial G}{\partial \sigma_{P_j}} = 2E_{\vec{f},\vec{P}} \left[\left(x_1(P;t_f) W_{1j}(t_f) + x_2(P;t_f) W_{2j}(t_f) \right) \cdot \left(\frac{P_j - P_j^O}{\sigma_{P_j}} \right) \right] .$$

All quantities that appear in this expression are available from the computer

simulation. Thus, we are now able to calculate the complete set of quantities necessary for the solution of the first stage or subsystem tolerance design problem. Of course, in utilizing any of the derived expressions involving expectations of random variables, the expectations are replaced by sample averages from many computer runs.

One very significant feature of the proposed theory is that nowhere in the development has it been necessary to make any assumption about the joint probability distribution of the subsystem parameters. Of course, when the theory is applied to any specific missile system, the system parameter values used in the simulation must be sampled from the appropriate joint distribution function, either assumed or known.

The outline of the formulation and solution of the optimum subsystem tolerance design procedure is now complete. We will now describe the second stage or component tolerance design method.

OPTIMUM COMPONENT TOLERANCES . Having solved the subsystem tolerance design problem, we are still faced with the problem of allocating the subsystem parameter tolerances to the components or piece parts of the subsystem, since these are the tolerances that must be considered by the circuit designer and manufacturer. Before proceeding with the formulation of the second stage problem, it should be noted that the application of the method for component tolerance design is not dependent upon the results obtained from subsystem tolerance design. For example, in some electronic circuits a set of tolerances in the overall circuit parameters which are known to result in circuit success may be specified. These circuit tolerances are then substituted for the optimum subsystem tolerances in the optimum component tolerance procedure. Thus, the component tolerance design procedure is useful for standard circuits or subsystems which have been developed for use in several systems.

Let the m system hardware parameters be random variables denoted by R_α, $\alpha = 1, 2, \ldots, m$. As a measure of the tolerance on the component parameter R_α we will choose the RMS deviation of R_α from its nominal or design value, denoted by σ_{R_α}. In most cases the nominal value of R_α will be identical to its mean. The subsystem parameters P_k, $k = 1, 2, \ldots L$, are functions of the random variables R_α. Since σ_{P_k} depends on the

component parameter tolerances,

$$\sigma_{P_k} = \sigma_{P_k}(\sigma_{R_1}, \sigma_{R_2}, \ldots, \sigma_{R_m}) = \sigma_{P_k}(\vec{\sigma}_R).$$

Assume that restrictions or specifications have been placed on the σ_{P_k} either by the optimum methods described above or by some other method. Let the form of these specifications be

$$\sigma_{P_k}(\vec{\sigma}_R) \leq S_k \qquad\qquad k = 1, 2, \ldots, L.$$

As before we would like to choose the component tolerances to be as large as possible but yet satisfy all of the above restrictions on the subsystem parameter tolerances. Thus, we introduce a similar objective or "cost" function. Let C_α be the "cost" of the component tolerance σ_{R_α},

$$C_\alpha = K_\alpha/\sigma_{R_\alpha}, \qquad 0 < \sigma_{R_\alpha} \leq \delta_\alpha,$$

$$C_\alpha = K_\alpha/\delta_\alpha, \qquad \sigma_{R_\alpha} > \delta_\alpha.$$

Then the total cost is

$$C(\vec{\sigma}_R) = \sum_{\alpha=1}^{L} C_\alpha.$$

Notice that in the present objective function we have introduced a constraint on the range of component tolerances, i. e., $0 < \sigma_{R_J} \leq \delta_\alpha$. The reason for this is that there is little value, if any, to be gained by increasing the tolerance above some specified level. Thus, we have the nonlinear programming problem

$$\text{Minimize:} \qquad C(\vec{\sigma}_R) = \sum_{\alpha=1}^{L} K_\alpha / \sigma_{R_\alpha}$$

subject to the constraints

$$S_k - \sigma_{P_k}(\vec{\sigma}_R) \geq 0, \qquad\qquad R = 1, 2, \ldots, m,$$

$$0 < \sigma_R \leq \delta_\alpha, \qquad\qquad \alpha = 1, 2, \ldots, L.$$

The remarks made about the subsystem tolerance cost model also apply in the present situation.

In order to solve the present nonlinear programming problem, we will again apply Carroll's "Created Response Surface Technique" to modify the programming problem. For component tolerance design the modified problem is

$$\text{Minimize:} \quad H_n(\vec{\sigma}_R) = \sum_{\alpha=1}^{L} \frac{r_\alpha^0}{\sigma_{R_\alpha}} + \beta_n \sum_{k=1}^{m} \frac{W_r}{(S_k - \sigma_{P_k}(\vec{\sigma}_R))}$$

for a finite decreasing sequence of values β_n ending in $\beta_n = 0$ and subject to the constraints

$$S_k - \sigma_{P_k}(\vec{\sigma}_R) \geq 0, \qquad\qquad k = 1, 2, \ldots, m,$$

$$0 < \sigma_{R_\alpha} \leq \delta_\alpha, \qquad\qquad 1, 2, \ldots, L.$$

The modification consists of, as before, the addition of a weighted sum of the receprocals of the subsystem constraint functions to the function being minimized. There are two differences in the procedure used here which did not appear in the prior discussion of Carroll's method. One is the constants, W_k, which weight the individual constraints among themselves. These relative weighting constants did not appear in subsystem tolerance design, since we considered only one constraint in that problem. The second is that the restrictions on the range of the component tolerances will not be handled by Carroll's modification. Since these restrictions are linear and separable they are more easily handled by another procedure.

SOLUTION PROCESS. We will now consider the gradient process which has been used successfully for the solution of the modified nonlinear programming problem. Given an initial set of values for the component tolerances, which we shall assume satisfy the constraints and some initial value for β_1, say

$B = 1$, calculate the partial derivatives, $\partial H_1 / \partial \sigma_{R_\alpha} \big|$ (initial value) and increment the value of σ_{R_α} in the direction of the negative α^{th} gradient component,

$$\Delta \sigma_{R_\alpha} = -K_\alpha \frac{\partial H_1}{\partial \sigma_{R_\alpha}} = -K_\alpha \left\{ \frac{-r_\alpha^0}{\sigma_{R_\alpha}^2} + \theta_1 \sum_{k=1}^{m} \frac{W_k \partial \sigma_{P_k} / \partial \sigma_{R_\alpha}}{(S_k - \sigma_{P_R}(\vec{\sigma}_k))^2} \right\},$$

$$K_\alpha > 0.$$

Since H_1 will decrease momentarily in the direction determined by the increments, if the initial choice of the increment should cause H_1 to increase, the size of the increments are decreased until the new value of H_1 has decreased. Thus, the value of the modified objective function will decrease at each step of the solution process. If the increments should cause the restrictions on the range of the component tolerances, i.e., $0 < \sigma_{R_\alpha} \leq \delta_\alpha$, to be violated, the appropriate increments are decreased by the amount necessary to place the affected component tolerances on the constraint boundary. If any of the constraints on the subsystem parameter tolerances are violated, the following correction cycle is employed to return the affected subsystem tolerances to the interior of the constraint set. Let I denote the set of constraints which have been violated,

$$I = \left\{ i: (S_i - \sigma_{P_i}) \leq 0 \right\},$$

and let A denote the set of component tolerances which contribute linearly to the violation of these constraints,

$$A = \left\{ \alpha: \frac{\partial \sigma_{P_i}}{\partial \sigma_{R_\alpha}} \Delta \sigma_{R_\alpha} > 0 , \ i \in I \right\}$$

form the total linear contribution to the violation of each of the constraints,

$$C_i = \sum_{\alpha \in A} \frac{\partial \sigma_{P_i}}{\partial \sigma_{R_\alpha}} \cdot \Delta \sigma_{R_\alpha} \quad , \quad i \in I.$$

Each of the quantities

$$1/C_i \qquad \frac{\partial \sigma_{P_i}}{\partial \sigma_{R_\alpha}} \qquad \Delta \sigma_{R_\alpha} \leq 1 \qquad i \in I, \qquad \in A,$$

represent the relative contribution of the increment $\Delta \sigma_{R_\alpha}$ to the violation of the ith constraint. Denote the largest of these relative contributions for each α by M_α ,

$$M_\alpha = \underset{i \in I}{\text{Max}} \quad \frac{1}{C_i} \quad \frac{\partial \sigma_{P_i}}{\partial \sigma_{R_\alpha}} \Delta \sigma_{R_\alpha} , \qquad \alpha \in A.$$

In order to restore the subsystem tolerances to the constraint set,

$$\text{replace} \quad \Delta \sigma_{R_\alpha} \quad \text{by} \quad \Delta \sigma_{R_\alpha} (1 - M_\alpha).$$

Several cycles of this procedure may be necessary to return to the interior of the constraint set. When $\beta_n = 0$, M_α is also used to modify the basic step size in the direction of the gradient components, i.e., when $\beta_n = 0$,

$$\Delta \sigma_R = \frac{K_\alpha \cdot r_\alpha^0}{\sigma_{R_\alpha}^2}$$

K_α is replaced by $K_\alpha(1-M_\alpha)$ each time a constraint is violated. Since, when $\beta_n = 0$, there is no penalty function term to aid in non-violation of the constraints, this procedure greatly reduces the basic increment size for those component parameters which have become chronic contributors to constraint violations.

CALCULATION OF THE DERIVATIVES $\dfrac{\partial \sigma_{P_k}}{\partial \sigma_{R_\alpha}}$.   In the application

of the method of steepest descent to the solution of the nonlinear programming problem the values of σ_{R_α} are incremented according to the rule

$$\triangle \sigma_{R_\alpha} = -K_\alpha \frac{\partial H}{\partial \sigma_{R_\alpha}} \qquad \alpha = 1, 2, \ldots, m.$$

From the expression for $H_n(\vec{\sigma}_R)$ given previously in (2-1)

$$\frac{\partial H_n}{\partial \sigma_{R_\alpha}} = -\frac{r_\alpha^o}{\sigma_{R_\alpha}^2} + \beta_n \sum_{k=1}^{L} \frac{W_k}{(S_k - \sigma_{P_k})^2} \frac{\partial \sigma_{x_k}}{\partial \sigma_{R_\alpha}}$$

The only undetermined factors in this expression are the derivatives

$$\frac{\partial \sigma_k}{\partial \sigma_{R_\alpha}} .$$

The kth subsystem parameter, P_k, is a random variable which is a

function of R_α,

$$P_k = p_k(\vec{R}) = p_k(R_1, R_2, \ldots, R_m).$$

In a great many cases the functional dependence of P_k on R_α will be unknown, however, all that is required for the tolerance optimization procedure is that P_k and $\dfrac{\partial P_k}{\partial R_\alpha}$ are calculable pointwise. The RMS deviation of P_k about its nominal value is given by

$$\sigma_{P_k} = \left\{ E_{\vec{R}} \left[(P_k - p_k^o)^2 \right] \right\}^{\frac{1}{2}}$$

Let U_α be a random variable distributed according to the same law as R_α, but with zero mean and unit standard deviation. Then

$$R_\alpha = \mu_{R_\alpha} + \sigma_{R_\alpha} U_\alpha \qquad\qquad \alpha = 1, 2, \ldots, m$$

With this substitution for R_α, $\sigma_{P_k}^2$ becomes

$$\sigma_{P_k}^2 = E_U \cdot \left[(P_k (\mu_{R_1} + \sigma_{R_1} U_1, \ldots, \mu_{R_m} + \sigma_{R_m} U_m) - p_k^0)^2 \right]$$

Taking the derivative of both sides of this equation with respect to σ_{R_α},

$$2\sigma_{P_k} \cdot \frac{\partial \sigma_{P_k}}{\partial \sigma_{R_\alpha}} = \frac{\partial}{\partial \sigma_{R_\alpha}} E_{\vec{U}} \left[(P_k (\mu_{R_1} + \sigma_{R_1} U_1, \ldots, \mu_{R_m} + \sigma_{R_m} U_m) - p_k^0)^2 \right]$$

Interchanging the order of differentiation and expectation on the right hand side of the above equation results in,

$$2\sigma_{P_k} \frac{\partial \sigma_{R_k}}{\partial \sigma_{R_\alpha}} = E_{\vec{U}} \left[\frac{\partial}{\partial \sigma_\alpha} (P_k (\mu_{R_1} + \sigma_{R_1} U_1, \ldots, \sigma_{R_m} U_m) - p_k^0)^2 \right]$$

$$\sigma_{P_k} \frac{\partial \sigma_{P_k}}{\partial \sigma_{R_\alpha}} = E_{\vec{U}} \left[(P_k - p_k^0) \frac{\partial P_k}{\partial R_\alpha} \frac{\partial R_\alpha}{\partial \sigma_{R_\alpha}} \right] \quad ,$$

or since

$$\frac{\partial R_\alpha}{\partial \sigma_{R_\alpha}} = U_\alpha \quad ,$$

$$\frac{\partial \sigma_{P_k}}{\partial \sigma_{R_\alpha}} = E_{\vec{U}} \left[\left(\frac{P_k - p_k^0}{\sigma_{P_k}} \right) \frac{\partial P_k}{\partial R_\alpha} U_\alpha \right].$$

In utilizing this expression for $\partial \sigma_{P_k} / \partial \sigma_R$ or any other quantity involving expected values of random variables in the computational process, the expectations are replaced by their sample estimates.

In order to calculate $\partial \sigma_{P_k} / \partial \sigma_R$ it is necessary to obtain the quantities $\partial P_k / \partial R_\alpha$. While these partial derivatives are not always available analytically, they can at least be approximated numerically. In the important case of systems describable by linear, constant coefficient differential equations and the P_k are given functions of the linear system poles and zeros, we will obtain an explicit expression for their point-wise evaluation. If the system contains time varying and/or nonlinear elements, some of the subsystem parameters P_k will quite often be identical to or known functions of the component parameters of the nonlinear and time varying elements. In most cases the values $\partial P_k / \partial R_\alpha$ will be directly calculable. In a few cases they may have to be estimated by difference approximation.

$\partial P_k / \partial R_\alpha$ FOR LINEAR CONSTANT COEFFICIENT SYSTEMS. If a subsystem can be described by linear, constant coefficient differential equations, it is possible to develop a rather general method for component tolerance design. Since the optimization and tolerance design method presented here is simulation oriented, the natural choice for the subsystem parameters for any linear, constant coefficient portion of the system is the set of transfer function coefficients or the set of transfer function poles and zeros. The procedure set forth for hardware tolerance design of a linear constant coefficient system will consider the transfer function poles and zeros as the subsystem parameters. However, the extension of the procedure to transfer function coefficients or any specified function of the poles and zeros, either analytical or empirical is obvious.

Either the numerator or denominator of the subsystem transfer function may be written as a polynomial in the Laplace transform variable S. The polynomial coefficients will be functions of the component parameters. Let

$$\triangle(r_1, r_2, \ldots, r_L; S) = (\vec{r}; S) = \left(\sum_{n=0}^{N} a_n(\vec{r}) S^n \right)$$

be either the numerator or denominator of the transfer function. This polynomial can also be expressed in terms of its zeros, the subsystem parameters

$$\triangle(\vec{r}; s) = a_n(\vec{r}) \cdot \prod_{i=1}^{N} (S - p_i(\vec{r})).$$

The functional form of p_j's is usually unknown. At the nominal values of the components, $r_i = r_i^o$,

$$\triangle(\vec{r}^o; S) = a_N^o \cdot \prod_{i=1}^{N} (S - p_i^o).$$

For small perturbations of the, δr_i, from the nominal values, the perturbation in zeros is

$$\delta p_i = \sum_{\alpha=1}^{L} \frac{\partial p_i}{\partial r_\alpha} \Big]_{r_\alpha^o} \cdot \delta r_\alpha .$$

The derivatives $\dfrac{\partial p_i}{\partial r_\alpha}$ can be written in terms of the polynomial coefficients as

$$\frac{\partial p_i}{\partial r_\alpha} = \sum_{n=o}^{N} \frac{\partial p_i}{\partial a_n} \frac{\partial a_n}{\partial r_\alpha} \qquad \begin{array}{l} i = 1, 2, \ldots, N \\ \alpha = 1, 2, \ldots, L. \end{array}$$

A computer method developed by Travis Guye at the Flight Simulation Laboratory, WSMR, uses polynomial interpolation to generate the transfer function coefficients. Since Δ is a polynomial, the polynomial coefficients can be exactly calculated in this way by evaluating the polynomial at N+1 values of S. If the values $S=m=0,1,2,\ldots,N$ are used, the polynomial coefficients are given by

$$a_n(\vec{r}) = \sum_{m=0}^{N} S_{nm}^{N}\ \Delta(\vec{r};m)\ ,$$

where the S_{nm}^{N} are the elements of a precomputed $(N+1) \times (N+1)$ matrix. Then the derivatives $\dfrac{\partial a_n}{\partial r_\alpha}$ can be written as

$$\frac{\partial a_n}{\partial r_\alpha} = \sum_{m=0}^{N} S_{nm}^{N} \cdot \frac{\partial \Delta(\vec{r};m)}{\partial r_\alpha}\ .$$

The derivatives $\partial \Delta / \partial r_\alpha$ are easily evaluated from a signal flow graph or block diagram representation of the system.

We must now evaluate the derivatives $\partial p_i / \partial a_n$. If the polynomial coefficients are perturbed from their nominal values, and only first order infinitesimals retained in the resulting expression for Δ, these derivatives are easily determined to be

$$\frac{\partial p_i}{\partial a_n}\Bigg]_{\vec{r}^{0}} = \frac{-(p_i^{0})^{n}}{a_n^{0} \displaystyle\prod_{k \neq i}^{N} (p_i^{0} - p_k^{0})}\ .$$

Then the desired derivatives are

$$\frac{\partial p_i}{\partial r_\alpha} = \sum_{n=0}^{N} \frac{\partial p_i}{\partial a_n} \sum_{m=0}^{N} S_{nm}^{N} \frac{\partial \Delta(\vec{r};m)}{\partial r_\alpha}$$

$$\frac{\partial p_i}{\partial r_\alpha} = \frac{-1}{a_n(\vec{r}) \prod_{k\neq i}^{N} (p_i(\vec{r}) - p_k(\vec{r}))} \sum_{n=0}^{N} \sum_{m=0}^{N} \left(\right.$$

$$p_i^n(\vec{r}) \quad S_{nm}^{N} \quad \frac{\partial \Delta(\vec{r};m)}{\partial M_\alpha} \left.\right).$$

A LINEAR EXAMPLE. As an example of optimum component tolerance design, consider the passive network, which might be an element of a missile control system.
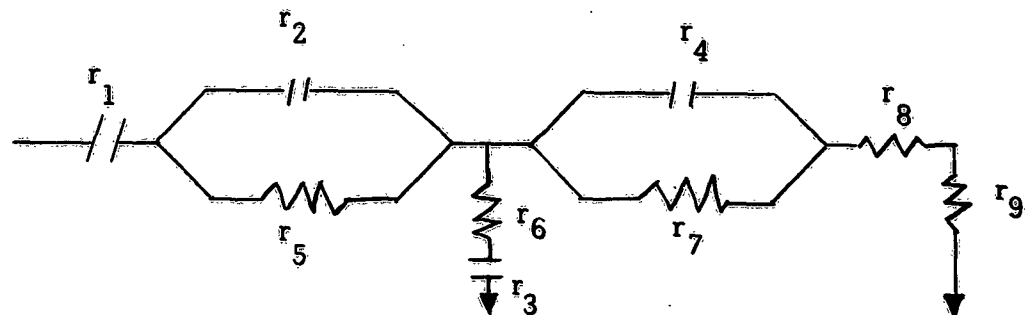
The nominal component values are $r_1^0 = .51$, $r_2^0 = .036$, $r_3^0 = .091$, $r_4^0 = .43$, $r_5^0 = .235$, $r_6^0 = .0619$, $r_7^0 = 1.0$, $r_8^0 = .348$, $r_9^0 = 1.87$

The nominal voltage transfer function is

$$\frac{V_o}{V_i} = \frac{.9537S \left(S/_{2.326}+1\right)\left(S/_{117.6}+1\right)\left(S/_{177}+1\right)}{\left(S/_{.4571}+1\right)\left(S/_{3.554}+1\right)\left(S/_{34.98}+1\right)\left(S/_{752.9}+1\right)} .$$

As subsystem parameters, we will consider only the gain, the smallest zero, and the two smallest poles. Thus, the nominal values of the subsystem parameters are $p_1^o = .9537$, $p_2^o = 2.326$, $p_3^o = -.4571$, $p_4^o = -3.554$. The subsystem parameter tolerances are restricted to be less than or equal to 10% of parameter nominal value.

$$\sigma_{P_1} \leq .1 \left|p_1^o\right| = .09537, \quad \sigma_{P_2} \leq .1 \left|p_2^o\right| = .2326,$$

$$\sigma_P^3 \leq .1 \left|p_3^o\right| = .04571, \quad \sigma_{P_4} \leq .1 \left|p_4^o\right| = .3554.$$

The maximum component tolerance level will be set at 25% of the component nominal value,

$$\sigma_{R_\alpha} \leq .25 \; r_\alpha^o \qquad \alpha = 1, 2, \ldots, 9.$$

The numerical results of this example are summarized in Figure 2. The initial values for each of the component tolerances was 10% of nominal. The final solution is on the boundaries

$$\sigma_{P_1} = .09537$$

$$\sigma_{P_2} = .2326,$$

$$\sigma_{R_2} = .09$$

$$\sigma_{R_3} = .0227$$

$$\sigma_{R_5} = .0588$$

	σ_{r_1}	σ_{r_2}	σ_{r_3}	σ_{r_4}	σ_{r_5}	σ_{r_6}	σ_{r_7}	σ_{r_8}	σ_{r_9}	σ_{x_1}	σ_{x_2}	σ_{x_3}	σ_{x_4}	H
INITIAL	.0255	.0018	.0045	.0215	.0117	.0031	.0500	.0174	.0935	.0690	.1883	.0272	.2434	192.3
% OF NOMINAL	10	10	10	10	10	10	10	10	10	7.23	8.10	5.95	6.85	—
FINAL	.0389	.0900	.0227	.0269	.0588	.0155	.0602	.0870	.1144	.0954	.2326	.0424	.3068	82.08
% OF NOMINAL	7.63	2.5	2.5	6.26	2.5	2.5	6.02	2.5	6.12	10	10	9.28	8.63	—

Summary of Numerical Results for Example Problem
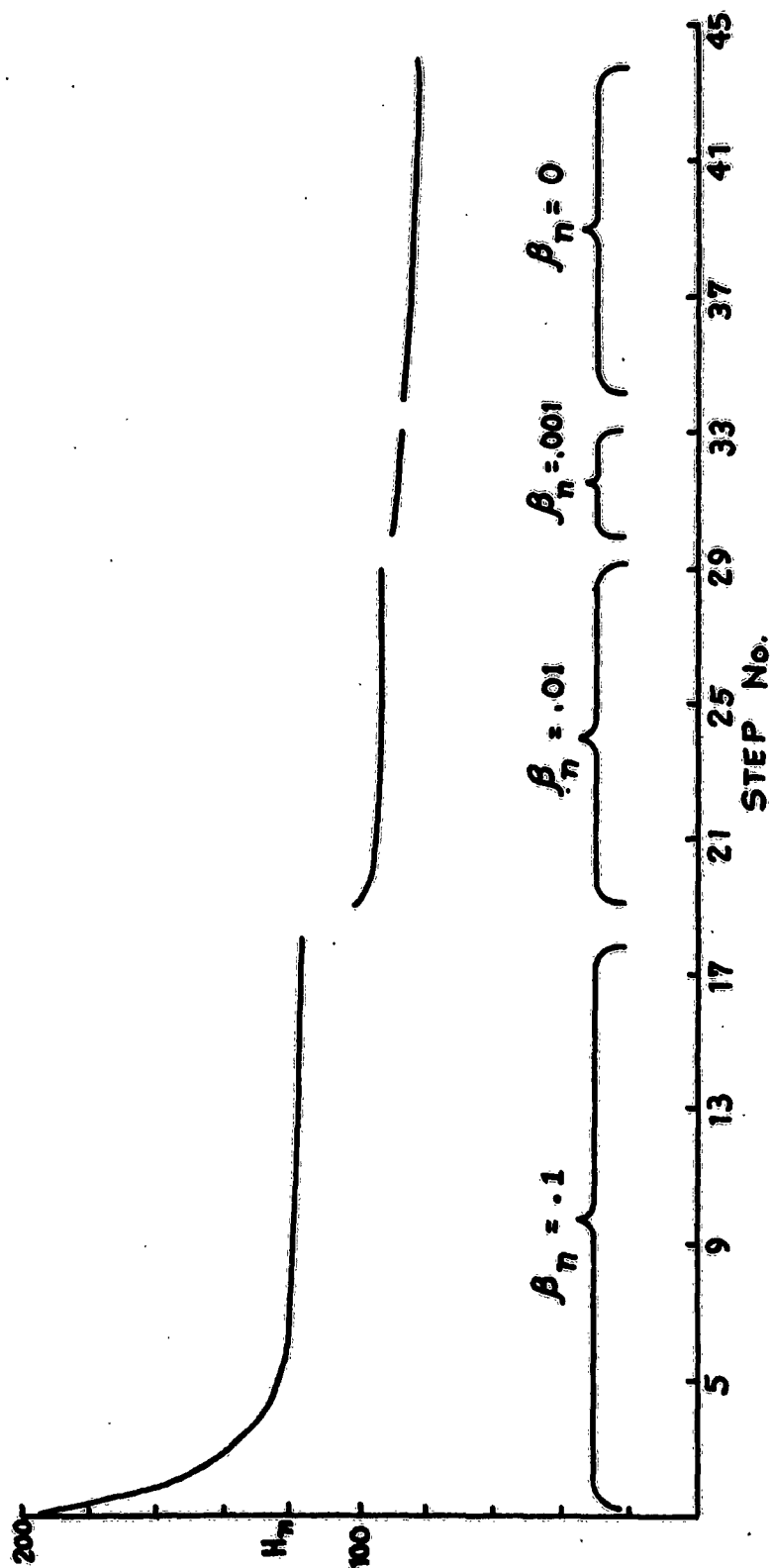
Figure 2

$$\sigma_{R_6} = .0155$$

$$\sigma_{R_8} = .087$$

Since σ_{P_1} depends only on σ_{R_1} and σ_{R_9} and σ_{P_2} on σ_{R_4} and σ_{R_7}, and the remaining independent variables are at their upper limit, the solution cannot reach the constraint boundaries $\sigma_{P_3} = .04571$ and $\sigma_{P_4} = .3554$.

A SECOND FORMULATION OF OPTIMUM TOLERANCE DESIGN. We will now consider another formulation of a tolerance cost model. This model will be very similar to the previous one, but we will use a different tolerance measure.

Let $r_\alpha^O + P_\alpha$ and $r_\alpha^O - N_\alpha$ be the upper and lower tolerance limits, respectively of the random component parameter R. Then the tolerance on the component is $+100\ P_\alpha /r_\alpha^O$ % and $-100 N_\alpha /r_\alpha^O$ %. These ideas are expressed pictorially in Figure 3.
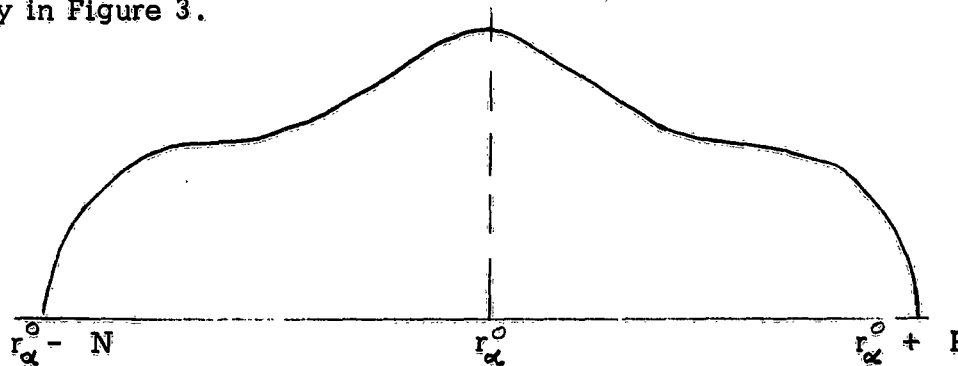
POSSIBLE DENSITY FUNCTION OF COMPONENT PARAMETER VALUE

Figure 3

The tolerance optimization method using these independent variables does not achieve the generality of the previous formulation since it will not be invariant to the probability distribution law of R_α. However, the use of the upper and lower tolerance limits provides a most definite tolerance measure and allows the use of a nonsymetric tolerance on R_α.

Let the "cost" of positive and negative tolerances, P_α and N_α, on R_α be inversely proportional to $P_\alpha + N_\alpha$. Then the total tolerance cost is

$$C(\vec{P}, \vec{N}) = \sum_{\alpha=1}^{L} \frac{r_\alpha^0}{P_\alpha + N_\alpha}, \quad 0 < P \leq \delta_\alpha, \quad 0 < N_\alpha \leq \delta_\alpha.$$

Notice that either P_α or N_α may be zero without inflicting an infinitely severe penalty.

The nonlinear programming problem generated by the present formulation is

$$\text{Minimize:} \qquad C(\vec{P}, \vec{N}) = \sum_{\alpha=1}^{L} \frac{r_\alpha^0}{P_\alpha + N_\alpha}$$

subject to the constraints

$$S_k - \sigma_{X_k}(\vec{P}, \vec{N}) \geq 0, \qquad\qquad k = 1, 2, \ldots, m,$$

$$0 < P_\alpha \leq \delta_\alpha, \quad 0 < N_\alpha \leq \delta_\alpha, \qquad \alpha = 1, 2, \ldots, L.$$

Two probability distribution functions, the uniform and truncated normal, have been considered for use with this problem. However, the amount of computation associated with the truncated normal is prohibitive.

For the numerical solution of the nonlinear programming problem by a gradient method expressions for the derivatives $\dfrac{\partial \sigma_{P_k}}{\partial P}$ and $\partial \sigma_{P_k} / \partial N_\alpha$ will be required. If the component parameter values, R_α, have a joint uniform distribution, these derivatives are

$$\frac{\partial \sigma_{X_k}}{\partial P_\alpha} = E_{\vec{R}}\left[\left(\frac{X_k(\vec{R}) - x_k^o}{\sigma_{X_k}}\right) \frac{\partial X_k}{\partial R_\alpha} \left(\frac{R_\alpha - r_\alpha^o + N_\alpha}{P_\alpha + N_\alpha}\right)\right]$$

$$\frac{\partial \sigma_{X_k}}{\partial N_\alpha} = E_{\vec{R}}\left[\left(\frac{X_k(R) - x_k^o}{\sigma_{X_k}}\right) \frac{\partial X_k}{\partial R_\alpha} \left(\frac{R_\alpha - r_\alpha^o + P_\alpha}{P_\alpha + N_\alpha}\right)\right].$$

The numerical solution proceeds as before.

RESEARCH AND DEVELOPMENT IS A MARKOV CHAIN

Sidney Sobelman

Management Sciences and Data Systems Division
Picatinny Arsenal
Dover, New Jersey

ABSTRACT. It is possible and useful to show that the steps taken in RandD or other investigative effort do in fact form a Markov chain. The "states" of the system must be identified on a basis of relative independence with respect to the probability of success or failure to complete each. An absorbing state is recognized which, when reached, signals termination. The Markov chain developed is of the "Recurrent Events" example with the added absorbing state. Generalization of the model to $\underline{n}$ states is described and partitioning to include time scheduling values appears possible.

STATES. The most basic set of states to describe an investigative or developmental process or operation is considered to consist of the phases: Analyze, Design, Fabricate, Test, and Report. We can speak of being successful or failing in the completion of each of these phases or states - relatively independently of the success or failure in another state. Although there is a probability of being successful or failure, the declaration, realization, or decision that we are now successful or have failed is to be "catastrophic", that is, decisive and sharply so. For example, successful completion of the analysis state means we have created the necessary and sufficient data to design the item or model (whether iconic, analog, or symbolic). Failure to complete the Analysis means the inability to proceed any further onto Design and we proceed to the Report state for a concluding report and/or action. A successful completion in Design means a step into Fabrication of the model, in Fabrication a step into Testing the model, and in Testing a step into the absorbing state of Reporting, including all the necessary action of standardizing, documenting, and issuing reports. A failure in each of the Design, Fabricate, or Test states means a return to the action of Analyzing what went wrong in light of the original analysis and its calculations establishing the design of the model, its tolerances and dimensions, and its design of experiment.

SYMBOLS. The probability of completion, or success, is p and of failure q, where $p+q = 1$. Following convention, the first state of the Markov chain will be State zero, thus the states are:

E_0 = Analyze (or Study, Feasibility Study, Evaluation, Problem Statement, etc.)

E_1 = Design (based on Analysis of a Model, Product, Organization, etc.)

E_2 = Fabricate (an iconic, analog, or symbolic model, or its logic program).

E_3 = Test (the model or run a simulation)

E_4 = Report (for implementation of applying the model or the product it models)

THE MARKOV PROCESS.   The Markov process is:

	E_0	E_1	E_2	E_3	E_4
E_0	O	P_0	O	O	q_0
E_1	q_1	O	P_1	O	O
E_2	q_2	O	O	P_2	O
E_3	q_3	O	O	O	P_3
E_4	O	O	O	O	1

where State E_4 is the absorbing state, otherwise failure in any state returns one to the "Analysis" state. This is identical to the "Recursion" example of Markov chain described by Feller, except for the absorbing state. As will be seen later, the submatrix Q of the canonical form will be of the recursion type exactly.

The canonical form is:

$$P = \begin{bmatrix} I & O \\ \hline R & Q \end{bmatrix}$$

=

	E_4	E_0	E_1	E_2	E_3
E_4	1	0	0	0	0
E_0	q_0	0	p_0	0	0
E_1	0	q_1	0	p_1	0
E_2	0	q_2	0	0	p_2
E_3	p_3	q_3	0	0	0

The Q matrix is <u>regular</u>, hence <u>ergodic</u>, as shown by:

$$Q = \begin{bmatrix} 0 & p & 0 & 0 \\ q & 0 & p & 0 \\ q & 0 & 0 & p \\ q & 0 & 0 & 0 \end{bmatrix} = \begin{bmatrix} 0 & * & 0 & 0 \\ * & 0 & * & 0 \\ * & 0 & 0 & * \\ * & 0 & 0 & 0 \end{bmatrix}$$

$$Q^2 = \begin{bmatrix} * & 0 & * & 0 \\ * & * & 0 & * \\ * & * & 0 & 0 \\ 0 & * & 0 & 0 \end{bmatrix}$$

$$Q^4 = \begin{bmatrix} * & * & * & 0 \\ * & * & * & * \\ * & * & * & * \\ * & * & 0 & * \end{bmatrix}$$

$$Q^8 = \begin{bmatrix} * & * & * & * \\ * & * & * & * \\ * & * & * & * \\ * & * & * & * \end{bmatrix}$$ Q.E.D.

First, let us determine the "fundamental matrix", N, from $(I-Q)^{-1}$.

$$I-Q = \begin{bmatrix} 1 & -p_0 & 0 & 0 \\ -q_1 & 1 & -p_1 & 0 \\ -q_2 & 0 & 1 & -p_2 \\ -q_3 & 0 & 0 & 1 \end{bmatrix}$$

Then, $N = (I-Q)^{-1}$ equals

$$(1/M) \begin{bmatrix} 1 & p_0 & p_0 p_1 & p_0 p_1 p_2 \\ (p_1 q_2 + q_1 + p_1 p_2 q_3) & 1 & p_1 & p_1 p_2 \\ (q_2 + p_2 q_3) & (p_0 p_2 q_3 + p_0 q_2) & (1-p_0 q_1) & p_2(1-p_0 q_1) \\ q_3 & p_0 q_3 & p_0 p_1 q_3 & (1-p_0 q_1 - p_0 p_1 q_2) \end{bmatrix}$$

where $M = 1 - p_0 q_1 - p_0 p_1 q_2 - p_0 p_1 p_2 q_3$. This is a _regular_ Markov chain.

Hence, there is some time at which it is possible to be in any of the states regardless of the starting state. But the prime condition is the one where the starting state is Analysis, or State E_0.

The entries in N, the _fundamental_ matrix of the absorbing chain, gives the _mean number of times_ in each nonabsorbing state for each possible nonabsorbing starting state. Since we are interested only in the case where the starting state is Analysis, the mean number of times we will be in each of the nonabsorbing states are:

$$1/M \qquad \text{for ANALYSIS } (E_0)$$

$$p_0/M \qquad \text{for DESIGN} \quad (E_1)$$

$$p_0 p_1/M \qquad \text{for FABRICATE } (E_2)$$

$$p_0 p_1 p_2/M \qquad \text{for TEST} \qquad (E_3)$$

Adding these values, or in effect obtaining the value of NC where C is a column vector with all entries 1, we obtain the <u>mean time, or number of steps required before being absorbed.</u> This value is:

$$NC = (1 + p_0 + p_0 p_1 + p_0 p_1 p_2)/M .$$

The probability that the Markov chain will end up in the absorbing state is given by NR, where R is the absorbing state portion of the canonical form. Since, again, we are interested only when starting in state E_0, Analysis, the product of the first row of N times the column vector of R yields:

$$NR = (q_0 + p_0 p_1 p_2 p_3)/M .$$

The Markov chain model described herein is very similar to the "Recurrent Events" chain described by Feller in his text, except for the last state which is an absorbing state and the first state which "goes to pot" or cancellation of the project with a probability q_0. A "success run" can exist from state E_0 to the absorbing state with a probability of: $p_0 p_1 p_2 p_3/M$ and the probability that a return to state E_0 will be required before final completion (i. e, absorption in state 4):

$$1 - (p_0 p_1 p_2 p_3/M)$$

EXAMPLE

The probabilities of successful completion of each state at each try are estimated to be, for a particular system:

$$E_0, \quad p_0 = 0.98 \qquad , \quad q_0 = 0.02$$

$$E_1, \quad p_1 = 0.80 \qquad , \quad q_1 = 0.20$$

$$E_2, \quad p_2 = 0.95 \quad , \quad q_2 = 0.05$$

$$E_3, \quad p_3 = 0.60 \quad , \quad q_3 = 0.40$$

$$N = \frac{1}{.4669}
\begin{bmatrix}
1 & .9800 & .7840 & .7448 \\
.5440 & 1 & .8000 & .7600 \\
.4300 & .4214 & .8040 & .7638 \\
.4000 & .3920 & .3136 & .7648
\end{bmatrix}
=
\begin{bmatrix}
2.14 & 2.10 & 1.68 & 1.60 \\
1.17 & 2.14 & 1.71 & 1.63 \\
.92 & .90 & 1.72 & 1.64 \\
.86 & .84 & .67 & 1.64
\end{bmatrix} .$$

The mean number of times in each nonabsorbing state is 2.14 for Analysis, 2.10 for Design, 1.68 for Fabricate, and 1.60 for Test. The number of steps required before being absorbed (full completion) is equal to the sum of these, i.e. 7.52 or at least 7 steps, where for a completely successful run there would be 4 steps. The probability of completion is equal to NR = .46688/.46690 = 0.999%.

The probability of having a "success run" without any returns to the initial state = .44688/.46690 = 0.957.

GENERALIZATION TO n STATES. A sharpening and improvement of the results to be obtained by this type of analysis may be possible by extending the phases to a larger number than that the five states described herein. For example, the Analyze state is often treated as either or both an initial or preliminary Feasibility Study and a later Engineering Analysis phase. In a similar manner, Design is taken in steps such as: a. A laboratory, or hand-made breadboard design, b. A pilot lot, pilot plant trial design, a first flight model design, and c. A design for first production run or for system flight trials. If each of these three designs is followed by the states of Fabricate and Test, then a total nine states are recognized where we had three before in our first, elementary Markov model. A Markov chain has just been described going from E_0 to E_{11}, the final absorbing state of "Report."

To arrive at the $\underline{n}$ -State model, inductive, or step-wise, development can be used. Thus, for the Markov chain having three states of E_0, E_1, and E_2,

$$Q = \begin{array}{c} E_0 \\ E_1 \end{array} \begin{bmatrix} 0 & p_0 \\ q_1 & 0 \end{bmatrix}$$

$$I-Q = \begin{bmatrix} 1 & -p_0 \\ -q_1 & 1 \end{bmatrix}$$

$$\text{and } N = \begin{bmatrix} I - Q \end{bmatrix}^{-1} = \frac{1}{1-p_0 q_1} \cdot \begin{bmatrix} 1 & p_0 \\ q_1 & 1 \end{bmatrix} .$$

For four states E_0, ..., E_3:

$$N = \frac{1}{1-p_0 q_1 - p_0 p_1 q_2} \cdot \begin{bmatrix} 1 & p_0 & p_0 p_1 \\ (q_1 + p_1 q_2) & 1 & p_1 \\ q_2 & p_0 q_2 & (1-p_0 q_1) \end{bmatrix} .$$

And to repeat what we had previously developed for five states, E_0 --- E_4:

$$(1/M) \begin{bmatrix} 1 & p_0 & p_0 p_1 & p_0 p_1 p_2 \\ (q_1 + p_1 q_2 + p_1 p_2 q_3) & 1 & p_1 & p_1 p_2 \\ (q_2 + p_2 q_3) & (p_0 q_2 + p_0 p_2 q_3) & (1-p_0 q_1) & p_2(1-p_0 q_1) \\ q_3 & p_0 q_3 & p_0 p_1 q_3 & (1-p_0 q_1 - p_0 p_1 q_2) \end{bmatrix} .$$

By induction, we can then arrive at the fundamental matrix, N, for six states. However, we are only concerned with the condition of starting out with State E_0 and of always returning there when a failure occurs, therefore, we are not interested in any rows of the matrix except the first; asterisks are therefore inserted in the following matrix for all rows but the first:

$$N = (1/K) \cdot \begin{bmatrix} 1 & p_0 & p_0 p_1 & p_0 p_1 p_2 & p_0 p_1 p_2 p_3 \\ * & * & * & * & * \\ * & * & * & * & * \\ * & * & * & * & * \\ * & * & * & * & * \end{bmatrix}$$

where $K = 1 - p_0 q_1 - p_0 p_1 q_2 - p_0 p_1 p_2 q_3 - p_0 p_1 p_2 p_3 q_4$.

In addition, C equals a single column matrix of one's and as before:

$$R = \begin{bmatrix} q_0 \\ 0 \\ 0 \\ 0 \\ p_4 \end{bmatrix}.$$

Generalizing, the denominator of the N matrix is designed as Z and equals:

$$Z = 1 - \sum_3^n \left(q_{n-2} \cdot \prod_3^n p_{n-3} \right).$$

The related estimates and probabilities are for n states, where E_0 is the initial starting state and E_n is the absorbing state:

Mean Number of times in each nonabsorbing state:

For State E_0, $= 1/z$

For State E_i $= (\prod_1^{n-1} p_{i-1})/z$
$0 < i < n$

The sum of these individual state probabilities, or the matrix product of NC, equals the mean number of steps required before being absorbed, that is, reaching the completion or mop-up phase. This is equal to:

$$\left[1 + \sum_1^{n-2} (\prod p_{i-1}) \right] /z.$$

The probability of completion, that is the probability of reaching the absorbing state, is NR and is equal to:

$$(q_0 + \prod_1^{n-2} p_{i-1}) / z .$$

The probability of having a "success run" to completion, that is, there are no failures and returns to the Analyze phase, is equal to:

$$(\prod_1^{n-2} p_{i-1}) / z .$$

DETERMINATION OF PROBABILITY VALUES. Although not the
purpose of the paper, the determination of the probability of completing
a phase or "step" in the Markov chain of RandD is very important to the
use of the described technique. Very briefly, several methods exist
for getting an estimate of a "step" probability. In all of these methods,
it appears important to consider each relatively broad "step" or "phase"
as an independent set of smaller phases, activities (as in PERT network
diagram), or component developments, each of which is in effect a sub-
set having a relative independence of its own.

It can now be conceived that the probability of the set can be cal-
culated using value judgments of each of the components or sub-set
made by the development engineer. Component or system reliability,
similar to that calculated for hardware systems, can be determined.

Another technique considers relating the probability of completing
an operation (such as our "independent set" or phase) to the number of
phases that have to be completed in that operation. Thus, the greater
the number of sub-sets, or internal phases in an operation, the smaller
the probability of its completion. This is described in the text by Flagle,
Huggins, and Roy (Operations Research and Systems Engineering) and
in this writer's report (A Modern Dynamic Approach to Product Develop-
ment.)

Although subject to question on the basis of rigorous mathematical
or statistical grounds, the probability of completing a major phase or
step can be calculated using PERT/TIME three-time-estimates and the
variances calculated from these for each of the detail steps or activities
comprising the major phase or step. The nature of a net-work branch, such
as whether it is in parallel or series with another branch, should be
considered in calculating the "system reliability" of the major phase
or "step". However, if one can identify a Markov chain for this sub-set
of PERT activities, particularly if a ground-rule for such network con-
struction is that activities between events must be relatively independent,
then we can use the Markov chain approach described in the basic part
of this paper.

EXTENSION TO INCLUDE TIME AND SCHEDULING. The preceeding
discussion considered several states with moves or "steps", of any

magnitude, from one state to another. We spoke of the mean number of times in a nonabsorbing state, but not of how long we would be in that state timewise. Suppose we now partition the transition matrix into sufficiently small and equal sub-steps each corresponding to a unit of time, such as a day, week, or month. Within one state we then move progressively from one time substate to the next -- unless a failure occurs at that substate level. The probability of a state is then the product of the time sub-state probabilities along the major diagonal of the imbedded time matrix.

In the context of this partitioning operation, we have subtly changed our meaning of probability. No longer do we have a "probability of completion", but instead we can now speak of the "probability of completion on time."

α -CLASSIFICATION OF MICROFIBERS

M. A. Sadowsky and M. A. Hussain
Watervliet Arsenal, Watervliet, New York

OBJECTIVE. Microfibers and microflakes are used to form composite materials of greatly increased strength. Individually, microfibers may belong to several (probably 3 or 4) distinct types which show different elastic behavior in tension and bending. The objective of this report is to work out the theoretical characteristics of the different types of microfibers in order to classify the actual experimental microfibers and to better understand their mode of action and the expectation one may associate with them.

EQUILIBRATION EQUATIONS OF ANALYTICAL STATICS.

By linear fiber we mean a fiber whose thickness is zero exactly. It is a one-dimensional arc of a curve suitable to open the discussion as a mathematical abstraction. Statical equilibrium equations apply to any linear fiber regardless of its physical background. We shall use the length of arc s as a coordinate along the fiber and we introduce the following quantities as internal forces and internal moment acting within the fiber: the tension force $P = P(s)$, the shearing force $Q = Q(s)$ and the bending moment $M = M(s)$. The positive directions of all quantities involved are shown in Fig. 1.

Since the microfiber is imbedded in an elastic matrix substance, a normal stress $\sigma = \sigma(s)$ and a tangential stress $\tau = \tau(s)$ are applied to the fiber by the matrix as shown in Fig. 1. As such stresses may be applied on either side, say σ^*, τ^* on one side and σ^{**}, τ^{**} on the other side, we note that σ and τ mean the resultant of such a bilateral application in the sense of

$$(1) \qquad \sigma = \sigma^* - \sigma^{**} , \quad \tau = \tau^* - \tau^{**}.$$

The assignment of a small thickness to the microfibers in Fig. 1 is only symbolic as the linear microfiber has zero thickness. Consequently, the distribution of either stress on the sides marked * and ** is immaterial, since it is only the resultant effect σ, τ that counts. The equilibrium equations obtained by analytical statics read
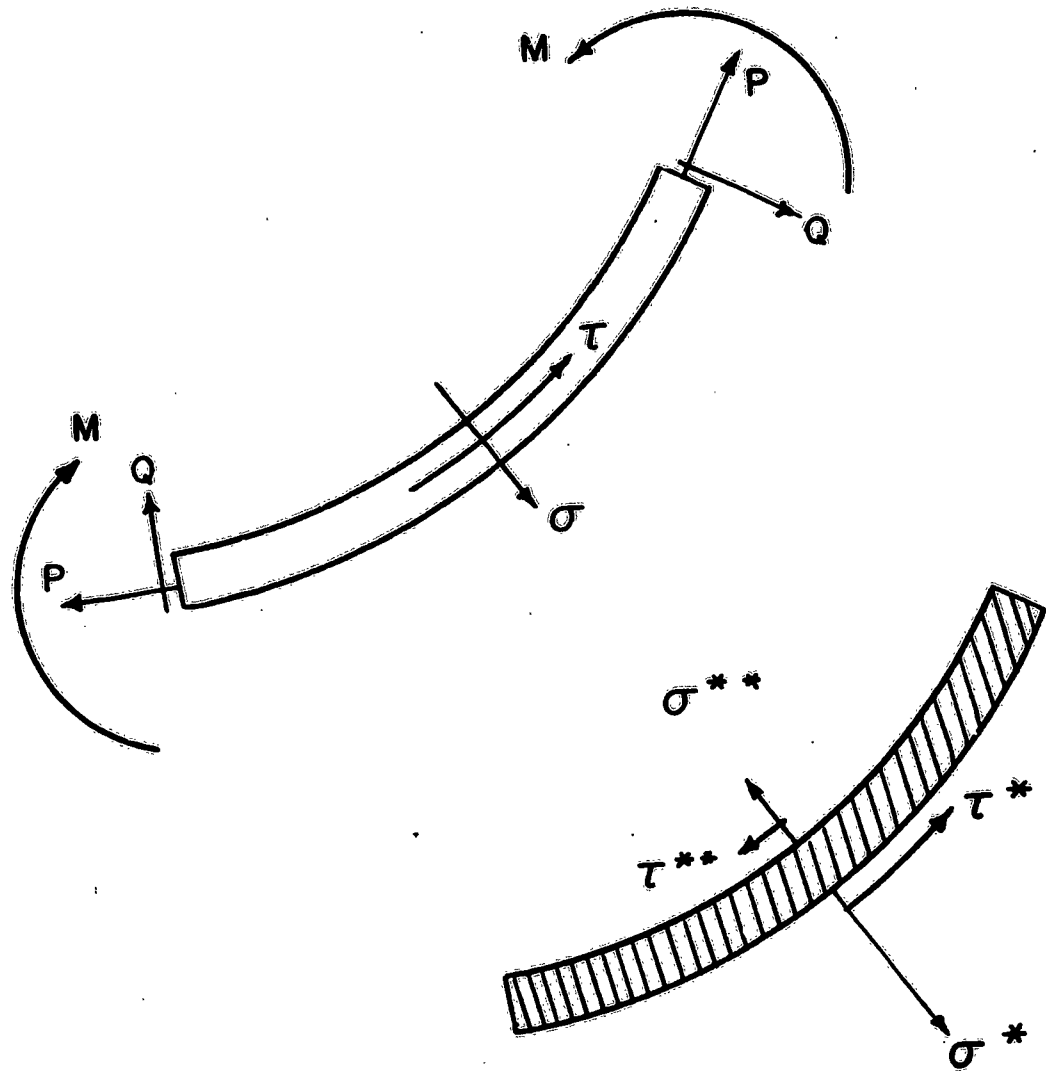
Figure 1. External Stresses and Internal Resultants in a Linear Fiber

(2)
$$\sigma + \frac{dQ}{ds} - P\frac{d\phi}{ds} = 0,$$

(3)
$$T + \frac{dP}{ds} + Q\frac{d\phi}{ds} = 0,$$

(4)
$$\frac{dM}{ds} - Q = 0.$$

ON THE IDEALIZED ELASTIC PROPERTIES OF MICROFIBERS. When a microfiber is treated analytically as a one-dimensional line, either as a line in space or as a line in the cross section figure in plane strain, that line must be thought of as the limiting case of an ordinary elastic body - a three-dimensional body in space or a two-dimensional cross section figure in plane strain. To fix ideas, let us develop the subject referring to plane strain. The limiting process consists in the narrow dimension of the body skrinking towards zero. As long as the narrow dimension goes on shrinking (and thus has not yet reached its limit value of zero) we have a very slender elongated elastic body to which the usual elasticity concepts and methods apply fully. In the limit, however, when all that is present is a line, we have a new formation (a linear microfiber) which is governed by characteristic rules of its own. "Rules" means, essentially, stress-strain relations.

Rules characteristic of linear fibers could be devised (and sometimes are devised) by arbitrary statements of the kind that say, typically, "let us consider a fiber in which the following (specified) is a cause leading to the following (specified) effect, and let the relation between cause and effect be as follows (specified)." We emphatically reject this approach as being too formal and basically void of a physical background. The actual microfibers used are not linear, but slender elongated full dimensional bodies of physical elastic nature. For the practical use of microfibers it is this pre-limit slender elongated fiber in which we are interested. The limit concept is a mere mathematical device introduced to bring out the characteristic features of fiber action in a conspicuous way. Also, the use of the limit concept of a linear

microfiber facilitates the mathematical treatment of special cases. But bearing in mind the physical foundations of the actual fibers, we now declare the following principle as a necessary (and indispensably necessary) prerequisite to any linear fiber characterization we may wish to operate with:

Physical Principle Prerequisite to the Acceptance of a Linear Fiber:

All specific individual relations characterizing a particular linear microfiber must be derivable as limit forms of relations given by the theory of elasticity for a thin slender replacement fiber when the thin dimension of the replacement fiber shrinks towards zero in the limit.

We have discussed the behavior of the narrow dimension δ of the fiber, namely

$$(5) \qquad \delta \longrightarrow 0 \ .$$

Figure 3 shows a few steps in the progressing process $\delta \longrightarrow 0$ for a fiber in uniaxial tension produced by a constant total tension force P. On top, the force has not yet been applied, and the unstrained length of the fiber is shown. The application of P causes an extension ΔL of the fiber, determined by

$$(6) \qquad \Delta L = L \, \epsilon = \frac{L}{E} \, \sigma = \frac{LP}{E\delta} \ .$$

As $\delta \longrightarrow 0$, $\Delta L \longrightarrow \infty$, and thus the limit is a linear fiber not capable of maintaining a finite tension P. This result is due to the fact that E was held constant in the process $\delta \longrightarrow 0$. This is not a logical or physical necessity as we may assume that while δ is going through the sequence $\delta_1, \delta_2, \delta_3 \ldots \longrightarrow 0$ the fibers are being exchanged and E goes correspondingly, through some sequence $E_1, E_2, E_3 \ldots \ldots$ giving us a chance to introduce the behavior of the product $E\delta$ during the limit process as we see fit.
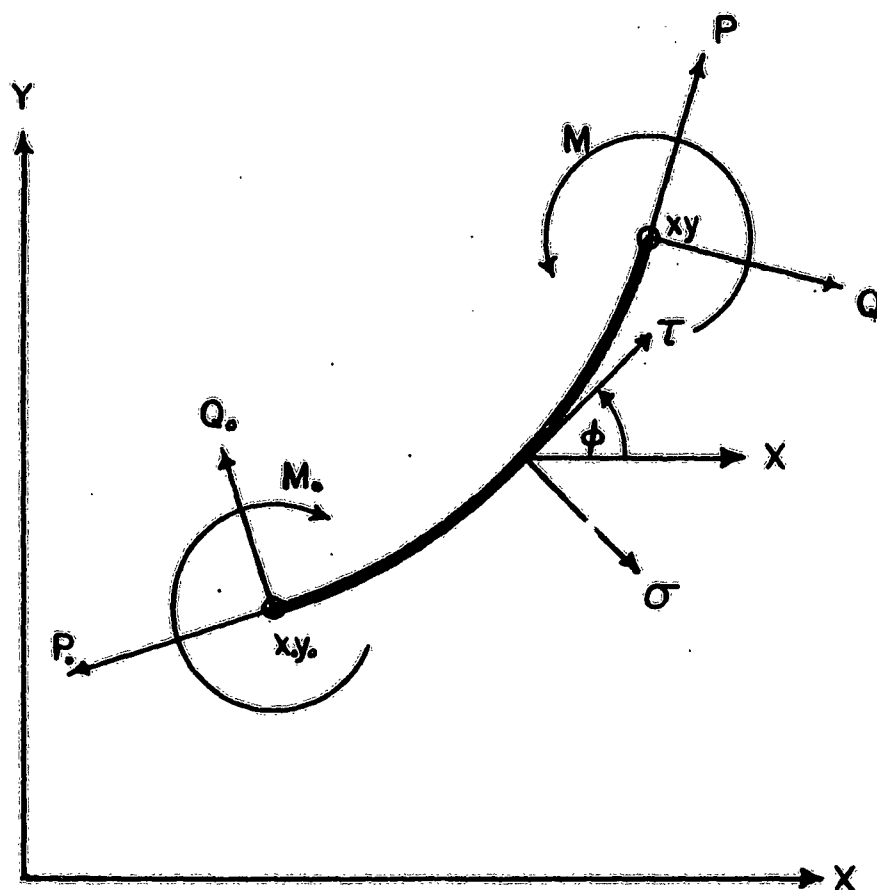
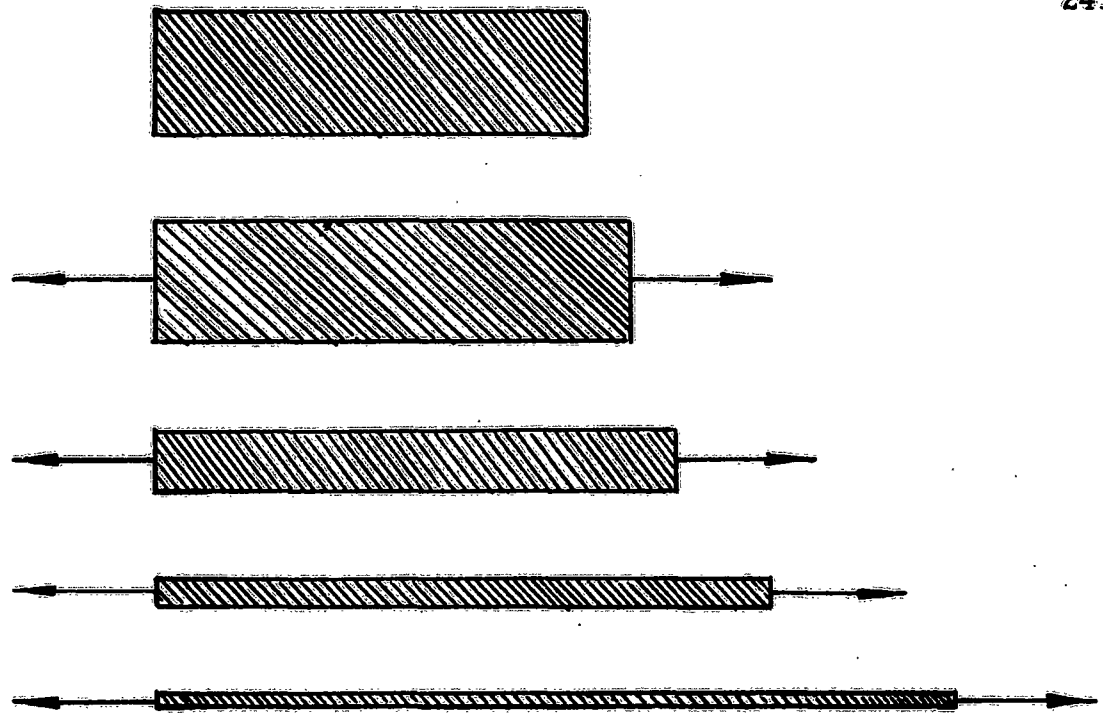Figure 2.   Free Body Diagram for a Fiber

Figure 3. Fiber $\alpha = 0$: Failure to Produce a Limit

Research publications dealing with the experimental aspects of microfiber production show a concentration of interest on tensile strength. The knowledge of the tensile strength and of the moduli of elasticity E and G would have sufficed for a mathematical analysis of microfiber action without involving possibilities that may not be physically available, while the determination of tensile strength alone without knowledge of E and G does not enable us to pinpoint the preferred theoretical variant.

Lacking experimental data on E in microfibers, we make an assumption capable of covering a wide range of possibilities. We assume that E grows inversely as a power α of δ , namely

$$(7) \qquad E = \frac{c}{\delta^{\alpha}} \, ,$$

in which c is some constant. We can now typify linear microfibers by the α - value used in the limiting process to obtain them. The formula for ΔL Eq. (6) now becomes

$$(8) \qquad \Delta L = \frac{L P \delta^{\alpha - 1}}{c} \, .$$

The fiber discussed in Fig. 3 belongs to the type $\alpha = 0$ since E was held constant. The type $\alpha = 1$ will have E δ = c, therefore

$$(9) \qquad \Delta L = \frac{L P}{C}$$

valid for any fiber of the sequence $\delta_1, \quad \delta_2, \ldots \to 0$ before the limit formation and also for the limiting linear microfiber $\delta \to 0$. This case is illustrated in Fig. 4. The limit is a fiber which is elastically extensible according to Eq. (9).

Should we bend each fiber of the pre-limit set $\delta_1, \quad \delta_2, \ldots$ into a circular arc shape by applying equal opposite moments M at the ends of the fibers, the relation
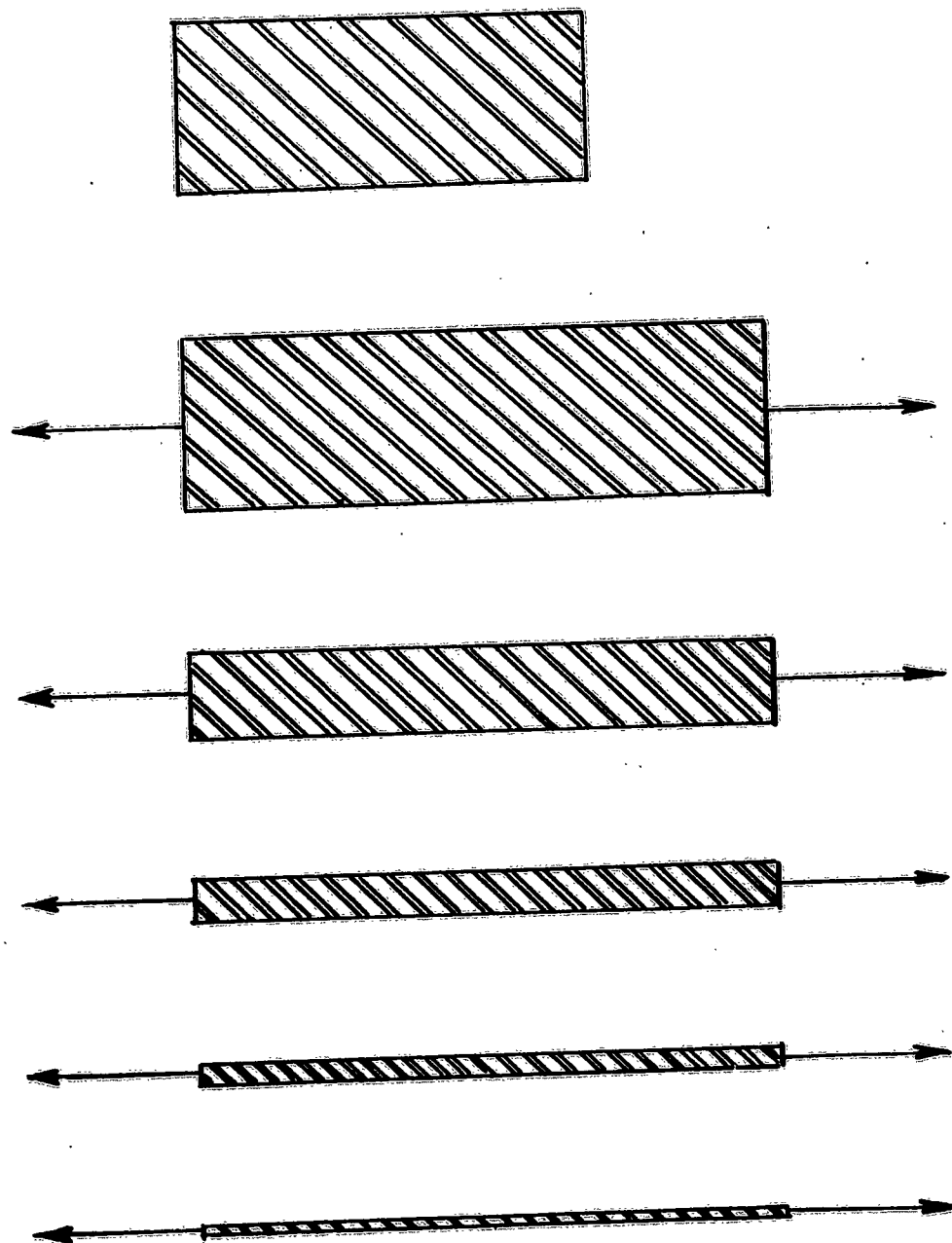
Figure 4. Fiber $\alpha = 1$: Elastically Extensible Fiber in the Limit

(10)
$$M = \frac{EI}{R}$$

would show the value of the bending moment M needed to produce a given curvature $\frac{1}{R}$ in the fiber. With $I = \frac{\delta^3}{12}$ and $E = \frac{c}{\delta^\alpha}$ we have

(11)
$$M = \frac{c\delta^{3-\alpha}}{12 R}$$

For $\alpha = 1$ (Fig. 4), $M \rightarrow 0$ as $\delta \rightarrow 0$. The $\alpha = 1$ linear fiber is thus flexible in the limp way - no bending moment is required to bend it into any curved shape. With respect to bending, it resembles a chain (but not with respect to elongation).

Turning now to $\alpha = 2$, we have

(12)
$$\Delta L = \frac{LP\delta}{c} \longrightarrow 0 \qquad M = \frac{c\delta}{12R} \longrightarrow 0, \quad \delta \rightarrow 0$$

from Eqs. (8) and (11). The linear microfiber is now inextensible under a finite force p and flexible in the limp way. This fiber resembles a chain in both aspects. The limiting set for ΔL is shown in Fig. 5. For $\alpha = 3$ we have

(13)
$$\Delta L = \frac{LP\delta^2}{c} \longrightarrow 0, \quad M = \frac{c}{12R}, \quad \text{as } \delta \rightarrow 0.$$

This is an inextensible and elastically flexible fiber: the bending moment M is proportional to the curvature produced, $\frac{1}{R}$.

Beginning with $\alpha = 4$ we have, in the limit,

$$\Delta L = 0 \qquad \frac{1}{R} = 0$$

for every P and M : the linear fiber is a rigid body incapable of any deformation (no elongation, no bending).

We have thus arrived at the following types of linear fibers:

$\alpha = 0$ no fiber at all results in the limit (limp extensibiliy, limp flexibility)

$\alpha = 1$.   elastically extensible, limp flexible

$\alpha = 2$.   inextensible, limp flexible

$\alpha = 3$.   inextensible, elastically flexible

$\alpha \geqslant 4$.   rigid.

We note a conspicuous absence: the absence of an elastically extensible elastically flexible linear microfiber.

Using equilibrium equations (2), (3), and (4) further particulars can be determined for the different fibers and compiled in a detailed exposition such as in Table 1 at the end of this report. No new assumptions are involved, the classification and tabulation take care of themselves along the following lines: if $\epsilon = 0$, the fiber is inextensible, and P becomes a reaction force not involved in an elastic stress-strain law. If ϵ does not vanish, P is either zero (limp extensibility) or related to ϵ (elastic extensibility). If $\frac{1}{R} = 0$, the fiber is inflexible and M becomes a reaction moment not involved in an elastic stress-strain law. If $\frac{1}{R}$ does not vanish, M is either zero (limp flexibility) or related to $\frac{1}{R}$ (elastic flexibility). If $P = 0$, the fiber is limp extensible. If P does not vanish, the fiber is either elastically extensible or inextensible. If $M = 0$, the fiber is limp flexible. If M does not vanish, the fiber is either elastically flexible or inflexible.

Reading the table by columns down we see how the character of the fibers changes from a limp, forceless and stressless start at $\alpha = 0$ to absolute rigidity at $\alpha = 4$. The change takes place in four consecutive stiffening steps in which limpness is first replaced by elasticity and then by rigidity.

NECESSITY OF A GENERAL ACCEPTANCE TEST FOR α - FIBERS.

The simple uniaxial tension tests illustrated in Figs. 3-5 served the purpose of general orientation and led to the four classifications $\alpha = 1$, $\alpha = 2$, $\alpha = 3$, $\alpha \geq 4$ of microfibers. The special character of uniaxial tension tests becomes obvious in the enumeration of quantities that vanish in the test, in other words, of quantities that do not appear in the test in which, consequently, the corresponding causative physical properties of linear fibers are not engaged:

$$(15) \qquad M = Q = \sigma = \tau = \frac{1}{R} = 0.$$

The flexural test (bending by a moment) is accompanied by the following set of vanishing values:

$$(16) \qquad P = Q = \sigma = \tau = \epsilon = 0.$$

The only values tested are P and ϵ in (15) and M and $\frac{1}{R}$ in (16). Q, σ, τ have been left out of testing altogether. Such limited testing is insufficient for the final acceptance of the α - fibers ($\alpha = 1, 2, 3, 4$).

The final acceptance of α - fibers should be decided upon by subjecting the candidate fibers for $\alpha = 1, 2, 3, 4$ to a general test in which as many of the quantities

$$(17) \qquad P, Q, M, \sigma, \tau, \epsilon, \frac{1}{R}$$

should actually develop (be different from zero) as the fiber type may produce. In a limp fiber $M = 0$, in an inextensible fiber $\epsilon = 0$, and so forth. Such zeros we will request considering their appearance as a general confirmation of the properties of limpness, inextensibility, and so forth. Furthermore, the tested microfibers ought to be curved, to get away from the specialized rectilinear shape with $\frac{d\phi}{ds} = 0$.
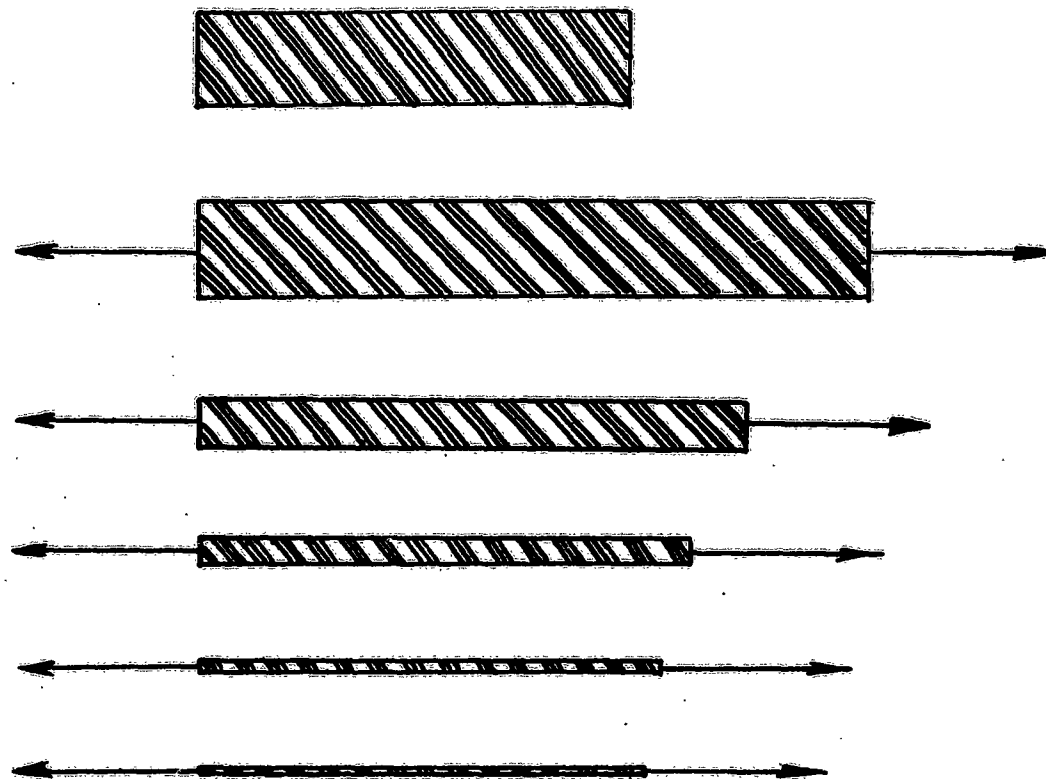
Figure 5. Fiber $\alpha = 2$: Inextensible Fiber in the Limit

Furthermore, each linear microfiber should be arrived at as the limiting case $\delta \rightarrow 0$ of a fully solved elasticity problem in which a slender $\delta > 0$ body is bonded to a matrix filler. The elasticity problem should be void of any unwanted symmetries which would reduce the number of independent features.

THE ACCEPTANCE TEST. We consider an infinite elastic matrix body filling the exterior of the circle $r = a$ (Fig. 6). Bonded to it along the circle $r = a$ is the δ-body which is a ring of outer radius a and inner radius b. Obviously,

(18)
$$\delta = a - b.$$

The elasticity constants of the matrix are denoted by E, G and ν ; those of the δ- ring by E', G' and ν'. In the stiffening process of the δ - body, Eq. (7), we assume that ν' remains constant (it would be limited to the range $0 \leq \nu' \leq \frac{1}{2}$ anyway). The analytical part of the test is simplified if we put $\nu = \nu'$.

The stiffening equation (7) is set up best in dimensionless form

(19)
$$\frac{G'}{G} = \left(\frac{L}{\delta}\right)^{\alpha}$$

in which L has the dimension of a length, same as δ, by Eq. (18).

In testing, the matrix substance is subjected to the state of pure shearing stress at infinity:

(20)
$$\sigma_x = 1 , \quad \sigma_y = -1 , \quad \tau_{xy} = 0 ,$$

while the inner surface of the δ-ring (at r = b) remains free from boundary tractions σ_r and $\tau_{r\theta}$. We have a problem of linear elasticity for the composite body consisting of the matrix substance with the δ-ring bonded to it along r = a. The problem was solved and the characterizations Eq. (14) have been checked as to their general validity. The results, affirmative in all cases, are shown in the following table:
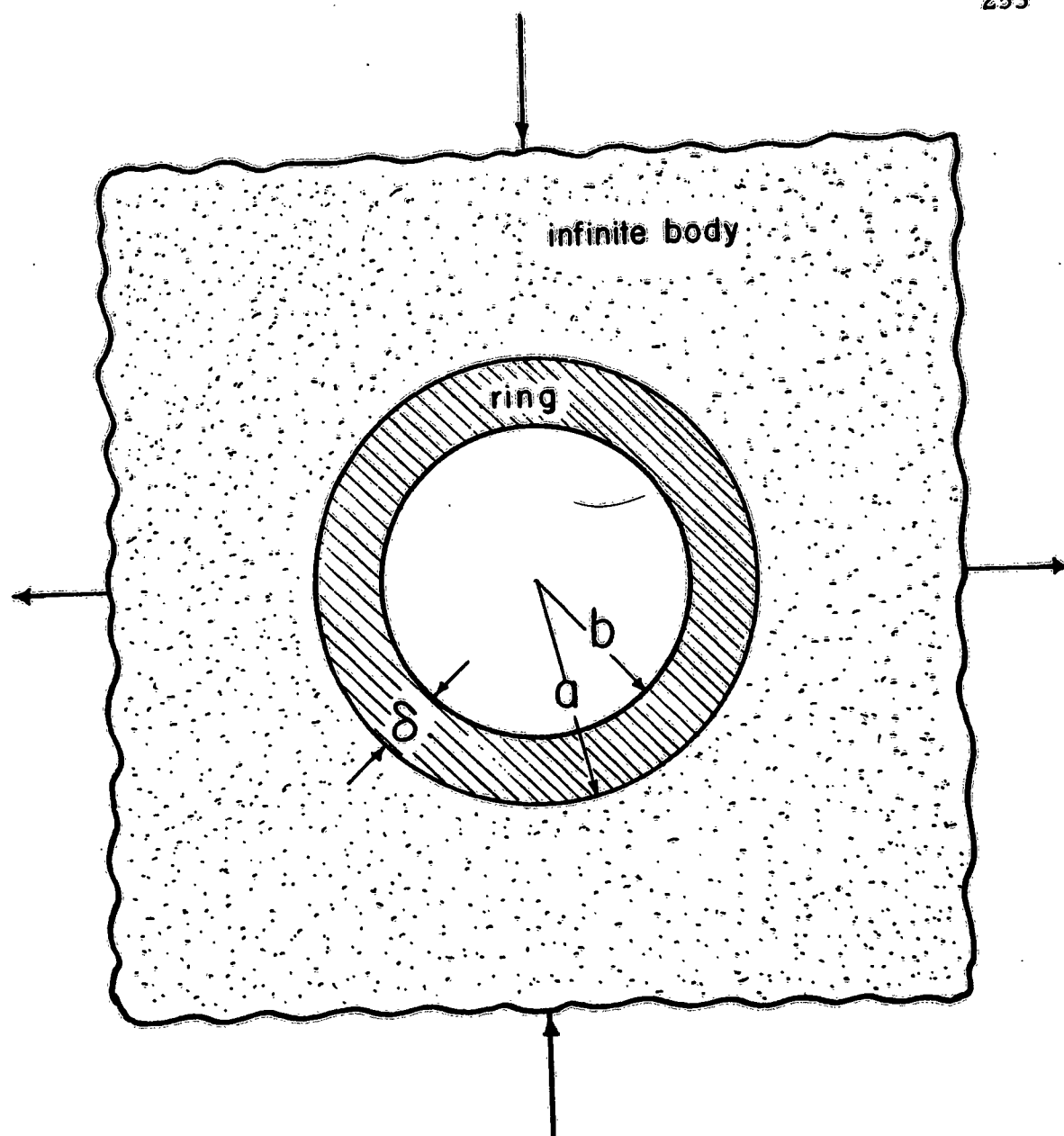
Figure 6. Composition of δ-Ring and Filler Body

α	Vanishing forces and stresses	Vanishing geometric strains / Geometric fiber characterization	present forces and stresses	Present geometric strains	Physical Law (Stress-strain law)
0	P=Q=M=σ=T=0	none	none	ε.... limp extensibility(since P=o) $\frac{1}{R}$.... limp flexibility (since M=o)	none
1	Q=M=0	none	P, σ, T	ε $\frac{1}{R}$.... limp flexibility(since M=o)	ε=C,P elastic extensibility
2	Q=M=0	ε=0 inextensible	P, σ, T	$\frac{1}{R}$.... limp flexibility(since M=0)	none
3	none	ε=0 inextensible	P,Q,M,σ,T	$\frac{1}{R}$	$\frac{1}{R}$ = C₂M elastic flexibility
4	none	ε=0, $\frac{1}{R}$=0 inextensible and inflexible= rigid	P,Q,M,σ,T	none	none

Table 1. Classification and Characterization of Elastostatically Consistent Linear Fibers

THIN CYLINDRICAL SHELLS UNDER LOCAL AXIAL LOADINGS

John Mescall

U. S. ARMY MATERIALS RESEARCH AGENCY
Watertown, Massachusetts   02172

INTRODUCTION.   It frequently happens in pressure vessel and missile construction that an axial load is transmitted into the wall of a thin cylindrical shell by means of a heavy ring attached to the cylinder.   This ring distributes the load fairly uniformly into the cylinder.   For reasons of economy or weight-saving, it is sometimes desirable to replace the solid ring by a series of brackets or angle irons.   The resulting non-uniform distribution of axial load can result in a significant increase in the local stress level in the cylinder.   This situation thus provides an interesting and useful problem in the asymmetric deformation of thin shells. Solutions and numerical results for similar localized radial (normal) and tangential (in the circumferential direction) loadings on simply supported cylinders have been presented by Bijlaard [1, 2] .   However, the related problem of a distributed tangential loading in the axial direction was not discussed.   It is our intention, then, to supplement these results by examining the solution and presenting some numerical results for localized axial loadings on thin cylindrical shells.

In the specific application described earlier, the axial load is not applied directly to the shell's middle surface but usually at a distance greater than half the thickness away from the middle surface.   Thus, there is also developed a radial load with an axial variation, i.e., a longitudinal moment, to use Bijlaard's nomenclature.   The desired solution to the physical problem is then a properly weighted combination of these two loading conditions.

In the ensuing discussion, the governing differential equations of equilibrium selected are those due to Flügge rather than those employed by Bijlaard.   This approach affords, as a by-product, an opportunity to compare results of Flugge's non-honogeneous equations with those of Bijlaard's for a wide range of shell parameters.   Hoff [3] and Kempner [4] have made similar comparisons with Donnell's equations for the corresponding homogeneous equations and for line loadings.

Recently, Nash and Bridgland [5] discussed line radial loadings on thin cylindrical shells using Flügge's equations and suggested the use of the finite Fourier transform in obtaining solutions. This technique has been employed in the present discussion of distributed axial loads.

BASIC EQUATIONS AND FORMULATION OF PROBLEM. We consider a thin circular cylindrical shell of radius a and thickness h. Young's modulus and Poisson's ratio are denoted by E and ν respectively, while x*, Θ and Z denote coordinates in the axial, circumferential and radial (positive when inward) directions. Corresponding displacement components for a point on the shell's middle surface are u*, v*, and w*. It is convenient to deal with the dimensionless displacement components u, v and w, defined by u = u*/a, v = v*/a and w = w*/a, as well as with dimensionless middle-surface coordinates x = x*/a and Θ.

Flügge's equations for the equilibrium of thin circular cylindrical shells [6] may then be written in the dimensionless form

$$u'' + \left(\frac{1-\nu}{2}\right)\ddot{u} + \left(\frac{1+\nu}{2}\right)\dot{v}' - \nu w' + k^2\left[w''' + \left(\frac{1-\nu}{2}\right)(\ddot{u} - \ddot{w}')\right] = -\frac{ap_x}{C}$$

(1)
$$\ddot{v} + \left(\frac{1-\nu}{2}\right)v'' + \left(\frac{1+\nu}{2}\right)\dot{u}' - \dot{w} + k^2\left[\left(\frac{3-\nu}{2}\right)\dot{w}'' + \frac{3(1-\nu)}{2}v''\right] = -\frac{a^2 p_\Theta}{C}$$

$$\nabla^4 w + 2\ddot{w} + w + \left(\frac{3-\nu}{2}\right)\dot{v}'' + u''' - \left(\frac{1-\nu}{2}\right)\ddot{u}' + \frac{1}{k^2}\left[w - \dot{v} - \nu u'\right] = \frac{a^2 p_r}{D}$$

where dots indicate differentiation with respect to Θ, and primes indicate differentiation with respect to x; p_x, p_Θ and p_r are the components of applied surface loading in the axial, circumferential and radial directions, $k^2 = h^2/12a^2$, $C = Eh/(1-\nu^2)$, $D = Eh^3/12(1-\nu^2)$, and

$$\nabla^4 w \equiv w'''' + 2\ddot{w}'' + \ddddot{w} .$$

When Equations (1) have been solved for u, v, and w for a prescribed loading condition, stress resultants and moments in the cylinder may be obtained from the following relations:

$$N_x = C \left[u' + \nu (\dot{v} - w) \right] + \bar{D} \, \ddot{w}$$

$$N_\Theta = C \left[\dot{v} + \nu u' - w \right] - \bar{D} \left[w + \ddot{w} \right]$$

$$N_{x\Theta} = C \left(\frac{1-\nu}{2} \right) \left[\dot{u} + v' \right] + \bar{D} \left(\frac{1-\nu}{2} \right) \left[v' + \dot{w}' \right]$$

$$N_{\Theta x} = C \left(\frac{1-\nu}{2} \right) \left[\dot{u} + v' \right] + D \left(\frac{1-\nu}{2} \right) \left[\dot{u} - \dot{w}' \right]$$

(2)

$$M_x = -\bar{D} a \left[w'' + \nu \ddot{w} + u' + \nu \, \dot{v} \right]$$

$$M_\Theta = -\bar{D} a \left[w + \ddot{w} + \nu \, w'' \right]$$

$$M_{x\Theta} = -\bar{D} a (1 - \nu) \left[\dot{w}' + v' \right]$$

$$M_{\Theta x} = -\bar{D} a (1 - \nu) \left[\dot{w}' + \frac{1}{2} (v' - \dot{u}) \right]$$

$$\bar{D} \equiv D/a^2 .$$

We consider the following specific loading and boundary conditions.
An axial load of intensity p_x is distributed over a set of N rectangular
areas (pads) periodically located around the circumference of the cylinder
(see Figure 1). Let the length in the axial direction of each pad be $2a\delta$
and the x coordinate of the center of each pad be x_o; let the length of
each pad in the Θ direction be $2a\Theta_1$, while the Θ coordinate of the center
of the first pad is $\Theta = 0$. The distributed applied load is assumed to be
balanced by a uniform axial compression N_x at the base of the cylinder.
This desired loading system may be considered as the superposition of
the following two systems:
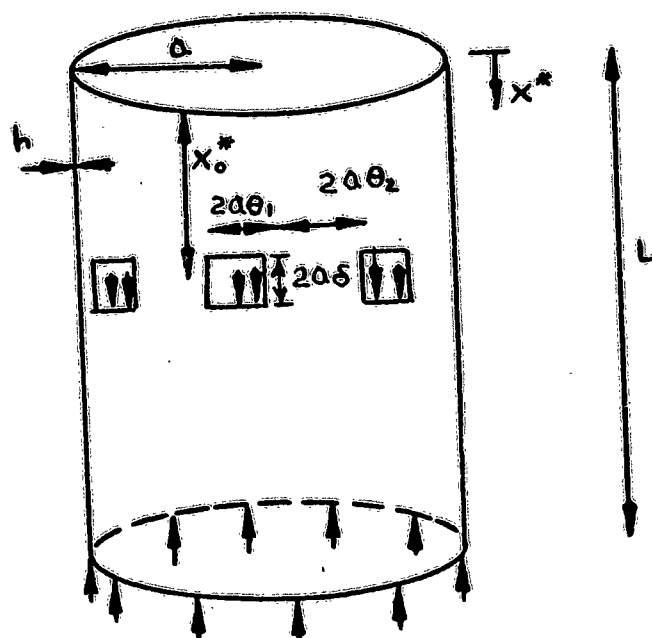
FIG. 1

FIG. 2

1. A rotationally symmetric distribution of uniform axial load acting over a band of length $2a\delta$, centered about $x=x_o$, and balanced by a uniform compression, N_x, at the base of the cylinder.

2. A self-equilibrating distribution of tangential axial load acting over the same area, (see Figure 2).

The solution to the first of these systems is trivial. Hence, the given problem is reduced to the solution of equilibrium equations when $p_\Theta = p_r = O$ and $p_x(x, \Theta)$ has the form of a step function in x for $\Theta = \Theta_o$ and a rectangular wave function in Θ for $x_o - \delta \leq x \leq x_o + \delta$, (see Figure 3).

Algebraically, then,

$$p_x(x, \Theta) = p_1 \qquad 2(m-1)(\Theta_1 + \Theta_2) - \Theta_1 \leq \Theta \leq 2(m-1)(\Theta_1 + \Theta_2) + \Theta_1$$

(3)

$$= -p_2 \qquad 2(m-1)(\Theta_1 + \Theta_2) + \Theta_1 \leq \Theta \leq 2m(\Theta_1 + \Theta_2) - \Theta_1$$

where $m=1, 2, \ldots$ N, $\Theta_1 + \Theta_2 = \pi/N$, $x_o - \delta \leq x \leq x_o + \delta$.

For x outside this range, p_x vanishes identically. The condition that the load be self-equilibrating is that $p_1\Theta_1 = p_2\Theta_2$. Finally, we consider boundary conditions of simple support at the ends, i.e., $w = v = N_x = M_x = o$ at $x=o$, L/a.

METHOD OF SOLUTION. We assume the following forms for the displacements:

$$w = \sum_{n=1}^{\infty} F_{1n}(\Theta) \sin(\lambda x)$$

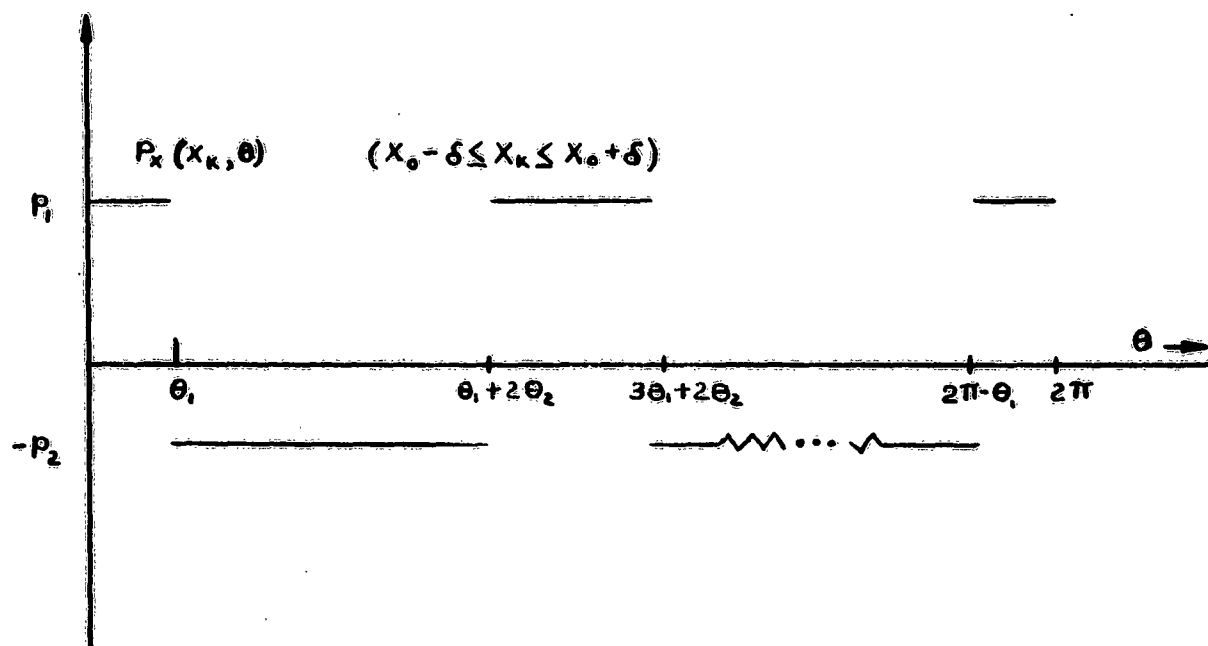(4) $$v = \sum_{n=1}^{\infty} F_{2n}(\Theta) \sin(\lambda x)$$

FIG 3

$$u = F_{3o}(\Theta) + \sum_{n=1}^{\infty} F_{3n}(\Theta) \cos(\lambda x)$$

$$\text{where } \lambda = \frac{n\pi a}{L} .$$

This form ensures simply supported edges at x=o, L/a. We further expand the applied load $p_x(x, \Theta)$ in a Fourier cosine series in x, obtaining:

$$p_x(x, \Theta) = \frac{a_o(\Theta)}{2} + \sum_{n=1}^{\infty} a_n(\Theta) \cos(\lambda x)$$

$$(5) \qquad a_n(\Theta) = \frac{4}{n\pi} p(\Theta) \cos(\lambda x_o) \sin(\lambda \delta)$$

$$a_o(\Theta) = \frac{4\delta a p(\Theta)}{L} .$$

Insertion of these expansions into the equilibrium equations (1) leads to a set of 3n ordinary differential equations for $F_{in}(\Theta)$ whose solution may rather compactly be obtained by means of the finite Fourier transform. The essential facts regarding this transform may be listed as follows. The finite Fourier transform of a function of $f(\Theta)$ is defined as:

$$f^*(S) = F\left[f(\Theta)\right] = \frac{1}{2\pi} \int_0^{2\pi} f(\Theta) e^{-iS\Theta} d\Theta.$$

The inverse transform is given by

$$f(\Theta) = F^{-1}\left[f^*(S)\right] = \sum_{S=-\infty}^{\infty} f^*(S) e^{iS\Theta} ,$$

Army Mathematicians

while the following useful relation holds [7]

$$\bar{F}\left[\frac{df}{d\Theta}\right] = iS\, f^*(S) \quad .$$

Application of the transform then reduces the equilibrium equations to a set of $3n$ algebraic equations to be solved for the transforms of $F_{mn}(\Theta)$:

$$\bar{F}_{1n}{}^*(S)\left\{k^2 q^4 + 2k^2 q^2(1-\lambda^2) + \left[1+k^2(1+\lambda^4)\right]\right\} + \bar{F}_{2n}{}^*(S)\left\{-q\left[1+k^2\lambda^2(\tfrac{3-\nu}{2})\right]\right\}$$

$$+ F_{3n}{}^*(S)\left\{\lambda k^2 q^2(\tfrac{1-\nu}{2}) + \lambda(\nu + \lambda^2 k^2)\right\} = 0$$

(6)

$$F_{1n}{}^*(S)\left\{-q\left[1+\lambda^2 k^2(\tfrac{3-\nu}{2})\right]\right\} + F_{2n}{}^*(S)\left\{q^2-\lambda^2(\tfrac{1-\nu}{2})(1+3k^2)\right\}$$

$$+ F_{3n}{}^*(S)\left\{-q\lambda(\tfrac{1+\nu}{2})\right\} = 0$$

$$F_{1n}{}^*(S)\left\{q^2\lambda k^2(\tfrac{1-\nu}{2}) + \lambda(\nu + \lambda^2 k^2)\right\} + F_{2n}{}^*(S)\left\{-\lambda q(\tfrac{1+\nu}{2})\right\}$$

$$+ F_{3n}{}^*(S)\left\{\lambda^2 - q^2(1+k^2)(\tfrac{1-\nu}{2})\right\} = \frac{a\, a_n}{C}\, F\left\{p(\Theta)\right\}$$

where $q = iS$.

The transform of $p(\Theta)$, the Θ-dependence of the load function is easily found to be

$$F\left[p(\Theta)\right] = \frac{1}{\pi S}\left\{p_1 \sin(S\,\Theta_1)\sum_{m=1}^{N} e^{-2(m-1)(\Theta_1+\Theta_2)\,iS}\right.$$

$$-p_2 \sin(S\Theta_2) \sum_{m=1}^{N} e^{-(2m-1)(\Theta_1+\Theta_2) iS} \Big\}$$

(7)

$$= \frac{N}{\pi S}\Big\{ p_1 \sin(S\Theta_1) - (-1)^k p_2 \sin(S\Theta_2) \Big\} \qquad s = kN$$

$$k = 1, 2, 3 \ldots$$

$$= \quad 0 \qquad\qquad\qquad\qquad\qquad\qquad\qquad\quad s \neq kN.$$

With this information, simple algebra permits an explicit solution for the transforms of $F_{mn}(\Theta)$. Inserting these into the inversion formula and taking account of the odd or even character of the resulting expressions leads directly to the following results for $F_{mn}(\Theta)$:

$$F_{mn}(\Theta) = \frac{2a\, a_n\, N(p_1+p_2)}{C\pi k^2} \sum_{S=N,\,2N\ldots}^{\infty} \frac{A_{mn}(S)\, \sin(S\Theta_1)}{S\, B_n(S)} \cos(S\Theta)$$

(8)

$$m = 1, 3$$

$$F_{2n}(\Theta) = \frac{2a\, a_n\, Ni(p_1+p_2)}{C\pi k^2} \sum_{S=N,\,2N\ldots}^{\infty} \frac{A_{2n}(S)\, \sin(S\Theta_1)}{S\, B_n(S)} \sin(S\Theta)$$

where

$$A_{1n}(S) = \Big\{ S^4 \lambda k^2 + S^2 \Big[3\lambda^3 k^4 (\tfrac{1-\nu}{2}) + \lambda \Big] - (1+3k^2)(\lambda^5 k^2 + \nu\lambda^3) \Big\}$$

$$A_{2n}(S) = iS \Big\{ -S^4 k^2 \lambda \, (\tfrac{1+\nu}{1-\nu}) - S^2 \Big[\lambda^3 (2k^2(\tfrac{1+\nu}{1-\nu}) + \tfrac{3-\nu}{2} k^4) - \lambda k^2 (\tfrac{1-3\nu}{1-\nu}) \Big]$$

$$+ \frac{2}{1-\nu} \Big[\lambda^5 \Big(k^4(\tfrac{3-\nu}{2}) - k^2 \, (\tfrac{1+\nu}{2}) \Big) + \lambda^3 k^2 \Big(1+(\tfrac{3-\nu}{2})\nu \Big)$$

$$+ \lambda \Big(\nu - \tfrac{1+\nu}{2}\, (1+k^2) \Big) \Big] \Big\}$$

$$A_{3n}(S) = \frac{2k^2}{1-\nu} \left\{ S^6 + S^4 \left[-2 + \frac{\lambda^2}{2} \left(5 - \nu + 3k^2(1-\nu) \right) \right] \right.$$

$$+ S^2 \left[\lambda^4 \left((2-\nu) + k^2 (3(1-\nu) - (\frac{3-\nu}{2})^2) \right) \right.$$

$$\left. - \lambda^2 \left(4 - 2\nu + k^2(3-3\nu) \right) + 1 \right]$$

$$\left. + \left[\lambda^6 (1+3k^2)(\frac{1-\nu}{2}) + \lambda^2 (1+k^2)(3+1/k^2)(\frac{1-\nu}{2}) \right] \right\}$$

$$B_n(S) = \left\{ S^8(1+k^2) + S^6 \left[-2(1+k^2) + \lambda^2 \left(4 + k^2(\frac{7-3\nu}{2}) + k^4 (\frac{3(1-\nu)}{2}) \right) \right] \right.$$

(9)
$$+ S^4 \left[\lambda^4 (6 + 3k^2(2-\nu) - \nu^2 k^4) \right.$$

$$\left. - \lambda^2 \left(2(4-\nu) + k^2 (7-5\nu) + k^4 3(1-\nu) + (1+k^2) \right) \right]$$

$$+ S^2 \left[\lambda^6 (4 + \frac{(11-3\nu)}{2} k^2 + \frac{9(1-\nu)}{2} k^4) \right.$$

$$- 3\lambda^4 (2 + (2-\nu+\nu^2) k^2)$$

$$\left. + \lambda^2 (2(2-\nu) + \frac{7(1-\nu)}{2} k^2 + \frac{3(1-\nu)k^4}{2}) \right]$$

$$\left. + (1+3k^2) \lambda^4 \left[1 + \frac{1-\nu}{k^2} \lambda^2 - 2\nu\lambda^2 + (1-k^2) \lambda^4 \right] \right\} \quad .$$

Equations (8) and (4) thus provide representations for the displacements u, v, w and, so, a solution to the problem in the form of a double Fourier series in x and Θ. It is readily established that these series for displacements converge and, in fact, coverge sufficiently rapidly that they

may be differentiated to provide convergent series for the stress result-
ants and couples. To complete the stress analysis of the cylinder under
tangential axial loadings over a series of N pads, it is necessary to
superimpose upon the stresses due to the above self-equilibrating load
system those due to a rotationally symmetric band of tangential axial
loads, (see Figure 2). We must, therefore, add to N_x the terms:

$$\bar{N}_x = 0 \quad , \qquad 0 \leq x \leq x_o - \delta$$

$$(10) \qquad = \frac{-N_o(x - x_o + \delta)}{2\delta} \quad , \qquad x_o - \delta \leq x \leq x_o + \delta \ (\text{all } \Theta)$$

$$= -N_o \quad , \qquad x_o + \delta \leq x \leq L$$

where $N_o = 2\delta a p_2$. Finally, we note that the intensity of $p_x(x, \Theta)$ over
the periodic pad areas then has a magnitude of $p_1 + p_2$.

LONGITUDINAL MOMENT SOLUTION To account for the fact that the
axial load is not applied at the middle surface of the shell, we assume
that there is a net longitudinal moment exerted over the area beneath
each pad, and that this moment may be described in terms of a radial
pressure distribution whose intensity is proportional to its algebraic
distance from x_o:

$$p_r(x, \Theta) = \bar{p}(\Theta) (x - x_o) \qquad x_o - \delta \leq x \leq x_o + \delta$$

where $\bar{p}(\Theta)$ has a unit value, say p_o, beneath a pad and vanishes elsewhere.

The solution for this type of loading may be obtained most exped-
iently by utilizing Nash and Bridgland's [5] basic results for a radial
line load acting over a portion of the circumference at $x = \xi$. Their
solution for this problem may be written in the form

$$w = \sum_{n=1}^{\infty} F_{1n}(\Theta) \sin(\lambda x)$$

$$v = \sum_{n=1}^{\infty} F_{2n}(\Theta) \sin(\lambda x)$$

(11)

$$u = \sum_{n=1}^{\infty} F_{3n}(\Theta) \cos(\lambda x),$$

where

$$F_{mn}(\Theta) = \frac{2(1-\nu^2)a^2}{Eh\, k^2 L} \sin(\lambda\zeta) \left\{ p^*(O)E_{mn}(O) + 2\sum_{S=1}^{\infty} p^*(S)E_{mn}^*(S) \cos S\Theta \right\}$$

$$m=1,3$$

(12)

$$F_{2n}(\Theta) = \frac{2(1-\nu^2)a^2}{Eh\, k^2 L} \sin(\lambda\zeta) \left\{ 2i \sum_{S=1}^{\infty} p^*(S)\, E_{2n}^*(S) \sin S\Theta \right\},$$

$p^*(S)$ is the finite Fourier transform of $p(\Theta)$,

(13)
$$E_{mn}^*(S) = \frac{\overline{A}_{mn}(S)}{\overline{B}_m(S)}$$

and

$$\overline{A}_{1n}(S) = S^4(1+k^2) + \lambda^2 S^2\left[2 + 2(1-\nu)k^2 + 3\left(\frac{1-\nu}{2}\right)k^4\right] + \lambda^4\left[1+3k^2\right]$$

(14A)

$$\overline{A}_{2n}(S) = -iS\left\{S^2\left[(1+k^2) + k^2\lambda^2\left(2+\frac{3-\nu}{2}k^2\right)\right] + \lambda^2\left[2+\nu+2k^2\lambda^2\right]\right\}$$

$$\overline{A}_{3n}(S) = \lambda\left\{k^2 S^4 + S^2\left[1+3\left(\frac{1-\nu}{2}\right)k^2\lambda^2\right] - (1+3k^2)\left[\nu+k^2\lambda^2\right]\cdot\lambda^2\right\}$$

$$\bar{\bar{B}}_n(S) = S^8(1+k^2) + S^6\left\{\lambda^2\left[4+\frac{7-3\nu}{2}k^2+\frac{3(1-\nu)}{2}k^4\right]-2(1+k^2)\right\}$$

$$+S^4\left\{\lambda^4\left[6+3(2-\nu)k^2-\nu^2k^4\right]-\lambda^2\left[2(4-\nu)+(7-5\nu)k^2+3(1-\nu)k^4\right]+(1+k^2)\right\}$$

$$+\lambda^2S^2\left\{\lambda^4\left[4+(\frac{11-3\nu}{2})k^2+9(\frac{1-\nu}{2})k^4\right]-3\lambda^2\left[2+(2-\nu+\nu^2)k^2)\right]\right.$$

$$\left.+\left[2(2-\nu)+7(\frac{1-\nu}{2})k^2+3(\frac{1-\nu}{2})k^4\right]\right\}$$

(14B)

$$+(1+3k^2)\lambda^4\left[1+\frac{1-\nu^2}{k^2}-2\nu\lambda^2+(1-k^2)\lambda^4\right].$$

We may treat this solution as a kernel and integrate suitably to obtain the desired solution for the radial load with axial variation. For example, if the displacement w of Reference 5 is denoted momentarily by $w_5(x,\Theta,\xi)$, then the displacement $w(x,\Theta)$ due to a band of radial pressure varying linearly about x_o and within a band of length $2a\delta$ is given by

$$w(x,\Theta) = \int_{x_o-\delta}^{x_o+\delta}(\xi-x_o)\,w_5(x,\Theta,\xi)\,d\xi$$

(15)

$$= \sum_{n=1}^{\infty}\bar{\bar{F}}_{1n}(\Theta)\left\{\int_{x_o-\delta}^{x_o+\delta}(\xi-x_o)\sin(\lambda\xi)d\xi\right\}\sin(\lambda x)$$

where

$$\bar{F}_{1n}(\Theta)\sin(\lambda\xi) = F_{1n}(\Theta).$$

Since

$$\int_{x_0 - \delta}^{x_0 + \delta} (\xi - x_0) \sin(\lambda \xi) \, d\xi = \frac{2}{\lambda^2} \cos(\lambda x_0) \left\{ \sin(\lambda \delta) - \lambda \delta \cos(\lambda \delta) \right\},$$

it follows that the desired solution for a distribution of longitudinal moment acting over a series of N pads may be expressed by Equations (11) thru (14), provided $F_{mn}(\Theta)$ $m = 1, 2, 3$ are modified by being multiplied by the quantity

$$\frac{2}{\lambda^2} \cot(\lambda x_0) \left\{ \sin(\lambda \delta) - \lambda \delta \cos(\lambda \delta) \right\},$$

and provided that in $F_{mn}(\Theta)$, $p^*(S)$ is given by

$$p^*(S) = F\left\{ p(\Theta) \right\} = \frac{1}{\pi S} \left\{ p_0 \sin(S\Theta_1) \sum_{m=1}^{N} e^{-2(m-1)(\Theta_1 + \Theta_2)iS} \right\}$$

(16)

$$= \frac{1}{\pi S} \, p_0 \sin(S\Theta_1) \left\{ N \right\}, S = k \cdot N$$

$$(k-1, 2, \dots)$$

$$= 0 \qquad\qquad , S \neq k \cdot N \ .$$

NUMERICAL EXAMPLE AND DISCUSSION. By way of illustration of the preceding results, computations have been made for a cylindrical shell with the parameters

$$a = 10'', \qquad L = 35'', \qquad h = .04'',$$

$$X_o = .8, \qquad E = 10^7 \text{psi} \qquad \nu = .3$$

having three areas over which the axial load is exerted with parameters $\delta = .10$ and $\Theta_1 = .025$. (These correspond to three brackets, two inches in length and one-half inch in width, located eight inches from the top of the cylinder). Figures 4a, b, c and d present stress and moment resultants for the case of a self-equilibrating axial load, while Figures 5a, b, c and d present similar results for the case of a longitudinal moment M acting over the same areas. If such a configuration were used, for example, to transmit into the cylindrical shell a total load (force) of 1500 pounds, and if the distance from the middle surface of the shell to the application of the load were, say, one-quarter inch, then $p_1 = 500$ psi and M = 125 in-lbs. The following distribution of stresses on the inner and outer surfaces of the cylinder would result along $\Theta=0$:

TABLE I

ax	σx_{in}	σx_{out}	$\sigma \Theta_{in}$	$\sigma \Theta_{out}$
9	-21, 662	+20, 980	-18, 523	+35, 909
9-1/2	+522	-734	-8, 491	+12, 853
10	-300	-1, 500	-5, 796	+4, 946
10-1/2	-1, 482	-1, 080	-4, 025	+2, 875
12	-1, 637	-1, 233	-1, 174	1, 314

In Reference 2, Bijlaard presents extensive numerical results for localized loading of cylindrical shells by radial loads and by longitudinal moments. This provides an opportunity to compare the results of Flügge's
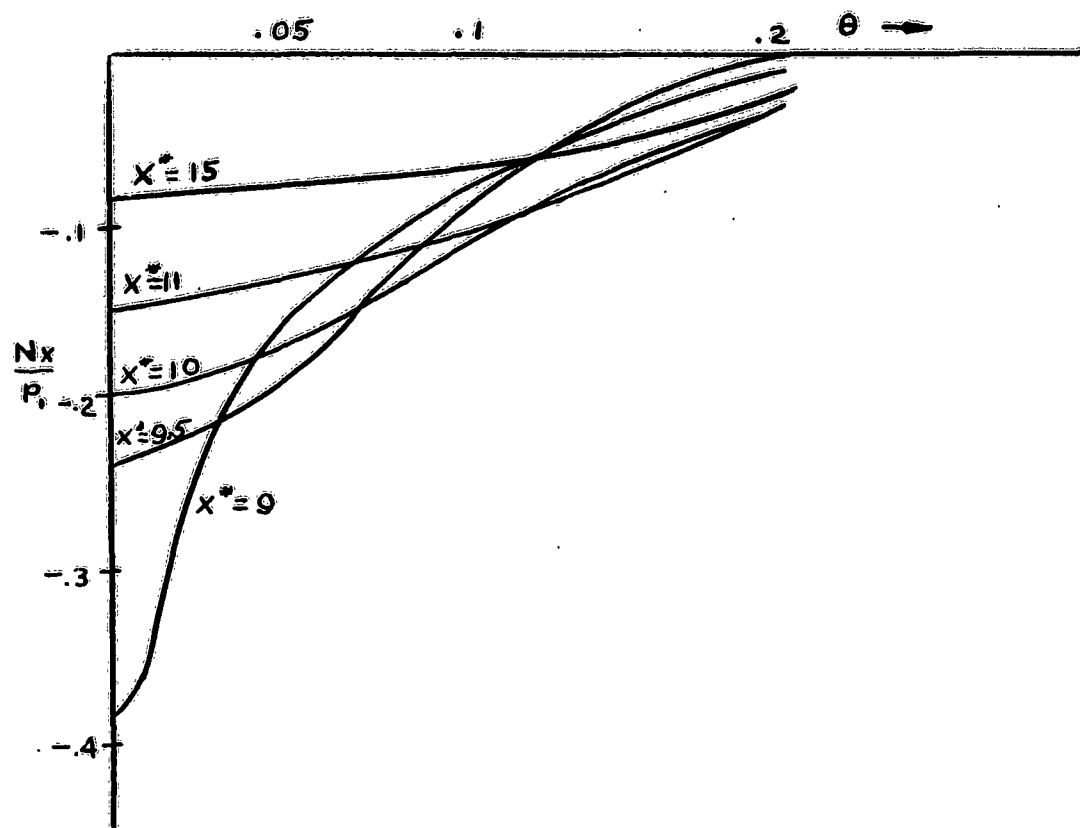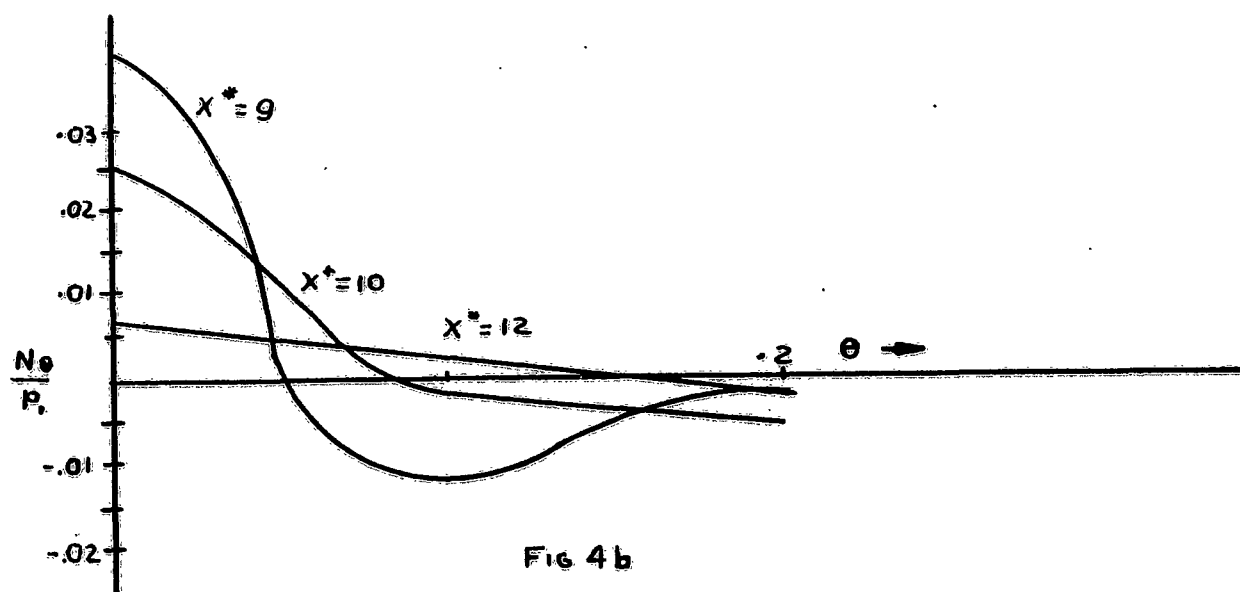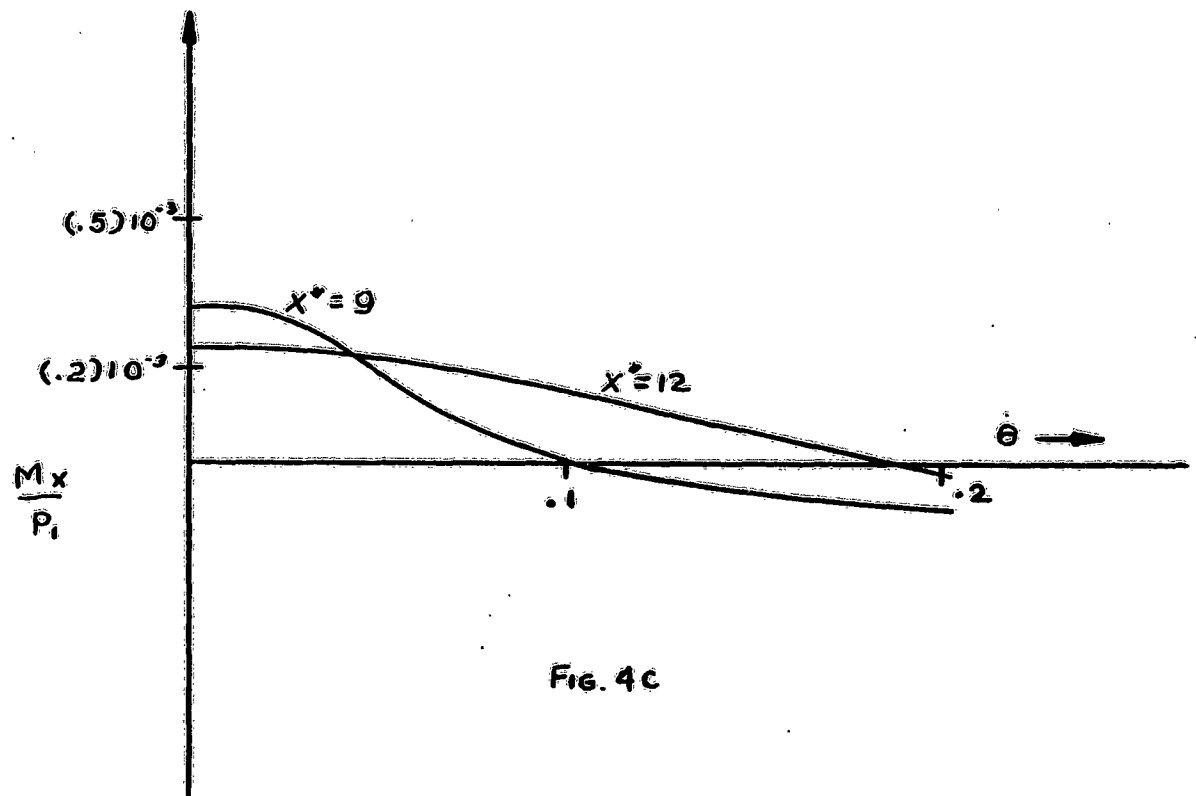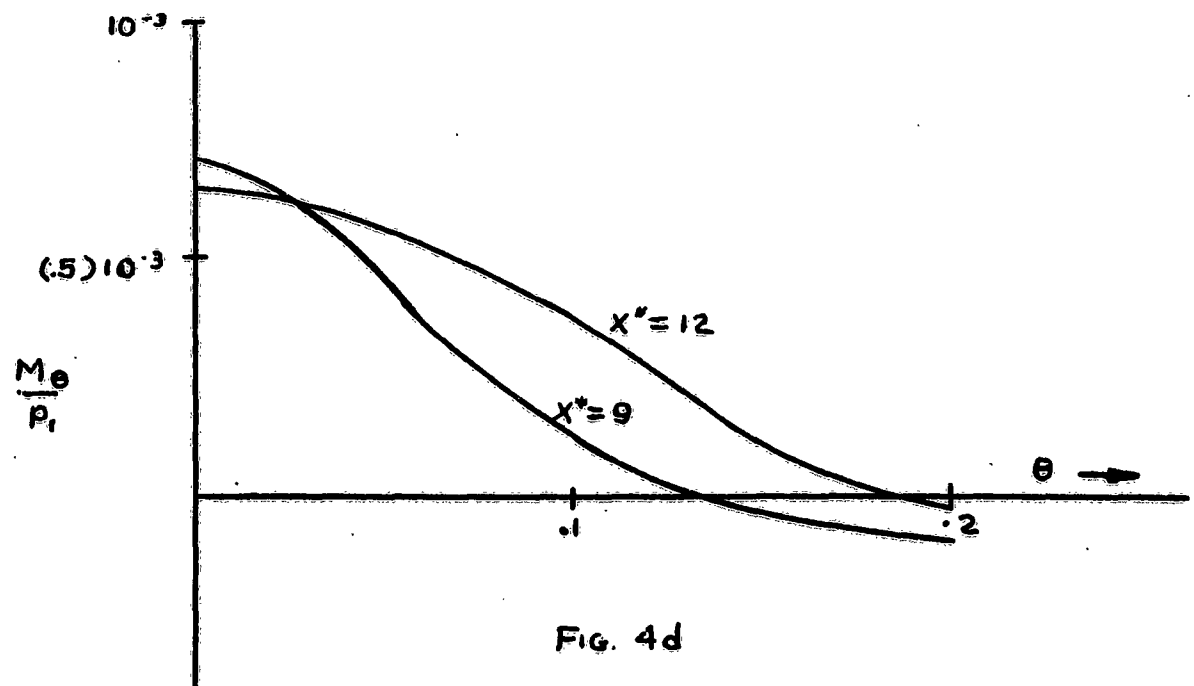
Fig. 4a

Fig 4b

Fig. 4c

Fig. 4d

Fig. 5a

Fig. 5 b

FOR $X^* = 9.5, 10$ VALUES
OF M_X ARE TOO SMALL
TO APPEAR ON THIS PLOT
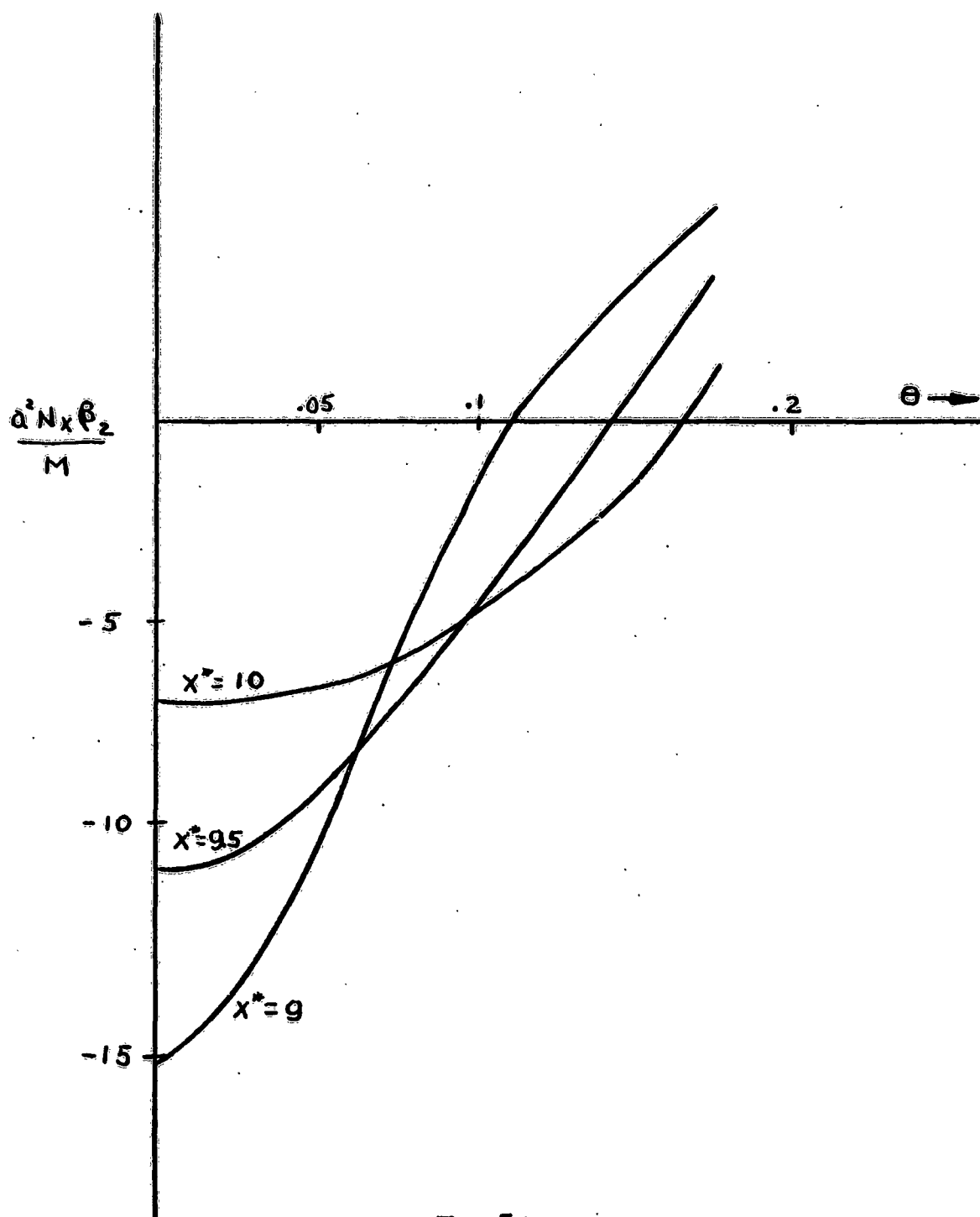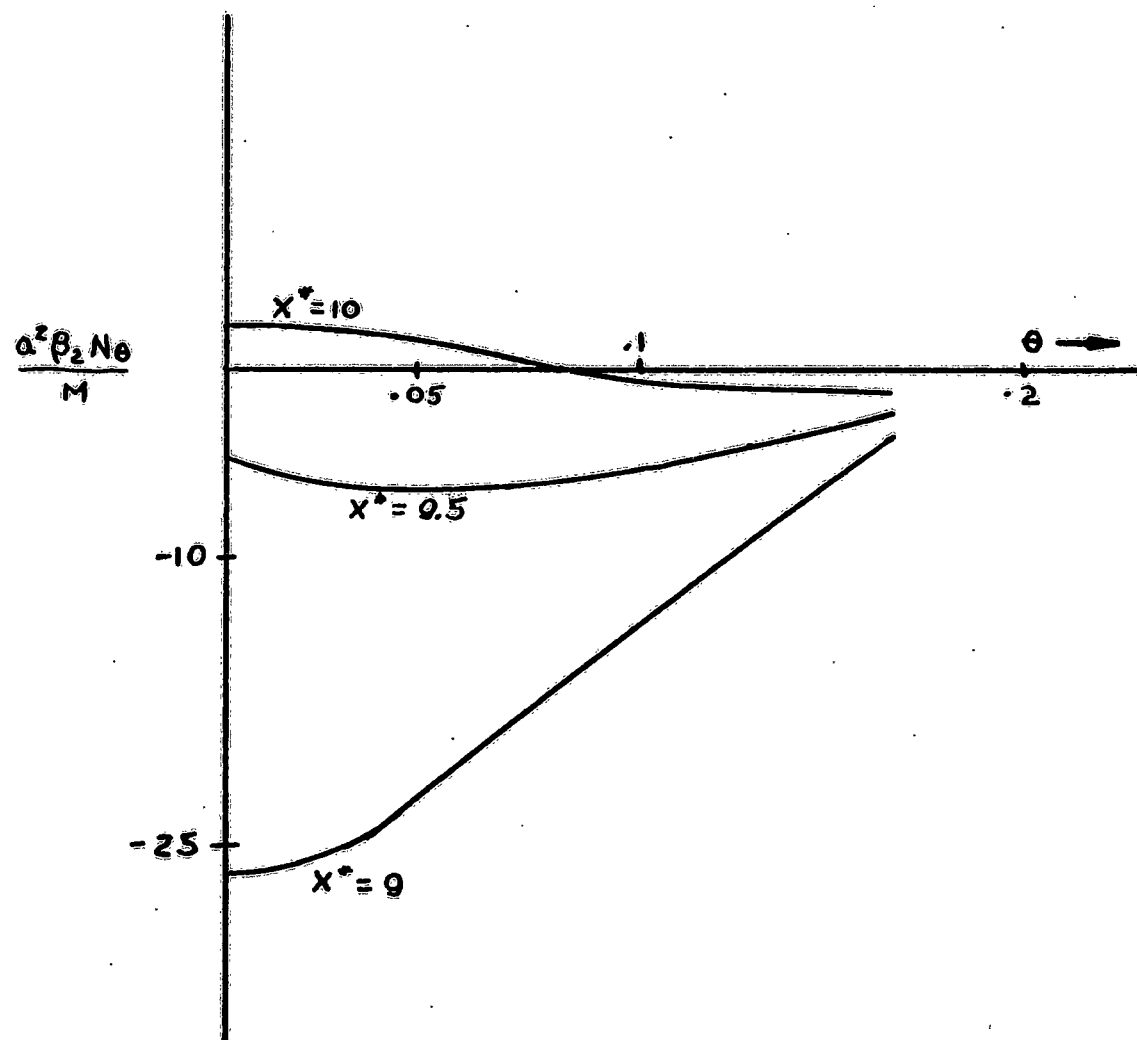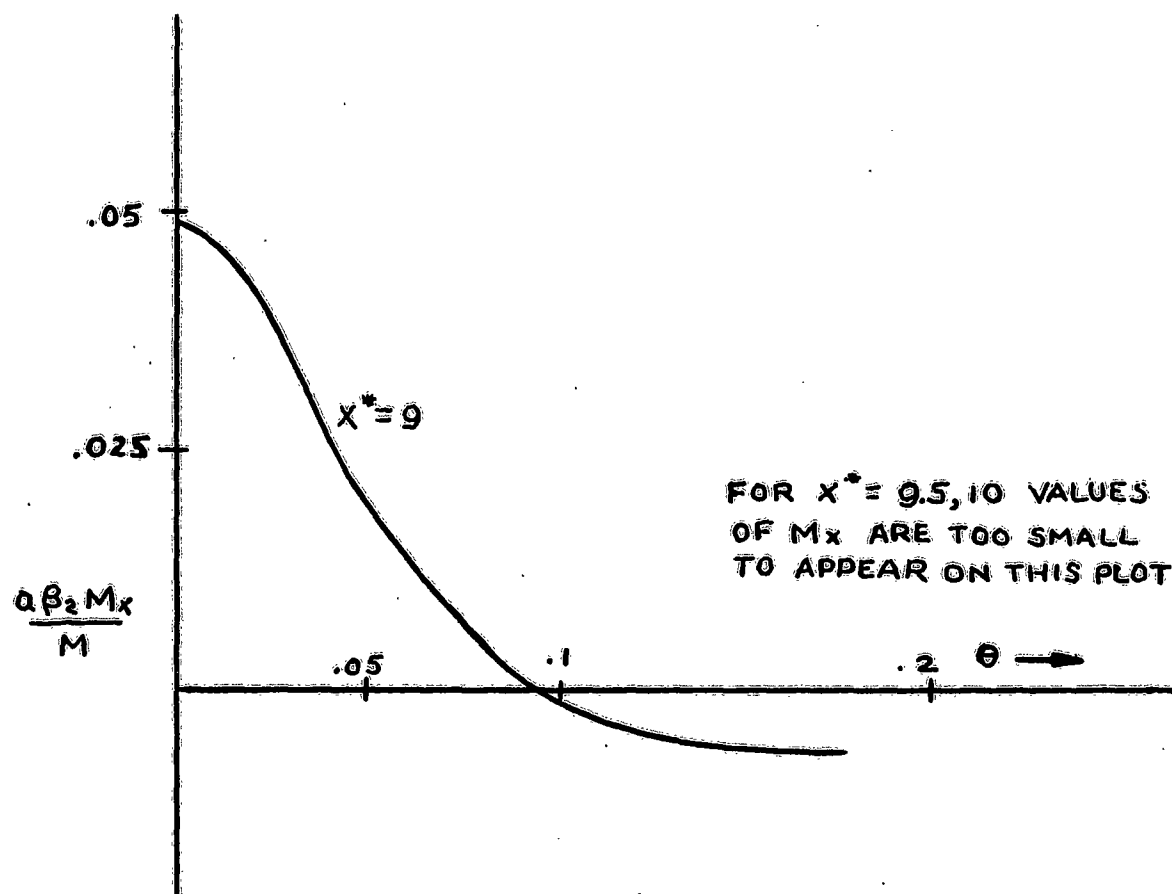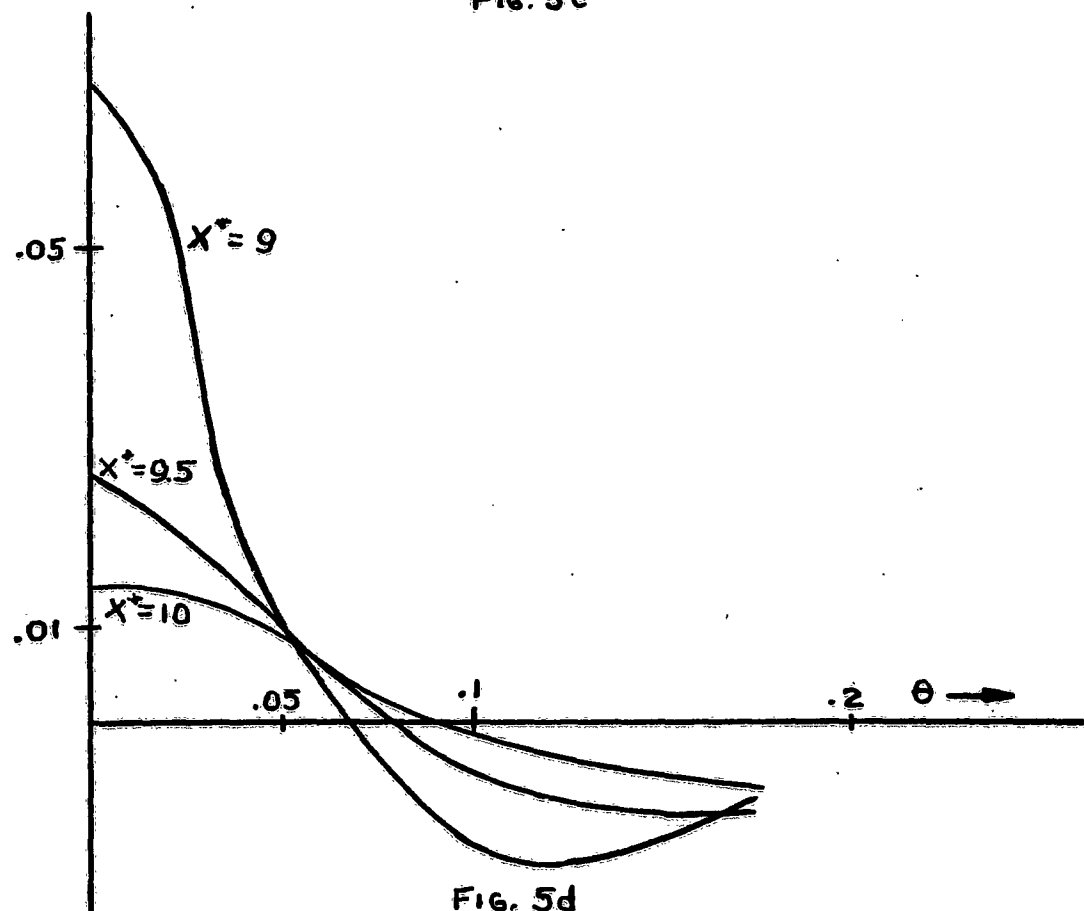
FIG. 5C

FIG. 5d

equations for distributed loads with those employed by Bijlaard for a wide range of shell parameters. Furthermore, the comparison can be made on the basis of actual stresses in the shell rather than on the basis of displacements. Tables II and III typify the results of such comparisons. (In these tables, we employ Bijlaard's notation in which $\alpha = \ell/a$, $\gamma = a/h$, $\beta_1 = \Theta_1$, $\beta_2 = \delta$, and for these computations $\beta_1 = \beta_2$). For radial loads, we observe that maximum differences occur when both β and γ are small, and that as γ increases, N_x and N_Θ tend to agree; but if $\beta << 1$ results for M_x and M_Θ by the two methods may still disagree when γ is quite large.

TABLE II

(Radial Load P)

β	γ	aN_x/P		aN_Θ/P		M_x/P		M_Θ/P	
		F.	B.	F.	B.	F.	B.	F.	B.
$\frac{1}{128}$	5	-1.0	-.9	-.666	-1.1	.346	.39	.356	.43
$\frac{1}{128}$	50	-9.10	-9.	-9.90	-10.	.225	.275	.254	.33
$\frac{1}{128}$	300	-55.2	-55	-57.2	-57	.159	.175	.195	.25
$\frac{1}{8}$	5	-.850	-.8	-.712	-.9	.114	.112	.153	.155
$\frac{1}{8}$	50	-6.42	-6.5	-3.46	-3.5	.031	.031	.071	.070
$\frac{1}{8}$	300	-25.	-25.	-5.2	-5.3	.011	.011	.032	.031

TABLE III
(Longitudinal Moment M)

β	γ	$a^2\beta N_x/M$		$a^2\beta N_\theta/M$		$a\beta M_x/M$		$a\beta M_\theta/M$	
		F.	B.	F.	B.	F.	B.	F.	B.
$\frac{1}{32}$	5	-.048	-.088	+.053	-.033	+.107	+.108	+.066	+.066
$\frac{1}{32}$	50	-.464	-.42	-1.72	-1.8	+.101	+.101	+.063	+.063
$\frac{1}{32}$	300	-7.55	-7.6	-27.5	-27.5	+.078	+.081	+.050	+.053
$\frac{1}{8}$	5	-.096	-.06	-.169	-.25	+.100	+.10	+.060	+.060
$\frac{1}{8}$	50	-1.86	-1.8	-5.63	-5.6	+.054	+.054	+.0367	+.036
$\frac{1}{8}$	300	-10.3	-10.3	-18.5	-18.5	+.0098	+.010	+.0086	+.009

TABLE III
(Longitudinal Moment M)

β	γ	$a^2\beta N_X/M$		$a^2\beta N_\theta/M$		$a\beta M_X/M$		$a\beta M_\theta/M$	
		F.	B.	F.	B.	F.	B.	F.	B.
$\frac{1}{32}$	5	-.048	-.088	+.053	-.033	+.107	+.108	+.066	+.066
$\frac{1}{32}$	50	-.464	-.42	-1.72	-1.8	+.101	+.101	+.063	+.063
$\frac{1}{32}$	300	-7.55	-7.6	-27.5	-27.5	+.078	+.081	+.050	+.053
$\frac{1}{8}$	5	-.096	-.06	-.169	-.25	+.100	+.10	+.060	+.060
$\frac{1}{8}$	50	-1.86	-1.8	-5.63	-5.6	+.054	+.054	+.0367	+.036
$\frac{1}{8}$	300	-10.3	-10.3	-18.5	-18.5	+.0098	+.010	+.0086	+.009

REFERENCES

1. BIJLAARD, P. P.   "Stresses from Local Loadings in Cylindrical
    Pressure Vessels," Trans. ASME, v. 77, 1955.

2. BIJLAARD, P. P.   "Additional Data on Stresses in Cylindrical Shells
    Under Local Loading," Welding Research Council Bulletin Series,
    No. 50, May 1959.

3. HOFF, N. J.   "On the Accuracy of Donnell's Equations," Jnl of
    Applied Mechanics, Trans. ASME, vol. 77, 1955, p. 329.

4. KEMPNER, J.   "Remarks on Donnell's Equations," Jnl of Applied
    Mechanics, Trans. ASME, vol. 77, 1955, p. 117.

5. NASH, W. A., and BRIDGLAND, T. F. JR.   "Line-Loadings on
    Finite Length Cylindrical Shells - Solution by the Finite Fourier
    Transform," Quarterly Journal of Mechanics and Applied Mathe-
    matics, vol. XIV, Part 2, 1961.

6. FLUGGE, W.   "Stresses in Shells," Springer-Verlag, Berlin/Göttingen/
    Heildelberg, 1960.

7. SNEDDON, I.   "Fourier Transforms," McGraw-Hill, New York, 1951.

RECTANGULAR TENSILE SHEET WITH EDGE CRACKS

Oscar L. Bowie
Materials Engineering Laboratory, U. S. Army
Materials Research Agency, Watertown, Massachusetts 02172

ABSTRACT.   Complex variable methods are applied to the plane elastic problem of a rectangular tensile sheet with edge cracks. A mapping function is used which is sufficiently flexible to account for both variations of crack length and length/width ratios of the sheet on the stresses local to the crack tips. Numerical results are carried out and compared with the approximation derived from Westergaard's solution.

CONTENTS

I. INTRODUCTION

A model frequently used in fracture mechanics is the rectangular tensile sheet with edge cracks (Figure 1). The plane elastic solution has not been solved previously although an approximation is used to estimate the elastic stresses local to the crack tip. This approximation depends on a modification of Westergaard's[1] solution for a series of equally spaced colinear cracks in an infinite sheet. Load-free conditions on the lateral edges of a strip defined by the perpendicular bisectors of two consecutive cracks are partially satisfied by Westergaard's solution and it is argued physically that the effect of the error is negligible in the vicinity of the crack tip. R. J. Tait[2] has considered the infinite strip of finite width with edge cracks; however, the mixed boundary conditions he considers on the lateral edges lead back to the Westergaard solution.

Due to controversy as to the accuracy of the modified Westergaard solution for this and related problems, e.g., Bluhm,[3] a procedure for an accurate stress analysis of this problem class would seem appropriate. In the present report, an analysis is considered which, in addition to eliminating the error in edge loading, accounts for the effect of the length/width ratio for finite rectangular sheet. Furthermore, other important problems in this area can be handled by this technique.

Although the basic plan of analysis is similar to that used by the author[4] for a plate with radial cracks originating at the boundary of an internal circular hole, several modifications were required. In Section IV an argument is made as to the character of the stresses at the crack roots in terms of the stress function and the exact mapping function. The result is also applicable to polynomial approximations of the geometry. In the numerical computation of results, it was necessary to overcome a convergence difficulty encountered in the truncation of the exact system. A satisfactory alternate plan of truncation was found whereby the stresses at the crack tips could be calculated with reliable accuracy.

II. INITIAL FORMULATION

The rectangular sheet under tension weakened by edge cracks (Figure 1) will be considered as lying in the complex Z-plane ($Z = x + iy$) with the center of the sheet described by $Z = 0$. The complex variable methods of Muskhelishvili[5] depend on the representation of the well-known Airy stress function, $U(x,y)$ in terms of two analytic functions of the complex variable, Z, namely, $\varphi(Z)$ and $\psi(Z)$, where

$$U(x,y) = \text{Re} \left[\bar{Z} \, \varphi(Z) + \int^{Z} \psi(Z)dZ \right]. \tag{1}$$

Figure I. Z - PLANE.

To facilitate the consideration of boundary conditions, an auxiliary complex plane, the ζ-plane, is introduced and a functional relationship,

$$Z = \omega(\zeta), \qquad \ldots (2)$$

is found such that the unit circle, $\zeta = \sigma = e^{i\theta}$, and its interior in the ζ-plane map into the boundary and interior, respectively, of the region in Figure 1. The mapping function, $\omega(\zeta)$, (described in Section III) is analytic interior to the unit circle but contains singularities necessary to the description of corner points on the unit circle itself.

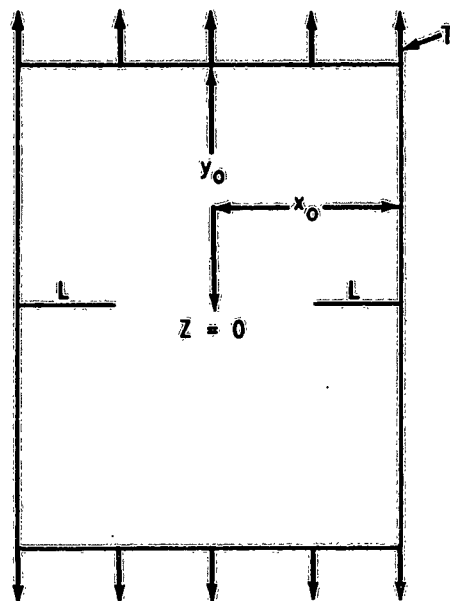The stress functions $\varphi(Z)$ and $\psi(Z)$ can be considered as functions of ζ. New notation can be minimized by designating $\varphi(Z) \equiv \varphi[\omega(\zeta)]$ as $\varphi(\zeta)$, etc., which leads to such definitions as $\varphi'(Z) = \varphi'(\zeta)/\omega'(\zeta)$, etc. (Primes are used to denote differentiation.) Thus, the stresses and displacements in rectangular coordinates can be written as

$$\sigma_y + \sigma_x = 4 \text{ Re } [\varphi'(\zeta)/\omega'(\zeta)], \qquad \ldots (3)$$

$$\sigma_y - \sigma_x + 2i\ \tau_{xy} = 2\{\overline{\omega(\zeta)}\ [\varphi'(\zeta)/\omega'(\zeta)]' + \psi'(\zeta)\}/\omega'(\zeta), \quad \ldots (4)$$

$$2\mu\ (u+iv) = \eta\varphi(\zeta) - \omega(\zeta)\ \overline{\varphi'(\zeta)/\omega'(\zeta)} - \overline{\psi(\zeta)}, \qquad \ldots (5)$$

where μ and η are constants depending on the material and bars denote complex conjugates.

The loading conditions in Figure 1 can be expressed conveniently in terms of the force resultant. Along an arc of the material with element ds, we denote the horizontal and vertical forces by Xds and Yds, respectively. If the arc is taken as the boundary of Figure 1, then s can be considered as a function of σ. Then,

$$\varphi(\sigma) + \omega(\sigma)\ \overline{\varphi'(\sigma)/\omega'(\sigma)} + \overline{\psi(\sigma)} = i \int^{s} (X+iY)ds = g(\sigma). \quad \ldots (6)$$

The solution requires the determination of the functions $\varphi(\zeta)$ and $\psi(\zeta)$ which are analytic for $|\zeta|<1$ and satisfy the loading condition (6). The

problem will be considered both in terms of power series expansions of the exact solution and an alternative polynomial approximation of the exact geometry.

III. THE MAPPING FUNCTION

By application of the Schwartz-Christoffel transformation, it was found that the required mapping function corresponds to an appropriate branch of

$$Z = \omega(\zeta) = -i \int_0^{\zeta} \left[(\zeta^2+1)/(1-2\zeta^2\cos 2\alpha+\zeta^4)^{1/2}(1-2\zeta^2\cos 2\beta+\zeta^4)^{1/2} \right] d\zeta \quad \ldots (7)$$

In (7), $0 < \alpha < \beta < \pi/2$, and these two parameters can be varied to obtain desired ratios of y_0/x_0 and L/x_0. The choice of branch was made by defining

$$\omega(1) = iy_0. \qquad \ldots (8)$$

Thus, $\omega(e^{i\alpha}) = -x_0 + iy_0$, $\omega(e^{i\beta}) = -x_0$, $\omega(i) = -x_0 + L$, etc.

By considering the mapping function on the unit circle, it can be shown by well-known substitutions used in elliptic integrals that

$$x_0 = \frac{1}{2\sin\beta} \int_0^{\frac{\pi}{2}} \frac{d\varphi}{(1-\lambda^2\sin^2\varphi)^{1/2}} = \frac{1}{2\sin\beta} K(\lambda), \qquad \ldots (9)$$

$$y_0 = \frac{1}{2\sin\beta} \int_1^{1/\lambda} \frac{ds}{(s^2-1)^{1/2}(1-\lambda^2 s^2)^{1/2}} = \frac{1}{2\sin\beta} K(\sqrt{1-\lambda^2}), \qquad \ldots (10)$$

$$L = x_0 - \frac{1}{2\sin\beta} \int_0^{\beta} \frac{d\varphi}{(1-\lambda^2\sin^2\varphi)^{1/2}} = x_0 - \frac{1}{2\sin\beta} F(\lambda,\beta), \qquad \ldots (11)$$

where

$$\lambda = (\sin\alpha)/\sin\beta. \qquad \ldots (12)$$

These integrals are standard elliptic integrals of the first kind and are well tabulated. A fixed y_0/x_0 ratio determines λ from (9) and (10). A fixed L/x_0 ratio then determines β and hence α. This computation was carried out by interpolation from existing tables. (An asymptotic relation between α and β for large y_0/x_0 ratios was derived in a study by E. W. Ross, Jr., and A. Kaplan.)

The mapping function has eight branch points falling on the unit circle (Figure 2). In addition to these corner-describing singularities, the crack tips are described by the roots of $\omega'(\sigma) = 0$ which occur at $\zeta = \pm 1$.
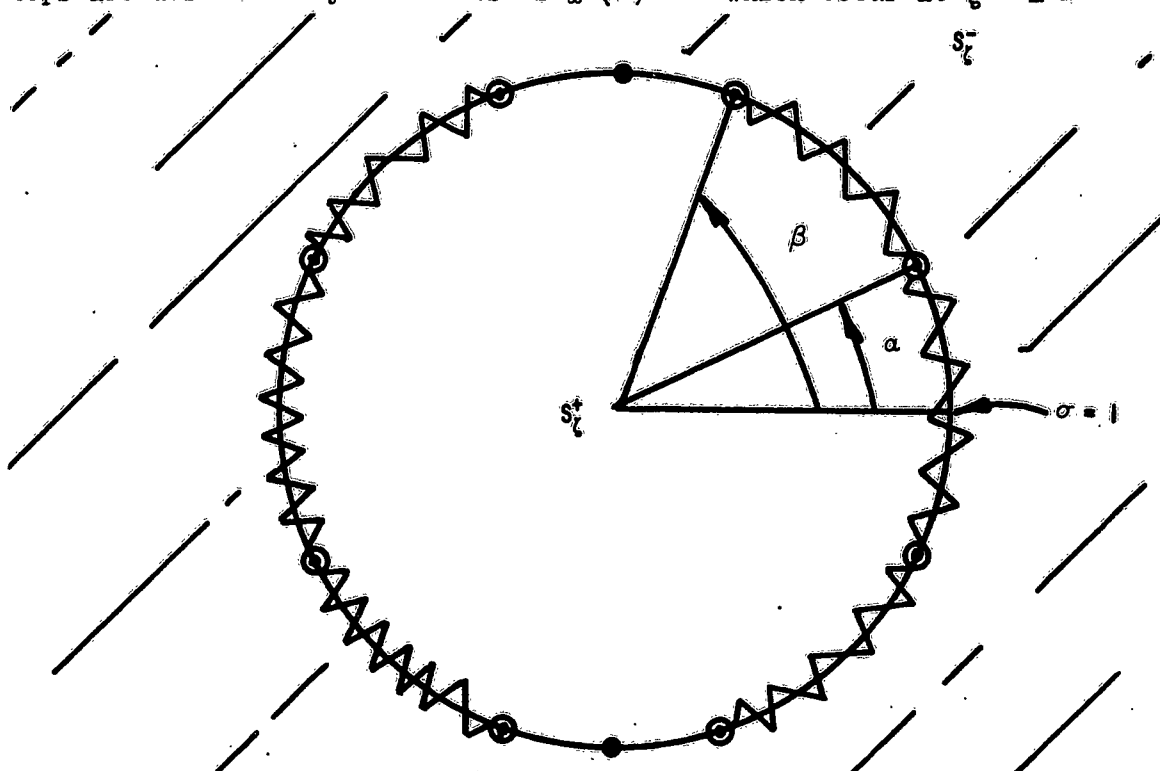

Figure 2. ζ - PLANE.

It is convenient to consider the mapping function as defined on an appropriate Riemann surface. The branch cuts can be chosen as the two intervals of the unit circle shown as the wavy arcs in Figure 2. The top sheet of the surface will be defined as including S_ζ^+ which maps into the physical region occupied by the sheet. Clearly the mapping function can be continued analytically across the uncut intervals of the unit circle into S_ζ^- in the top sheet. By our choice of branch cuts, the uncut intervals on the unit circle correspond to the crack intervals situated along the real axis in the Z-plane. Thus, by Schwartz's reflection principle, the analytic continuation of $\omega(\zeta)$ into S_ζ^- is defined as

$$\omega(\zeta) = \overline{\omega(1/\bar{\zeta})} \quad \zeta \epsilon S_\zeta^-. \qquad \qquad \ldots (13)$$

The mapping function can be expressed in series form as

$$Z = \omega(\zeta) = -i \sum_{n=1}^{\infty} A_n \zeta^{2n-1}, \quad \zeta \epsilon S_\zeta^+ \qquad \ldots (14)$$

where the mapping coefficients A_n are real. Although the A_n's can be related to integrals involving the elliptic functions, it is simpler computationally to calculate them from easily derived recursive formulae.[6]

IV. STRESSES IN THE NEIGHBORHOOD OF THE CRACK TIPS

The character of the stresses in the neighborhood of the crack tips will now be examined in terms of the present formulation. From other investigations of this problem type, it can be expected that σ_{max} in the vicinity of the crack tip will vary as $r^{-1/2}$ where r is the radial distance measured from the crack tip. The determination of the factor of proportionality and its variation with the geometric parameters is the primary concern of this investigation.

An argument particularly useful for analyzing the situation for the exact mapping function will now be carried out utilizing the elegant extension concept of Muskhelishvili. In brief, the function $\omega(\zeta)$ is extended into S_ζ^- by defining

$$\varphi(\zeta) = -\omega(\zeta)\,\bar{\varphi}'\,(1/\zeta)/\,\bar{\omega}'(1/\zeta) - \bar{\psi}(1/\zeta), \quad \zeta \epsilon S_\zeta^-, \qquad \ldots (15)$$

where the bar notation above is defined by

$$\bar{f}(1/\zeta) = \overline{f(1/\bar{\zeta})}. \qquad \ldots (16)$$

In (15), $\omega(\zeta)$ for $\zeta \epsilon S_\zeta^-$ will be considered defined by (14). The form of extension above for the case of polynomial mapping functions of the circular regions is due to Kartzivadze.[7]

The extended definition of $\varphi(\zeta)$ is clearly analytic for all finite points in S_ζ^-. Its structure at infinity is determined by the structures of the defining functions. The function $\psi(\zeta)$ can now be expressed as

$$\psi(\zeta) = -\bar{\varphi}(1/\zeta) - \bar{\omega}(1/\zeta)\,\varphi'(\zeta)/\omega'(\zeta), \quad \zeta \epsilon S_\zeta^+. \qquad \ldots (17)$$

Thus, the boundary condition (6) can be replaced by

$$\varphi^+(\sigma) - \varphi^-(\sigma) + [\omega^+(\sigma) - \omega^-(\sigma)]\overline{\varphi'^+(\sigma)}/\overline{\omega'^+(\sigma)} = g(\sigma), \qquad \ldots (18)$$

where the notations $f^+(\sigma)$ and $f^-(\sigma)$ are defined as the values of $f(\zeta)$ as $\zeta \rightarrow \sigma$ through S_ζ^+ and S_ζ^-, respectively.

It will now be assumed that $\varphi'^+(\sigma)$ is bounded on intervals of the unit circle corresponding to unloaded portions of the original geometry. (The validity of this assumption can be verified by an a postiori argument.) It then follows that on the uncut intervals of the unit circle in the present problem, Equation 18 reduces to

$$\varphi^+(\sigma) - \varphi^-(\sigma) = g(\sigma). \qquad \ldots (19)$$

In the present problem $g(\sigma)$ can be considered as vanishing on one of the intervals of the unit circle corresponding to a crack description by a suitable choice of $s = 0$. On this interval, therefore $\varphi^+ = \varphi^-$. Thus $\varphi(\zeta)$ can be considered as analytically continued across this interval by (15). In particular, $\varphi(\zeta)$ is analytic on this interval of the unit circle. The analyticity of $\varphi(\zeta)$ and $\omega(\zeta)$ on this interval in turn establish the analyticity of $\omega'(\zeta)$ $\psi(\zeta)$ at the same points from (17).

The argument above is purposely restrictive for the sake of brevity. The conclusion is valid when $g(\sigma)$ is constant on a crack interval. This can be verified by altering the definition of (15) and utilizing the independence of the stress state to constants added to $\varphi(\zeta)$ and $\psi(\zeta)$. Generalization of the argument to the case of applied loads acting on the cracks is straightforward. For most practical load systems,[5] the structure of $\varphi(\zeta)$ on the crack interval will differ from an analytic function by a Cauchy integral with a density function $g(\sigma)$.

Having established the properties of $\varphi(\zeta)$ and $\psi(\zeta)$ on the intervals of the unit circle containing the crack tip, it is now a straightforward matter to determine the structure of the stresses in the vicinity of the crack tip. Let σ_0 denote a point on the unit circle corresponding to a crack tip in the physical plane. Then the expansions

$$Z = \omega(\sigma_0) + \omega''(\sigma_0)(\zeta-\sigma_0)^2/2! + \cdots, \qquad \ldots (20)$$

$$\varphi(\zeta) = \varphi(\zeta_0) + \varphi'(\sigma_0)(\zeta-\sigma_0) + \cdots, \qquad \ldots (21)$$

are valid in a complete neighborhood of $\zeta = \sigma_0$. If

$$Z - \omega(\sigma_0) = re^{it}, \qquad \ldots (22)$$

then by reversion of series,

$$\zeta - \sigma_0 \approx \sqrt{2r}\, e^{it/2}/\sqrt{\omega''(\sigma_0)}. \qquad \qquad \ldots (23)$$

From (3), (20), (21), and (23), in the vicinity of the crack tip,

$$\sigma_y + \sigma_x \approx 4\,\text{Re}\,\{\varphi'(\sigma_0)e^{-it/2}/\sqrt{2r\omega''(\sigma_0)}\}. \qquad \ldots (24)$$

Similarly, from (4), (17), (20), (21), and (23),

$$\sigma_y - \sigma_x + 2i\,\tau_{xy} \approx \frac{2e^{-it/2}}{\sqrt{2r\omega''(\sigma_0)}}\left| \frac{\overline{\varphi'(\sigma_0)}}{\sigma_0^2} - \frac{\varphi'(\sigma_0)}{2\sigma_0^4} - \frac{\varphi'(\sigma_0)}{2}e^{-2it} \right|. \qquad \ldots (25)$$

In the conventional description, the stress concentration factor K is defined by

$$\sigma_{max} = \sigma_y \approx \frac{KT}{\sqrt{2r}}\,(\cos t/2)\,[1+(\sin t/2)(\sin 3t/2)]. \qquad \ldots (26)$$

In the present problem, choosing the crack tip corresponding to $\sigma_0 = 1$ leads to

$$K = 2\varphi'(1)/\sqrt{\omega''(1)}. \qquad \qquad \ldots (27).$$

The final result is obviously valid for polynomial approximations of the exact mapping function as well since no contradictions of the local behavior are introduced.

V. DETERMINATION OF $\varphi'(1)$ BY POWER SERIES

In this section, we consider a power series development of the solution for the determination of $\varphi'(1)$. The following representations are assumed:

$$\varphi(\zeta) = T\omega(\zeta)/4 + iT\sum_{n=1}^{\infty}\alpha_n\,\zeta^{2n-1}, \quad \zeta \in S_\zeta^+, \qquad \ldots (28)$$

$$\psi(\zeta) = T\omega(\zeta)/2 + iAT\zeta/(\zeta^2+1) + iT\sum_{n=1}^{\infty}\beta_n\,\zeta^{2n-1}, \quad \zeta \in S_\zeta^+. \qquad \ldots (29)$$

The first term of each of these representations corresponds to the elementary solution were there no cracks in the geometry. The coefficients A, α_n and β_n are real from symmetry considerations. The simple poles at $\zeta = \pm 1$ in $\psi(\zeta)$ are consistent with the structure indicated in (17), in fact,

$$A = 2i \; \omega(i)\varphi'(i)/T\omega''(i). \qquad \ldots (30)$$

It will be sufficient for the present purpose to determine the α_n's since

$$\varphi'(i) = -iT \sum_{n=1}^{\infty} (2n-1)\alpha_n(-1)^n. \qquad \ldots (31)$$

It is convenient to express the boundary condition (6) as

$$\overline{\omega'(\sigma)} \; \varphi(\sigma) + \omega(\sigma)\overline{\varphi'(\sigma)} + \overline{\omega'(\sigma)} \; \overline{\psi(\sigma)} = \overline{\omega'(\sigma)} \; g(\sigma). \qquad \ldots (32)$$

We write the Fourier expansion

$$g(\sigma) - \frac{T}{2}\left[\omega(\sigma) + \overline{\omega(\sigma)}\right] = i \; T \sum_{n=-\infty}^{\infty} C_{2n-1} \; \sigma^{2n-1} \qquad \ldots (33)$$

where

$$C_{2k-1} = \frac{2}{(2k-1)\pi} \int_{\beta}^{\frac{\pi}{2}} x(\theta) \cos (2k-1)\theta d\theta, \; k = 1,2,\cdots \qquad \ldots (34)$$

$$C_{-2k-1} = -C_{2k+1}, \; k = 0, 1, 2, \cdots.$$

Inserting the appropriate series expansions into (32) and equating properly coefficients of equal powers of σ, from the positive powers of σ one finds

$$\sum_{n=1}^{\infty} (2n-1)\left[\alpha_n \; A_{n+p-1} + A_n \; \alpha_{n+p-1}\right] = +d_p \qquad \ldots (35)$$

$$p = 1, 2, \cdots$$

$$d_p = \sum_{n=1}^{\infty} (2n-1)A_n \; C_{2(p+n)-3}, \; p = 1, 2, \cdots. \qquad \ldots (36)$$

The solution of the infinite linear system (35) determines the coefficients α_n.

VI. TRUNCATION OF THE SYSTEM

The initial numerical procedure carried out followed the conventional study of the numerical convergence of $\varphi'(i)$ for sequences of truncations of the system (35). For the parameter range, large y_O/x_O in conjunction with small values of L/x_O, this procedure proved fairly effective. Beyond this range, however, the rate of convergence presented serious practical difficulties in the determination of accurate values of $\varphi'(i)$. A plausible explanation of the difficulty can be found by a study of the convergence of the series form of the mapping function. Examination of $\omega_T'(i)$ and $\omega_T''(i)$, where $\omega_T(\zeta)$ denotes the truncated mapping series, indicates that a substantial error in these quantities can occur by indiscriminate truncation. On the other hand, from physical considerations, the solution should be somewhat sensitive to the representation of the geometry in the vicinity of the crack root.

An effective alternative truncation plan was found by considering selected truncations of the series for the mapping function. In particular,

$$\omega_T(\zeta) = -i \sum_{n=1}^{M+2} \epsilon_n \zeta^{2n-1}, \qquad \ldots (37)$$

where $\epsilon_n = A_n$, $n = 1, 2, \cdots, M$; $\epsilon_{M+1} = -R$; $\epsilon_{M+2} = -S$;

$$2(2M+1)R = S_M - 2(M+1)T_M - (-1)^M Q, \qquad \ldots (38)$$

$$2(2M+3)S = S_M - 2MT_M - (-1)^M Q,$$

$$T_M = (-1)^M \sum_{n=1}^{M} (2n-1)A_n(-1)^n, \quad S_M = (-1)^M \sum_{n=1}^{M} (2n-1)(2n-2)A_n(-1)^n,$$

and

$$Q = \omega''(i) = -1/2 \cos \alpha \cos \beta. \qquad \ldots (39)$$

With this definition of $\omega_T(\zeta)$, satisfaction of $\omega_T'(i) = 0$ and $\omega_T''(i) = Q$ is assured. The choice of M is made from an examination of the partial sums of the exact mapping function and selecting those values of M for which $\omega'(i) \approx 0$ and $\omega''(i) \approx Q$ simultaneously. Thus, corrections of the

geometry in the vicinity of the crack tips can be made with little disturbance of the over-all configuration.

Modification of the previous setup is minor. The major change involves the assumed form of $\varphi(\zeta)$. In particular, we assume

$$\varphi(\zeta) = T \, \omega_T(\zeta)/4 + i \, T \sum_{n=1}^{\infty} C_{2n-1} \, \zeta^{2n-1} + i \, T \sum_{n=1}^{M+2} \alpha_n' \, \zeta^{2n-1}. \quad . \quad .(40)$$

The coefficients C_{2K-1} are calculated from (34) with $\dot{x}(\theta)$ now computed from $Z = \omega_T(\zeta)$. The system for the determination of the α_n' can be written as

$$\sum_{n=1}^{M+3-p} (2n-1) \left[\epsilon_n \alpha_{n+p-1}' + \alpha_n' \, \epsilon_{n+p-1} + C_{2n-1} \, \epsilon_{n+p-1} \right] = 0,$$

$$p = 1, 2, \cdots, M+2. \quad . \quad .(41)$$

Calculation of $\varphi'(i)$ requires the evaluation of

$$\varphi'(i) = -iT \left[\sum_{n=1}^{\infty} (-1)^n (2n-1)C_{2n-1} + \sum_{n=1}^{M+2} (-1)^n (2n-1)\alpha_n' \right]$$

$$= -iT[\Sigma_1 + \Sigma_2]. \quad . \quad .(42)$$

Evaluation of Σ_1 can be made directly from the relation

$$\Sigma_1 = -\frac{1}{\pi} \int_{\beta}^{\pi/2} \dot{x}(\theta) \, d\theta/\cos\theta. \quad . \quad .(43)$$

Evaluation of Σ_2 requires the solution of the system of equations (41).

VII. NUMERICAL RESULTS

The analysis was carried out numerically for the two cases $y_0/x_0 = 1.00$ and $y_0/x_0 = 3.00$. The truncation plan of Section VI proved to be very effective for $y_0/x_0 = 1.00$. Both the conventional truncation plan for the exact solution and the alternative plan of Section 6 were used in the study of $y_0/x_0 = 3.00$.

The numerical results for $y_0/x_0 = 3.00$ are contained in Table I. The values of α and β have been rounded to four decimal places for convenience of presentation. The term Σ_1 which is the dominant contribution

302

TABLE I

EVALUATION OF K FOR $y_0/x_0 = 1.00$

α	β	x_0	L	L/x_0	Σ_1	Σ_2	$i\varphi'(i)$	K	K_A	K/K_A
.7703	1.3963	0.9413	0.1246	.1324	.346	.055	.401	0.401	0.356	1.13
.7519	1.3090	0.9598	0.1896	.1975	.348	.057	.405	0.498	0.442	1.13
.7268	1.2217	0.9865	0.2577	.2612	.353	.063	.416	0.595	0.522	1.14
.6956	1.1345	1.0229	0.3308	.3234	.359	.069	.428	0.690	0.602	1.15
.6591	1.0472	1.0705	0.4109	.3838	.372	.074	.446	0.793	0.685	1.16
.6178	0.9599	1.1317	0.5007	.4424	.387	.076	.463	0.895	0.775	1.16
.5236	0.7854	1.3110	0.7269	.5544	.434	.070	.504	1.120	0.995	1.13
.4718	0.6981	1.4422	0.8769	.6080	.470	.063	.533	1.250	1.140	1.10
.3614	0.5236	1.8541	1.3185	.7111	.575	.050	.625	1.590	1.560	1.02
.3035	0.4363	2.1936	1.6691	.7609	.683	.041	.724	1.900	1.880	1.01

to $\varphi'(i)$ can be considered as accurately computed to $\pm$ .001. Evaluation of Σ_2 depended on the solution of the system (41). In general, three values of M were selected for each set of the parameters to study the convergence. For the most part it was possible to select $0 < M_1 < 50$, $50 < M_2 < 100$, $100 < M_3 < 150$. A study of the convergence of Σ_2 with respect to M leads to the assertion that $i\varphi'(i)$ is numerically correct to within one percent.

The numerical results for $y_0/x_0 = 3.00$ are contained in Table II.

TABLE II

EVALUATION OF K FOR $y_0/x_0 = 3.00$

α	β	x_0	L	L/x_0	Σ_1	Σ_2	$i\varphi'(i)$	K	K_A	K/K_A
.0354	1.3963	0.7978	0.0887	.1112	--	--	.283	0.334	0.299	1.12
.0347	1.3090	0.8134	0.1356	.1667	--	--	.287	0.413	0.373	1.11
.0337	1.2217	0.8361	0.1858	.2222	--	--	.293	0.485	0.440	1.10
.0311	1.0472	0.9072	0.3024	.3333	--	--	.311	0.622	0.577	1.08
.0294	0.9599	0.9591	0.3730	.3889	.297	.027	.324	0.694	0.654	1.06
.0254	0.7854	1.1111	0.5556	.5001	.342	.019	.361	0.858	0.841	1.02
.0152	0.4363	1.8590	1.3441	.7230	.575	.015*	.590	1.590	1.590	1.00

*Obtained by extrapolation.

For the first four sets of parameters, the exact system outlined in Section V was considered. Systematic truncation of (35) was successfully carried out for the shorter crack lengths to yield reliably accurate values of $\varphi'(i)$. As the crack length increased this plan became uneconomical and was abandoned in favor of the alternative truncation scheme. It was necessary to find Σ_2 by extrapolation for the largest crack length shown in Table II due to the limitations of the digital computer used in solving the systems. Again, $i\varphi'(i)$ in Table II can be considered accurate to one percent.

The author is indebted to Mr. Donald Neal of the Army Materials Research Agency for programming the analysis for a digital computer.

A matter of considerable interest is the comparison of the calculated results with the approximate stress concentration factor K_A derived from the Westergaard solution. This factor, e.g., Irwin,[8] can be written as

$$\frac{K_A}{T} = \left[\frac{2x_0}{\pi} \tan \frac{\pi L}{2x_0}\right]^{1/2} . \qquad \ldots (44)$$

The appropriate K_A's are listed in Tables I and II along with the ratios K/K_A.

For deep cracks the approximation K_A is clearly very good. For short cracks K_A differs from the exact solution by approximately 13 percent. This result is consistent with work by Bueckner,[9] who showed that for an edge crack in an elastic half plane $K \to 1.13 \sqrt{L}$. As $L \to 0$ in (44), $K_A \to \sqrt{L}$. For small crack depths therefore the 13 percent error in K_A is consistent to both analyses. The effect of length of the strip can be seen for intermediate crack depths by comparing Tables I and II. It is evident from this comparison that the ratio $y_0/x_0 = 3.00$ is effectively infinite as far as effects on K are concerned.

VIII. SUMMARY

It has been shown that the complex variable approach using conformal mapping provides an effective numerical procedure for determining the stress concentration in edge cracks in rectangular sheet. Convergence difficulties encountered with increasing crack depth can be minimized by truncation of the series form of the mapping function in a manner preserving key properties of the geometry local to the crack tip.

For edge cracks in a rectangular tensile sheet the numerical results of this report indicate that the approximate stress concentration factor derived from Westergaard's solution is in error by 13 percent for short cracks but increases fairly rapidly in accuracy with increasing crack depth.

REFERENCES

1. WESTERGAARD, H. M. Bearing Pressures and Cracks. Transactions, ASME, v. 61, 1939, p. A-49 to A-53.

2. TAIT, R. J. Crack in Strip Finite Width. See SNEDDON, I. N., Crack Problems in the Mathematical Theory of Elasticity, North Carolina State College, Raleigh, North Carolina, May 1961.

3. BLUHM, J. I. Fracture Mechanics. Presented at Automotive Engineering Congress, 1963, Paper 655C.

4. BOWIE, O. L. Analysis of an Infinite Plate Containing Radial Cracks Originating at the Boundary of an Internal Circular Hole. Journal of Mathematics and Physics, v. 25, April 1956, p. 60-71.

5. MUSKHELISHVILI, N. I. Some Basic Problems of the Mathematical Theory of Elasticity. P. Noordhoff, Ltd., Groningen, Holland, 1953.

6. BOWIE, O. L. Rectangular Tensile Bar Weakened by Surface Cracks. Part I, Stress Analysis, Watertown Arsenal Laboratories, WAL TR 811.8/5, March 1963.

7. KARTZIVADZE, I. N. The Fundamental Problems of the Theory of Elasticity for the Elastic Circle. Comptes rendus de l'Académie des Sciences de l'U. R. SS. 20, v. XII, 1943, p. 95-104.

8. IRWIN, G. R. The Crack Extension-Force for a Crack at a Free Surface Boundary. Naval Research Laboratory, Washington, D. C., NRL Report 5120, 1958.

9. BUECKNER, H. F. Some Stress Singularities and Their Computation by Means of Integral Equations. Boundary Problems in Differential Equations, University of Wisconsin Press, Madison, Wisconsin, 1960.

For the first four sets of parameters, the exact system outlined in Section V was considered. Systematic truncation of (35) was successfully carried out for the shorter crack lengths to yield reliably accurate values of $\varphi'(i)$. As the crack length increased this plan became uneconomical and was abandoned in favor of the alternative truncation scheme. It was necessary to find Σ_2 by extrapolation for the largest crack length shown in Table II due to the limitations of the digital computer used in solving the systems. Again, $i\varphi'(i)$ in Table II can be considered accurate to one percent.

The author is indebted to Mr. Donald Neal of the Army Materials Research Agency for programming the analysis for a digital computer.

A matter of considerable interest is the comparison of the calculated results with the approximate stress concentration factor K_A derived from the Westergaard solution. This factor, e.g., Irwin,[8] can be written as

$$\frac{K_A}{T} = \left[\frac{2x_0}{\pi} \tan \frac{\pi L}{2x_0} \right]^{1/2} . \qquad \qquad \ldots (44)$$

The appropriate K_A's are listed in Tables I and II along with the ratios K/K_A.

For deep cracks the approximation K_A is clearly very good. For short cracks K_A differs from the exact solution by approximately 13 percent. This result is consistent with work by Bueckner,[9] who showed that for an edge crack in an elastic half plane $K \to 1.13 \sqrt{L}$. As $L \to 0$ in (44), $K_A \to \sqrt{L}$. For small crack depths therefore the 13 percent error in K_A is consistent to both analyses. The effect of length of the strip can be seen for intermediate crack depths by comparing Tables I and II. It is evident from this comparison that the ratio $y_0/x_0 = 3.00$ is effectively infinite as far as effects on K are concerned.

VIII. SUMMARY

It has been shown that the complex variable approach using conformal mapping provides an effective numerical procedure for determining the stress concentration in edge cracks in rectangular sheet. Convergence difficulties encountered with increasing crack depth can be minimized by truncation of the series form of the mapping function in a manner preserving key properties of the geometry local to the crack tip.

For edge cracks in a rectangular tensile sheet the numerical results of this report indicate that the approximate stress concentration factor derived from Westergaard's solution is in error by 13 percent for short cracks but increases fairly rapidly in accuracy with increasing crack depth.

REFERENCES

1. WESTERGAARD, H. M. Bearing Pressures and Cracks. Transactions, ASME, v. 61, 1939, p. A-49 to A-53.

2. TAIT, R. J. Crack in Strip Finite Width. See SNEDDON, I. N., Crack Problems in the Mathematical Theory of Elasticity, North Carolina State College, Raleigh, North Carolina, May 1961.

3. BLUHM, J. I. Fracture Mechanics. Presented at Automotive Engineering Congress, 1963, Paper 655C.

4. BOWIE, O. L. Analysis of an Infinite Plate Containing Radial Cracks Originating at the Boundary of an Internal Circular Hole. Journal of Mathematics and Physics, v. 25, April 1956, p. 60-71.

5. MUSKHELISHVILI, N. I. Some Basic Problems of the Mathematical Theory of Elasticity. P. Noordhoff, Ltd., Groningen, Holland, 1953.

6. BOWIE, O. L. Rectangular Tensile Bar Weakened by Surface Cracks. Part I, Stress Analysis, Watertown Arsenal Laboratories, WAL TR 811.8/5, March 1963.

7. KARTZIVADZE, I. N. The Fundamental Problems of the Theory of Elasticity for the Elastic Circle. Comptes rendus de l'Académie des Sciences de l'U. R. SS. 20, v. XII, 1943, p. 95-104.

8. IRWIN, G. R. The Crack Extension-Force for a Crack at a Free Surface Boundary. Naval Research Laboratory, Washington, D. C., NRL Report 5120, 1958.

9. BUECKNER, H. F. Some Stress Singularities and Their Computation by Means of Integral Equations. Boundary Problems in Differential Equations, University of Wisconsin Press, Madison, Wisconsin, 1960.

THE PROPAGATION OF SHOCK WAVES THROUGH SOIL - ANALYTICAL METHODS AND PROBLEMS

Dietrich E. Gudzent

Structures and Mechanics Laboratory,
Directorate of Research and Development,
U. S. Army Missile Command
Redstone Arsenal

I would like to give you a brief survey of the analytical methods and problems involved in the study of the propagation of shock waves induced by underground explosions. I also would like to direct your attention to the places where the question marks are and where future research is badly needed.

Structures and Mechanics Laboratory, Army Missile Command came in touch with this problem because we have to worry about the safety of missiles housed in underground silos, especially in respect to sympathetic detonations.

Let us assume that a certain number of silos are clustered to a nest, that the nests are a certain distance from each other, and that a number of nests are integrated into a system (Fig. 1). It is possible that a missile blowup can occur. In such a case we have to provide means that only one nest may be destroyed while all other nests remain operational. Or, in other words, the radius of destruction, r_d, must be related to the inter-nest distance, ℓ , by the inequality

$$r_d < \ell$$

This requirement may be achieved by

1. suitable design of silos and nests
2. choosing proper distance "ℓ" between two nests
3. using means to attenuate the propagating shock wave between adjacent nests.

We can try to achieve a solution in two different ways, either by experimental investigations or by theoretical considerations.
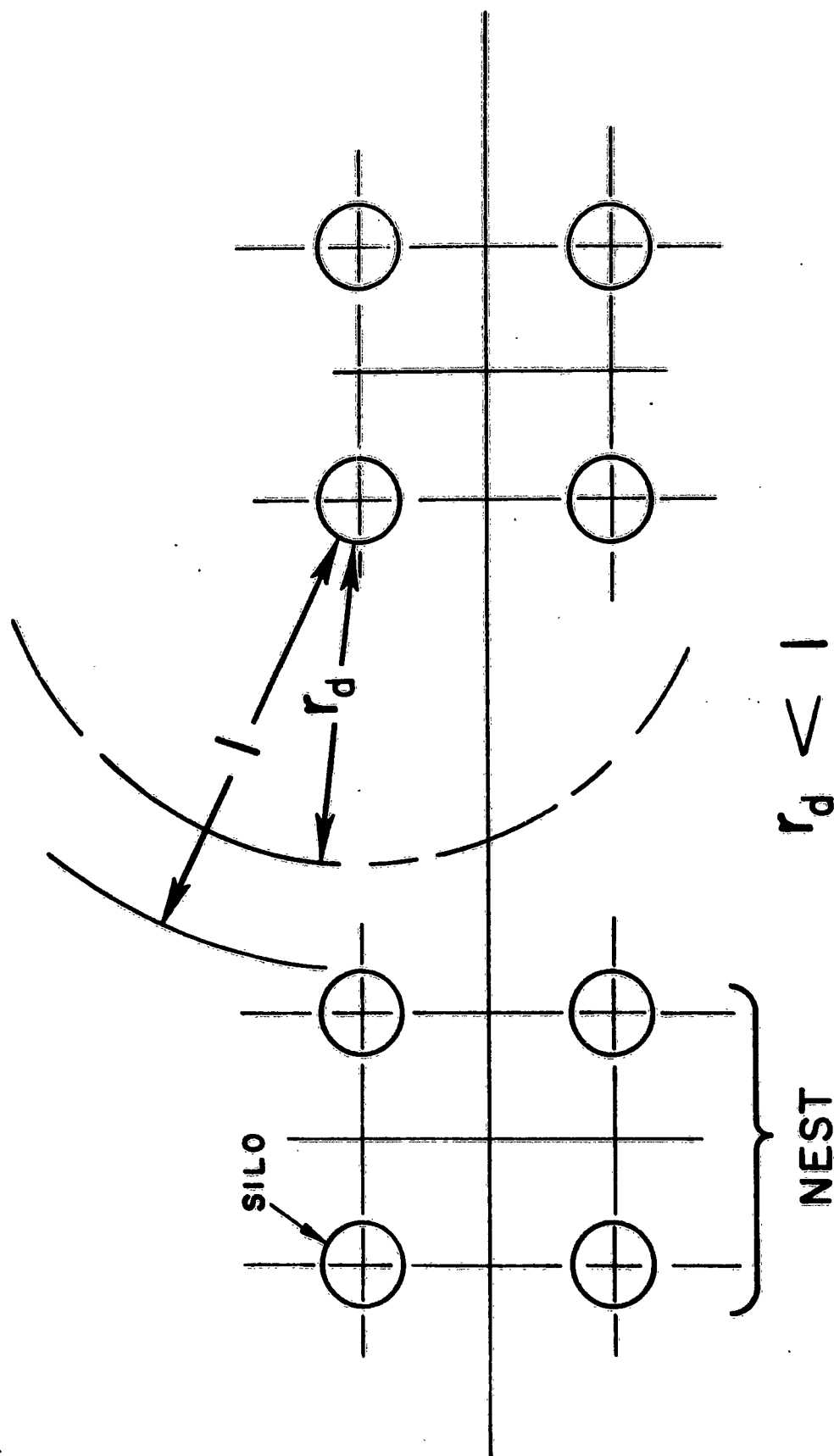
FIG I

$r_d < I$

Let me first discuss experimental investigations.

Little has been done to date in full-scale experiments but numerous scaled experiments have been performed.

In 1946 Lampson published his very extensive and comprehensive report relating measured phenomena from underground explosions to damage on underground structures. Lampson derived a currently well known model law to extend the results of properly designed experiments over a range of scale factors.

According to this, if D_1 is the distance from an explosion of a material of reference weight, W_1, with which a certain overpressure or dynamic pressure is attained, then for any weight of explosive, W, this same pressure will occur at a distance, D, given by

$$\frac{D}{D_1} = \left(\frac{W}{W_1} \right)^{\frac{1}{3}}$$

This law has been widely used in current literature despite the fact that many authors have found discrepancies between it and actual measurements. This is not too surprising because the law is well established only for a gaseous medium which follows the law of state of an ideal gas. We shall not expect that solid material behaves like an ideal gas. As long as we do not have a law of state for soil, we will have difficulties in establishing scaling procedures for investigation of explosions.

For this reason many scientists have developed empirical formulae for the attenuation of a shock wave versus distance. As an example, Townsend, Langseth, and Perkins published the formula

$$A_r = A_o^{-\eta \, \ell n \, r}$$

where A_r is the acceleration at the distance r, and A_o is the acceleration for the distance zero. The value of n has been found to be 4.3 in sand and 4.2 in clay, varying with distance.

Now, I would like to mention some theoretical consideration. This part of the discussion consists of a description of the requirements for the time-location relationship of the propagating wave after an underground explosion and its action upon the next nest, considering

1. type of wave,
2. frequency distribution,
3. kind of soil,
4. type of explosion of detonation, and
5. design criteria of silos and nests.

At the present time no general equation of such nature exists due to the complexity of the problem and the contributing unknown factors and functions. However, treatments are available for certain aspects of the problem.

In order to treat the propagation of waves through soil it is necessary to assume idealized behavior of the soil with regard to deformation. The most common idealizations are represented by the model of the elastic medium and the locking medium. It is not necessary here to discuss the behavior of an elastic medium except to note that in some cases rock may be considered as ideally elastic.

The locking medium is characterized by a certain behavior of the stress-strain relation of granular masses which may be described as follows:

First Stage: On initial compression a slightly non-linear elastic behavior exists.

Second Stage: Further compression may produce a plastic flow and some gradual breaking of grains resulting in a softening or plastic response.

Third Stage: Additional pressure produces a rather sudden rearrangement of granules into a less compressible state accompanied by large volumetric changes and by permanent strains, manifested by the upturning of the stress-strain curve.

Because of the complexity of the mathematical model describing such behavior, the stress-strain relation has been idealized by various

curves as shown in Fig. 2a, b, c, and d, the simplest being that of
Fig. 2a.   This stress-strain diagram implies that upon initial loading
the medium exerts no resistance until a critical value of the strain (or
density) is reached.   Beyond this critical strain the material becomes
incompressible.   Modifications of the material behavior affect either
the initial behavior of the material, making it elastic (Fig. b) or elasto-
plastic (Figure. c), or they influence the behavior after the critical
strain is reached by permitting a certain amount of residual elasticity,
leading to the bi-linear model of Fig. d.   At lower levels of compression,
where the governing phenomenon is not that of incompressibility but rather
that of a gradual but irreversible volume change, the behavior of the
medium may be characterized by the stress-strain curve of Fig. e.

As an example, sand may be considered as an idealized locking
medium.   Other types of soil such as clay are located between the
elastic and the locking medium.

Time limits a comprehensive discussion of famous mathematical
treatments given by Hutton, Skalak, Salvadori, Weidlinger, and
Wiedermann, to mention a few.   I would like to present only one example:
a very recently published paper by Jordan in England.   He gives a
thorough mathematical treatment and arrives at solutions which can be
numerically evaluated.   A detailed description of the theory is beyond
the scope of my presentation today, but to give an idea I will outline here
some basic steps of his approach.   Jordan assumes an infinite, cylindri-
cal hole in the solid body, partially filled with explosives.   The explosive
is lighted on one end; the explosion travels through the material in the
hole and a shock wave is created showing a certain time delay.

Cylindrical coordinates, (r, θ, z), are used, with the origin at the
center of the source; z extends along the axis of the hole.   The radius
of the infinitely long cylindrical hole is a , the displacement components
in the r and z directions are μ_r and μ_z, respectively, and component
μ_θ is absent for reasons of symmetry.   After introducing convenient
non-dimensional coordinates, the equation of propagation of the wave is
obtained as

$$\frac{\partial^2 U}{\partial T^2} = \text{grad div } U - \frac{\mu}{(\lambda + 2\mu)} \cdot \text{curl curl } U$$

(a)

(b)

(c)

(d)

(e)
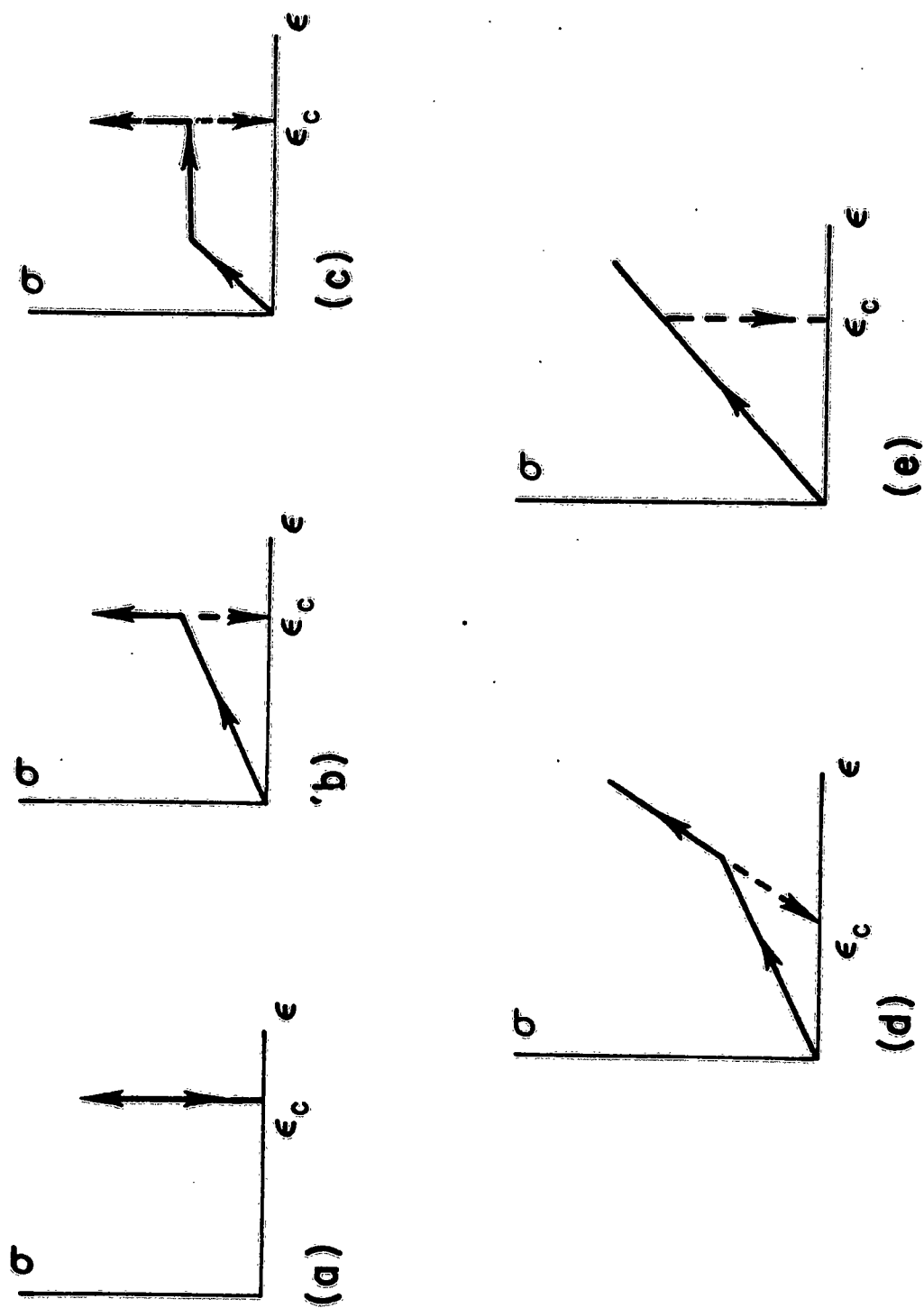
IDEALIZED STRESS – STRAIN CURVES

FIG 2

To solve this equation, first curl $\mathcal{U}$ and then div $\mathcal{U}$ is equal to zero, which "trick" yields two solveable equations

$$\frac{\partial^2 \mathcal{U}}{\partial T^2} - grad\ div\ \mathcal{U} = 0$$

$$\frac{\partial^2 \mathcal{U}}{\partial T^2} + m\ curl\ curl\ \mathcal{U} = 0$$

solutions of which have to be combined linearly. Splitting into scalar components the equations become the following:

$$\frac{\partial^2 \mathcal{U}_R}{\partial T^2} - \frac{\partial}{\partial R}\left\{\frac{1}{R}\frac{\partial}{\partial R}(R\,\mathcal{U}_R)\right\} - \frac{\partial^2 \mathcal{U}_z}{\partial R\,\partial Z} = 0$$

$$\frac{\partial^2 \mathcal{U}_z}{\partial T^2} - \frac{\partial}{\partial Z}\left\{\frac{1}{R}\frac{\partial}{\partial R}(R\,\mathcal{U}_R)\right\} - \frac{\partial^2 \mathcal{U}_z}{\partial Z^2} = 0$$

$$\frac{1}{m}\frac{\partial^2 \mathcal{U}_R}{\partial T^2} + \frac{\partial^2 \mathcal{U}_R}{\partial Z^2} + \frac{\partial^2 \mathcal{U}_z}{\partial R\,\partial Z} = 0$$

$$\frac{1}{m}\frac{\partial^2 \mathcal{U}_z}{\partial T^2} + \frac{1}{R}\frac{1}{\partial R}\left\{R\frac{\partial \mathcal{U}_z}{\partial R}\right\} - \frac{\partial^2 \mathcal{U}_R}{\partial R\,\partial Z} = 0.$$

The solutions have to satisfy the following boundary conditions: radial components of stress equals the negative value of the Lamé constant times H(T) at r = a and T > 0 lateral components along the cylindrical surface equals zero, again for r = a, T > 0, and all displacements equal zero for T < 0.

The equations and boundary conditions can be satisfied if a double Fourier transform is used, which transforms the four equations into

$$\frac{d}{dR}\left\{\frac{1}{R}\frac{d}{dR}\left(R u_R''\right)\right\} + \left(h^2 - n^2\right) u_R'' = 0$$

$$\frac{d u_z''}{dR} - i n\, u_R'' = 0$$

$$\frac{d u_z''}{dR} - \frac{\mathcal{S}^2}{i n}\, u_R'' = 0$$

$$\frac{1}{R}\frac{d}{dR}\left\{R\frac{d u_z''}{dR}\right\} + h^2 u_z'' - i n \frac{1}{R}\frac{d}{dR}\left(R u_R''\right) = 0$$

together with suitable transformation of the boundary conditions.

By applying the method of "steepest descent" from calculus of variation it is seen that this system can be solved by Hankel-Functions (Bessel Functions of third kind):

$$u_R'' = \mathcal{S}\, H_1'^{(2)}\left(\mathcal{S} R\right)_1 \qquad u_z'' = -i n\, H_0^{(2)}\left(\mathcal{S} R\right)$$

and

$$u_R'' = i n\, H_1^{(2)}\left(\mathcal{S} R\right)_1 \qquad u_z'' = \mathcal{S}\, H_0^{(2)}\left(\mathcal{S} R\right)$$

where the following abbreviations are used:

$$\mathcal{S} = \left(h^2 - n^2\right)^{1/2} \qquad \mathcal{S} = \left(k^2 - n^2\right)^{1/2} \qquad k = m^{-1/2} h$$

and h and n are the parameters used in the Fourier transform. The boundary conditions need careful consideration to determine their effects on the path of integration in order to aviod certain difficulties arising from branch points (poles) occuring in the functions.

Jordan's paper investigates in detail these singularities and the expendability in different regions surrounding the cylinder separately for dilation wave stresses and for shear wave stresses. Fig. 3 may be given as an example. The theoretical solution must be brought in a suitable form for numerical evaluation. This can be done for large speed of detonation, while no such evaluation has been obtained for smaller speeds. Also in the case where the computation is feasible it is very lengthy and to a certain extent inaccurate because the maximum of the waves can only be found by interpolating between equally spaced points for which the computations were made. Another source of inaccuracy is that damping and dispersion of the waves have not been considered. From the complexity of the mathematical theory of even this very much simplified problem, Jordan concludes that experimental studies are necessary and that it must be expected that the interpretation of experimental results will be by no means straightforward. The experimental work done up to date does not give an adequate description of the propagation of the wave.

Based primarily on the material which I have presented here and on additional investigations not discussed today we conclude that:

(1) Publications on experiments to date do not give the desired answer to our specific problem, principally due to the following reasons:

a. Most of the experimental works were not intended to solve exactly the same problem with which we are concerned. Many neglect phenomena or circumstances which are vital to our task, i.e. (a) using spherically shaped instead of cylindrically shaped charges, or (b) directly burying the charges into the soil neglecting an air gap, or (c) using different type of explosives.

b. Most of the experimental works give too little consideration to the theory of similitude and so prevent satisfactory extrapolation to larger or smaller dimensions, i.e. application of a scaling law to underground explosions which is well established only for air blasts.

For that reason we are initiating at Army Missile Command a critical comparison of all important information dealing with experimental data in an effort to establish an integrated picture by interlinking the more or less isolated data of independent reports. Further-
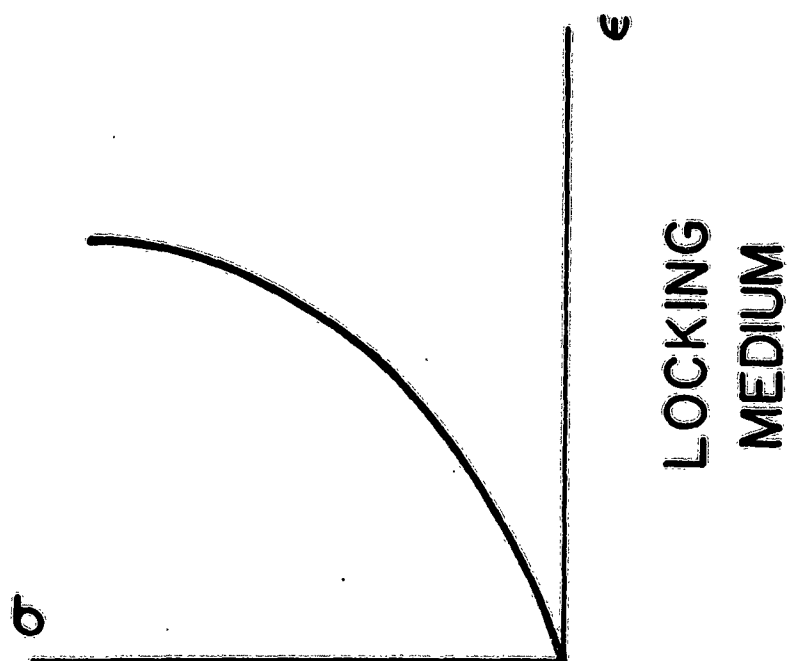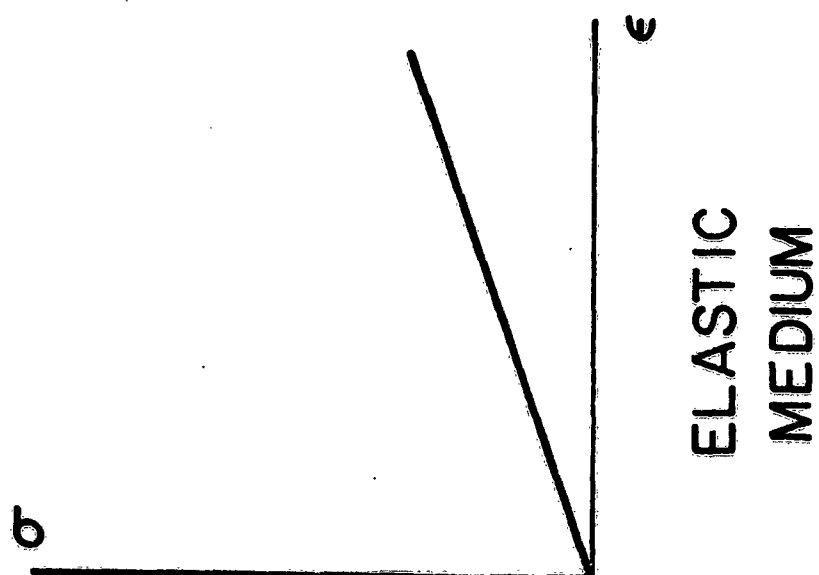
ELASTIC
MEDIUM

LOCKING
MEDIUM

FIG 3

more, we will conduct our own experiments to fill existing gaps of information or to gain specific data for theoretical investigations.

(2) The theoretical works do not present the desired answer to our specific problem due principally to the fact that one or more assumptions and/or simplifications necessary for mathematical treatment do not agree with the conditions of our problems. For that reason we will conduct a critical investigation of the most important theoretical approaches to determine to what extent they are applicable to our problem, and we plan to apply the most promising approaches to our special requirements.

(3) We will compare theoretical results with the experimental data. We want to give attention to the development of equations of state for solids with the objective of establishing a theoretically well-founded scaling procedure for experiments in soils.

(4) Finally, we are going to include studies of the interaction of a shock wave with buried structures in the above-mentioned investigations with the ultimate goal of establishing the design criteria for silos subjected to heavy dynamic loads from underground explosions.

REFERENCES

1. Hutton, R. E. , Ground Motion Resulting from Nuclear Surface Detonations; Shock, Vibration and Associated Environments, Part III, pp. 1, 1960, OSD Bulletin No. 28.

2. Skalak, R. , Wave Propagation in a Plastic-Elastic Medium; The Mitre Corporation Report No. 39852-SR-18: On the Application of the Theory of Locking Media to Ground Shock Phenomena, Bedford, Mass.

3. Salvadori, M. G. , Skalak, R. , and Weidlinger, P. , Spherical Waves in an Ideal Locking Medium; The Mitre Corporation Report No. 39852-SR-18: On the Application of the Theory of Locking Media to Ground Shock Phenomena, Bedford, Massachusetts, 1960.

4. Weidlinger, P. , On the Application of the Theory of Locking Media to Ground Shock Pehnomena, The Mitre Corporation SR-18, 1960.

5.   Wiedermann, A. H., A Concept for Soil-Structure Interaction Due to Ground Shock Waves;   Shock, Vibration and Associated Environments, Part III, pp. 100, 1961, OSD Bulletin No. 29.

6.   Jordan, D. W., The Stress Wave from a Finite, Cylindrical Explosive Source;   Journal of Mathematics and Mechanics 11, pp. 503, 1962.

TRANSFORMATION FROM HYPERBOLIC
COORDINATES TO RECTANGULAR UTM

Duncan Harken

U. S. Army Engineer Geodesy,
Intelligence and Mapping Research and Development Agency*

The transformation of hyperbolic coordinates, given directly by electromagnetic wave phase comparison techniques, to UTM (Universal Transverse Mercator) rectangular coordinates, for the normal mapping procedures and applications, involves straightforward geometrical relations which can be resolved analytically by straightforward algebraic techniques.

One current application to SHREPE (Short Range Electronic Position Equipment) involves the use of three sending stations -- a Master Station and two Slave Stations, the latter under the control of the Master Station for simultaneity of signal emission. A receiver located in the vicinity of these three stations is equipped to measure the differences in times of arrival of signals from the Master Station and each of the two Slaves. Considering that all electro-magnetic waves are propagated with the same velocity, these differences in <u>time</u> are proportional to differences in <u>distance</u> (since s = vt).

Referred to rectangular coordinates X, Y, let the master station be located at the point M(a, b) and the two slave stations (with simultaneous signals syncronized by and from the master station) be at the points S(c, h) and T(f, g). Determination of the location of any wandering point P(x, y) receiving signals from the sending stations is based on the differences of the times of arrival of the signals from these stations. Inasmuch as the velocity of signal propagation is constant, the time of arrival of any signal is proportional to the distance

$$s = vt \quad \text{or} \quad t = s/v$$

---

* The author is no longer with this agency.
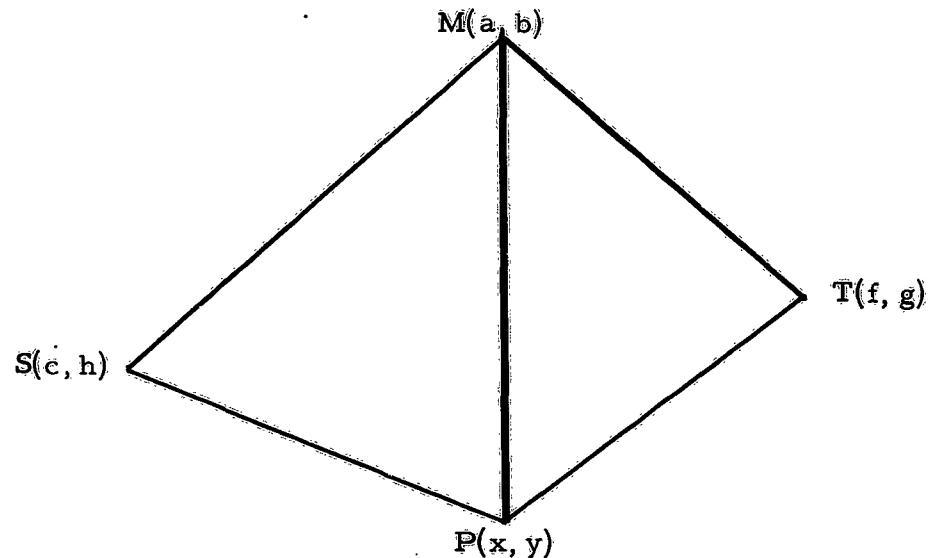
where

s = distance between sending and receiving stations (ft.)

t = propagation time (sec.)

v = velocity of signal propagation (ft./sec.)

(Actually, v = c = velocity of light = for electromagnetic waves)
This situation is determined entirely by the geometry

This determines the differences in distances (which are proportional to
propagation intervals) as

$$d_1 = \sqrt{(x-a)^2 + (y-b)^2} - \sqrt{(x-c)^2 + (y-h)^2}$$

$$d_2 = \sqrt{(x-a)^2 + (y-b)^2} - \sqrt{(x-f)^2 + (y-g)^2}$$

These conditions can better be put in the form

$$\sqrt{(x-a)^2 + (y-b)^2} \quad = \quad \begin{cases} d_1 + \sqrt{(x-c)^2 + (y-h)^2} \\ \\ d_2 + \sqrt{(x-f)^2 + (y-g)^2} \end{cases}$$

so that radicals can be eliminated by successive squaring, always with one radical isolated on one side of the equation. The resulting conditions can be represented as a pair of quadratic in x and y:

$$A_i x^2 + 2B_i xy + C_i y^2 + D_i x + E_i y + F_i = 0 \qquad (i = 1, 2)$$

where

$$A_1 = 4\left[(c-a)^2 - d_1^2 \right] \qquad\qquad A_2 = 4\left[(f-a)^2 - d_2^2 \right]$$

$$B_1 = 4\left[(c-a)(h-b) \right] \qquad\qquad B_2 = 4(f-a)(g-b)$$

$$C_1 = 4\left[(h-b)^2 - d_1^2 \right] \qquad\qquad C_2 = 4\left[(g-b)^2 - d_2^2 \right]$$

$$D_1 = 4\left[(c-a)(a^2+b^2-c^2-h^2-d_1^2) + 2cd_1^2 \right] \qquad D_2 = 4\left[(f-a)(a^2+b^2-f^2-g^2-d_2^2) + 2fd_2^2 \right]$$

$$E_1 = 4\left[(h-b)(a^2+b^2-c^2-h^2-d_1^2) + 2hd_1^2 \right] \qquad E_2 = 4\left[(g-b)(a^2+b^2-f^2-g^2-d_2^2) + 2gd_2^2 \right]$$

$$F_1 = (a^2+b^2-c^2-h^2-d_1^2)^2 - 4d_1^2(c^2+h^2) \qquad F_2 = (a^2+b^2-f^2-g^2-d_2^2)^2 - 4d_2^2(f^2+g^2)$$

The two quadratic in x and y can be thought of as representing two conics. Their common solution, resulting from their conditions being simultaneous, is then represented by the points of intersection of the two conics. The coordinates of these common solutions (or intersections) are given by the eliminants, hereinafter developed.

This above pair of quadratics in both x and y can be expressed with special emphasis as quadratic in x

$$A_i x^2 + (2B_i y + D_i)x + (C_i y^2 + E_i y + F_i) = 0 \qquad (i = 1, 2)$$

and as quadratics in y

$$C_i y^2 + (2B_i x + E_i) y + (A_i x^2 + D_i x + F_i) = 0 \quad (i = 1, 2)$$

As a possible simplification for observing duality relationships, the quadratics in x may be written

$$ax^2 + bx + c = 0$$

$$Ax^2 + Bx + C = 0$$

where

$$a = A_1 \qquad\qquad b = 2B_1 y + D_1 \qquad\qquad c = C_1 y^2 + E_1 y + F_1$$

$$A = A_2 \qquad\qquad B = 2B_2 y + D_2 \qquad\qquad C = C_2 y^2 + E_2 y + F_2$$

Elimination of x can now be accomplished by SYLVESTER'S Dialytic method:

$$\begin{vmatrix} a & b & c & o \\ o & a & b & c \\ A & B & C & o \\ o & A & B & C \end{vmatrix}$$

This resultant eliminant can be expanded by minors (or by LAPLACE's cascade method):

$$a \begin{vmatrix} a & b & c \\ B & C & o \\ A & B & C \end{vmatrix} + A \begin{vmatrix} b & c & o \\ a & b & c \\ A & B & C \end{vmatrix} = o$$

resulting in

$$a^2C^2 + acB^2 - abBC$$

$$- 2acAC = 0$$

$$+ A^2c^2 + ACb^2 - ABbc$$

The above eliminant can be expressed in its original unabbreviated form as

$$
\begin{vmatrix}
A_1 & 2B_1y + D_1 & C_1y^2 + E_1y + F_1 & 0 \\
0 & A_1 & 2B_1y + D_1 & C_1y^2 + E_1y + F_1 \\
A_2 & 2B_2y + D_2 & C_2y^2 + E_2y + F_2 & 0 \\
0 & A_2 & 2B_2y + D_2 & C_2y^2 + E_2y + F_2
\end{vmatrix} = 0
$$

and expanded as above (amounting to simple substitution in the final result). This elimination of x from the two simultaneous quadratic equations by SYLVESTER'S dialytic (or any other) method results in a quartic equation in y. Similar elimination of y leads to a quartic in x, resulting from

$$
\begin{vmatrix}
C_1 & 2B_1x + E_1 & A_1x^2 + D_1x + F_1 & 0 \\
C_2 & 2B_1x + E_2 & A_2x^2 + D_2x + F_2 & 0 \\
0 & C_1 & 2B_1x + E_1 & A_1x^2 + D_1x + F_1 \\
0 & C_2 & 2B_2x + E_2 & A_2x^2 + D_2x + F_2
\end{vmatrix} = 0
$$

These quartics in x and y can be solved by HORNER's method for the numerical solution of algebraic equations of higher degree with numerical coefficients. The resulting values of x and y are the rectangular coordinates of the point P (x, y). Any ambiguity resulting from multiple real values of x and y will have to be resolved by means of the known practical situation at hand -- which will permit only values within certain ranges.

MEMBRANE NATURAL FREQUENCIES FOR AXISYMMETRIC

VIBRATION OF DEEP SPHERICAL CAPS

Edward W. Ross, Jr.
Materials Engineering Laboratory, U. S. Army Materials
Research Agency, Watertown, Massachusetts 02172

ABSTRACT. This paper contains the results of an analysis of the natural frequencies for the axially symmetric vibration of a thin shell in the form of a segment of a sphere with a free edge. In the present analysis only the membrane theory is used, i.e., bending effects are neglected. The effects of both the longitudinal (i.e., in-surface) and transverse (perpendicular-to-the-surface) inertias are retained, and the entire range of opening angles is considered. The main body of the results is obtained by numerical solution of the frequency equation although a number of limiting cases (high frequencies, shallow shells, and shells with small holes) are treated analytically.

CONTENTS

I. INTRODUCTION

In comparison with the enormous volume of work that has appeared in the literature concerning statics of thin shells, the work on shell dynamics is much less extensive, and largely limited to certain special cases such as circular cylindrical shells and shallow shells. Naghdi and Kalnins[1] give a short historical summary of work on vibrations of deep shells and have themselves found the lowest natural frequency of vibration for a free-edged hemisphere by the bending theory, as well as the natural frequencies for non-axially symmetric vibrations of a hemisphere by the membrane theory. Much earlier, of course, Love[2] and Lamb[3] had given the natural frequencies for axially symmetric vibrations of hemispheres and complete spherical shells, respectively, by the membrane theory. Shallow-shell vibrations have been discussed in a number of papers by Reissner and co-workers, see Reference 4 and the references given there, and a paper by Naghdi and Kalnins.[5]

The present report presents the calculation by the membrane theory of the natural frequencies for a thin shell in the form of a spherical segment. The vibration is assumed to be axially symmetric and torsion-free. The membrane equations adopted are those for small deflections of a classically elastic shell, with both longitudinal and transverse inertia terms retained. The edge is assumed to be free.
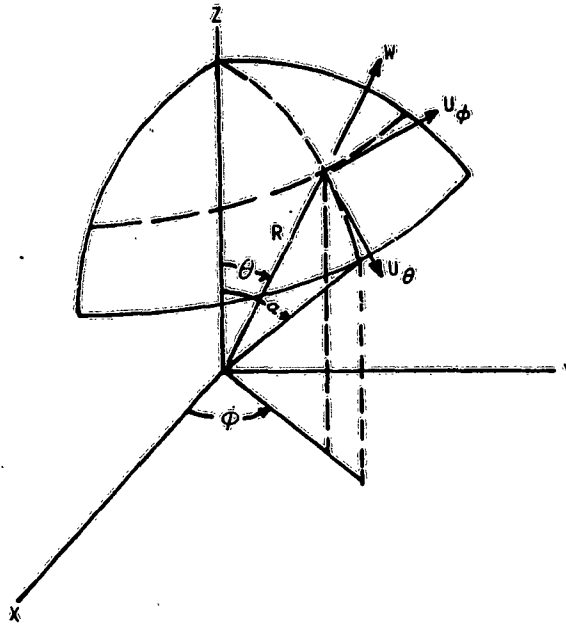
Section II contains the basic equations of the dynamic membrane theory, which are then specialized for the particular problem considered here. These are finally reduced to Legendre's equation, whose solutions, when inserted in the homogeneous boundary conditions, give a transcendental equation that must be solved for the frequency. In Section III there is, first, a short summary of formulas relating to Legendre functions that are useful in treating this frequency equation; then several special cases are discussed for which the frequency equation may be simplified; and finally the numerical calculation of the frequencies is carried out. Section IV contains a brief discussion of the results.

II. SOLUTION OF THE DYNAMIC MEMBRANE EQUATIONS FOR THE SPHERE

The basic geometry of the spherical shell segment, or deep spherical cap, is shown in Figure 1.

We adopt spherical surface coordinates θ, ϕ as shown in Figure 1 and express the differential equations in terms of the usual physical stress - resultant components, N_θ, N_ϕ and $N_{\theta\phi} = N_{\phi\theta}$, and displacement components, U_θ, U_ϕ and W. The definitions and sign conventions for these quantities are shown in Figures 1 and 2. The equations of motion in the absence of applied forces are

$$\frac{\partial}{\partial \theta} (N_\theta \sin \theta) + \frac{\partial N_{\theta\phi}}{\partial \phi} - N_\phi \cos \theta = \rho h R \sin \theta \frac{\partial^2 U_\theta}{dt^2} \qquad (1)$$

19-066-1073/AMC-63

Figure 1. ONE QUADRANT OF A DEEP SPHERICAL CAP WITH SEMI-ANGLE α, SHOWING THE SIGN CONVENTIONS FOR U_θ, U_ϕ, W.
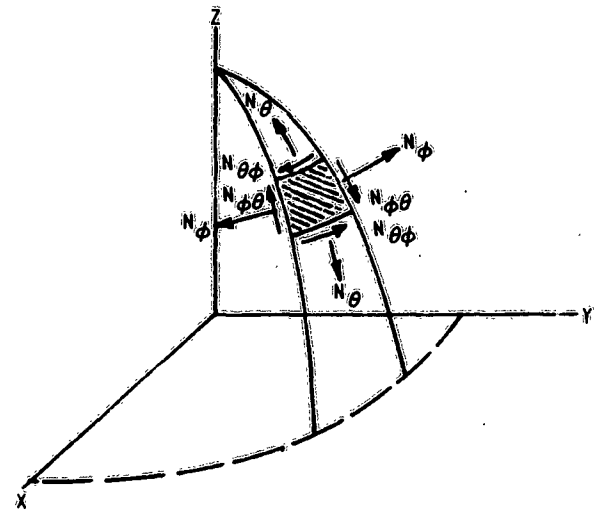
19-066-1074/AMC-63

Figure 2. DEFINITIONS AND SIGN CONVENTIONS FOR PHYSICAL STRESS-RESULTANTS N_θ, N_ϕ, $N_{\theta\phi}$.

$$\frac{\partial}{\partial\theta}(N_{\theta\phi}\sin\theta) + \frac{\partial N_\phi}{\partial\phi} + \cos\theta\, N_{\theta\phi} = \rho h R \sin\theta\, \frac{\partial^2 U_\phi}{\partial t^2} \tag{2}$$

$$-(N_\theta + N_\phi) = \rho h R\, \frac{\partial^2 W}{\partial t^2} \tag{3}$$

and the stress-displacement relations are

$$N_\theta = \frac{Eh}{(1-\nu^2)R}\left[W(1+\nu) + \frac{\partial U_\theta}{\partial\theta} + \nu U_\theta \cot\theta + \nu \csc\theta\, \frac{\partial U_\phi}{\partial\phi}\right] \tag{4}$$

$$N_\phi = \frac{Eh}{(1-\nu^2)R}\left[W(1+\nu) + U_\theta \cot\theta + \csc\theta\, \frac{\partial U_\phi}{\partial\phi} + \nu\, \frac{\partial U_\theta}{\partial\theta}\right] \tag{5}$$

$$N_{\theta\phi} = \frac{Eh}{2(1+\nu)R}\left[\frac{\partial U_\phi}{\partial\theta} - U_\phi \cot\theta + \csc\theta\, \frac{\partial U_\theta}{\partial\phi}\right]. \tag{6}$$

In these equations ρ is the mass-density of the shell material, h is the shell thickness, R is the radius of middle-surface of the shell, E is Young's modulus and ν is Poisson's ratio.

For torsionless axisymmetric deformations we have $U_\phi = N_{\theta\phi} = \frac{\partial}{\partial\phi} = 0$ and the equations that are not identically satisfied become

$$\frac{\partial}{\partial\theta} (N_\theta \sin \theta) - N_\phi \cos \theta = \rho h R \sin \theta \frac{\partial^2 U_\theta}{\partial t^2} \tag{7}$$

$$- (N_\theta + N_\phi) = \rho h R \frac{\partial^2 W}{\partial t^2} \tag{8}$$

$$N_\theta = \frac{Eh}{(1 - \nu^2)R} \left[(1 + \nu)W + \frac{\partial U_\theta}{\partial_\theta} + \nu U_\theta \cot \theta \right] \tag{9}$$

$$N_\phi = \frac{Eh}{(1 - \nu^2)R} \left[(1 + \nu)W + U_\theta \cot \theta + \nu \frac{\partial U_\theta}{\partial\theta} \right] . \tag{10}$$

If we set

$$U_\theta = ue^{i\omega t}, \quad W = we^{i\omega t}, \quad M = \Omega^2 = \frac{\omega^2 R \rho}{E} \tag{11}$$

we obtain upon substituting (9), (10) into (7), (8)

$$\frac{\partial^2 u}{\partial\theta^2} + \frac{\partial u}{\partial\theta} \cot \theta + u \left[(1 - \nu^2)M - \nu - \cot^2\theta \right] + (1 + \nu) \frac{\partial w}{\partial\theta} = 0 \tag{12}$$

$$\frac{\partial u}{\partial\theta} + u \cot \theta + w \left[2 - (1 - \nu) M \right] = 0 . \tag{13}$$

To obtain a single equation in a single unknown, we may eliminate either U or W between these equations. It seems to lead to a slightly easier final equation if we retain W and eliminate U although at first sight this appears more roundabout. When we do it, the results are

$$u = \left[\frac{1 - M}{1 + (1 + \nu)M} \right] \frac{\partial w}{\partial\theta} \tag{14}$$

$$\frac{\partial^2 w}{\partial\theta^2} + \cot \theta \frac{\partial w}{\partial\theta} + cw = 0 \tag{15}$$

where

$$c = \frac{[1 + (1 + \nu)M] [(1 - \nu)M - 2]}{M - 1} . \tag{16}$$

If we set

$$c = \lambda (\lambda + 1) , \tag{17}$$

(15) is in the form of Legendre's equation. Since the shell is closed at $\theta = 0$ the solution $Q_\lambda (\cos \theta)$ must be discarded and so w is given by

$$w = P_\lambda(\cos \theta) \tag{18}$$

apart from an immaterial arbitrary constant. Here $P_\lambda(\cos \theta)$ is the Legendre function of the first kind of degree λ.

The boundary condition at the free edge $\theta = a$ is

$$N_\theta\Big|_{\theta = a} = 0,$$

and with the aid of (9), (11), (13), and (14) this gives the condition

$$\left[w + \frac{\cot \theta}{1 + (1 + \nu)M} \frac{\partial w}{\partial \theta}\right]\Bigg|_{\theta = a} = 0 \tag{19}$$

Thus substituting (18) into (19), we may express the boundary condition as either

$$[1 + (1 + \nu)M + \lambda \cot^2 a]P_\lambda(\cos a) - \lambda \cot a \csc a \, P_{\lambda - 1}(\cos a) = 0 \tag{20}$$

or, setting $y = \cos a$ and multiplying through by $\sin^2 a$,

$$\lambda y P_{\lambda - 1}(y) - \{1 + (1 + \nu)M + y^2[\lambda - 1 - (1 + \nu)M]\}P_\lambda(y) = 0 , \tag{21}$$

where we have used the familiar formula for expressing the derivative of a Legendre function as a linear combination of two Legendre functions of different degrees. Equations 16, 17, and 20 or 21 form the basis for the calculations of the natural frequencies that are described in the next section.

III. CALCULATION OF THE NATURAL FREQUENCIES

It is convenient first to record some formulas for the behavior of the Legendre functions $P_\lambda (\cos \theta)$ in various cases. These may all be found in Erdelyi.[6]

There are two series representations for the Legendre functions, each appropriate to a particular part of the range $0 \leq \theta < \pi$. Near $\theta = 0$ a very convenient representation is the hypergeometric series

$$P_\lambda(\cos \theta) = \sum_{n=0}^{\infty} C_n(z) , \tag{22}$$

where

$$z = \sin^2 \frac{\theta}{2} \tag{23}$$

$$C_n(z) = -\frac{\sin \lambda\pi}{\pi} \frac{\Gamma(n-\lambda)\,\Gamma(n+\lambda+1)}{[\Gamma(n+1)]^2}\, z^n . \tag{24}$$

If we set $\gamma = \pi - \theta$, a representation of $P_\lambda(\cos \gamma)$ near $\gamma = \pi$ is given in terms of θ by

$$P_\lambda(\cos \gamma) = P_\lambda(\cos \theta)\left\{\cos \lambda\pi - \frac{\sin \lambda\pi}{\pi}\left[\log\left(\frac{1-z}{z}\right) - 2\psi(\lambda) + 2\psi(0)\right]\right\}$$

$$-\frac{2}{\pi}\sin \lambda\pi \sum_{n=0}^{\infty} C_n(z)\, W_n \tag{25}$$

where

$$W_n = \psi(n) - \psi(0) \tag{26}$$

and $\psi(\lambda)$ is the logarithmic derivative of the factorial function.

The various series terms are easily calculated sequentially by the formulas

$$C_0 = 1 \tag{27}$$

$$W_0 = 0 \tag{28}$$

and

$$C_n(z) = C_{n-1}(z)\left[1 - \frac{1}{n} - \frac{A}{n^2}\right]z^2 \qquad n \geq 1 \tag{29}$$

$$W_n = W_{n-1} + \frac{1}{n} \qquad n \geq 1 \tag{30}$$

where

$$A = \lambda(\lambda+1) . \tag{31}$$

When λ is an integer the representations (22) and (25) remain valid and $P_\lambda(\cos \theta)$ reduces to a Legendre polynominal. Only in this case is $P_\lambda(\cos \theta)$ finite at $\theta = \pi$.

The expansions of $P_\lambda(\cos \theta)$ and $dP_\lambda(\cos \theta)/d\theta$ about $\theta = \pi/2$ were used in the numerical calculation of natural frequencies having $\lambda = -\frac{1}{2} + ib$ and are described in Appendix C. When $|\lambda|$ is large we have the asymptotic representation

$$P_\lambda(\cos \theta) \sim \sqrt{\frac{2}{\pi\sin \theta}}\, \frac{\Gamma(\lambda+1)}{\Gamma\left(\lambda+\frac{3}{2}\right)} \sum_{n=0}^{\infty} (-1)^n \left[\frac{\Gamma\left(n+\frac{1}{2}\right)}{\Gamma\left(\frac{1}{2}\right)}\right]^2 \frac{\Gamma\left(\lambda+\frac{3}{2}\right)}{\Gamma\left(n+\lambda+\frac{3}{2}\right)}$$

$$\cdot \frac{\sin\left[\left(\lambda+n+\frac{1}{2}\right)\theta + \frac{\pi}{4} + \frac{n\pi}{2}\right]}{n!\,(2\sin \theta)^n}; \tag{32}$$

this expansion converges if $\pi/6 < \theta < \frac{5\pi}{6}$. If θ is small the asymptotic representation

$$\bar{P}_\lambda(\cos\ \theta) = J_o(a) + \sin^2\left(\frac{\theta}{2}\right)\left[\frac{a}{6}\ J_3(a) - J_2(a) + \frac{1}{2a}\ J_1(a)\right] + O\left(\sin^4\ \frac{\theta}{2}\right), \quad (33)$$

where $a = \left(\lambda + \frac{1}{2}\right)2\ \sin\ (\theta/2)$, is valid.

The natural frequencies of the system under discussion are found for any value of $y = \cos\ \alpha$ by solving (16), (17) and (21) for $\Omega = M^{\frac{1}{2}}$. In general this must be done numerically and the procedures for carrying it out will be described later. However, a good deal of information can be gained by considering various limiting cases of these equations analytically.

In the first place (16) and (17) together specify a quadratic relation between $M = \Omega^2$ and λ which may be written either

$$\lambda^2 + \lambda - \frac{[1 + (1 + \nu)M]\ [1 - \nu)M - 2]}{M - 1} = 0 \qquad (34)$$

or

$$M^2 - \left[\frac{1 + 3\nu + \lambda(\lambda + 1)}{1 - \nu^2}\right]M + \left[\frac{\lambda(\lambda + 1) - 2}{1 - \nu^2}\right] = 0\ . \qquad (35)$$

Since only real frequencies are of interest, we are concerned only with the case $M \geq 0$. Also λ enters (34), (35), and (21) only in the combination $A = \lambda\ (\lambda + 1)$, hence among the real values of λ, only the range $\lambda \geq -\frac{1}{2}$ need be considered. However, there are sometimes real, positive solutions for M when $\lambda(\lambda + 1) < -\frac{1}{2}$, in which case λ is complex but of the special form

$$\lambda = -\frac{1}{2} + ib \quad \text{or} \quad \lambda(\lambda + 1) = -\left(b^2 + \frac{1}{4}\right). \qquad (36)$$

A qualitative graph of M versus $\lambda(\lambda + 1)$ is shown in Figure 3. It is evident
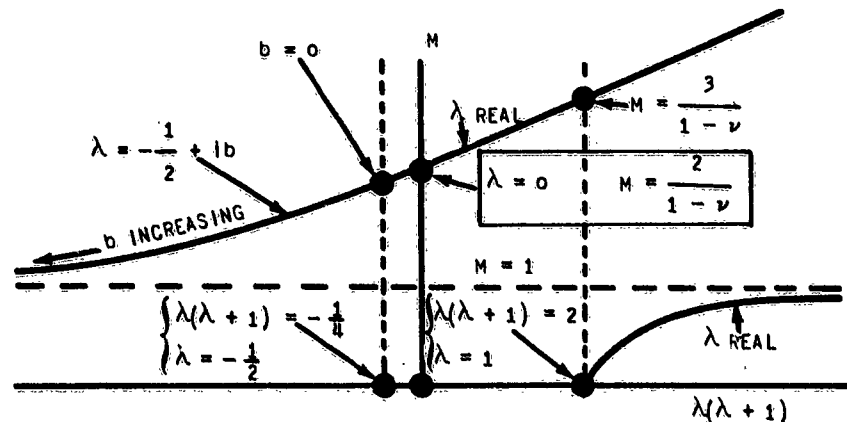

Figure 3. SKETCH OF THE RELATIONS BETWEEN $M = \Omega^2$ AND $\lambda(\lambda + 1)$.

that for $\lambda > 1$, there are two M-values, i.e., two natural frequencies, associated with each λ-value. We give separate names to these, designating the low-frequency branch (with $M < 1$) by M_L and the high-frequency branch (with $M > 1$) by M_H. The asymptotic behaviors for large $|\lambda(\lambda + 1)|$ of these branches are

$$\Omega_H^2 = M_H \sim 1 + \frac{(1 + \nu)(2 + \nu)}{b^2 + \frac{1}{4}} \quad \text{as } b\to\infty, \lambda(\lambda + 1)\to - \infty \tag{37}$$

$$\Omega_H^2 = M_H \sim \frac{\lambda(\lambda + 1)}{1 - \nu^2} + \frac{\nu(3 + \nu)}{1 - \nu^2} \quad \text{as } \lambda\to + \infty \tag{38}$$

$$\Omega_L^2 = M_L \sim 1 - \frac{(1 + \nu)(2 + \nu)}{\lambda(\lambda + 1)} \quad \text{as } \lambda\to\infty. \tag{39}$$

One special value of α is easily dealt with. When $\alpha = \pi/2$ the frequency equation 21 reduces to

$$P_\lambda(0) = 0 ,$$

of which the only real solutions are

$$\lambda = 2K + 1 . \tag{40}$$

From Figure 3 we see that in (40)

$$K = 0,1,2,3,\dots$$

for $M > 1$, but

$$K = 1,2,3, \dots$$

for $M < 1$.

It is convenient also to introduce the following notation. The value of λ obtained from simultaneously solving (21 and (35), taking $M = M_H$, will be designated as λ_H; similarly, if $M = M_L$ is taken, the resulting λ will be designated λ_L. Then (40) can be written

$$\lambda_H(\pi/2) = (2K + 1) \qquad K = 0,1,2,3, \dots$$

$$\lambda_L(\pi/2) = (2K + 1) \qquad K = 1,2,3, \dots \tag{40a}$$

We now consider various special cases.

(a) Large values of $|\lambda|$

Of the various limiting cases, we consider first $|\lambda| \to \infty$ and α not near 0 or π. In this case we may replace $P_\lambda (\cos \alpha)$ and $P_{\lambda-1} (\cos \alpha)$ in (21) by the first two terms in their asymptotic expansions (39), and this leads, after some reduction, to

$$\lambda \cos \alpha \left[\sin (\beta - \alpha) - \frac{\sin (\beta + \frac{\pi}{2})}{8(\lambda + \frac{1}{2})\sin \alpha} \right] - \left[\lambda \cos^2\alpha + G \sin^2\alpha \right]\left[1 + \frac{1}{2\lambda} \right]^{-1} \left[\sin \beta \right.$$

$$\left. - \frac{\sin(\beta + \alpha + \frac{\pi}{2})}{8(\lambda + \frac{3}{2}) \sin \alpha} \right] = o\ (1) \tag{41}$$

where

$$\beta = (\lambda + \frac{1}{2})\alpha + \frac{\pi}{4} , \tag{42}$$

$$G = 1 + (1 + \nu)M . \tag{43}$$

After further reduction we can write the limiting form of the frequency equation, (21), as

$$\lambda \cos \alpha \sin \alpha \cos \beta[1 + o(\lambda^{-1})] + \sin \beta(G \sin^2\alpha - \frac{3}{8} \cos^2\alpha) = o(\lambda^{-1}) \tag{44}$$

whence

$$\tan \beta \approx \frac{-\lambda}{G \tan \alpha - \frac{3}{8} \cot \alpha} \tag{45}$$

or

$$\lambda \approx - \frac{1}{2} - \frac{\pi}{4\alpha} + \frac{1}{\alpha} \tan^{-1}\left\{ \frac{-\lambda}{G \tan \alpha - \frac{3}{8} \cot \alpha} \right\} . \tag{46}$$

Fairly accurate results are obtainable for surprisingly small values of λ by the following process. Obtain G as a function of λ from (37), (38), or (39), insert this in (46), solve iteratively for λ and then find the final value of Ω (or M) from (35). M and Ω can of course also be found from the approximate formulas (37) to (39), but for moderate values of λ, and $\alpha \neq 0$, π, (46) is somewhat more accurate than (37) to (39), and this accuracy would be wasted if (35) were not used in the final calculation of M. The accuracy of (46) is aided by the fact that it happens to give exactly the correct set of values for $\lambda = \pi/2$.

The approximate analysis described above is carried out in the ensuing paragraphs for the three cases generated by the three approximate representations (37) to (39). We must always keep in mind that the asymptotic approximations that lead to (46) are not generally valid near $a = 0$ and $a = \pi$ and may also lead to appreciable error if $\lambda = 0$ (1).

In the first case we set $\lambda = -\frac{1}{2} + ib$ and $G = 2 + \nu$ and obtain from (45) after some manipulation that, as $b \to \infty$,

$$(2 + \nu) \tan^2 a + b \tan a - \frac{3}{8} \approx 0 . \tag{47}$$

A curve of Ω_H versus a is generated by solving this for a as a function of b and combining the result with the solution of (35) for Ω as a function of b, provided the proper solution branch is chosen for each equation. The results of this are shown in Figure 4 and Tables I and III (where this branch is designated as $\lambda_H^{(-1)}$ and $\Omega_H^{(-1)}$). The two solutions of (47) are given approximately by

$$\tan a = -\frac{b}{2+\nu}$$

$$\tan a = \frac{b}{8b}$$

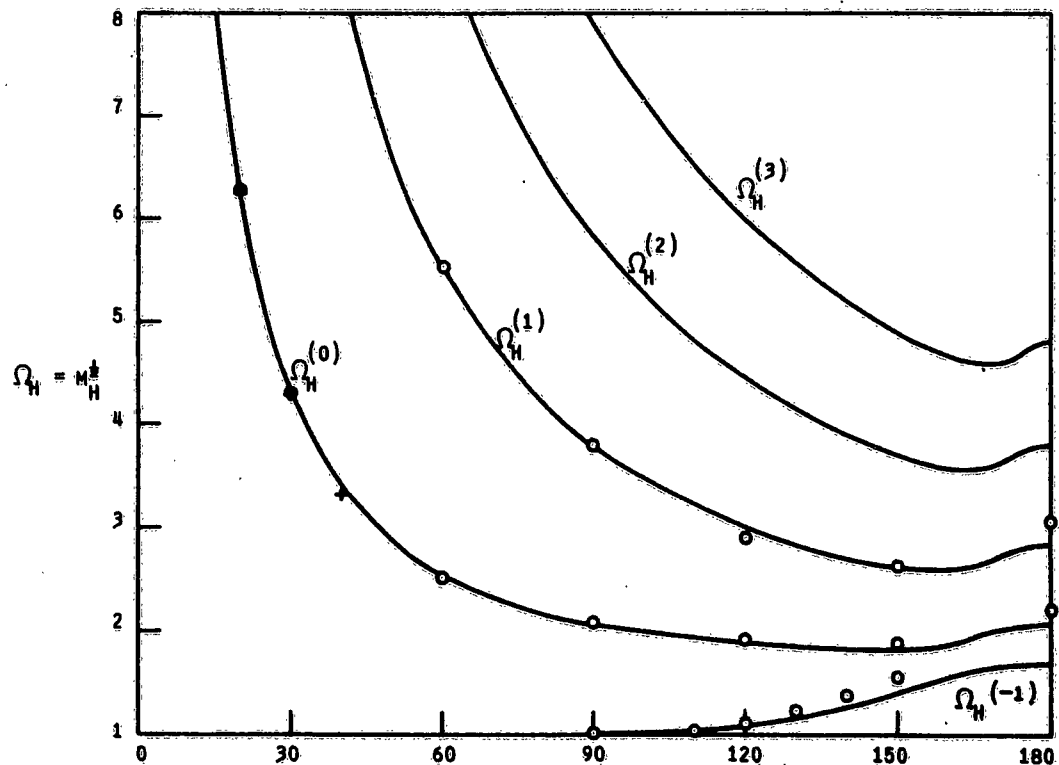
Figure 4. DEPENDENCE OF NATURAL FREQUENCY, $\Omega = wR/\sqrt{E/\rho}$, ON SEMI-ANGLE, a, FOR THE FIVE LOWEST BRANCHES OF THE UPPER FAMILY, Ω_4. O AND + DENOTE POINTS GIVEN BY THE APPROXIMATION (46) FOR HIGH λ-VALUES AND (61) FOR SHALLOW SHELLS, RESPECTIVELY.

of which the second is useless since our approximate equations are not applicable near $a = 0$ or π. If the first of these is combined with (37), we obtain

$$\Omega_H^{(-1)} \sim \left[1 + \left(\frac{1 + \nu}{2 + \nu} \right) \cot^2 a \right]^{\frac{1}{2}}$$

(48)

as a simple approximation to the frequency curve. This, and the preceding equation, predict that as $b \to \infty$, $a \to \pi/2$ from above and $\Omega_H^{(-1)} \to 1$ from above.

In the second case we find from (38) that

$$G \approx \frac{\lambda(\lambda + 1)}{1 + \nu} \quad ,$$

and (46) then reduces to

$$\lambda \approx -\frac{1}{2} - \frac{\pi}{4a} + \frac{1}{a} \tan^{-1} \left[-\frac{(1 - \nu)}{(\lambda + 1) \tan a} \right]$$

except near $a = 0$ or π, where (46) itself is unreliable. This has many solutions corresponding to the multiple branches of the $\tan^{-1}$ function; we may represent these branches explicitly by writing the equation as

$$\lambda \approx -\frac{1}{2} + \frac{\pi}{a} \left(K + \frac{3}{4} \right) + \frac{1}{a} \tan^{-1} \left[-\frac{(1 - \nu)}{(\lambda + 1)} \cot a \right] ,$$

(49)

where $K = 0,1,2,\ldots$, and then specifying that

$$-\pi/2 < \tan^{-1} \left[-\frac{(1 - \nu) \cot a}{\lambda + 1} \right] < \pi/2 .$$

Equation 49 can be solved iteratively for $\lambda = \lambda_H$ as a function of a. If this is combined with the solution of (35) for $\Omega_H = M_H^{\frac{1}{2}}$ as a function of λ, we obtain an approximate solution for Ω_H as a function of a. This approximation is tabulated (Tables I and III) at a few points for the two branches of the high-frequency family obtained by taking $K = 0,1$ in (49), and the points are graphed in Figure 4, along with the solution obtained by numerical analysis of (21) and (35).

A simpler approximation, valid only for very large λ is found by neglecting

$$\frac{1}{a} \tan^{-1} \left[-\frac{(1 - \nu)}{\lambda + 1} \cot a \right]$$

in (49). This gives

$$\lambda_H \approx -\frac{1}{2} + \frac{\pi}{a} \left(K + \frac{3}{4} \right)$$

(50)

and then (38) leads to

$$\Omega_H^{(K)} \approx \frac{1}{\sqrt{1-\nu^2}}\left[\frac{\pi}{a}\left(K + \frac{3}{4}\right)\right],$$ (51)

The third case, where $M_L \to 1$ from below as $\lambda \to \infty$, is a little more involved than the preceding ones. Setting $G = 2 + \nu$ the approximate equation (46) becomes

$$\lambda \approx -\frac{1}{2} - \frac{\pi}{4a} + \frac{1}{a}\tan^{-1}\left[\frac{-\lambda}{(2 + \nu)\tan a - \frac{3}{8}\cot a}\right],$$

and again there are many solutions. We may make the solutions explicit by writing

$$\lambda \approx -\frac{1}{2} + \frac{\pi}{a}\left(K + \frac{3}{4}\right) + \frac{1}{a}\tan^{-1}\left[\frac{-\lambda}{(2 + \nu)\tan a - \frac{3}{8}\cot a}\right],$$ (52)

where $K = 1,2,3\ldots$, and making the following set of specifications:

Let a_0 be the root between 0 and $\pi/2$ of

$$\tan^2 a = 3/8\left[(2 + \nu)\right]$$

(for $\nu = .3$, $a_0 \approx 22° \approx .384$). Then

    (i) if $a < a_0$,

$$-\pi < \tan^{-1}\left[\frac{-\lambda}{(2 + \nu)\tan a - \frac{3}{8}\cot a}\right] < -\pi/2 \;;$$

    (ii) if $a_0 < a < \pi - a_0$

$$-\pi/2 < \tan^{-1}\left[\frac{-\lambda}{(2 + \nu)\tan a - \frac{3}{8}\cot a}\right] < \pi/2$$

    (iii) if $\pi - a_0 < a < \pi$

$$\pi/2 < \tan^{-1}\left[\frac{-\lambda}{(2 + \nu)\tan a - \frac{3}{8}\cot a}\right] < \pi$$

    (iv) if $a = a_0$ $\tan^{-1}\left[\frac{-\lambda}{(2 + \nu)\tan a - \frac{3}{8}\cot a}\right] = -\pi/2$

$$a = \pi - a_0 \qquad\qquad\qquad\qquad\qquad = \pi/2 \;.$$

With these specifications we have for $\lambda = \lambda_L$

$$\text{at } \bar{a} = a_o, \qquad \lambda_L = -\frac{1}{2} + \frac{\pi}{a_o}\left(K + \frac{1}{4}\right)$$

$$\text{at } \bar{a} = \pi/2, \qquad \lambda_L = 2K + 1$$

$$\text{at } \bar{a} = \pi - a_o, \quad \lambda_L = -\frac{1}{2} + \frac{K + \frac{5}{4}}{1 - \frac{a_o}{\pi}}$$

$$\text{at } \bar{a} = \pi, \qquad \lambda_L = K + \frac{5}{4} .$$

The values at $a = \pi/2$ are exact. The exact values at $\bar{a} = \pi$, as we shall see, are $\lambda_L = K + 1$, so the above approximate values are not too atrocious even in this limiting case for which the approximations made in deriving them are not reliable.

Approximate curves, $\Omega_L^{(K)}$ versus a, of the low-frequency family are obtained by solving (52) for $\lambda = \lambda_L$, substituting into (35) and then solving for $\Omega_L = M_L^{\frac{1}{2}}$. These calculations were carried out for some of the a-values, and the results for $K = 1,2$ and 3 are shown in Tables II and IV and Figure 5.

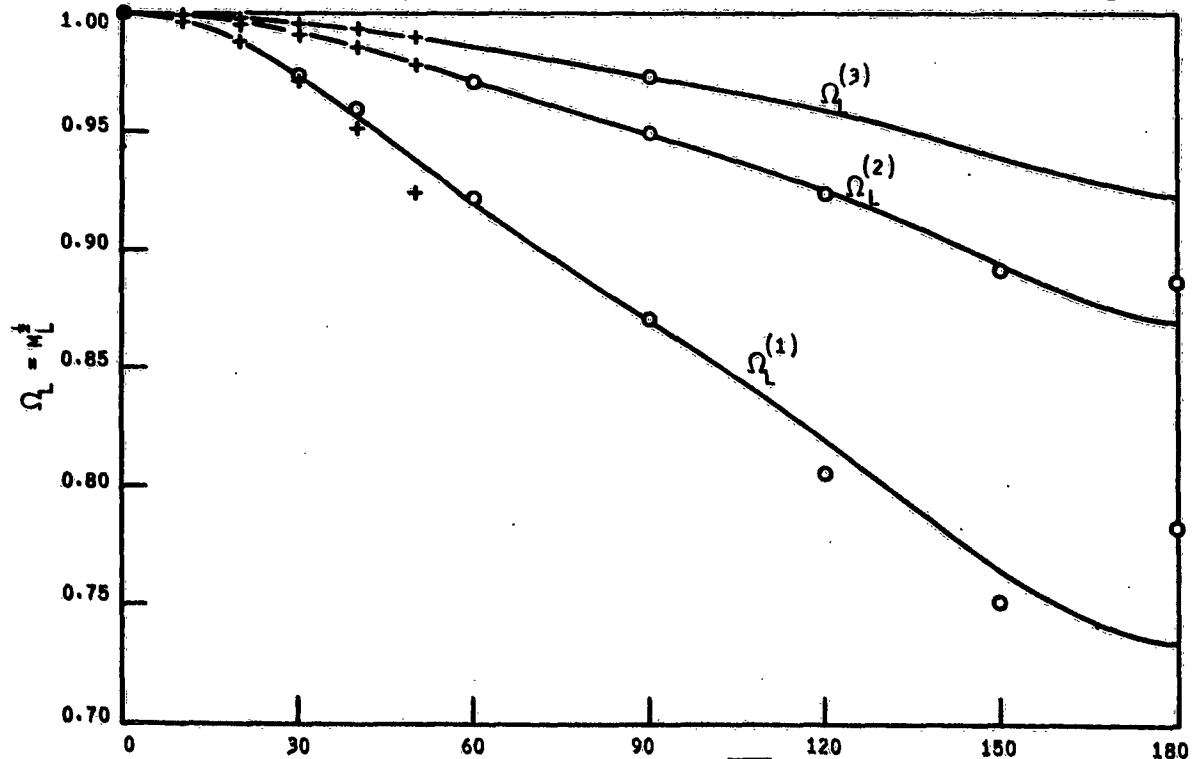
Figure 5. DEPENDENCE OF NATURAL FREQUENCY, $\Omega = wR\sqrt{E/\rho}$, ON SEMI-ANGLE, a, FOR THE THREE LOWEST BRANCHES OF THE LOWER FAMILY, Ω_L. O AND + DENOTE POINTS GIVEN BY THE APPROXIMATION (52) FOR HIGH λ-VALUES AND (59) FOR SHALLOW SHELLS, RESPECTIVELY.

Simpler but less accurate approximations to these curves are obtained by setting

$$\tan^{-1}\left[\frac{-\lambda}{(2 + \nu)\tan\alpha - \frac{3}{8}\cot\alpha}\right] \approx -\pi/2 \quad \text{for } 0 < \alpha < \pi/2$$

$$\approx \pi/2 \quad \text{for } \pi/2 < \alpha < \pi$$

so that

$$\lambda_L \approx -\frac{1}{2} + \frac{\pi}{\alpha}\left(K + \frac{1}{4}\right) \quad 0 < \alpha < \pi/2 \tag{53}$$

$$\lambda_L \approx -\frac{1}{2} + \frac{\pi}{\alpha}\left(K + \frac{5}{4}\right) \quad \pi/2 < \alpha < \pi. \tag{54}$$

These are then combined with (39) to obtain

$$\Omega_L^{(K)}(a) \approx \left\{1 - \left(\frac{a}{\pi}\right)^2 \frac{(1 + \nu)(2 + \nu)}{\left(j + \frac{1}{4}\right)^2}\right\}^{1/2} \tag{55}$$

where

$$j = K \quad \text{for } 0 < \alpha < \pi/2$$

$$= K + 1 \quad \text{for } \pi/2 < \alpha < \pi.$$

These very simple representations of the curves of the low-frequency family are not accurate near $\alpha = \pi/2$ nor are they very reliable near $\alpha = 0$ or π.

(b) Shallow Shells

The second limiting case that is of interest is the behavior of the frequency curves as $\alpha \to 0$, $y \to 1$, i.e., the limiting behavior for shallow shells. In this connection we observe that (21) is trivially satisfied by setting $a = 0$, $y = 1$, but this root is spurious since we have multiplied (20) by $\sin^2 \alpha$ in arriving at (21). If we use the representations (33), and make the definitions

$$\epsilon = 2 \sin\frac{a}{2}$$

$$a = \left(\lambda + \frac{1}{2}\right)\epsilon \quad ,$$

then (21) implies (see Appendix A, equation A-5)

$$\left(\frac{1}{4} - \frac{G}{\lambda}\right)J_0(a) + \left(\frac{\lambda + \frac{1}{2}}{a}\right)J_1(a) + \frac{1}{4}J_2(a) = 0 (\epsilon). \tag{56}$$

We now consider various implications of (56). First when $\lambda = O(1)$, then as $\epsilon \to 0$, $a \to 0$, and

$$J_o(a) \to 1$$

$$J_1(a) \sim \frac{a}{2}$$

$$J_2(a) \sim \left(\frac{a}{2}\right)^2$$

and so (56) implies

$$\lambda(\lambda + 1) = 2G + O(\epsilon) = 2[1 + (1 + \nu)M] + O(\epsilon) . \tag{57}$$

Since (16) and (17) already specify a relation between $\lambda(\lambda + 1)$ and M that does not agree with (57) for $M > 0$ and $\nu > 0$, we conclude that the system of equations (35) and (21) has no solutions when $\epsilon \to 0$ and $\lambda = O(1)$, i.e., there are no natural frequencies for shallow shells except those for which $\lambda \to \infty$. This is suggested by the asymptotic relations (50) and (53) but these are not necessarily valid near $a = o$, so the present discussion puts this conclusion on firmer ground.

For large values of λ and small values of ϵ we consider the high- and low-frequency cases separately. For the low-frequency case, as $\lambda \to \infty$, $G \sim 2 + \nu$ and the leading term gives just

$$J_1(a)/a = O(\epsilon)$$

whence

$$\lambda_L + \frac{1}{2} = \frac{a_K}{2 \sin \frac{a}{2}} \quad , \quad K = 1,2,3,\ldots \tag{58}$$

where a_K is the K-th positive zero of $J_1(a)$. The first three zeros are, to three decimal places,

$$a_1 = 3.832$$

$$a_2 = 7.016$$

$$a_3 = 10.173 .$$

Since the values of λ are large near $a = 0$, it is accurate enough to use (39) and obtain the behavior near $a = 0$ of the low-frequency curves in the form

$$\Omega_L^{(K)} \sim \left\{ 1 - \frac{4(1 + \nu)(2 + \nu)}{a_K^2} \sin^2(a/2) \right\}^{\frac{1}{2}} \quad K = 1,2,3 . \tag{59}$$

In the high-frequency case $G \sim \lambda(\lambda + 1)/(1 - \nu)$ and the limiting form of (56) as $\lambda \to \infty$ is

$$a \, J_0 \, (a) - (1 - \nu) \, J_1 \, (a) = 0 .$$

For $\nu = .3$ the first three roots of this are

$$\bar{a}_0 = 2.049$$

$$\bar{a}_1 = 5.389$$

$$\bar{a}_2 = 8.572 ,$$

which can be combined with

$$\lambda_H + \frac{1}{2} = \frac{\bar{a}_K}{2 \sin \, (a/2)} \tag{60}$$

and with (38) to get the following asymptotic behaviors for the first three high-frequency curves near $a = 0$,

$$\Omega_H^{(K)} = \frac{\bar{a}_K}{2 \sqrt{1 - \nu^2} \, \sin \, (a/2)} , \qquad K = 0,1,2. \tag{61}$$

If the results (50), (51), (53), and (55) are applied near $a = 0$, it is seen that they do not differ too much from the results (58) to (61), despite the fact that the approximations for large λ are not necessarily accurate near $a = 0$. The worst discrepancy is in the high-frequency case for $K = 0$, where instead of

$$\lambda_H + \frac{1}{2} \approx \frac{\bar{a}_0}{a} \approx \frac{2.05}{a}$$

(50) gives

$$\lambda_H + \frac{1}{2} = \frac{3\pi}{4a} \approx \frac{2.36}{a} .$$

The predictions of (58) to (61) near $a = 0$ are given in Tables I to IV and shown in Figures 4 and 5, where they may be seen to join fairly smoothly with the results from the numerical calculations using (35) and (21).

(c) Shells with Small Holes

The final limiting case that is of interest is the behavior near $a = \pi$, i.e., the natural frequencies for a spherical shell with a small hole in it. For this purpose the representation (25) is combined with (21) to obtain the limiting form of the frequency equation near $a = \pi$

$$\frac{\sin \lambda \pi}{\pi} \left\{ 2 + \sigma^2 \left[G - \frac{1}{2} \lambda(\lambda + 1) \right] \left[\pi \cot \lambda \pi + 2 \log \, \sin\left(\frac{\sigma}{2}\right) + 2 \, \psi(o) \right] + \sigma \left[\frac{\lambda(\lambda + 1)}{2} - 1 \right] \right. $$
$$\left. + 0 \, (\sigma^4 \ln \sigma) \right\} = 0$$

where $\sigma = \pi - \alpha$. This is derived in Appendix B. Then it is clear that, as $\sigma \to 0$, λ must approach one of the integers. Keeping only the leading terms in the above equation we get

$$\frac{2 \tan \lambda \pi}{\pi} \left\{ 1 + \left[G - \frac{1}{2} \lambda (\lambda + 1) \right] \sigma^2 \log \sin\left(\frac{\sigma}{2}\right) \right\} + \left[G - \frac{1}{2} \lambda (\lambda + 1) \right] \sigma^2 = 0 . \quad (62)$$

Setting $\lambda = n + \epsilon$, we obtain for the limiting behavior as $\sigma \to 0$,

$$\sigma^2 \sim \frac{4}{\pi} \frac{\tan \epsilon \pi}{[n(n + 1) - 2G]} \qquad \text{as } \epsilon \to 0 \qquad (63)$$

where n may be taken as a non-negative integer without loss of generality. This limiting behavior is correct for any of these n; however, when n is very large, the representation (63) is accurate only for very small σ - values because the neglected quantity

$$\left[G - \frac{1}{2} \lambda (\lambda + 1) \right] \sigma^2 \log \sin \left(\frac{\sigma}{2}\right)$$

in the first term of (62) increases very rapidly as σ increases when λ is large. By means of (16) and (17) it is easy to verify that

$$\lambda(\lambda + 1) - 2G = (1 + \nu)M [1 + (1 + \nu)M]/(1 - M) ,$$

and so we have in an obvious notation

$$\lambda_L(\lambda_L + 1) - 2G_L > 0$$

$$\lambda_H(\lambda_H + 1) - 2G_H < 0 .$$

Hence, if (62) is to be satisfied for real angles σ, we must have

$$\epsilon < 0 \qquad \text{for } M < 1$$

$$\epsilon > 0 \qquad \text{for } M > 1 ,$$

i.e., λ_H decreases and λ_L increases as σ increases. Then near $\alpha = \pi$

$$\frac{d\lambda_L}{d\alpha} < 0$$

$$\frac{d\lambda_H}{d\alpha} > 0 .$$

Since (see Figure 4) $dM/d\lambda > 0$ for $\lambda > - 1/2$, we have

$$\left.\begin{array}{l} \dfrac{dM_L}{d\alpha} < 0 \\[3mm] \dfrac{dM_H}{d\alpha} > 0 \end{array}\right\} \quad \text{or} \quad \left\{\begin{array}{l} \dfrac{d\Omega_L}{d\alpha} < 0 \\[3mm] \dfrac{d\Omega_H}{d\alpha} > 0 \end{array}\right\} \tag{64}$$

near $\alpha = \pi$. Also we see from Figure 4 that when $0 < M < 1$, $\lambda > 1$. Thus at $\alpha = \pi$

$$\lambda_L = K + 1 \qquad K = 1,2,3,\ldots \tag{65}$$

and the high-frequency curves have

$$\lambda_H = K \qquad K = 0,1,2,\ldots \tag{66}$$

Equation 63 is not especially accurate, and no approximate numerical results have been derived from it.

(d) Summary of Results

The results in the foregoing cases enable us to construct a reasonably clear picture of the curves of Ω versus α. These fall into two general families, Ω_H (α) and Ω_L (α) with

$$\Omega_H > 1$$

$$\Omega_L < 1 ,$$

and each family has a countably infinite number of branches, $\Omega_H^{(K)}$ (α) and $\Omega_L^{(K)}$ (α), respectively. The gross features of these two families are described below.

For $K \geq 0$ the curve $\Omega_H^{(K)}$ (α) becomes positively infinite at $\alpha = 0$, (see Equation 61), decreases steadily as α increases from zero until it reaches a minimum and thereafter increases until $\alpha = \pi$ (see Equation 64). The minimum occurs at about $\alpha = 145°$ for the branch with $K = 0$ and moves toward $\alpha = \pi$ as one proceeds to branches with larger K-values. For large K-values the minimum occurs very close to $\alpha = \pi$.

The curve $\Omega_H^{(-1)}$ (α) is somewhat different in nature. It starts at $\alpha = \pi$ with the lowest frequency of any of the $\Omega_H^{(K)}$ (α), decreases as α decreases and approaches 1 from above (see Equation 48) as $\alpha \rightarrow \pi/2$. For $\alpha < \pi/2$, $\Omega_H^{(-1)}$ is absent and $\Omega_H^{(0)}$ is the lowest of the $\Omega_H^{(K)}$ (α).

The curves of the low-frequency family, $\Omega_L^{(K)}$ (α) for $K = 1,2,3$, all decrease monotonically as α increases from 0 to π (see Equation 55 and 64).

In addition to the foregoing approximate analyses of special, limiting cases, the natural frequencies were also found by numerical solution of the

frequency equation at $10°$ increments in a, taking $\nu = .3$. The numerical treatment of these frequency equations is described in Appendix C. The results for $\lambda_H^{(K)}(a)$ and $\Omega_H^{(K)}(a)$, where $K = -1,0,1,2,3$, are shown in Tables I and III respectively, and $\Omega_H^{(K)}(a)$ are graphed in Figure 4. $\lambda_L^{(K)}(a)$ and $\Omega_L^{(K)}(a)$ (where $K = 1,2,3$) are shown in Tables II and IV, and $\Omega_L^{(K)}(a)$ are graphed in Figure 5. Tables I to IV also show the results given by the approximations (a) for large values of $|\lambda|$ and (b) for shallow shells.

IV. DISCUSSION

It should be mentioned at the outset that in general the inextensional modes of vibration of shells give frequencies that are proportional to h, whereas the membrane (extensional) modes of vibration have frequencies independent of h. Therefore the natural frequencies of inextensional modes of vibration for sufficiently thin shells must be lower than those of membrane modes. However, axisymmetric deformation of a shell of revolution always involves some extension of the middle surface, hence the inextensional modes cannot occur and in this restricted situation the extensional modes are of greater importance than would otherwise be the case.

The primary purpose in carrying out these calculations of natural frequencies is to obtain an estimate of the natural frequencies of axisymmetric vibration for a shell in the form of a deep spherical cap. The question naturally arises, how are these estimates likely to compare with those of the more accurate thin shell theory that includes both bending and stretching effects. It is difficult to say anything conclusive about this comparison, but a few observations are pertinent.

First, statical analyses of thin shells have shown that in the axisymmetric case employing membrane theory is tantamount to retaining lengths of order R and neglecting those of order $\sqrt{hR}$, whereas the general bending plus membrane theory requires retention of terms of order $\sqrt{hR}$ or larger but neglect of terms of order h. It seems reasonable to suppose, therefore, that the membrane theory will be useful for predicting the frequencies associated with the lower-order eigenfunctions, which do not change too rapidly over a length of order R. In the present problem, this means that the results are meaningful for moderate values of $|\lambda|$ but are questionable when $|\lambda|$ is too large. Now, all our results for shallow shells (i.e., small values of a) involve large values of λ and are therefore suspect. Also the case $\lambda = -\frac{1}{2} + ib$, when b is large, is doubtful, so the behavior of the lowest branch of our high-frequency family is uncertain near $a = \pi/2$. Otherwise, we conclude that the results for the lowest few branches of both the high-and low-frequency families are probably useful estimates of the more exact natural frequency results when h/R is small enough.

Second, the membrane natural frequencies are independent of h, but those given by the bending theory and the exact elastic theory depend on h. One cannot therefore use the membrane theory to estimate the dependence of

the natural frequencies on h. In general, however, one expects that inclusion of bending effects would amount to making the shell stiffer, and hence the membrane natural frequencies should be lower bounds for the corresponding natural frequencies calculated from the bending theory.

Third, we may compare the results obtained here with those of three previously calculated special cases. To begin with, the results for $a = \pi$ agree with Lamb's calculations[3] for the membrane frequencies of a complete sphere, and so we conclude that the effect of a small hole at one pole of a sphere executing axially symmetric vibrations is negligible, at least as far as the lower natural frequencies are concerned. Higher frequencies are probably affected, but the membrane theory does not give these accurately in any case. Next, the results of Naghdi and Kalnins[1] for a free-edge hemisphere show general agreement with the results here. As h/R → o their results apparently approach the membrane value from above although the calculations were not carried out for h/R < .01. Finally, in the shallow shell bending case calculated by Reissner,[4] the limiting result $\Omega \to 1$ as $h \to 0$ for all branches of the frequency curve is obtained, in agreement with the behavior of the low-frequency family in the present calculations. While this tends to indicate that the membrane analysis is fairly good even in this unfavorable limiting case, too much importance should not be attached to this agreement. Reissner's theory neglects the effect of longitudinal inertia (which is retained in the membrane theory used here) so the inclusion of bending in Reissner's theory is not the only difference between the two theories.

We conclude from these observations that the membrane theory provides useful information about the natural frequencies whose mode shapes do not change too rapidly.

Finally it is interesting to observe the effect on the frequencies of changes in a. Here we would anticipate the operation of two opposed effects. First, if a flat, circular plate with free edges executes axisymmetric transverse vibrations, its natural frequencies are decreased by an increase in radius. In the bending of a spherical shell, an increase in a is similar to an increase in radius for the plate in that both produce an increase in area of the middle surface, so we might expect increases in a to cause decreases in natural frequency. On the other hand, the curvature of the shell ought to have a stiffening tendency that would cause increase of the natural frequencies as a increases. This second effect is likely to be important only for the lower values of λ. For, when λ is large and real, the eigenfunctions oscillate many times within $o \leq \theta \leq \pi$ so that, crudely speaking, the shell does not curve appreciably within any one oscillation and hence the effect of curvature is probably not felt by the oscillation.

The frequency curves of the present membrane theory give some evidence of the action of these two conflicting influences. Their general trend is to decrease as a increases except that the curves with the smallest values of λ (i.e., the lowest two curves of the upper family) experience a reversal for $\pi/2 < a < \pi$. These are the curves that are most likely to be affected

by the shell curvature if the foregoing speculations are correct. For the curves with larger values of λ there is either no reversal (in the lower family) or (for the upper family) the reversal takes place over a rather small range near $\alpha = \pi$ in which the membrane theory may need to be supplemented by bending effects to obtain accurate results.

TABLE I

HIGH-FREQUENCY VALUES OF λ

Dependence of $\lambda_H^{(K)}$ on a for $-1\le K\le 3$, as calculated numerically. $\tilde{\lambda}_H^{(K)}$ is derived from the approximation for large $|\lambda|$, (49) and (47). $\hat{\lambda}_H^{(K)}$ is derived from the shallow-shell approximation, (60). For $90°<a\le 160°$, $\lambda_H^{(-1)} = -\frac{1}{2} + ib$ and the tabular entries are the b values.

a	b	$\lambda_H^{(0)}$	$\lambda_H^{(1)}$	$\lambda_H^{(2)}$	$\lambda_H^{(3)}$	b	$\tilde{\lambda}_H^{(0)}$	$\tilde{\lambda}_H^{(1)}$	$\hat{\lambda}_H^{(0)}$	$\hat{\lambda}_H^{(1)}$
0		∞	∞						∞	∞
10									11.26	30.42
15		7.397								
20		5.462					5.417		5.400	15.02
30		3.543	9.816				3.487	9.786	3.458	9.811
40		2.593	7.250						2.485	7.378
50		2.027	5.714	9.344						
60		1.648	4.692	7.712			1.603	4.682		
70		1.374	3.964	6.548	9.125					
80		1.165	3.421	5.676	7.829					
90		1.000	3.000	5.000	7.000		1.000	3.000		
100	13.09	0.866	2.666	4.481	6.256	12.96				
110	6.416	0.756	2.394	4.022	5.653	6.183				
120	4.121	0.666	2.172	3.660	5.152	3.767	0.778	2.062		
130	2.903	0.593	1.990	3.358	4.731	2.320				
140	2.084	0.544	1.844	3.107	4.377	1.483				
150	1.408	0.534	1.742	2.906	4.081	0.676	0.643	1.758		
160	0.783	0.637	1.716	2.774	3.855					
170	-0.111*	0.898	1.865	2.822	3.782					
175	-0.020*	0.977	1.965	2.944	3.817					
180	0*	1.000	2.000	3.000	4.000		1.250	2.250		

*These entries are values of $\lambda_H^{(-1)}$

TABLE II

LOW-FREQUENCY VALUES OF λ

Dependence of $\lambda_L^{(K)}$ on a for $K = 1, 2, 3$, as calculated numerically from (21) and (35). $\tilde{\lambda}_L^{(K)}$ is derived from the approximation for large $|\lambda|$, (52). $\hat{\lambda}_L^{(K)}$ is derived from the shallow-shell approximation, (58).

a	$\lambda_L^{(1)}$	$\lambda_L^{(2)}$	$\lambda_L^{(3)}$	$\tilde{\lambda}_L^{(1)}$	$\tilde{\lambda}_L^{(2)}$	$\hat{\lambda}_L^{(1)}$	$\hat{\lambda}_L^{(2)}$	$\hat{\lambda}_L^{(3)}$
0	∞	∞	∞			∞	∞	∞
10						21.48	39.75	57.58
20	10.702					10.53	19.70	28.65
30	7.161			7.179	13.10	6.903	13.05	19.06
40	5.454	9.825		5.502		5.102	9.757	14.30
50	4.485	7.914				4.034	7.801	11.48
60	3.884	6.698	9.586	3.875	6.737			
70	3.490	5.898	8.348					
80	3.213	5.371	7.532					
90	3.000	5.000	7.000	3.000	5.000			
100	2.816	4.680	6.543					
110	2.649	4.365	6.072					
120	2.496	4.065	5.621	2.396	4.015			
130	2.359	3.793	5.217					
140	2.242	3.553	4.862					
150	2.144	3.347	4.555	2.079	3.323			
160	2.069	3.177	4.296					
170	2.019	3.053	4.095					
175								
180	2.000	3.000	4.000	2.250	3.250			

TABLE III

HIGH-FREQUENCY VALUES OF Ω

Dependence of $\Omega_H^{(K)}$ on a for $-1\leq K\leq 3$, as calculated numerically from (21) and (35). $\hat\Omega_H^{(K)}$ is derived from the approximation for large λ, (52) and (35). $\tilde\Omega_H^{(K)}$ is derived from the shallow-shell approximation, (61).

a	$\Omega_H^{(-1)}$	$\Omega_H^{(o)}$	$\Omega_H^{(1)}$	$\Omega_H^{(2)}$	$\Omega_H^{(3)}$	$\hat\Omega_H^{(-1)}$	$\hat\Omega_H^{(o)}$	$\hat\Omega_H^{(1)}$	$\tilde\Omega_H^{(o)}$	$\tilde\Omega_H^{(1)}$
0									∞	∞
10									12.36	32.43
15										
20		6.321					6.276		6.258	16.30
30		4.354	10.85				4.309	10.82	4.270	10.85
40		3.411	8.177						3.318	8.311
50		2.878	6.582	10.36						
60		2.546	5.527	8.658			2.511	5.518		
70		2.327	4.782	7.447	10.13					
80		2.177	4.231	6.543	8.884					
90		2.070	3.810	5.844	7.917		2.073	3.812		
100	1.009	1.992	3.461	5.290	7.146	1.009				
110	1.036	1.935	3.220	4.841	6.519	1.038				
120	1.083	1.891	3.011	4.473	6.001	1.098	1.948	2.812		
130	1.156	1.861	2.844	4.168	5.567	1.225				
140	1.262	1.840	2.715	3.917	5.203	1.391				
150	1.408	1.836	2.625	3.717	4.901	1.559	1.895	2.842		
160	1.560	1.879	2.604	3.588	4.671					
170	1.674	2.010	2.733	3.634	4.607					
175	1.687	2.056	2.822	3.755	4.734					
180	1.689	2.070	2.853	3.810	4.818		2.239	3.086		

TABLE IV

LOW-FREQUENCY VALUES OF Ω

Dependence of $\Omega_L^{(K)}$ on α for $K = 1, 2, 3$, as calculated numerically from (21) and (35). $\tilde{\Omega}_L^{(K)}$ is derived from the approximation for large λ, (52) and (35). $\hat{\Omega}_L^{(K)}$ is derived from the shallow-shell approximation, (59).

α	$\Omega_L^{(1)}$	$\Omega_L^{(2)}$	$\Omega_L^{(3)}$	$\tilde{\Omega}_L^{(1)}$	$\tilde{\Omega}_L^{(2)}$	$\hat{\Omega}_L^{(1)}$	$\hat{\Omega}_L^{(2)}$	$\hat{\Omega}_L^{(3)}$
0	1.000	1.000	1.000			1.000	1.000	1.000
10						.997	.999	1.000
20	.988					.988	.996	.998
30	.974			.974	.992	.972	.992	.996
40	.957	.986		.957		.851	.986	.993
50	.938	.979				.824	.978	.990
60	.919	.871	.985	.922	.971			
70	.901	.963	.981					
80	.885	.956	.976					
90	.870	.949	.973	.870	.949			
100	.854	.942	.969					
110	.838	.935	.965					
120	.820	.925	.959	.806	.923			
130	.801	.915	.953					
140	.782	.904	.946					
150	.765	.893	.940	.751	.892			
160	.750	.883	.933					
170	.739	.874	.926					
180	.734	.870	.923	.783	.887			

APPENDIX A

LIMITING BEHAVIOR OF FREQUENCY EQUATION
FOR SHALLOW SHELLS

In this Appendix we wish to derive the limiting form of Equation 20 as $a \to 0$. To this end we rewrite (20) as

$$\left(\frac{G}{\lambda} + \cot^2 a\right) P_\lambda - \cot^2 a \, \sec a \, P_{\lambda-1} = 0 \, . \tag{A-1}$$

Setting

$$\epsilon = 2 \sin\frac{a}{2} \, , \tag{A-2}$$

and using the approximations

$$\cot^2 a = \frac{1}{\epsilon^2} - 1 + O(\epsilon^2)$$

$$\cot^2 a \, \sec a = \frac{1}{\epsilon^2} - \frac{1}{2} + O(\epsilon^2) \, ,$$

Equation A-1 becomes

$$\frac{1}{\epsilon^2}\left(P_\lambda - P_{\lambda-1}\right) + \left(\frac{G}{\lambda} - 1\right) P_\lambda + \frac{1}{2} P_{\lambda-1} = 0 \, (\epsilon^2) \, . \tag{A-3}$$

From (33) we have

$$P_\lambda = J_0(a) + \frac{\epsilon^2}{4}\left[\frac{1}{2a} J_1(a) - J_2(a) + \frac{a}{6} J_3(a)\right] + O(\epsilon^4)$$

where

$$a = \left(\lambda + \frac{1}{2}\right) \epsilon \, , \tag{A-4}$$

and also

$$P_{\lambda-1} = J_0(a-\epsilon) + \frac{\epsilon^2}{4}\left[\frac{1}{2(a-\epsilon)} J_1(a-\epsilon) - J_2(a-\epsilon) + \left(\frac{a-\epsilon}{6}\right)J_3(a-\epsilon)\right] + O(\epsilon^4)$$

$$= J_0(a) + \epsilon J_1(a) - \frac{\epsilon^2}{4}\left[J_0(a) - J_2(a)\right] + \frac{\epsilon^2}{4}\left[\frac{1}{2a} J_1(a) - J_2(a)\right.$$

$$\left. + \frac{a}{6} J_3(a)\right] + O(\epsilon^3) \, .$$

where $J_o(a - \epsilon)$ has been expanded in a Taylor series about a, and the formulas for the derivatives of the Bessel functions have been used.

Then

$$\frac{1}{\epsilon^2}\Big(P_\lambda - P_{\lambda-1}\Big) = -\frac{1}{\epsilon} J_1(a) + \frac{1}{4}\Big[J_o(a) - J_2(a)\Big] + O(\epsilon) \; ,$$

and substituting into (A-3) gives

$$\Big(\frac{1}{4} - \frac{G}{\lambda}\Big)J_o(a) + \frac{1}{\epsilon} J_1(a) + \frac{1}{4} J_2(a) = O(\epsilon) \; .$$

Using (A-4) we obtain

$$\Big(\frac{1}{4} - \frac{G}{\lambda}\Big) J_o(a) + \left(\frac{\lambda + \frac{1}{2}}{a}\right) J_1(a) + \frac{1}{4} J_2(a) = O(\epsilon) \tag{A-5}$$

which is the limiting form of (20) as $\alpha \to 0$.

APPENDIX B

LIMITING BEHAVIOR OF THE FREQUENCY EQUATION NEAR $a = \pi$.

For this purpose we take (20) in the form

$$(G + \lambda \cot^2 a) \, P_\lambda(\cos a) - \lambda \cot^2 a \, \sec a \, P_{\lambda-1}(\cos a) = 0 \qquad \text{(B-1)}$$

and let $a = \pi - \sigma$, whence

$$\cot^2 a = \frac{1}{\sigma^2} - 1 + O(\sigma^2)$$

$$\sec a = -1 - \frac{\sigma^2}{2} + O(\sigma^4)$$

Using these in (B-1), we get

$$\frac{\lambda}{\sigma^2}(P_\lambda + P_{\lambda-1}) + (G - \lambda) P_\lambda - \frac{\lambda}{2} P_{\lambda-1} = O(\sigma^2) . \qquad \text{(B-2)}$$

Now the formula (25) will be used to obtain the leading terms in the behavior of $P_\lambda(\cos a)$ and $P_{\lambda-1}(\cos a)$ near $a = \pi$. We obtain

$$P_\lambda(\cos a) = \frac{\sin \lambda\pi}{\pi}\left\{ H\left(1 - A\frac{\sigma^2}{4}\right) + \frac{\sigma^2}{4}\left(1 + 2A\right) + O(\sigma^4 \ln \sigma)\right\}$$

$$P_{\lambda-1}(\cos a) = - \frac{\sin \lambda\pi}{\pi}\left\{ H\left(1 - A\frac{\sigma^2}{4} + \frac{\lambda\sigma^2}{2}\right) - \frac{2}{\lambda} + \frac{\sigma^2}{4}(1 + 2A - 2 - 2\lambda)\right.$$
$$\left. + O(\sigma^4 \ln \sigma)\right\}$$

where

$$A = \lambda(\lambda + 1)$$

$$H = 2 \log \sin\left(\frac{1}{2}\sigma\right) + \psi(\lambda) + \psi(- \lambda - 1) - 2 \psi(0) \qquad \text{(B-3)}$$

and repeated use has been made of the identity

$$\psi(t) = \psi(t - 1) + \frac{1}{t} .$$

From this the relation

$$\frac{\lambda}{\sigma^2}\left(P_\lambda + P_{\lambda-1}\right) = \frac{\sin \lambda\pi}{\pi}\left\{\frac{2}{\sigma^2} + \frac{A}{2} - \frac{H \lambda^2}{2} + O(\sigma^2 \ln \sigma)\right\}$$

follows. Putting this and the previous expressions into (B-2) we obtain

$$\frac{\sin \lambda \pi}{\pi} \left\{ \frac{2}{\sigma^2} + H\left(G - \frac{A}{2}\right) + \frac{A}{2} - 1 + O\left(\sigma^2 \ln \sigma\right) \right\} = 0 .$$

In (B-3) use is made of the identity

$$\pi(- \lambda - 1) = \psi(\lambda) + \pi \cot \lambda \pi$$

so that

$$H = 2\left[\log \sin \frac{\sigma}{2} + \psi(\lambda) - \psi(0)\right] + \pi \cot \lambda \pi .$$

Then (B-2) can be written

$$\frac{\sin \lambda \pi}{\pi} \left\{ 2 + \sigma^2 \left(G - \frac{A}{2}\right)\left[2 \log \sin\left(\frac{\sigma}{2}\right) + 2\psi(\lambda) - 2\psi(0) + \pi \cot \lambda \pi\right] \right.$$

$$\left. + \sigma^2 \left(\frac{A}{2} - 1\right) + O\left(\sigma^4 \ln \sigma\right) \right\} = 0. \qquad (B-4)$$

This formula, B-4, is the desired limiting form of (20) when $\alpha \to \pi$.

APPENDIX C

NUMERICAL COMPUTATION OF λ AND Ω

The numerical computation of λ and Ω for various a - values is based on (35) and either (21) or (19). In a great majority of the calculations (35) and (21) were used, and so we shall describe the process of solution for that case first.

By means of (35) M can be calculated if λ is given, hence we may regard (21) as a single transcendental equation for λ. However, there are usually two values of M, which we have called M_H and M_L, for each λ - value, and so the transcendental equation for λ changes slightly with the choice of M. Choosing M_H leads to frequencies of the higher family, choosing M_L leads to frequencies of the lower family, and within each family there are of course several solutions for M and λ corresponding to the different branches (i.e., K - values). In describing the process below, we consider the problems of finding just one root (i.e., a single λ and a single M), taking the same choice of M throughout, and keeping a fixed.

If our transcendental equation is denoted by

$$E(\lambda) = 0$$

then the process starts with an initial guess for λ and $\Delta\lambda$. The basic process consists of calculating new values $\overline{\lambda}$ and $\overline{\Delta\lambda}$ from the formulas

$$\overline{\lambda} = \lambda - \frac{E(\lambda)}{S(\lambda)}$$

$$\overline{\Delta\lambda} = -\frac{E(\overline{\lambda})}{S(\lambda)}$$

where

$$S(\lambda) = \frac{E(\lambda + \Delta\lambda) - E(\lambda)}{\Delta\lambda} .$$

This process is continued until $E(\lambda)$ becomes small and successive values of λ differ by a sufficiently small amount, at which point M and finally Ω are calculated. This basic process was changed somewhat in practice to insure that at each step $E(\lambda + \Delta\lambda)$ and $E(\lambda)$ had opposite signs. The resulting values of λ and Ω in Tables I to IV have errors that do not exceed 1×10^{-3} in absolute value.

The above process was used for all the branches of both the high- and low-frequency families except the portion of the high-frequency curve for $K = -1$ that has $\lambda = -\frac{1}{2} + ib$. For these points (19) was used instead of (21), and in the numerical analysis b played the role of λ in the above description, see below.

Except in the case where $\lambda = \frac{1}{2} + ib$, the Legendre functions for $0 < a \leq 90°$ were all calculated from (22) and for $90° < a < 180°$ from (25). When $\lambda = -\frac{1}{2} + ib$ the quantities $P_{-\frac{1}{2}+ib}(\cos a)$ and $dP_{-\frac{1}{2}+ib}(\cos a)/da$ were calculated from the following formulas, derivable from those given in Reference 6.

$$P_{-\frac{1}{2}+ib}(\cos a) = P_{-\frac{1}{2}+ib}(0) \, U(x^2) - \frac{\cosh b\pi}{\pi P_{-\frac{1}{2}+ib}(0)} \, x \, V(x^2)$$

$$\frac{dP_{-\frac{1}{2}+ib}(\cos a)}{da} = \sin a \left\{ - \left(b^2 + \frac{1}{4} \right) x \, U'(x^2) P_{-\frac{1}{2}+ib}(0) \right.$$
$$\left. + \frac{\cosh b\pi}{\pi P_{-\frac{1}{2}+ib}(0)} \left[V(x^2) + \frac{\left(\frac{9}{4} + b^2 \right)}{3} x^2 \, V'(x^2) \right] \right\}$$

where $U(x^2)$, $V(x^2)$, $U'(x^2)$, $V'(x^2)$ are defined by

$$x = \cos a, \quad A = - \left(b^2 + \frac{1}{4} \right) = \lambda(\lambda + 1)$$

$$U(x^2) = \sum_{n=0}^{\infty} U_n(x^2), \quad V(x^2) = \sum_{n=0}^{\infty} V_n(x^2)$$

$$U'(x^2) = \sum_{n=0}^{\infty} U'_n(x^2), \quad V'(x^2) = \sum_{n=0}^{\infty} V'_n(x^2)$$

$$U_0 = V_0 = U'_0 = V'_0 = 1$$

$$U_n/U_{n-1} = x^2 \left[1 - \frac{1}{n} - \frac{1}{2n} \frac{A}{(2n-1)} \right]$$

$$V_n/V_{n-1} = x^2 \left[1 - \frac{1}{n} - \frac{1}{2n} \left(\frac{A-2}{2n+1} \right) \right]$$

$$U'_n/U'_{n-1} = x^2 \left[1 - \frac{1}{2n} \frac{A}{(2n+1)} \right]$$

$$V'_n/V'_{n-1} = x^2 \left[1 - \frac{1}{2n} \frac{A-2}{(2n+3)} \right] .$$

The frequency equation (19) reduces to

$$[1 + (1 + \nu)M]U(x^2) + Ax^2 U'(x^2) + \frac{(-x)\cosh b\pi}{\pi[P_{-\frac{1}{2}+ib}(0)]^2} \left[(1 + \nu)MV(x^2) + \left(\frac{A-2}{3} \right) x^2 V'(x^2) \right] = 0 .$$

and this (together with Equation 35), was then solved for b, and so
Ω , by the process described above.

The author wishes to thank Mr. James MacLaughlin who did
the programming and carrying out of these computations on the IBM
1620 computer at the Army Materials Research Agency.

REFERENCES

1. NAGHDI, P. M., and KALNINS, A.   On Vibrations of Elastic
   Spherical Shells.   Journal of Applied Mechanics, Transac-
   tions ASME, Series E, v. 84, 1962, p. 65-72.

2. LOVE, A. E. H.   The Small Free Vibrations and Deformation of
   a Thin Elastic Shell.   Philosophical Transactions of the Royal
   Society, London, Series A, v. 179, 1888, p. 491-546.

3. LAMB, H.   On the Vibrations of a Spherical Shell.   Proceedings
   of the London Mathematical Society, London, v. 14, 1882,
   p. 50-56.

4. REISSNER, E.   On Axi-Symmetrical Vibrations of Shallow, Spher-
   ical Shells.   Quarterly of Applied Mathematics, v. 13, 1955,
   p. 279-290.

5. NAGHDI, P. M., and KALNIN, S. A.   Axi-Summetric Vibrations
   of Shallow Spherical Shells.   Journal of the Acoustical Society
   of America, v. 32, 1960, p. 342-347.

6. ERDELYI, A., et al.   Higher Transcendental Functions., v. 1.
   McGraw-Hill Co., New York, 1953, p. 120-181.

COORDINATE SYSTEMS AND ERROR ANALYSES[*]

Hodge W. Doss, Jr.
Institute of Science and Technology,
The University of Michigan

Air traffic control, air defense and other surveillance systems are dependent on the accurate location of objects in three dimensional space. In connection with the evaluation of such systems, it is paramount to know how location accuracy has been designed into the system. Acquisition, tracking and data transmission accuracy are concerned with three important system functions which need to be considered. The design of these functions are determined by geometrical consideration as well as hardware state-of-the-art considerations. It is the purpose of this paper to delve into these functions and illustrate a procedure by which one can formulate a model of the system in question. Such models enable one to conduct step by step error analyses of target location accuracy.

Figure 1 is a block diagram of a possible system. Illustrated are system functions which provide the means by which coordinate data is obtained, processed and transmitted to remote center for decision making. The functions shown do not correspond to any particular system and are given here only as hypothetical examples.

An evaluation of a data-processing system which utilizes coordinate date (geographically oriented with respect to different locations in the system) requires extensive knowledge of the mathematical relations involved in the orientation of this system. Coordinate-data accuracy is dependent on the type of system function employed, and is closely related to the mathematical model used in the design of system functions. Evaluation techniques are dependent on the coordinate transformations which are accomplished by the system.

In Figure 2, we have indicated how target coordinate data might be handled by the functions of a hypothetical system. The target is introduced as having a longitude, latitude, and height above sea level. A radar at a point on the ground sees this position as a slant range, azimuth,

---

Fig. 1

Target → Sensor → Coordinate Data Converter → Transmitter → Receiver → Tracking Correlation Prediction → Transmitter Receiver → Decision Action → Target

Fig. 2

λ, L, h — τ_1 → r, θ, α — η → x, y, h Analog — ν → x, y, h Digital — τ_2 → u, ν, h — ρ → $\bar{u}, \bar{\nu}, \bar{h}$ — τ_3 → X, Y, H — δ → $\Delta\lambda, \Delta L, \Delta h$
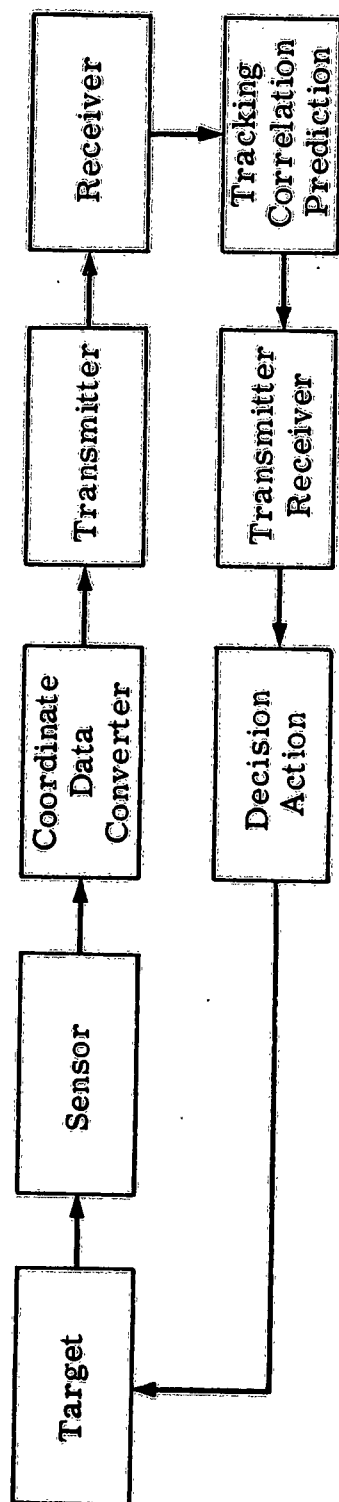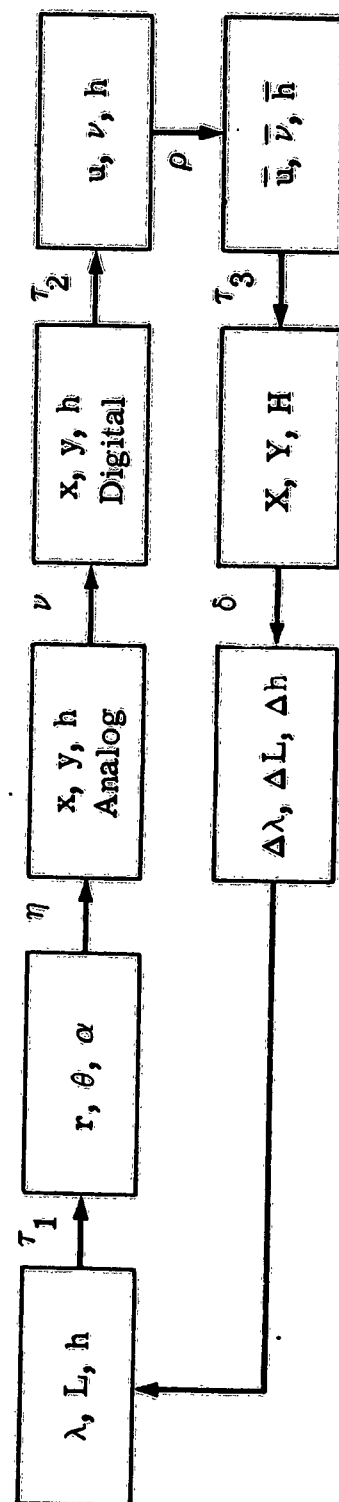
and angle of elevation. These data then appear, after going through
the coordinate conversion, as analog x, y, h coordinates. Coordinates
are then transformed by the analog to digital converter into a digital
form of x, y, h. In quantitized form, the data is then pulse code modulated
for transmission and sent to a central receiving section which is
physically remote to the sensor. It appears there as u, v, h, which are
transformed versions of the x, y, h. In the tracking and correlation
function, we find that u, v, h for one sighting are put together with
other sightings in a correlation and tracking phase. Eventually $\bar{u}, \bar{v}, \bar{h}$
are produced as the best or most likely position of the target. This
track position is then possibly sent to some other location, in which
case the coordinates would appear there as a transformed version of
$\bar{u}, \bar{v}, \bar{h}$ which we have denoted as X, Y, H. These final target location
values are then used in the system for ACTION relative to the target.
In an air traffic control situation, for example, the action could be to
give a new altitude or new velocity vector. Although the velocity
vector has not been shown in the diagram of Figure 2, one expects
that such systems predict positions periodically and include a velocity
vector for each of the targets in the system.

Relative to the figures which we have seen and the illustrated
system functions, we wish to define a set of coordinate mappings which
illustrate mathematically the action taken by the system. In Figure 2,
we have indicated coordinate mappings by lower case Greek letters
placed on the arrows which connect the blocks of the diagram. We
define these mappings in the following way. There exists a set of
functions f_1, f_2, and f_3 such that

$$r = f_1(\lambda, L, h),$$

and

$$\theta = f_2(\lambda, L, h),$$

$$\alpha = f_3(\lambda, L, h).$$

f_1, f_2, and f_3 are defined in terms of (λ_R, L_R, h_R) the geographical
coordinates of the sensor. Let τ_1 denote the combined effect of f_1,
f_2, and f_3 on (λ, L, h) as inputs to obtain (r, θ, α). Thus τ_1 is a
mapping such that

$$(\lambda, L, h) \xrightarrow{\quad \tau_1 \quad} (r, \theta, \alpha).$$

τ_1 is a symbol for a system operation and also a symbol for a mathematical mapping of coordinate data. Similarly η is the mapping which maps radar coordinates into (x, y, h). Under more usual circumstances, η would map (r, θ, α) into (x, y, z). However, as an illustrative example, we will use a stereographic projection to define η such that $\eta(r, \theta, \alpha) = (x, y, h,)$. Each of the succeeding maps indicated in Figure 2 operate similarly and are defined to agree with this figure. τ_1 combined with η, as a series map, is indicated by the product $\eta \tau_1$, where the order agrees with regular functional notation.

So far we have considered only a relatively simple example in which a series block diagram is considered. However, in many systems, coordinate dat. is prepared by parallel operations. For example, a surveillance radar may provide slant range and azimuth while a height finder radar provides the height information. The parallel output from these two devices is then combined to form a three-dimensional picture of target location. In order to show this, we can combine mappings by using addition. Thus τ_{11} and τ_{12} may be the respective mappings of λ, L and h by the surveillance radar and the height radar. We then could indicate the overall mapping as $\tau_{11} + \tau_{12}$ operating on (λ, L, h) to produce two vector quantities which are (r, θ, O) and (O, O, z).

Hence our mapping diagram for τ_1 is replaced by
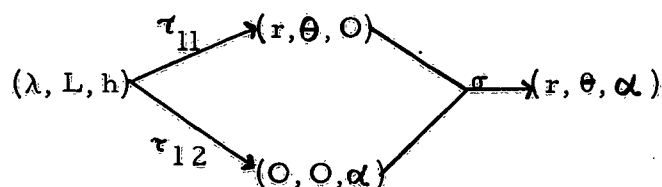
σ may be nothing more than a computer storage of (r, θ, α) and, for most pilot model constructions, would not be considered as a change in coordinates. If σ implied a round off procedure, however, then it would be quite important. In any case, we now have

$$\tau_1 = \sigma(\tau_{11} + \tau_{12}).$$

Letting

$$\Psi = \delta\, \tau_3\, \rho\, \tau_2\, \nu\, \eta\, \tau_1,$$

we have

$$(\lambda, L, h) \xrightarrow{\ \Psi\ } (\Delta\lambda,\ \Delta L,\ \Delta h)$$

as a model of the system. The individual mappings symbolized here are exact mathematical expressions which relate the contents of two adjoining blocks in the block diagram; hence Ψ is the exact mathematical model of our hypothetical system. In general Ψ is a combination of computable functions and may be programmed directly as a computer pilot model. We might remark at this point that our model, so far, is open ended. Should it be desirable, a mapping K could be defined to close the loop. Feedback in an automatic pilot control system could be the system function represented. In this case, our model would be

$$\Psi' = K\, \delta\, \tau_3\, \rho\, \tau_2\, \nu\, \eta\, \tau_1.$$

For hardware design of such systems, each of these mappings must be performed by a component or sub-system. In the process of generating such a design, approximations to the exact mappings are used in order to simplify the hardware. Thus, in the case of the sensor mapping τ_1 or $(\tau_{11} + \tau_{12})$ there are approximations which we shall denote by $\overline{\tau}_1$. $\overline{\tau}_1, \overline{\eta}, \overline{\nu}$ and, in general, the collective form $\overline{\Psi}$ are the designer's approximation to the exact mathematical conversions and transformations.

Let $\hat{\Psi}$ be the hardware approximation to $\overline{\Psi}$ and $\tilde{\Psi}$ the operational system approximation to $\hat{\Psi}$. $\tilde{\Psi}$ must be measured in the field and obtained by analysis of emperical data. $\hat{\Psi}$ can, for the most part, be obtained in the more controlled atmosphere of a laboratory. The system errors in which we are interested are like

$$\epsilon_1 = \psi(\lambda, L, h) - \overline{\psi}(\lambda, L, h)$$

$$= (\Delta\lambda, \Delta L, \Delta h) - (\Delta\overline{\lambda}, \Delta\overline{L}, \Delta\overline{h}),$$

$$\epsilon_2 = (\Delta\overline{\lambda}, \Delta\overline{L}, \Delta\overline{h}) - (\Delta\hat{\lambda}, \Delta\hat{L}, \Delta\hat{h}),$$

$$\epsilon_3 = (\Delta\lambda, \Delta L, \Delta h) - (\Delta\hat{\lambda}, \Delta\hat{L}, \Delta\hat{h})$$

and
$$= \epsilon_1 + \epsilon_2 ,$$

$$\epsilon_4 = (\Delta\lambda, \Delta L, \Delta h) - (\Delta\tilde{\lambda}, \Delta\tilde{L}, \Delta\tilde{h})$$

Once the errors of interest have been chosen, then one may use this procedure to conduct a step by step error analysis.

For an illustrative example, we turn to a specific problem area. In sending radar coordinate information oriented to the geographical location of the user, two problems arise: (1) the conversion of target location parameters to an easily transformed and easily transmitted code, and (2) the transformation of the converted parameters to another coordinate system. Approximations are required which make conversions, transformation, and transmission of data as simple and rapid as possible while maintaining required accuracy. It has been shown by Dr. Goldenberg and E. Wolf that approximations to a stereographic projection have many of the desired properties.[1]

The stereographic projection of a spherical earth presents an interesting illustration of an η and a τ, conversion and transformation, respectively. In Figure 3a and 3b, the stereographic projection image T' of a target T is shown relative to the radar coordinates of T. To obtain T', a line segment is drawn between T and C , where C is the center of the earth. T", as shown is then projected stereographically

---

[1] See Reference 1.

from $\overline{S}$ onto the target at S to give T' as the image point. The x and y coordinates of T' are called the stereographic coordinates of T. Let h be the distance $\overline{TT''}$ in Figure 3a. h is the sea-level altitude of T and is invariant under changes in the location of S. An $(x, y, h,)$ represents a unique point in space. Let x_t and y_t be the x, y coordinates of P. Then x_t, y_t, and z_t are Cartesian coordinates of T with origin at S.

After using the law of cosines on triangle CST and making a few trigonometric manipulations, one finds that

$$h = \sqrt{E^2 + 2E\, z_t + r^2} \; - E,$$

and

$$x = D \sin \theta,$$

$$y = D \cos \theta,$$

where

$$D = \left(1 + \frac{h}{E} - \frac{r^2 - h^2}{4E^2}\right)^{\frac{1}{2}} (r^2 - h^2)^{\frac{1}{2}} = \mu_1 (r^2 - h^2)^{\frac{1}{2}}$$

or

$$D = \left(1 + \frac{h}{E} - \frac{r^2 - h^2}{4E^2}\right)^{-1} (r^2 z_t^2)^{\frac{1}{2}} = \mu_2 (r^2 - z_t^2)^{\frac{1}{2}}.$$

Let η represent the three equations which give x, y and h. An interesting approximation $\overline{\eta}$ for η is given by

$$h \cong z_t + \frac{r^2}{2E}$$

and

$$D \cong (r^2 - h^2)^{\frac{1}{2}}$$
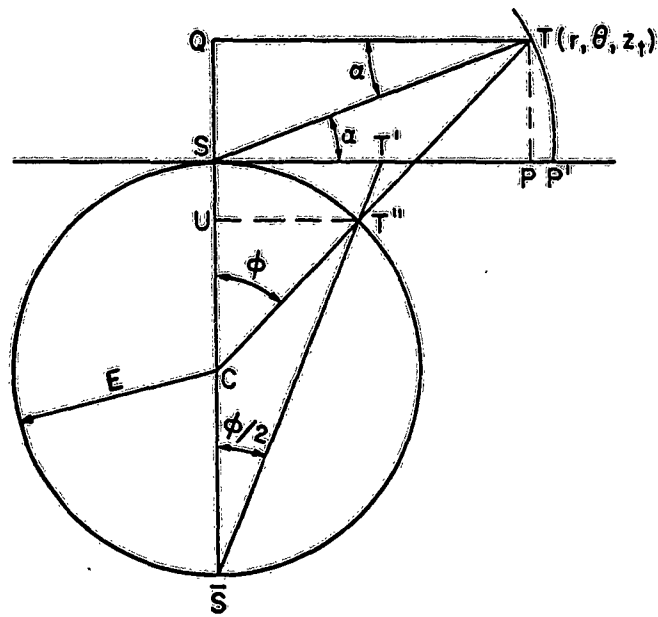
or

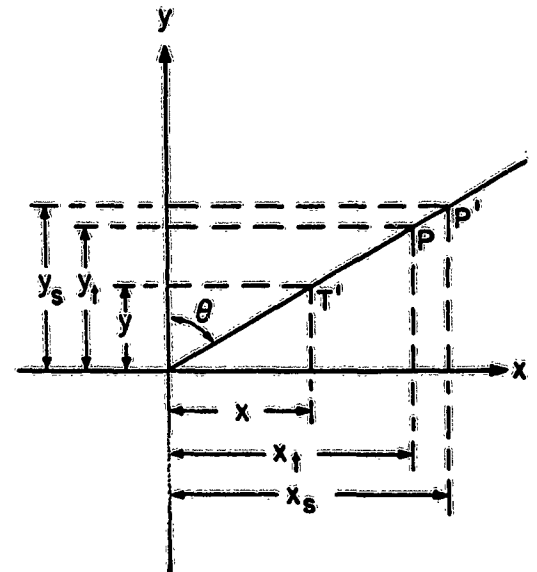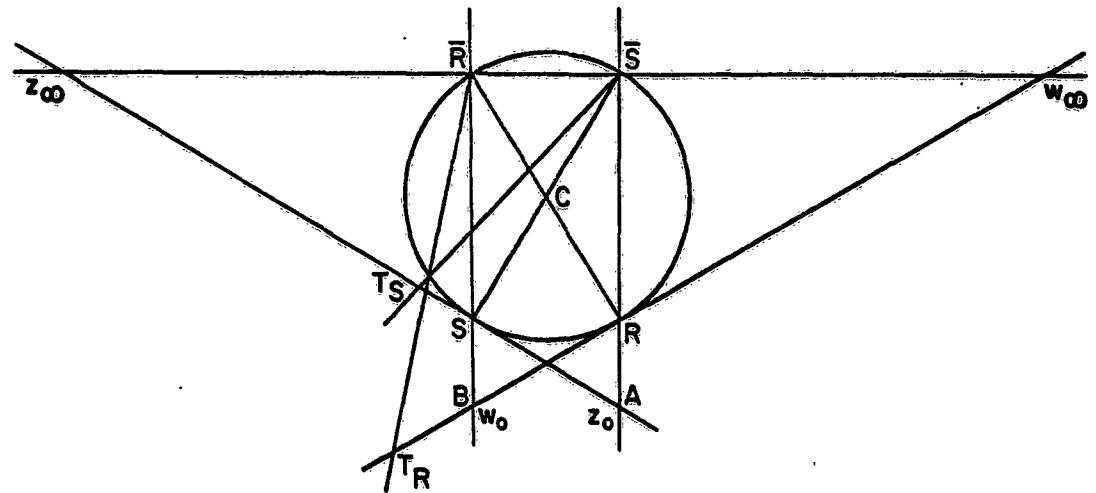$$D \cong .999 \, (r^2 - z_t^2)^{\frac{1}{2}}.$$

Figure 3a

Figure 3b

Figure 4

The approximations for D are obtained by assuming $\mu_1 \overset{\sim}{=} 1$ and $\mu_2 \overset{\sim}{=}$ .999. η and $\bar{\eta}$ are example conversion mappings and we shall refer to them later.

Transformation of stereographic coordinates from one tangent plane to another consists of an inverse stereographic projection from the S-plane to the sphere followed by a stereographic projection into the R-plane. Let $z = x+iy$ and $w = u+iv$. In Figure 4, T_S, the stereographic image of T in the S-plane, is at z and T_R, the corresponding image of T in the R-plane, is at w. Let $\tau_2(z) = w$ be the desired mapping. As the product of two conformal maps, it is conformal. This mapping is also 1-1 and hence analytic. From the geometry shown in Figure 4, we see that z_0 is the only zero of τ_2 and z_∞ is the only singular point. Since this analytic mapping has only one zero, one pole, and no other essential singularities, then, by well-known theorems about analytic functions, τ_2 is a linear fractional transformation of the form

$$w = \tau_2(z) = \frac{a+bz}{c+dz} \quad .$$

Using triangle congruency and similarity implications, $a, b, c,$ and d can be evaluated to give

$$w = \tau_2(x, y) = \frac{w_0 + ze^{-i\beta}}{1 - \frac{\bar{w}_0}{4E^2} ze^{-i\beta}} \quad .$$

where $w_0 = u_0 + iv_0$, $\bar{w}_0$ is the complex conjugate of w_0 and β is an orientation angle satisfying

$$\frac{w_0}{z_0} = -e^{-i\beta} \quad .$$

Using a spherical model of the earth, (λ_s, L_s) as the longitude and latitude of S, and (λ_R, L_R) as the geographical coordinates of R, one can use spherical trigonometry to show that

$$u_0 = 2E \frac{\sin \Delta\lambda \cos L_S}{1 + \sin L_R \sin L_S + \cos L_R \cos L_S \cos \Delta\lambda},$$

$$v_0 = 2E \frac{\sin L_S \cos L_R - \cos L_S \sin L_R \cos \Delta\lambda}{1 + \sin L_R \sin L_S + \cos L_R \cos L_S \cos \Delta\lambda}.$$

and

$$\tan \beta = \frac{\sin \Delta\lambda (\sin L_S + \sin L_R)}{\cos \Delta\lambda + \cos \Delta\lambda \sin L_S \sin L_R + \cos L_S \cos L_R},$$

with $\Delta\lambda = \lambda_R - \lambda_S$.

A series expansion of τ_2 produces

$$\tau_2(z) = w_0 + (1 + \frac{|w_0|^2}{4E^2}) \sum_{n=0}^{\infty} \frac{|w_0|^n D^{n+1}}{(4E^2)^n} e^{i \cdot [\pi - \theta + \beta - n(\theta - \beta - \gamma)]},$$

where

$$D = |z| \quad \text{and} \quad \gamma = \tan^{-1} \frac{v_0}{u_0}.$$

β has been replaced by $-\beta$ in this expansion to conform with the azimuth orientation of θ and γ. In component form, the first three terms of this series are

$$u = u_0 + k D \sin(\theta - \beta) + \frac{k |w_0| D^2}{4E^2} \sin [2(\theta - \beta) - \gamma]$$

$$v = v_0 + k D \cos(\theta - \beta) + \frac{k |w_0| D^2}{4E^2} \cos [2(\theta - \beta) - \gamma],$$

where

$$k = 1 + \frac{|w_0|^2}{4E^2}.$$

Let $\bar{\tau}_2$ be the approximation to τ_2 given by the above equations for u and v. The error in using $\bar{\tau}_2$ is

$$\left| \bar{\tau}_2(z) - \tau(z) \right| \cong \frac{\left| w_o \right|^2 D^3}{(4E^2)^2} \quad .$$

The error in $\bar{\eta}$, as discussed earlier, amounts to the assumption that

$$\text{(a)} \quad \mu_1 = (1 + \frac{h}{E} - \frac{r^2 - h^2}{4E^2})^{-\frac{1}{2}} \cong 1$$

and

$$\text{(b)} \quad h \cong z_t + \frac{r^2}{2E} \quad .$$

It can be shown[2] that $\mu_1^2 = \mu_2$ and

$$\frac{E}{E+h} < \mu_2 < \frac{E}{E+z_t} \quad .$$

Hence

$$\sqrt{\frac{E}{E+h}} < \mu_1 < \sqrt{\frac{E}{E+z_t}} \quad .$$

Thus, the greatest possible error given by (a) is bounded by

$$\epsilon_\mu = \sqrt{\frac{E}{E+h}} - 1$$

$$\cong - 0.00145 \quad .$$

_____

[2] A derivation of this result and a more extensive development for η and τ by stereographic projection is given in Reference 2.

If $h = 10$ nautical miles and $E = 3440$ nautical miles, $\overline{D}$, the approximate stereographic range, would be off by no more than -203 yards in each 100 nautical miles. The error in (b) is easily seen to be

$$\epsilon_h = \overline{h} - h = \frac{h^2}{2E} \quad ,$$

where $\overline{h}$, is obtained by (b). With h and E as before,

$$\epsilon_h = 20 \text{ yards}.$$

The output from the pilot models and analysis models which we have described are in the form of

$$\Delta V = V - \overline{V} ,$$

where V is a vector and $\overline{V}$ is an approximation to it. An analysis is needed to summarize and determine relationships between the set $\{\Delta V\}$ and system performance. A straightforward approach can be used to measure and predict accuracy of target location. By bringing in the purpose of such a system, one begins the evaluation of said system in terms of its mission. We have found in the past that a theory of system performance, and hence system control, has best been approached through a process of curve fitting to a polynomial in a number of variables. Heretofore most of this analysis has taken the form of a linear regression analysis. However, we are now considering extension to higher degree polynomials. A recent article[3] by John E. Walsh, of the System Development Corporation, on linearized nonlinear regression, provides a procedure for extension in Monte Carlo models.

This problem of curve fitting has been met before in the analysis of empirical data collected during field tests. In the type of computer pilot models that we are discussing, we have control of replication combined with a high degree of similitude relative to those system attributes under study. These pilot model representations are made with respect to hard-

---

[3] See Reference 3.

ware and the physical theories of hardware operation. The outputs from pilot models are very similar to real system outputs and, by analogy, similar analysis procedures appear reasonable. Moreover, serious play with pilot model and analysis procedures suggests new developments in each. We have only just begun this pilot model work at Michigan and our results so far are few and fragmentary. However, results to date are interesting and our intuitions appear justified.

In large scale systems design, error implications from a $\bar{\Psi}$ system design have often taken the form, in series type operations, of assuming the maximum error in target location to be the sum of the maximum errors in each step. Coupled with total recognition of electronic netting, these computer pilot models and corresponding analysis procedures should provide a more comprehensive design evaluation. In particular, coordinate systems, system geometry, and the corresponding netting procedures can be evaluated through pilot model calculations and analysis procedures similar to those discussed during this presentation. Probably the most important factor illustrated by this discussion is the possibility of synthesizing, from design specifications, a pilot model for eventual evaluation of system design. In so doing, one realizes the possibility that hardware design should include special considerations for built-in analysis procedures to be used for evaluation of the operational system.

REFERENCES

1. D. Goldenberg and E. Wolf, "A Common Coordinate System for the Utilization of Data from Several Radars," Technical Report No. 67, Lincoln Laboratory, Massachusetts Institute of Technology, Lexington, Mass., 13 September 1954 (UNCLASSIFIED).

2. Hodge W. Doss, Jr. et al, "A Description of Coordinate Conversion and Transformation in the SAGE and Missile Master Systems, Vol. 1," Report No. 2354-30-T, Institute of Science and Technology, The Univ of Michigan, Ann Arbor, Michigan, January 1961 (UNCLASSIFIED).

3. John E. Walsh, "Use of Linearized Nonlinear Regression for Simulations Involving Monte Carlo," Journal of the Operations Research Society of America, Vol. 11, No. 2, 228-235 (1963)

STABILITY OF CURVED FLOWS*

R. C. DiPrima
Department of Mathematics,
Rensselaer Polytechnic Institute, Troy, N. Y.

In this paper we will be concerned with reviewing the formulation of the linear hydrodynamic-stability problem for a viscous fluid between two infinitely long concentric rotating cylinders, a discussion of several related problems, and a discussion of recent work on nonlinear effects.

The general problem of the hydrodynamic stability of a viscous incompressible flow can be stated as follows: Consider a velocity distribution $\vec{v}(x,y,z)$, and pressure field $p(x,y,z)$ which are an exact time-independent solution of the Navier-Stokes equations. Suppose that at an initial time $t = 0$ this solution is slightly perturbed by arbitrary small disturbances, $\vec{v}'(x,y,z,t)$ in the velocity, and $p'(x,y,z,t)$ in the pressure. If the disturbances die out as $t \to \infty$, the flow is said to be stable; otherwise it is unstable. According to this definition an unstable flow does not necessarily lead to a turbulent motion; it may lead to a new laminar motion. Indeed, as we shall see, it is the latter situation which occurs in the stability of a viscous fluid between two concentric rotating cylinders.

In general, the basic time-independent flow field can be characterized by a Reynolds number $R = Vl/\nu$ where V and l are a representative velocity and length, and ν is the kinematic viscosity. For sufficiently small values of R we can anticipate that, because of the action of viscosity, all disturbances will be damped out, but as R is increased there will eventually be a value, say, R_c such that for $R > R_c$ at least one disturbance will not die out as $t \to \infty$. It is the determination of R_c, its dependence on the other parameters of the problem, and the form of the initially unstable disturbance which are of primary interest.

To solve the foregoing stability problem, it is necessary to trace the behavior in time of the solution of a very complicated system of nonlinear partial differential equations which also satisfies a set of homogeneous boundary conditions and given initial conditions. This is clearly a formidable problem and, for this reason, most investigations to date have only considered the linear-

---

stability problem obtained by neglecting quadratic terms in the disturbance quantities. In this case we obtain a system of linear partial differential equations for $\vec{v}'$ and p', in which time enters only through the term $\partial \vec{v}'/\partial t$. There are two standard methods of solving the linear-stability problem. One is to take a Laplace transform in time (thus introducing the initial conditions into the differential equations as nonhomogeneous terms), solve the resulting system of equations subject to the prescribed boundary conditions, take the inverse transform and study $\vec{v}'$ as $t \longrightarrow \infty$.

However, it is more common in practice to use a normal-mode analysis. It is clear because of the way in which time enters that if we separate variables by assuming $\vec{v}'(x, y, z, t) = T(t)\vec{v}''(x, y, z)$ and a similar expression for p', then $T(t) = e^{\sigma t}$. The functions $\vec{v}''$ and p'' must satisfy a system of linear homogeneous partial differential equations, and v'' a set of homogeneous boundary conditions. In general, nontrivial solutions will exist only for certain values of σ, the eigenvalues of the problem. If the corresponding systems of eigenfunctions or normal modes are complete in the sense that any arbitrary initial disturbance can be represented as a superposition of the normal modes, the two approaches will be equivalent.[1]

In this paper we will use the method of normal modes. Recalling what we said earlier about a critical Reynolds number, we can anticipate that for R sufficiently small __all__ of the eigenvalues will have real part of $\sigma < 0$, ($\mathrm{Re}\ \sigma < 0$); and hence any disturbance will die out. However, for $R > R_c$ there will be at least one eigenvalue with $\mathrm{Re}\ \sigma > 0$ which will lead to an exponentially growing mode, and the flow will be unstable. The value R_c is determined by the condition that at $R = R_c$ there are no eigenvalues with $\mathrm{Re}\ \sigma > 0$, but that there is at least one with $\mathrm{Re}\ \sigma = 0$ which becomes positive if R is increased beyond R_c.

---

[1] For an example of a stability problem for which the methods are not equivalent, see the paper by G. F. Carrier and C. T. Chang, "On an Initial Value Problem Concerning Taylor Instability of Incompressible Fluids," Quarterly of Applied Mathematics, Vol. 16, 1959, pp. 436-439. Also for recent related work see K. M. Case, "Hydrodynamic Stability and the Inviscid Limit," Journal of Fluid Mechanics, vol. 10, 1961, pp. 420-429; and C. C. Lin, "Some Mathematical Problems in the Theory of the Stability of Parallel Flows." Journal of Fluid Mechanics, vol. 10, 1961, pp. 430-438.

Even with the simplification introduced by linearizing the disturbance equations, the general eigenvalue problem is still prohibitive since we must solve a system of partial differential equations with three independent variables. With a few exceptions, in particular, some of the problems of interest in meteorology, attention has been focused on problems in which the basic velocity has only one nonzero component, and both the velocity and pressure distribution are functions of but one space variable. In this case it is possible to separate the dependence of the disturbance quantities on the two missing space variables and obtain a considerably simpler eigenvalue problem for σ associated with a system of <u>ordinary differential equations</u>. Such problems fall into two general classes — the stability of parallel[2] or nearly parallel flows such as Poiseuille flow and the boundary-layer flow; and the stability of revolving fluids such as Couette flow, or the flow over a concave wall. The two classes of problems are quite different, both in the physical mechanisms causing instability and in the mathematical techniques used to solve the corresponding eigenvalue problem. The problem of the stability of parallel flow is discussed in detail by Lin [1][3] in his excellent monograph, while the problem of the stability of Couette flow and related problems has been described in a comprehensive treatise by Chandrasekhar [2] . As we discuss the stability of Couette flow we will try to point out how it differs from the parallel-flow stability problem, and the significance of these differences.

The stability of Couette flow was first investigated both theoretically and experimentally by G. I. Taylor [3] in his famous paper of 1923. Taylor showed that as the speed of the inner cylinder is increased there is a point at which a new steady secondary motion appears. This secondary motion is of the form of toroidal vortices located periodically in the z-direction — they are usually referred to as Taylor vortices. Recent experiments [4, 5] show that, as the speed of the inner cylinder is increased beyond the critical speed, there is a second critical speed at which the vortices assume a wavy form in the azimuthal direction and move circumferentially around the cylinders; as the speed is increased even further the flow will eventually become turbulent.

Taylor's experimental work has been well verified by numerous experiments; however, there is some question as to what is the form of the initially unstable disturbance when $\mu = \Omega_2/\Omega_1$[4] is sufficiently negative, say, $\mu \sim -1$. This

---

[2] Some authors use the term parallel flow to denote a flow for which the streamlines do not converge or diverge in the flow direction. In the present paper we mean by parallel flow a flow for which the streamlines are straight lines.

[3] Numbers in brackets designate References at end of paper.

[4] The angular velocities of the inner and outer cylinders are Ω_1 and Ω_2 respectively.

will be discussed briefly in the section "Some Related Problems". Taylor's theoretical analysis for rotationally symmetric disturbances is complete. However, the numerical computations are limited to the case in which the gap between the cylinders is small compared to the mean radius (actually linear terms in this ratio were retained) and, except for a couple of cases, to values of $\mu > -1/2$. The reasons for these limitations will be made clear in the next section.

Recent theoretical work on the stability of Couette flow has been concerned primarily with the development of better mathematical techniques to solve the eigenvalue problem, the extension to finite gap, the extension to μ negative, and the consideration of nonrotationally symmetric disturbances.

STABILITY OF COUETTE FLOW. Now let us consider the stability of a viscous fluid between two infinitely long concentric rotating cylinders. Let r, θ, z denote the usual cylindrical coordinates, and R_1, R_2 and Ω_1, Ω_2 the radii and angular velocities of the inner and outer cylinders, respectively. Further, we denote the velocity components in the increasing r, θ, and z-directions by u_r, u_θ and u_z. An exact solution of the Navier-Stokes equations satisfying the boundary conditions $u_\theta = R_1 \Omega_1$ at R_1 and $R_1 \Omega_2$ at R_2 is the Couette velocity distribution:

(1) $u_z = 0,$ $u_r = 0,$ $u_\theta = V(r) = Ar + \dfrac{B}{r},$ $\dfrac{\partial p}{\partial r} = \rho \dfrac{V^2}{r}$

where

(2) $A = -\Omega_1 \eta^2 \dfrac{1 - (\mu/\eta^2)}{1 - \eta^2},$ $B = \Omega_1 R_1^2 \dfrac{1 - \mu}{1 - \eta^2},$

$\mu = \Omega_2/\Omega_1,$ $\eta = R_1/R_2.$

In this section we will be interested in considering the stability of the Couette velocity distribution to rotationally symmetric disturbances. The case of nonrotationally symmetric disturbances will be discussed in the next section.

If the fluid is inviscid, we know (Rayleigh's criterion) that a necessary and sufficient condition for the flow to be stable to rotationally symmetric

disturbances is that the square of the circulation increases radially outward[5].
For the velocity distribution (1) this gives that the flow is stable provided the
$\mu = \Omega_2/\Omega_1 > \eta^2 = (R_1/R_2)$. Synge [6] has extended this result and has

shown that for a viscous fluid $\mu > \eta^2$ is a sufficient condition for stability,
but not a necessary condition. Thus we can expect that viscosity will always
have a stabilizing effect.

If we substitute for $u_\theta(r, z, t)$

(3) $u_\theta(r, z, t) = V(r) + v'(r, z, t)$

and similar expressions for u_z, u_r, and p in the Navier-Stokes equations,
neglect quadratic terms, and eliminate p' and the axial disturbance velocity
w', we obtain two partial differential equations for v' and the radial disturbance
velocity u'. It is easy to show that it is possible to separate variables and
obtain solutions of the form

(4) $v'(r, z, t) = v(r)e^{\sigma t + i\lambda z}$, $u'(r, z, t) = u(r)e^{\sigma t + i\lambda z}$

Anticipating that the secondary motion is periodic in the axial direction, we
take λ to be real and positive; in general σ is complex. The ordinary differential
equations satisfied by $u(r)$ and $v(r)$ are

(5) $\{v(DD^* - \lambda^2) - \sigma\}(DD^* - \lambda^2)u = 2\lambda^2 \Omega(r)v,$

(6) $\{v(DD^* - \lambda^2) - \sigma\}v = (D^*V)u$

and the boundary conditions are

(7) $u = Du = v = 0$ at $r = R_1$ and R_2 .

---

[5] See, for example [2] , Sec. 66.

Here

$$(8) \qquad D = \frac{d}{dr}, \qquad D^* = \frac{d}{dr} + \frac{1}{r}, \qquad \Omega(r) = V/r$$

Equations (5), (6), and (7) when written in dimensionless form determine an eigenvalue problem for σ as a function of the parameters $\eta, \mu, a = \lambda d$ and $R = \Omega_1 R_1 d/v$ where $d = R_2 - R_1$. For fixed values of η and μ, which determine the geometry and the angular velocity up to scale factors, the condition Re $\sigma = 0$ determines R as a function of a and the imaginary part of σ, (Im σ). Since the instability is known to be a steady secondary motion, we can expect that the marginal state will be characterized not only by Re $\sigma = 0$ but also Im $\sigma = 0$; and hence the conditions for determining R as a function of a is $\sigma = 0$. This is known as the principle of exchange of stabilities. It has only been proved mathematically [7] in the one limiting case $d/R_1 \rightarrow 0$ and $\mu \rightarrow 1$. In this case the stability problem is identical with that for the convective instability of a layer of fluid heated from below. The minimum real positive value of R over all real a determines the critical value of R, say, R_c. The corresponding value of a determines the axial wave number.

Before discussing how we solve the eigenvalue problem (5), (6), and (7), let us first contrast the present problem with the typical stability problem in parallel flow. First, in parallel flow the critical disturbance is a two-dimensional disturbance[6] that is periodic in the flow direction and is oscillatory in time; whereas, for curved flow, the critical disturbance is three-dimensional, independent of the coordinate in the flow direction and is steady in time. Also, the curved flow stability problem leads to a sixth-order ordinary differential equation with real regular coefficients which in the limit $v \rightarrow 0$ reduces to a second-order differential equation with regular coefficients. In contrast, the parallel-flow stability problem leads to a fourth-order ordinary differential equation with regular complex valued coefficients (the Orr-Sommerfeld equation) which in the limit $v \rightarrow 0$ reduces to a second-order differential equation with a regular singular point. These differences are summarized in Table 1.

---

[6]That we need only consider two-dimensional disturbances follows from Squire's theorem; see Lin [2], p.27.

It is clear that there are essential differences between the two problems, and the mathematical techniques suitable for one problem may not be suitable for the other. For example, even though the solution of the Orr-Sommerfeld equations is regular for $\nu \neq 0$, we can expect that for ν small it will be rapidly varying in the neighborhood of the singular point of the reduced equation, and hence difficult to approximate. Indeed, the mathematical procedures used in solving the Orr-Sommerfeld equation, which involve an analysis of the asymptotic solutions of a differential equation for which the reduced equation is singular, are considerably more sophisticated than those needed for an investigation of the stability of Couette flow.

<u>Table 1</u>

Parallel flow	Couette flow
Two-dimensional disturbance	Three-dimensional disturbance
Periodic in coordinate direction of basic flow	Independent of the coordinate direction of the basic flow, periodic in the axial direction
Oscillatory disturbance	Steady secondary motion, principle of exchange of stabilities
Fourth-order ordinary d.e., regular but complex valued coefficients	Sixth-order ordinary d.e., regular and real valued coefficients
$\nu \to 0$ gives second-order d.e. with a regular singular point	$\nu \to 0$ gives second-order d.e. with regular coefficients

Turning now to the eigenvalue problem defined by equations (5), (6), and (7), we will consider the limiting case in which the gap $d = R_2 - R_1$ is small compared to the mean radius $R_0 = (R_1 + R_2)/2$. The small gap approximation allows two simplifications. The first is that, correct to terms $O(d/R_0)$, the variable coefficient differential operator DD^* can be replaced by the constant coefficient differential operator D^2; the second is the reduction of the number of parameters in the eigenvalue problem; i.e., $\eta \to 1$. To the same order of accuracy we can approximate Ω by a linear profile. Setting $\sigma = 0$ (the principle of exchange of stabilities), letting

(9) $r = R_0 + dx,$ $a = \lambda d,$ $T = -4A\,\Omega_1 d^4/\nu^2$

and denoting d/dx by D, we obtain

(10) $(D^2 - a^2)^2 u = \left\{ (1 + \mu)/2 - (1 - \mu)x \right\} v$,

(11) $(D^2 - a^2)v = -a^2 Tu$

In deriving equations (10) and (11) we have made the use of the fact that $D^*V = 2A$, and have rescaled u by a factor $-2Ad^2/a^2T$.

The boundary conditions (7) are to be applied at $x = \pm 1/2$. The dimensionless parameter T is known as the Taylor number; it has the form

(12) $T = 4R^2 \left(\dfrac{d}{R_1} \right) \dfrac{\eta^2 - \mu}{\eta(1 + \eta)}$

For $\mu = 0$, $\eta \rightarrow 1$, T reduces to $2R^2(d/R_1)$, which is the form commonly found in the engineering literature.

For a fixed value of $\mu < \eta'$ we wish to find the minimum positive value of T (This is equivalent to minimizing R) over all real positive a. The eigenvalue problem for $T = T(a, \mu)$ defined by equations (10) and (11) and the boundary conditions is a nonself-adjoint boundary-value problem; and the existence of a positive real eigenvalue T has only been shown rigorously for the case that the dimensionless angular velocity $\{(1 + \mu)/2 - (1 - \mu)x\}$ is greater than zero; i.e., the cylinders rotate in the same direction [8]. However, from a practical point of view, approximate calculations do indicate the existence of positive eigenvalues T for $\mu < 0$; and, of course, we can anticipate their existence from the experimental results. The fact that the eigenvalue problem is nonself-adjoint also complicates any discussion of the convergence of approximate iterative or expansion procedures. Again, from a practical point of view, a more serious difficulty occurs when $\mu < 0$. In this case the coefficient on the right-hand side of equation (10) vanishes at some point $x_1 = (1 + \mu)/2(1 - \mu)$ in the interval of interest. Then $\Omega(x)$ is positive for $-1/2 < x < x_1$ and negative for $x_1 < x < 1/2$. It follows from Rayleigh's criterion that the flow is "inviscidly" unstable in the inner region and inviscidly stable in the outer region. Thus we can expect that the corresponding eigenfunction will be relatively constant over the outer region, with its variation primarily taking place in the inner region; and hence will be fairly difficult to approximate. This

is particularly true as $x_1 \longrightarrow -1/2$; i.e., as $-\mu \longrightarrow \infty$.

Thus the problem of solving the eigenvalue problem defined by equations (11), (10), and (7) can be broken into three parts: $\mu > 0$, $-\mu \longrightarrow \infty$, and an intermediate range between large negative μ and $\mu = 0$. Actually it has been shown [9] that the asymptotic results for $-\mu \longrightarrow \infty$ can be expected to be satisfactory for $\mu < -1$. A variety of methods has been suggested for solving the eigenvalue problem. For $\mu > 0$ the eigenfunction does not vanish in the interval; hence is fairly easy to approximate, and as a result all methods are very satisfactory. As μ decreases beyond zero, however, the approximate methods require more and more iterations, or terms in a series representations for the eigenfunction, and hence become more and more unwieldy.

One method which involves a reasonable amount of work, and also yields accurate results for the behavior of T_c as $-\mu \longrightarrow \infty$ is a modified Galerkin method[7]. This method which was suggested by Chandrasekhar[8] is briefly as follows: First expand $v(x)$ in a complete set of functions (preferably orthogonal) satisfying the boundary conditions $v = 0$ at $x = \pm 1/2$; say,

$$v(x) = \sum_{n=1}^{\infty} \alpha_n v_n(x)$$

Corresponding to this expansion it is possible to write

$$u(x) = \sum_{n=1}^{\infty} \alpha_n u_n(x)$$

where the $u_n(x)$ are solutions of

(13) $(D^2 - a^2)^2 u_n = \left\{ (1 + \mu)/2 - (1 - \mu)x \right\} v_n(x)$

---

[7] An alternative method is to convert the boundary-value problem (11), (10) and (7) to a pair of simultaneous integral equations, which can then be solved by an iterative technique; see, for example, Kirchgassner [8] and the references given there

[8] See reference 2 for a detailed discussion.

satisfying $u_n = Du_n = 0$ at $x = \pm 1/2$. Substituting these series for
u and v in equation (11), and then requiring that the error in the equation be
orthogonal to the $v_n(x)$, leads to an infinite system of linear homogeneous
equations for the α_n. A necessary condition for the existence of a nontrivial
solution is that the determinant of the coefficients vanish; this determines the
eigenvalue equation. Approximate values for $T(a, \mu)$ are obtained by taking
a finite number of terms in the series for $v(x)$. How satisfactory the method
will be depends upon the number of terms required to obtain accurate results.

For $\mu > 0$ the eigenfunction is nearly symmetric, and just the one
term approximation $v_1 = \sqrt{2}$ $\cos \pi x$ gives a satisfactory result for T_c.
Of course, for $\mu > 0$, the standard Galerkin procedure with the approximating
functions $v_1 = x^2 - 1/4$ and $u_1 = (x^2 - 1/4)^2$ will also give good results.
For $\mu > 0$, T_c is given approximately by $T_c = 3416/(1 + \mu)$, and also
$a_c = 3.12$. The advantage of the modified Galerkin method lies in the fact
that for $\mu < 0$ part of the difficulties associated with the sign change of
Ω are overcome (in some sense) by solving equation (13) for the expansion
functions $u_n(x)$. Also, since one equation is satisfied, the size of the deter-
minantal eigenvalue equation is smaller by a factor of two than the one for the
corresponding approximation if both u and v are expanded in complete sets
of functions. Even so, at $\mu = -3$ it is necessary to take five terms in the
series for $v(x)$ in order to obtain T_c correct to 1 percent. The values of T_c
and a_c as a function of μ for $-4 < \mu < 1$ are given by Chandrasekhar [2].

For $-\mu \rightarrow \infty$, in which case the flow is inviscidly unstable in a
vanishingly thin region near the inner cylinder, it is clear that the proper
length scale is $d_1 = d/(1 - \mu)$, the distance from the inner cylinder to
the zero point of $\Omega(x)$, rather than the full gap $d = R_2 - R_1$. With this
idea in mind, Meksyn [10] using asymptotic methods and DiPrima [9] using
the Galerkin method have computed the limiting form of T_c as $-\mu \rightarrow \infty$.
More recently, Duty and Reid [11] have made an extensive investigation of
this case using asymptotic methods. Their results, which are undoubtedly
the most exact, show that as $(1 - \mu) \rightarrow \infty$, $T_c \rightarrow 1186.4 (1 - \mu)^4$
and $a_c \rightarrow 2.0018 (1 - \mu)$. [9] An extrapolation of the results of
Chandrasekhar using the modified Galerkin method to the case $-\mu \rightarrow \infty$

---

[9] D. L. Harris in an unpublished paper has obtained the constants 1178.6
and 2.034 by direct numerical integration

gives close agreement with these results.

Finally, it should be pointed out that if the differential equations that are involved have variable coefficients it may be very difficult or even impossible to compute the $u_n(x)$ and, hence, impossible to use the modified Galerkin method. Also if the principle of exchange of stabilities is not valid, the term (i Im σ) will appear in the differential equations; and the solution of the equation for $u_n(x)$ will be a fairly complicated complex-valued function. As a consequence the computations will be considerably longer; but, of course, such a problem can be expected to be more difficult than one for which the principle of exchange of stabilities holds (see following section).

SOME RELATED PROBLEMS. In this section we will discuss several problems related to the classic small-gap Taylor problem.

The Finite-Gap Problem. This problem is similar to the small-gap problem, the primary difference being that $DD^* = d^2/dr^2 + r^{-1}d/dr - r^{-2}$ can no longer be approximated by d^2/dr^2. Also, of course, the Taylor number T is a function of the additional parameter η: $T = T(\alpha, \mu, \eta)$. Since the differential equations have variable coefficients the use of the modified Galerkin method is fairly tedious. However, Chandrasekhar and Reid [12] have constructed an appropriate set of complete functions (a linear combination of Bessel functions), and Chandrasekhar [13] has solved the eigenvalue problem for a wide range of values of μ for $\eta = 1/2$. Some of the difficulties, including the necessity of having to resort to numerical integration to evaluate several of the integrals, can be avoided by considering the adjoint boundary-value problem. This also has been done by Chandrasekhar and Elbert [14], again for $\eta = 1/2$. Computations for other values of η have not been carried out by this method.

Witting [15] and Kirchgassner [8] have also considered the finite-gap problem. In the more complete work of Kirchgassner the differential equations are converted to simultaneous integral equations which are then solved by an iterative scheme. The variation of T_c with μ for $\eta = 1/2$ and with η for $\mu = 0$ and η in the range $1/2 < \eta < 1$ is given.

Recently Walowit, Tsao and DiPrima [16] have observed that as long as interest was restricted to the case $0 \leq \mu < \eta^2$ (the case $\mu = 0$ is of primary engineering interest) or μ not too negative, the variation of T_c with η can be obtained by a straightforward application of the Galerkin method. The expansion functions chosen for u and v were polynomials satisfying the

prescribed boundary conditions. With a simple change of variables all necessary integrals could be evaluated easily. The variation of T_c with η for $\mu = 0$ using four-term approximations for u and for v (the percentage difference between the two-term and four-term approximations is less than 2.5 percent for $0.2 < \eta < 1$) is shown in Fig. 1. Also shown is an approximate formula for η near 1 that was suggested by Taylor [3] , and various theoretical and experimental results of Taylor [3] , Lewis [17] , Donnelly [18] , and Caldwell and Donnelly [19] . For a discussion of the experimental results of Lewis, which indicate a hysteresis effect, the reader is referred to the paper by Caldwell and Donnelly. It is interesting to note that as $\eta \to 0$, i.e., as the gap becomes infinitely large ($R_1 \neq 0$), $T_c(\mu = 0, \eta)$ appears to behave as $C(1 + \eta)/2\eta^2$ where C is a constant. It follows that $(R_1^2 \Omega_1/v)^2 \to C/8$.

Nonrotationally Symmetric Disturbances. It has been observed when the gap between the cylinders is small and the outer cylinder is at rest, that at a Reynolds number of the order $1.1 R_c$ to $1.2 R_c$ the steady cellular motion assumes a wavy form in the aximuthal direction and moves with a definite wave velocity in this direction. An analysis of this "higher-order instability" of the distorted original velocity distribution plus the Taylor vortices has not been considered to date. However, the problem of the stability of Couette flow to nonrotationally symmetric disturbances; that is, disturbances of the form

(14) $v'(r, \theta, z, t) = v(r)e^{i(\sigma t + k\theta + \lambda z)}$.

where k is an integer, has recently been treated by DiPrima [20] .[10]

In the case of small gap and for $\mu = 0$, DiPrima found, using the Galerkin method, that R_c is a slowly increasing function of k. For $k = 4$ the value of R_c and the wave velocity are in qualitative agreement with the observed results. However, within the framework of linear theory, it is impossible to say which mode is preferred at speeds above the original critical speed. It also should be pointed out that since the disturbance is periodic in the direction of the basic flow, the stability problem has certain features of parallel-flow stability problems

---

10 The corresponding inviscid problem has been treated for $\mu > 0$ by E. Krueger and R.C. DiPrima, "Stability of Nonrotationally Symmetric Disturbances for Inviscid Flow Between Rotating Cylinders," Physics of Solids, vol. 5, 1962, pp. 1362 - 1367; and for $\mu < 0$ by F. Bisshopp, "Asymmetric Inviscid Modes of Instability in Couette Flow," The Physics of Fluids, vol. 6, 1963, pp. 212-217.
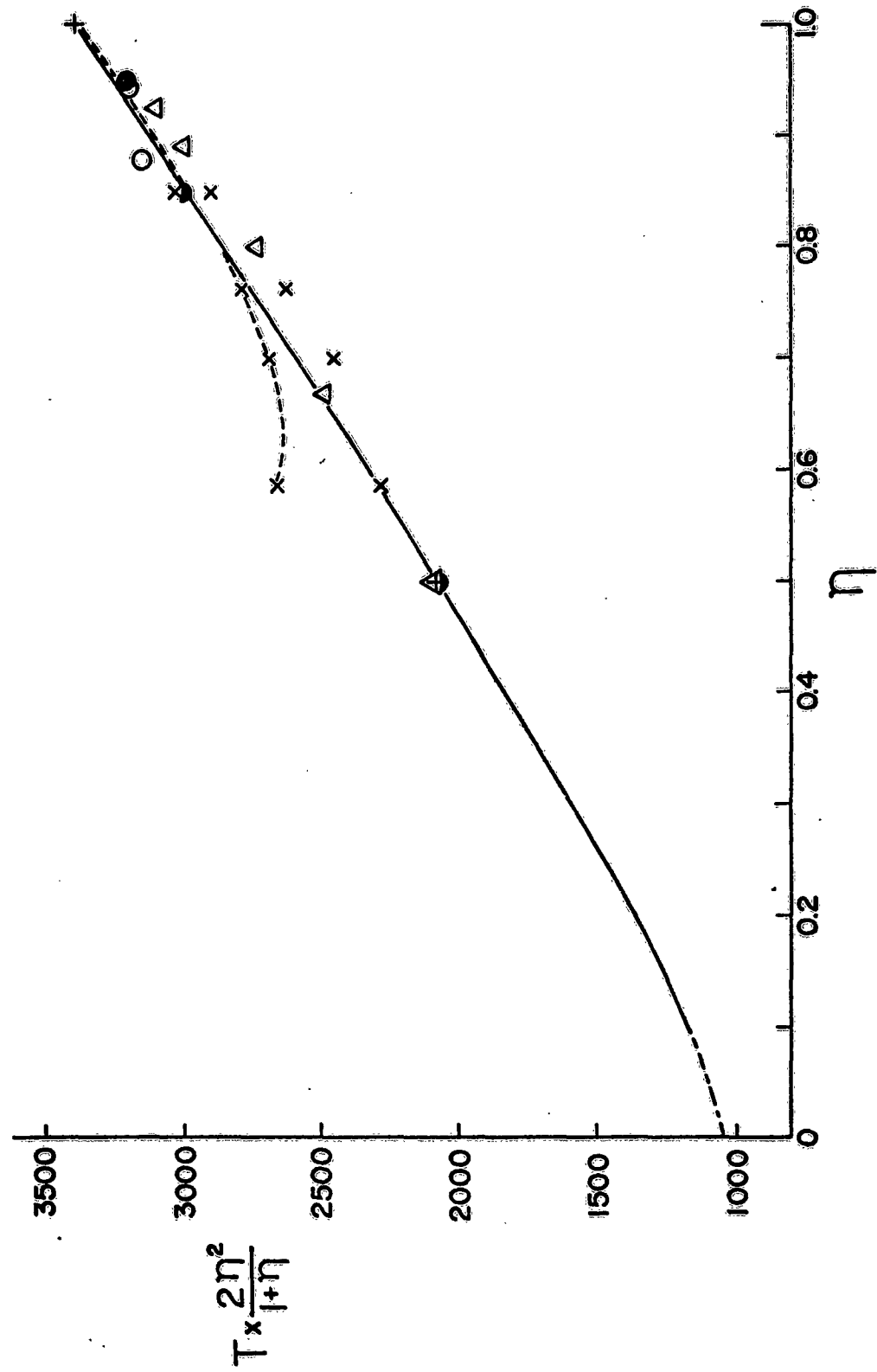
Fig. 1 Variation of T_c with for $\mathcal{H} = 0$. X, experiment, Lewis [17] . 0, experiment, Taylor [3] . ●, experiment, Donnelly [18] , and Donnelly and Caldwell [19] . +, theoretical, Chandrasekhar [14 . △, theoretical, Kirchgassner [8] --- finite-gap approximation, Taylor [3] . ------ theoretical, DePrima and Tsao [16] .

which make the solution more difficult to approximate. For example, the principle of exchange of stabilities is no longer valid. Also in contrast to the case $k = 0$, the reduced equation ($\mathcal{V} \to 0$) does have a singular point. While the results seem satisfactory, it is not clear at the present time that the methods that are so successful for $k = 0$ are equally satisfactory for $k \neq 0$.

Recently Krueger [21] has extended Di Prima's analysis to the case $\mu < 0$. His results are shown in Fig. 2, where $T_c(\xi)/T_c(\xi = 0)$ is plotted as a function of μ for several values of the dimensionless parameter $\xi = k(-4A/\Omega_1)^{1/2}$. These preliminary computations indicate that at negative values of $\mu \sim -3/4$ to -1 non-rotationally symmetric disturbances may be the most unstable. These computations do not show which mode will occur, and we should only accept these results as being indicative of the fact that for $\mu \sim -3/4$ the terms introduced by the azimuthal dependence of the disturbance may be destabilizing. A more complete mathematical investigation[11] is needed before a definite conclusion can be drawn; however, it should be pointed out that at $\mu = -1$, $k = 0$ the value of T_c is within 2 percent of the exact result. There is some confirmation for these results in the experimental results of Lewis [17] who observed, for $\mu < 0$, that in some cases "the motion changed straightway at the critical speed to the pulsating time." Also Nissan et al. [5] have observed that the difference between the critical speed for nonrotationally symmetric disturbances and rotationally symmetric disturbances decreases as $-\mu$ increases, and at $\mu \sim -0.7$ nonrotationally symmetric motions are observed at the onset of instability.

In concluding this section we should mention that other closely related problems which have been discussed in the recent literature include the stability of flow between rotating cylinders with a pressure gradient around the cylinders [22, 23] and the stability of flow between rotating cylinders with an axial pressure gradient [24, 25, 26]. For a discussion of these problems and the experimental results the reader is also referred to Chandrasekhar [2]. Also, a very interesting discussion of some unusual features of the first problem has recently been given by Hughes and Reid [27]. In regard to the second problem see also the recent experimental work of Snyder [28]. Finally, we mention that the effect of axial and azimuthal magnetic fields and radial temperature gradients on the stability of conducting fluids between rotating cylinders has also been considered.

---

[11] Since this paper was presented, more detailed and complete computations have been carried out by Krueger, Gross and DiPrima. These computations establish that for $\mu < -0.8$ nonrotationally symmetric disturbances do, indeed, occur at lower Taylor numbers than those for rotationally symmetric disturbances.
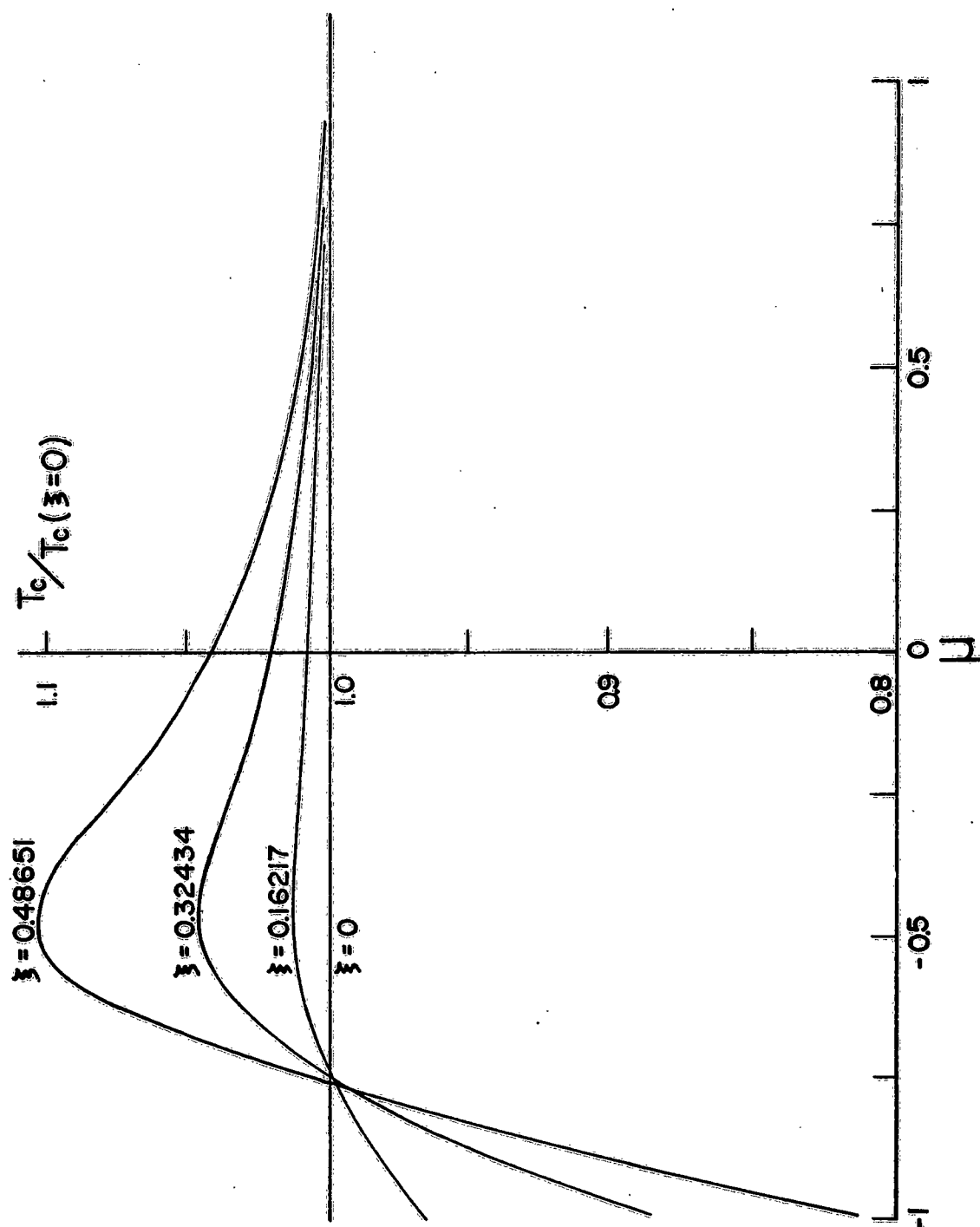
Fig. 2 Variation of T_c with μ for different values of $\xi = k(-4A/\Omega_1)^{1/2}$ as given by Krueger [21]

NONLINEAR EFFECTS.   As we have seen, the linear theory of hydrodynamic
stability predicts correctly the critical speed for the instability of Couette
flow; and further, the predicted axial spacing of the toroidal vortices is in
agreement with experiment. However, there are several questions which can
not be answered using linear theory. For example: (a) According to linear
theory an unstable disturbance will grow exponentially in time at speeds above
the critical speed, whereas actually a finite amplitude is reached and a new
equilibrium flow is established.[12] (b) At speeds above critical there is a
continuous interval of values of λ for which there exist growing disturbances,
yet a definite periodic motion is observed which indicates that the other modes
are damped out.

The answer to each of these problems can only be found by considering
nonlinear effects. In this section we will discuss (a), following the work of
Stuart [29, 30] and Davey [31] . By using nonlinear theory we will find that for
$R > R_c$ a disturbance with a specific axial wave number will reach an equilibrium
amplitude, which is independent of the initial condition. The question of the
preferred axial wave number for the Taylor problem has not been considered; however,
the corresponding question for the Benard problem has been investigated recently
by Segel [32] .

We should also mention that while we are going to consider nonlinear
effects in regard to the establishment of a new equilibrium flow, there are also
instability problems where it is doubtful that a new equilibrium flow is ever
reached. For example, in the instability of the boundary layer it would appear
that the initially growing oscillation becomes progressively less regular and
finally leads to turbulence. For the role of nonlinear effects in the breakdown
of boundary-layer flow the reader is referred to the interesting papers by Benney
and Lin [33] , Benney [34] , Greenspan and Benney [35] , and Stuart [36].

In our analysis of nonlinear effects in Couette flow instability we will
continue to assume that the velocity is independent of θ . Since the motion
is periodic in z of period $2\pi/\lambda$, it is convenient to divide the velocity into
a mean (with respect to z) velocity plus disturbance velocity; thus we write

---

[12]We might also note that using the normal-mode approach the eigenfunctions
are only determined up to a multiplicative constant. The amplitude can, of course,
be determined by considering the initial value problem. Even so, the disturbance
will grow exponentially.

$$u_\theta(r,z,t) = \overline{V}(r,t) + v'(r,z,t)$$

$$(15) \qquad\qquad\qquad\qquad = \overline{V}(r,t) + \sum_{n=1}^{\infty} v_n(r,t) \cos n\lambda z$$

and similar expressions for the other velocity components.[13] Here a bar denotes a mean value with respect to z, a prime denotes a disturbance quantity, and of course $\overline{v'} = 0$. The equations satisfied by the mean motion are obtained by substituting for the velocity and pressure in the Navier-Stokes equations, and then taking averages with respect to z. The equations for the disturbance quantities are obtained by subtracting the mean motion equations from the full equations. The main points which we wish to illustrate can be seen by considering the mean motion equation for $\overline{V}$, and the equation for the energy associated with the disturbance. These equations are

$$(16) \qquad \frac{\partial \overline{V}}{\partial t} + \frac{1}{r^2} \frac{\partial}{\partial r} (r^2 \overline{u'v'}) = \nu \left(\frac{\partial^2}{\partial r^2} + \frac{1}{r} \frac{\partial}{\partial r} - \frac{1}{r^2} \right) \overline{V}$$

and

$$\frac{\partial}{\partial t} \iint \frac{u'^2 + v'^2 + w'^2}{2} \, r\,dr\,dz$$

$$(17) \qquad\qquad = \iint (-\overline{u'v'}) \cdot \left(\frac{\partial \overline{V}}{\partial r} - \frac{\overline{V}}{r} \right) r\,dr\,dz \; - \; \nu$$

$$\times \iint (\xi'^2 + \eta'^2 + \zeta'^2) r\,dr\,dz$$

Equation (17) is obtained by multiplying the r, θ, and z-disturbance momentum equations by u', v', and w', and then integrating over the radial gap, and one wavelength in the z-direction; ξ', η' and ζ' are the r, θ, and z-components of the disturbance vorticity. The terms in equation (17) represent, respectively, the rate of change of the kinetic energy of the disturbance, the rate of transfer of kinetic energy from the mean motion to the disturbance, and the rate of viscous dissipation of kinetic energy. We should also note that, if quadratic

---

[13] In the following discussion we will usually refer to v' or $v_n(r,t)$; it is to be understood that we mean similar comments for the other velocity components.

terms in the disturbance quantities are neglected, the steady-state solution of equation (16) is precisely the Couette velocity distribution, equation (1).

Equations (16) and (17) show clearly the interaction between the mean motion and the disturbance. The mean motion is modified through the action of the Reynolds stress term $r^{-2} \partial(r^2 \overline{u'v'})/\partial r$ and, in turn, the modification of the mean flow changes the rate at which kinetic energy is transferred to the disturbance until eventually an equilibrium state is reached.

An approximate way of determining this equilibrium state is based on the so-called "shape assumption" suggested by Stuart [29]. The basic idea is that, at speeds above critical, the disturbance velocities and vorticity distributions are assumed to have the form given by the solution of the linearized stability problem, but to have an amplitude $A(t)$. For example,

$$v'(r,z,t) \; = \; A(t)v(r) \, \cos \lambda z$$

where $v(r)$ is the solution of the linearized stability problem at the given value of λ and angular velocity Ω_1. Then, if we neglect the time derivative in the mean motion equation (16) — near the equilibrium state it is small — we obtain

$$(18) \qquad \overline{V}(r,t) \; = \; V_{\lambda}(r) \; + \; A^2(t)V_1(r)$$

The term $V_{\lambda}(r)$ is precisely the Couette velocity distribution, and the second term represents the correction due to the Reynolds stress. Substituting for $\overline{V}$ in the disturbance equations, and evaluating the spatial integrals gives an equation for the amplitude $A(t)$ of the form

$$(19) \qquad \frac{dA^2}{dt} \; = \; 2A^2(a_0 \; + \; a_1 A^2)$$

where a_0 and a_1 are parameters which depend on the speed of rotation, and so on. In particular a_0 is precisely the amplification rate $\sigma > 0$ based on linear theory, which is what we should expect, since if we neglect terms $0(A^4)$ in equation (19) we obtain $A(t) \sim e^{a_0 t}$. If the term $2a_1 A^4$, which arises from the second term in equation (17) due to the distortion of $\overline{V}$, is retained, the solution of equation (19) is

$$(20) \qquad\qquad A^2(t) \;=\; \frac{K\sigma e^{2\sigma t}}{1 - a_1 K e^{2\sigma t}}$$

Here K is a constant which is determined by the initial conditions. As $t \to \infty$, $A(t) \to (-\sigma/a_1)^{1/2}$, and hence provided that $a_1 < 0$, we obtain an equilibrium disturbance amplitude $A_e = (-\sigma/a_1)^{1/2}$. Thus the effect of the nonlinear term is to modify the exponentially growing disturbance (according to linear theory) so that a finite amplitude equilibrium flow is eventually reached. Once A_e is known the equilibrium mean flow and the corresponding torque can be computed.

In the foregoing approximate analysis we have only taken account of the effect of the distortion of the mean motion by the action of the Reynolds stress. Recently Davey [31] has given a complete formal analysis of the nonlinear growth of Taylor vortices; and he found that, correct through terms $O(A^4)$, the equation for $A(t)$ is of the form (19), but that the constant a_1, which is indeed negative, represents the sum of three effects. These effects are the distortion of the mean motion due to the Reynolds stress; the transfer of energy from the fundamental mode $\cos \lambda z$ to its first harmonic $\cos 2\lambda z$; and finally the radial distortion of the fundamental.

In the analysis by Davey the Fourier series representation for v', equation (15), is substituted for v' in the disturbance equations. This gives an infinite system of nonlinear partial differential equations for the $v_n(r,t)$. These equations can be solved systematically by a separation of variables technique based on a suitable expansion of the velocities in powers of the amplitude $A(t)$. In particular $v_n(r,t)$ and $\bar{V}(r,t)$ are given by

$$(21) \qquad\qquad v_n(r,t) \;=\; \sum_{m=0}^{\infty} A^{n + 2m}(t) v_{nm}(r)$$

$$(22) \qquad\qquad \bar{V}(r,t) \;=\; V_\chi(r) + \sum_{m=1}^{\infty} A^{2m}(t) V_m(r)$$

and the amplitude $A(t)$ must satisfy

$$(23) \qquad\qquad \frac{dA}{dt} \;=\; \sigma A + \sum_{m=1}^{\infty} a_m A^{2m}(t)$$

The function v_{10} is the solution of the linearized stability equations corresponding to the basic flow $V_\theta(r)$ at a given speed above critical; i.e., $\sigma > 0$. The other functions $v_{nm}(r)$ are determined systematically as the solutions of nonhomogeneous ordinary differential equations. The constants a_1, a_2, $\ldots$ are also determined as part of the analysis.

For $\lambda = \lambda_c$ as predicted by linear theory, Davey has carried out the necessary computations to determine σ and a_1 as a function of Ω, in the three cases $\eta = 1/2$, $\mu = 0$; $\eta \to 1$, $\mu = 0$; and $\eta \to 1$, $\mu \to 1$. Knowing the amplitude of the disturbance, it is possible to compute the additional torque required to maintain the motion at $R > R_c$. The agreement between the theoretical and experimental values of the torque as a function of $R > R_c$ for $\eta = 1/2$, $\mu = 0$ is very good for an unexpectedly large range of R, $R_c < R < 2R_c$. For the case $\eta \to 1$, $\mu = 0$ the agreement is not as good, except for $R - R_c$ small ($R_c < R < 1.2R_c$). Finally, Davey's computations also show that as long as the cylinders rotate in the same direction the use of the shape assumption will give results in very close agreement with those obtained using the complete theory.

ACKNOWLEDGMENT

REFERENCES

1. C. C. Lin, The Theory of Hydrodynamic Stability, Cambridge University Press, Cambridge, England, 1955.

2. S. Chandrasekhar, Hydrodynamic and Hydromagnetic Stability, Oxford at the Clarendon Press, London, England, 1961.

3. G. I. Taylor, "Stability of a Viscous Liquid Contained Between Two Rotating Cylinders," Philosophical Transactions of The Royal Society of London, Series A, vol.223, 1923, pp. 289-343.

4. D. Coles, "Transition in Circular Couette Flow," paper presented at Tenth International Congress of Applied Mechanics, Stresa, Italy, August, 1960.

REFERENCES (Cont.)

5. A. Nissan, J. Nardacci, and C. Y. Ho, "Heat Transfer Characteristics of Fluids Moving in a Taylor System of Vortices. Parts I and II," to be published in the American Institute of Chemical Engineers Journal.

6. J. L. Synge, "On the Stability of a Viscous Liquid Between Rotating Coaxial Cylinders," Proceedings of the Royal Society of London, Series A, vol. 176, 1940, pp. 313-343.

7. Anne Pellew and R. V. Southwell, "On Maintained Convective Motion in a Fluid Heated From Below," Proceedings of The Royal Society of London, Series A, vol. 176, 1940, pp. 313-343.

8. K. Kirchgassner, "Die Instabilitat der Stromung zwischen zwei rotierenden Zylindern gegenuber Taylor-Wirbeln fur beliebige Spaltbreiten," Zeitschrift fur Mathematik und Physik, vol. 12, 1961, pp. 14-30.

9. R. C. DiPrima, "Application of the Galerkin Method to Problems in Hydrodynamic Stability," Quarterly of Applied Mathematics, vol. 13, 1955, pp. 55-62.

10. D. Meksyn, "Stability of Viscous Flow Between Rotating Cylinders. II. Cylinders Rotating in Opposite Directions. III. Integration of a Sixth Order Linear Equation," Proceedings of The Royal Society of London, Series A, vol. 187, 1946, pp. 480-491, 492-504.

11. R. L. Duty and W. H. Reid, "On the Stability of Viscous Flow Between Rotating Cylinders, I. Asymptotic Analysis," Brown University Technical Report 42, Nonr 562(07), 1961.

12. S. Chandrasekhar and W. H. Reid, "On the Expansion of Functions Which Satisfy Four Boundary Conditions," Proceedings of the National Academy of Science, vol. 43, 1957, pp. 521-527.

13. S. Chandrasekhar, "The Stability of Viscous Flow Between Rotating Cylinders. II," Proceedings of The Royal Society of London, Series A, vol. 246, 1958, pp. 301-311.

14. S. Chandrasekhar and Donna Elbert, "The Stability of Viscous Flow Between Rotating Cylinders. II," Proceedings of The Royal Society of London, Series A, vol. 268, 1952, pp. 145-152.

15. H. Witting, "Über den Einfluss der Stromlinienkrümmung auf die Stabilität laminarer Strömungen," Arch. Rat. Mech. Anal., vol 2, 1958, pp. 243-283.

16. J. Walowit, S. Tsao, and R. C. DiPrima, "Stability of Flow Between Arbitrarily Spaced Comentric Cylindrical Surfaces Including the Effect of a Radial Temperature Gradient", To appear in the Journal of Applied Mechanics.

17. J. W. Lewis, "An Experimental Study of the Motion of a Viscous Liquid Contained Between Two Coaxial Cylinders," Proceedings of The Royal Society of London, Series A, vol. 117, 1928, pp. 388-407.

18. R. J. Donnelly, "Experiments on the Stability of Viscous Flow Between Rotating Cylinders. I, Torque Measurements," Proceedings of the Royal Society of London, Series A, vol. 246, 1958, pp. 312-325.

19. D. R. Caldwell and R. J. Donnelly, "On the Reversibility of the Transition Past Instability in Couette Flow," Proceedings of The Royal Society of London, Series A, vol. 267, 1962, pp. 197-205.

20. R. C. DiPrima, "Stability of Nonrotating Symmetric Disturbances for Viscous Flow Between Rotating Cylinders," Physics of Fluids, vol. 4 1961, pp. 751-755.

21. E. R. Krueger, The Stability of Couette Flow and Spiral Flow, PhD thesis, Rensselaer Polytechnic Institute, Troy, N.Y., June, 1962.

22. R. C. DiPrima, "The Stability of Viscous Flow Between Rotating Concentric Cylinders With a Pressure Gradient Acting Round the Cylinders," Journal of Fluid Mechanics, vol. 6, 1959, pp. 462-468.

23. B. Meister, "Das Taylor-Deansche Stabilitatsproblem für Beliebige Spaltbreiten," Zeitschrift für Mathematik und Physik, vol. 13, 1962, pp. 83-91.

24. R. C. DiPrima, "The Stability of a Viscous Fluid Between Rotating Cylinders With an Axial Flow," Journal of Fluid Mechanics, vol. 9, 1960, pp. 621-631.

25. S. Chandrasekhar, "The Hydrodynamic Stability of Inviscid Flow Between Coaxial Cylinders," "The Hydrodynamic Stability of Viscid Flow Between Coaxial Cylinders," Proceedings of the National Academy of Science, vol. 46, 1960, pp. 141-143.

26. S. Chandrasekhar, "The Stability of Spiral Flow Between Rotating Cylinders," Proceedings of The Royal Society of London, Series A, vol. 265, 1962, pp. 188-197.

27. T. H. Hughes and W. H. Reid, "On the Stability of Viscous Flow Between Rotating Cylinders, III. The Effect of a Transverse Pressure Gradient," Brown University Technical Report 50, Nonr 562(07), 1962.

28. H. A. Snyder. "Experiments on the Stability of Spiral Flow at Low Axial Reynolds Numbers," Proceedings of The Royal Society of London, Series A, vol. 265, 1962, pp. 198-214.

29. J. T. Stuart, "On the Non-Linear Mechanics of Hydrodynamic Stability," Journal of Fluid Mechanics, vol. 4, 1958, pp. 1-21.

30. J. T. Stuart, "Non-Linear Effects in Hydrodynamic Stability," Proceedings of the Tenth International Congress of Applied Mechanics, Stresa, Italy, August, 1960, pp. 63-97.

31. A. Davey, "The Growth of Taylor Vortices in Flow Between Rotating Cylinders," Journal of Fluid Mechanics, vol. 14, 1962, pp. 336-368.

32. L. A. Segel, "The Non-Linear Interaction of Two Disturbances in the Thermal Convection Problem," Journal of Fluid Mechanics, vol. 14, 1962, pp. 97-114.

33. D. J. Benney and C. C. Lin, "On the Secondary Motion Induced by Oscillations in a Shear Flow," Physics of Fluids, vol. 3, 1960, pp. 656-657.

34. D. J. Benney, "A Non-Linear Theory for Oscillations in a Parallel
     Flow," Journal of Fluid Mechanics, vol. 10, 1961, pp. 209-236.

35. H. P. Greenspan and D. Benney, "On Shear Layer Instability,
     Breakdown and Transition," Journal of Fluid Mechanics, vol. 15,
     1963, 133-153.

36. J. T. Stuart, "On Three Dimensional Non-Linear Effects in the
     Stability of Parallel Flows," Advances in Aeronautical Sciences,
     vol. 3, 1962, pp. 121-142.

LIST OF ATTENDEES

Agee, W. S.
White Sands Missile Range
New Mexico

Beck, S.
Watervliet Arsenal
Watervliet, New York

Biser, E.
U. S. Army Electronic R D Lab.
Ft. Monmouth, New Jersey

Bowie, O.
Watertown Arsenal
U. S. Army Materials Research Agency
Watertown, Massachusetts

Bradley, J.
Ballistic Research Labs.
Aberdeen Proving Ground
Maryland

Brown, R.
U. S. Army Munitions Command
Frankford Arsenal
Philadelphia, Pennsylvania

Crnarich, L.
Picatinny Arsenal
Dover, New Jersey

Culbertson, G.
Hercules Powder Co. Representative
Radford, Virginia

Davis, J.
P ↑ P Lab., FRL
Picatinny Arsenal
Dover, New Jersey

DiPrima, R.
Rensselaer Polytechnic
   Institute
Troy, New York

Doss, H.
University of Michigan
Ann Arbor, Michigan

Dressel, F.
Army Research Office
Durham, North Carolina

Duffin, R.
Carnegie Institute of
   Technology
Pittsburg, Pennsylvania

Epstein, I.
U. S. Army Electronics
   R ↑ D Laboratory
Ft. Monmouth, New Jersey

Fitzpatrick, C.
Rock Island Arsenal
Rock Island, Illinois

Fleming, D.
Con. Armament
R ↑ D Establishment
Quebec, Canada

Frishman, F.
Mathematics Branch
Army Research Office
Washington, D. C.

Galbraith, A.
Army Research Office
Durham, North Carolina

LIST OF ATTENDEES (CONT.)

Gerhard, S.
Picatinny Arsenal
Dover, New Jersey

Glynn, J.
Frankford Arsenal
Philadelphia, Pennsylvania

Goldsmith, L.
Picatinny Arsenal
Dover, New Jersey

Greville, T. N. E.
Mathematics Research Center
University of Wisconsin
Madison, Wisconsin

Gudzent, D.
Army Missile Command
Redstone Arsenal
Huntsville, Alabama

Harkin, D.
Research and Analysis Division
Ft. Belvoir, Virginia

Harrison, J.
Research Analysis Corporation
MacLean, Virginia

Helmbold, R. L.
Combat Operations Research Group
Ft. Belvoir, Virginia

Howard, B.
U. S. Army Weapons Command
Rock Island Arsenal, Illinois

Hussain, M.
Watervliet Arsenal
Watervliet, New York

Inselmann, E.
Frankford Arsenal
U. S. Army Munitions Command
Philadelphia, Pennsylvania

Jakobowski, E.
Springfield Armory
Springfield, Massachusetts

Jaroszewski, E.
Picatinny Arsenal
Dover, New Jersey

Krueger, E.
Mathematics Research Center
University of Wisconsin
Madison, Wisconsin

Kurkjian, B.
Harry Diamond Labs.
Washington, D. C.

Lawler, J.
Office of the Scientific Director
QM, R & D Center
Natick, Massachusetts

Lehman, J.
Rensselaer Polytechnic
 Institute
Troy, New York

Lehnigk, S.
Army Missile Command
Redstone Arsenal
Huntsville, Alabama

Loatman, P.
Watervliet Arsenal
Watervliet, New York

Maisel, H.
U. S. Army Strategy and
 Tactics Analysis Group
Brooklyn, New York

LIST OF ATTENDEES (CONT.)

Mall, A.
Frankford Arsenal
Philadelphia, Pennsylvania

Matzkowitz, W.
W & SP Lab - Analytical Div.
Picatinny Arsenal
Dover, New Jersey

Mescall, J.
Watertown Arsenal
Watertown, Massachusetts

Murray, F.
U. S. Army Research Office
Durham, North Carolina

Nevel, D.
Cold Regions Research and
 Engineering Laboratory
Hanover, New Hampshire

O'Neil, J.
Springfield Armory
Springfield, Massachusetts

Parrish, G.
U. S. Army Research Office
Durham, North Carolina

Pascual, M.
Watervliet Arsenal
Watervliet, New York

Ross, E.
Watertown Arsenal
Watertown, Massachusetts

Sadowsky, M.
Watervliet Arsenal
Watervliet, New York

Scanlon, R.
Watervliet Arsenal
Watervliet, New York

Schmidt, T.
U. S. Army Research Office
Durham, North Carolina

Schmiedeshoff, F.
Watervliet Arsenal
Watervliet, New York

Scott, W.
Ballistic Research Laboratory
Aberdeen Proving Ground
Maryland

Sewell, W.
Army Research Office
Durham, North Carolina

Sloane, H.
Dugway Proving Ground
Dugway, Utah

Sobelman, S.
Picatinny Arsenal
Dover, New Jersey

Stoker, J.
Courant Institute of
 Mathematical Sciences
New York, New York

Struble, R.
North Carolina State College
Raleigh, North Carolina

Takagi, S.
Cold Regions Research and
 Engineering Laboratory
Hanover, New Hampshire

LIST OF ATTENDEES (CONT.)

Tyler, J.
Edgewood Arsenal
Edgewood Arsenal, Maryland

Wedemeyer, E.
Ballistic Research Lab.
Aberdeen Proving Ground
Maryland

Weigle, R.
Watervliet Arsenal
Watervliet, New York

Weinstein, J.
U. S. Army Electronics
R & D Laboratory
Monmouth, New Jersey

Wiesenfeld, L.
Picatinny Arsenal
Dover, New Jersey

Wouk, A.
Mathematics Research Center
University of Wisconsin
Madison, Wisconsin

Zaroodny, S.
Ballistic Research Lab.
Aberdeen Proving Ground
Maryland

Zweig, J.
Watervliet Arsenal
Watervliet, New York